



DISSERTATION

In Partial Fulfillment of the Requirements
for the Degree of Doctor of Philosophy
from TELECOM ParisTech

Specialization: Communication and Electronics

Rizwan Ghaffar

Interference Mitigation in Multi-Antenna Systems

Defense scheduled on the 26th of November 2010 before a committee
composed of:

Reviewers	Prof. Erik G. Larsson, Linköping University Prof. Giorgio Taricco, Politecnico di Torino
Examiner	Prof. David Gesbert, EURECOM
Thesis Supervisor	Prof. Raymond Knopp, EURECOM



THESE

présentée pour obtenir le grade de

Docteur de TELECOM ParisTech

Spécialité: Communication et Electronique

Rizwan Ghaffar

Atténuation d'Interférence dans les Systèmes Multi-Antennaires

Soutenance de thèse prévue le 26 Novembre 2010 devant le jury
composé de :

Rapporteurs	Prof. Erik G. Larsson, Linköping University Prof. Giorgio Taricco, Politecnico di Torino
Examineur	Prof. David Gesbert, EURECOM
Directeur de thèse	Prof. Raymond Knopp, EURECOM

Acknowledgements

I would like to extend my deep and sincere thanks to my adviser Prof. Raymond Knopp for his invaluable support and brilliant ideas. The interest and eagerness exhibited by him in this research work has been phenomenal, which has been complemented by his excellent technical knowledge and organizational skills. This work would not have been possible without his patient, consistent and professional guidance. He is indeed an excellent human being with great personal qualities and I am very thankful to him for his unconditional support during 3 years of my PhD.

I am also grateful to the committee members of my jury, Prof. Erik G. Larsson, Prof. Giorgio Taricco and Prof. David Gesbert for their valuable comments which not only helped to improve the quality of the thesis but also guided me for the possible future extension of this work.

I would like to thank all of my friends at EURECOM, all my former colleagues and current PhD students. I am particularly indebted to some fellow PhD students at EURECOM. I was extremely lucky to have the best persons as my office mates, Sara, Giuliana, Carina, Zuleita and Florian whom I consider my trustworthy friends. I am very grateful to Randa and Umer for many useful technical discussions during the course of my PhD. Randa and Umer, among other things, made extremely valuable suggestions to improve the quality of my thesis manuscript.

I would like to thank my wife, Sarah, who understood my concerns and spared me household chores, which would have definitely hindered the regular attention required for this research. This adds to the ever-growing list of favors that she has done for me. My daughter Mahnoor and my son Musa could not be absent from the list of people I should thank.

I would like to thank my brothers, Imran and Salman, and my sister, Nadia, for their immense love and support throughout my life. I would like to specially mention my elder brother, Imran, whose unconditional support for my academic career has indeed been phenomenal and I truly believe that without his support, I would not have achieved this position.

Finally, I would like to thank my parents who made immense sacrifices for me throughout their lives and stood by me unconditionally through all thick and thin. To this end, I would specially mention my father as not many fathers do what he has done for the better education of his children. And my mother, all my life her prayers have been invaluable, for which I can offer no compensation. I am truly convinced that my father in the heaven and my mother here are the happiest persons on my this accomplishment. As a matter of fact, although it is negligible compared to what they have offered to me, I dedicate my PhD to my parents.

Abstract

Achieving enhanced spectral efficiency and increased reliability are the leading objectives of upcoming wireless systems. Exploitation of spatial dimension and exhaustive use of frequency resources are considered as the principal approaches in the pursuit of these aspirations. However, it is imperative to devise strategies taking into account the practical constraints so that the ensuing solutions are implementable in the real world.

Ongoing standardizations in the wireless world are incorporating low dimensional MIMO systems due to the intricacy of realizing requisite antenna spacing in small mobile handsets, enormous feedback load requirements in case of multiuser (MU) MIMO transmissions combined with the added complexity of separate radio-frequency (RF) chains for each antenna and the corresponding cost considerations. In this thesis, we first deliberate on the dual stream bit interleaved coded modulation (BICM) MIMO OFDM systems which are considered as the baseline configuration of long term evolution (LTE). Standard receiver solutions for such schemes employ linear minimum mean square error (MMSE) successive stripping detectors whose optimality is constrained to Gaussian alphabets. We propose a low complexity matched filter (MF) based maximum likelihood (ML) detector and show that the proposed detector reduces one complex dimension of the system. This is a fundamental result as space and technology constraints shall be restricting future MIMO systems to low dimensionality. In the sequel, we show that the proposed detector is characterized by full diversity. For comparison purposes, the analysis of MMSE detector is also included which suffers from the deficit of one diversity order in the dual stream scenario. We further contemplate on the uniform rate, nonuniform power distribution and the uniform power, nonuniform rate distribution between the spatial streams which lead to the prioritized handling of data in MIMO broadcast systems. The low complexity detection is subsequently extended to higher-dimensional MIMO systems by a hybrid approach showing that there is a slight degradation in the performance with the increase in the dimensionality

of the system but it is concurrently coupled with a boost in the complexity savings.

To offset the impediment of less number of sufficiently spaced receive antennas on the users (handsets), the spatial dimension is exploited in terms of spatial separation of the users, i.e. spatial user multiplexing in the downlink of MU cellular systems. Modern wireless systems as LTE have proposed the employment of low resolution precoders which are based on the principle of equal gain transmission (EGT) necessitating 2 to 4 bits of feedback from the user equipment (UE). The efficient employment of these precoders for MU MIMO mode is not yet fully understood thereby leading to the perception that MU MIMO is not workable in LTE. We propose in this thesis a precoding strategy for LTE standardized precoders which encompasses geometrical interference alignment at the eNodeB (LTE notation for the base station) followed by the exploitation of the residual interference structure by the UEs. On one hand, this strategy relegates the interference by a geometric scheduling algorithm while on the other hand, UEs exploit the structure of residual interference in the detection process by the low complexity MF based detectors. The effect of EGT is then studied both for singleuser (SU) and MU MIMO systems and it is shown that while EGT is characterized by full diversity in SU MIMO, it suffers from a loss of diversity in MU MIMO.

In addition to the incorporation of spatial dimension in the pursuit of higher spectral efficiency in cellular communications, frequency resources will also be aggressively utilized by tightening the frequency reuse factor. Coupled with adaptive modulation and coding schemes and diversified data services, the performance will be limited by the interfering signals of diverse rates and strengths. In this scenario, we propose an interference suppression strategy which is characterized by exploiting the interference structure in the detection process. In the sequel, we study the effects of the rate and the strength of the interference and show that the proposed strategy exhibits a coding gain as either the interference gets stronger or the rate of interference trims down. Based on the characteristic of effective exploitation of the lower rate interference by the proposed strategy, we further propose a novel fractional frequency reuse (FFR) scheme which is more spectrally and energy efficient than the traditional FFR strategies.

Contents

Acknowledgements	i
Abstract	iii
Contents	v
List of Figures	ix
Acronyms	xv
Notations	xvii
1 Introduction	1
1.1 State of the Art Communication Systems	1
1.1.1 Multiple Input Multiple Output - MIMO	2
1.1.2 Orthogonal Frequency Division Multiplexing - OFDM	3
1.1.3 Bit Interleaved Coded Modulation - BICM	3
1.2 Challenges for Future Wireless Systems	4
1.2.1 Interference	4
1.2.2 From Single-User MIMO to Multiuser MIMO	5
1.3 Major Themes in the Thesis	6
1.3.1 Low Complexity Detection for SU MIMO Systems . .	6
1.3.2 Feasibility of MU MIMO for Future Wireless Systems	7
1.3.3 Interference Handling	8
1.4 Thesis Outline and Contributions	9
I Single User MIMO	15
2 Low Complexity Detection in BICM SISO System	17
2.1 Introduction	17
2.1.1 Contribution	18
2.1.2 Organization	18
2.2 System Model	19
2.3 Simplified Bit Metrics	21

2.3.1	QPSK	23
2.3.2	QAM16	23
2.3.3	QAM64	25
2.4	Simulation Results	29
2.5	Conclusions	29
3	Low Complexity Detection in BICM MIMO Systems	31
3.1	Introduction	31
3.1.1	The state of the Art	33
3.1.2	Contribution	34
3.1.3	Organization	35
3.2	System Model	35
3.3	An Information Theoretic View	37
3.4	State of the Art Detection Schemes	42
3.4.1	Linear MMSE Detector for SIC	42
3.4.2	Linear MMSE Detector for PIC	44
3.4.3	PEP Analysis	44
3.5	Proposed Low Complexity MF Based Detection Schemes	45
3.5.1	First Approach - Dual Stream Scenario	45
3.5.2	Second Approach - General Scenario	47
3.5.3	PEP Analysis	50
3.6	Dual Stream Broadcast Strategy	50
3.7	Extension to Higher Dimensions	52
3.7.1	Fast Fading Channel	52
3.7.2	Slow Fading Channels	53
3.8	Simulations	53
3.9	Conclusions	59
3.A	Mutual Information for Dual Stream Scenario	59
3.B	Low Complexity Bit Metrics	60
3.B.1	QPSK-QPSK	61
3.B.2	QAM16-QAM16	61
3.B.3	QAM64-QAM64	63
3.B.4	QAM16-QPSK	63
3.C	PEP Analysis of MMSE Detector	64
3.D	PEP Analysis of the MF Based Detector	68
3.E	$P(\hat{x}_{2,k} \neq x_{2,k})$	71

II	Interference Suppression	73
4	Interference Suppression in Future Cellular Systems	75
4.1	Introduction	75
4.1.1	The state of the Art	76
4.1.2	Contribution	77
4.1.3	Organization	78
4.2	System Model	79
4.2.1	Spatial Correlation Model	80
4.2.2	Correlation Structure	82
4.3	An Information Theoretic View	83
4.4	PEP Analysis	85
4.4.1	Low Complexity MF Based Detector	86
4.4.2	MMSE Detector	87
4.5	Simulation Results	87
4.6	Novel Fractional Frequency Reuse Scheme	94
4.7	Conclusions	100
4.A	Mutual Information for Discrete Alphabets	101
4.B	PEP Analysis of MF Based Detector	103
4.C	PEP Analysis of MMSE Detector	107
4.D	$P(\hat{x}_{2,k} \neq x_{2,k})$	108
III	Multuser MIMO	111
5	Making Multuser MIMO Work for LTE	113
5.1	Introduction	113
5.1.1	The State of the Art	114
5.1.2	Motivation	115
5.1.3	Contribution	115
5.1.4	Organization	116
5.2	LTE System Model	116
5.2.1	LTE - A Brief Overview	116
5.2.2	System Model	119
5.3	MU MIMO Mode	120
5.3.1	Single Antenna UEs	120
5.3.2	Dual Antenna UEs	129
5.4	Performance Analysis	131
5.5	Simulation Results	131
5.6	Conclusion	136

5.A	Mutual Information for Finite Alphabets	138
5.B	Near Optimal Linear Precoder	140
5.C	Diversity Analysis of EGT in SU MIMO	143
6	Conclusions and Future Perspectives	149
6.1	Conclusions	149
6.2	Future Perspectives	151
	Appendices	153
A	Summary of the Thesis in French	155
A.1	Abstract en Français	155
A.2	Introduction	156
A.2.1	Interférence	156
A.2.2	De Single-User MIMO à Multiuser MIMO	157
A.3	Contributions et cadre de cette thèse	158
A.4	Chapitre 2 - Détection de faible complexité dans le système SISO BICM	158
A.4.1	Modèle de Système	159
A.4.2	Métriques de Complexité Faible	160
A.5	Chapitre 3 - La détection de faible complexité dans les systèmes MIMO BICM	161
A.5.1	Modèle de Système	163
A.5.2	MF détecteur de faible complexité	163
A.6	Chapitre 4 - Suppression des interférences dans les futurs systèmes cellulaires	165
A.6.1	Modèle de Système	167
A.6.2	Analyse de l'information mutuelle	167
A.6.3	Suppression d'Interférence	169
A.6.4	Novel FFR	169
A.6.5	Chapitre 5 - MIMO multi-utilisateurs (MU MIMO) pour LTE	172
A.6.6	Modèle de Système	173
A.6.7	Stratégie de précodage at alignement géométrique d'interférence	173
A.6.8	Résultats de la simulation	175
	Bibliography	177

List of Figures

2.1	Block diagram of the transmitter. π indicates the interleaver while μ and χ indicate the labeling map and the constellation respectively.	19
2.2	Normalized constellations of QPSK, QAM16 and QAM64 with Gray mapping.	22
2.3	Metric for the first bit of QAM16. (a) shows 3 regions for the LLR where (b) shows the exact and approximated bit metric. In (b), continuous line indicates the exact bit metric while the dashed line indicates the approximated bit metric. Note that $ h $ and σ are taken as 1.	24
2.4	Metric for the first bit of QAM64. (a) shows 7 regions for the LLR where (b) shows the exact and the approximated bit metric.	27
2.5	Metric for the second bit of QAM64. (a) shows 3 regions for the LLR where (b) shows the exact and the approximated bit metric.	28
2.6	SISO System using punctured rate 1/2 turbo code of 3GPP LTE. Decoding iterations are 5.	30
3.1	Block diagram of the transmitter of dual stream BICM MIMO OFDM system. π_1 denotes the random interleaver, μ_1 the labeling map and χ_1 the signal set for the first stream.	35
3.2	Block diagram of the SIC receiver of dual stream BICM MIMO OFDM system.	37
3.3	Capacity of the dual stream system for Gaussian alphabets once the channel is known at the receiver. Both streams have equal power i.e. $\sigma_1^2 = \sigma_2^2$ in (3.3) and (3.4). Note that SNR is $(\sigma_1^2 + \sigma_2^2)/N_0$	38

3.4	Capacity of the 2×2 and 3×3 systems for Gaussian alphabets once the channel is known at the receiver. There are two scenarios of equal power with nonuniform rate distribution between the streams and equal rate with nonuniform power distribution between the streams. Note that for the case of equal power with nonuniform rate distribution for 2×2 system, $\sigma_1^2 = \sigma_2^2$ where for the case of equal rate with nonuniform power distribution, total power is optimally divided in σ_1^2 and σ_2^2 to equate $I(\mathbf{Y}; X_1 \mathbf{H})$ and $I(\mathbf{Y}; X_2 X_1, \mathbf{H})$. This optimal power distribution is shown in the next figure.	39
3.5	Optimized power distribution between the spatial streams. The objective is to equate their rates at each SNR value. Total power is normalized to 1.	40
3.6	Capacity of the first stream in the dual stream scenario for finite size alphabets once the channel is known at the receiver. Both the streams have equal power. Note that SNR includes the power of both the streams.	41
3.7	Capacity of the second stream in the dual stream scenario for finite size alphabets once the channel is known at the receiver. First stream has already been stripped off.	41
3.8	Performance of the first stream in 2×2 system. The channel is fast fading. Continuous lines indicate low complexity MF based detector while dashed lines indicate MMSE detector. Fig.(a) uses convolutional code while Fig.(b) employs 3GPP LTE turbo code.	55
3.9	2×2 and 3×3 systems with uniform rate and nonuniform power spatial streams. The channel is fast fading while convolutional code is used. Fig.(a) shows the performance in 2×2 system while Fig.(b) shows the performance in 3×3 system.	57
3.10	4×4 MIMO system with four spatial streams using QPSK. The channel is slow fading. Fig.(a) uses convolutional code while Fig.(b) employs 3GPP LTE turbo code.	58
4.1	Interference in single frequency reuse cellular network. x_1 is the desired signal while x_2 is the interfering signal.	79

4.2	Effect of the rate of interference stream x_2 on the mutual information of the desired stream x_1 . Interference strength is of the same strength as the desired stream, i.e. $\sigma_2^2/\sigma_1^2 = 1$. Random interference refers to the case once interference is not static but changes randomly between QPSK, QAM16 and QAM64.	83
4.3	Effect of the strength of interference stream x_2 on the mutual information of the desired stream x_1 . SNR is 4.5 dB for x_1 =QPSK, 11 dB for x_1 =QAM16 and 13 dB for x_1 =QAM64	85
4.4	Effect of the strength and the rate of interference stream x_2 on the detection of desired stream x_1 . Continuous lines indicate low complexity MF based detection while dashed lines indicate linear MMSE detection. In Fig.(a), x_1 is QAM16, SNR is 11 dB while 64-state, rate 1/2 convolutional code is used. In Fig.(b), x_1 is QAM64, SNR is 13 dB while LTE turbo code (rate 1/2) is used.	89
4.5	Blind detection and random interference. Random interference indicates that interference is randomly generated from all three constellations.	91
4.6	Effect of receive correlation. x_1 is QAM16 in (a) and QAM64 in (b).	92
4.7	Effect of transmit and receive correlation. Desired stream x_1 is QAM16 while interference stream x_2 is QPSK. Settings are same as in Fig. 4.6.	93
4.8	FFR in LTE. Frequency reuse factor for cell edge users is 3. .	94
4.9	Proposed FFR in LTE. Only one interference is ensured in the worst case scenario. Frequency reuse factor for cell edge users is 1.5.	95
4.10	Two ways of subcarrier assignment to the cell edge users. Blue users are high data rate while red users are low data rate users. Left figure shows the case of uniform rate streams while right figure shows the case of nonuniform rate streams.	96
4.11	Required SNR for the desired stream x_1 for different constellations of interference x_2 for the target FER of 10^{-2}	97

4.12	Optimizing required SNRs to achieve the desired FER on both streams. Continuous lines indicate the required SNRs to achieve the desired FER both for x_1 and x_2 while dashed line indicates the corresponding SNR of x_2 for the required SNR of x_1 for that particular value of σ_2^2/σ_1^2 . Dashed-dotted line indicates the point where both streams achieve the desired FER of 10^{-2} with minimum SNRs	99
5.1	Geometric alignment of interference. (a) shows the original channel from the eNodeB to the UE while (b) shows the effective channel of the desired signal while (c) shows the effective channel of the interference.	122
5.2	Sum rates of different precoding strategies. The eNodeB has two antennas while we consider two single antenna UEs. Both the UEs belong to QPSK constellations.	128
5.3	MU MIMO mode in LTE. Downlink fast fading channel with $n_t = 2$ and 2 single antenna UEs. 3GPP LTE rate 1/3 turbo code is used with different puncturing patterns.	133
5.4	MU MIMO mode in LTE. Downlink fast fading channel with eNodeB with 2 antennas and 2 dual antenna UEs. 3GPP LTE rate 1/3 turbo code is used with different puncturing patterns.	134
5.5	Interference sensitivity for MU MIMO mode in LTE. Three sets of simulations are shown. QPSK-QPSK indicates that both x_1 and x_2 both QPSK. 'Interference Actual' implies the case once UE knows the constellation of interference (x_2).	135
5.6	Diversity in SU and MU MIMO modes. Downlink slow fading channel (one channel realization per codeword) with $n_t = 2$ and 2 single antenna UEs. 3GPP LTE rate 1/3 turbo code is used with different puncturing patterns.	137
A.1	Schéma de l'émetteur. π indique l'entrelaceur alors que μ et χ indiquent la carte d'étiquetage et de la constellation, respectivement.	159
A.2	Schéma de l'émetteur de flux système dual BICM MIMO OFDM. π_1 désigne l'entrelaceur aléatoire pour le premier flux.	163
A.3	Intérférence dans un réseau cellulaire. x_1 est le signal désiré alors que x_2 est le signal d'interférence.	167

A.4	Effet du taux de flux d'interférence x_2 sur l'information mutuelle du flux désiré x_1 . Les interférences sont la force de la même force que le flux désiré, soit $\sigma_2^2/\sigma_1^2 = 1$. Interférences hasard fait référence à l'affaire une fois l'interférence n'est pas statique, mais change de manière aléatoire entre QPSK, QAM16 et QAM64.	168
A.5	Comparaison de suppression d'interférence et d'atténuation d'interférence.	170
A.6	FFR dans LTE. Facteur de réutilisation de fréquence pour les utilisateurs de bord de la cellule est de 3.	171
A.7	FFR Proposé en LTE. Une seule interférence est assurée dans le pire des cas. Facteur de réutilisation de fréquence pour les utilisateurs de bord de la cellule est de 1,5.	171
A.8	Alignement géométrique d'interférence. (a) montre la canal originale de la eNodeB à l'UE tandis que (b) montre le canal efficace du signal désiré while (c) montre le canal efficace de l'interférence.	175
A.9	MU MIMO mode en LTE	176

Acronyms

Here are the main acronyms used in this document. The meaning of an acronym is usually indicated once, when it first appears in the text.

3GPP	Third Generation Partnership Project
AWGN	Additive White Gaussian Noise
BICM	Bit Interleaved Coded Modulation
BICM-ID	Bit Interleaved Coded Modulation Iterative Decoding
BS	Base Station
CI	Channel Inversion
CP	Cyclic Prefix
CQI	Channel Quality Indicator
CSI	Channel State Information
CSIR	Channel State Information at the Receiver
CSIT	Channel State Information at the Transmitter
DFE	Decision Feedback Equalizer
DOF	Degrees of Freedom
DPC	Dirty Paper Coding
DVB	Digital Video Broadcast
EGT	Equal Gain Transmission
FDD	Frequency-Division Duplex
FFT	Fast Fourier Transform
HDTV	High Definition TV
ICI	Intercarrier Interference
IDFT	Inverse Discrete Fourier Transform
IFFT	Inverse Fast Fourier Transform
iid	Independent and Identically Distributed
ISI	Intersymbol Interference
LAN	Local Area Network
LDPC	Low-Density Parity-Check

LLR	Log-likelihood Ratio
LR	Lattice Reduction
LTE	Long Term Evolution
MAC	Multiple Access Channel
MAP	Maximum a Posteriori Probability
MGF	Moment Generating Function
MIMO	Multiple Input Multiple Output
MISO	Multiple Input Single Output
ML	Maximum Likelihood
MLC	Multilevel Code
MMSE	Minimum Mean Square Error
MRC	Maximum Ratio Combining
MS	Mobile Station
MSE	Mean Square Error
MU	Multiuser
PDF	Probability Density Function
PEP	Pairwise Error Probability
PIC	Parallel Interference Cancellation
QAM	Quadrature Amplitude Modulation
OFDM	Orthogonal Frequency Division Multiplexing
OFDMA	Orthogonal Frequency Division Multiplexing Access
QoS	Quality of Service
QPSK	Quadrature Phase-Shift Keying
RCI	Regularized Channel Inversion
RF	Radio-Frequency
SDTV	Standard definition TV
SIC	Successive Interference Cancellation
SIMO	Single Input Multiple Output
SINR	Signal to Interference and Noise Ratio
SISO	Single Input Single Output
SNR	Signal to Noise Ratio
STC	Space Time Coding
SU	Single-user
TDD	Time Division Duplex
THP	Tomlinson-Harashima precoding
UE	User Equipment
UEP	Unequal Error Protection
w.r.t.	with respect to
ZF	Zero Forcing

Notations

Here is a list of main operators and symbols used in this document. For vectors and matrices, the dimensions are frequently indicated when they appear in the text. We have tried to keep the notation consistent throughout the thesis, but rarely symbols have different definitions in different chapters and in that case they are defined very explicitly to avoid any confusion.

x or X	Scalar
\mathbf{x}	Vector
\mathbf{X}	Matrix
$h, \mathbf{h}, \mathbf{H}$	Channel (scalar, vector, matrix)
$z, \mathbf{z}, \mathbf{Z}$	Noise (scalar, vector, matrix)
$y, \mathbf{y}, \mathbf{Y}$	Received signal (scalar, vector, matrix)
$(\cdot)^*$	Conjugate operation
$(\cdot)^T$	Transpose operation
$(\cdot)^\dagger$	Hermitian operation
$(\cdot)_R$	Real part of a complex number
$(\cdot)_I$	Imaginary part of a complex number
$ x $	Absolute value of scalar
$\ \mathbf{x}\ $	Euclidean norm of vector
$Q(y)$	Gaussian Q-function i.e. $\frac{1}{\sqrt{2\pi}} \int_y^\infty e^{-x^2/2} dx$
$E(\cdot)$	Mathematical expectation
$\mathbf{A}_{M \times N}$	Matrix \mathbf{A} with M rows and N columns
$\mathbf{A}(i, j)$	Entry at the i -th row and j -th column of matrix \mathbf{A}
$\lambda_i(\mathbf{A})$	i -th eigenvalue of the matrix \mathbf{A}
$\text{vec}(\mathbf{A})$	Vectorization operator which stacks the columns of matrix \mathbf{A}
\mathbf{I}_n	$n \times n$ identity matrix
μ	Labeling map
\otimes	Kronecker product
\rightarrow	Quantization process

\bar{y}	Matched filter output of the received signal y
\mathcal{CN}	Complex Normal Distribution
\mathcal{C}	Complex space
\mathbb{C}^M	M -dimensional complex space
$\mathcal{H}(\cdot)$	$= -E \log p(\cdot)$ Entropy of the argument
\log	All logarithms are to the base 2
$I(\cdot; \cdot)$	Mutual information between the two arguments
n_t	Number of transmit antennas
n_r	Number of receive antennas
P_T	Transmit power constraint
χ	Constellation
$x \in \chi_b^i$	Subset of the signal set $x \in \chi$ whose labels have the value $b \in \{0, 1\}$ in the position i
M_1	$ \chi_1 $ i.e. cardinality of the constellation χ_1
M_2	$ \chi_2 $ i.e. cardinality of the constellation χ_2

Chapter 1

Introduction

Wireless communications is a rapidly growing segment of the communications industry, with the potential to provide high-speed and high-quality information exchange between countless and diverse gadgets. Potential applications enabled by this technology include multimedia internet-enabled cell phones, smart homes and appliances, automated highway systems, video teleconferencing, distance learning, and autonomous sensor networks. However, supporting these applications on wireless medium poses a significant technical challenge which has led to a flurry of research in wireless communication systems.

1.1 State of the Art Communication Systems

The major challenges in the design of future wireless communication systems are increased spectral efficiency and improved link reliability. A significant challenge in the pursuit of these objectives is the wireless channel which constitutes a hostile propagation medium as it suffers from frequency selectivity (caused by the multipath effects), fading (caused by the destructive addition of multipath components) and interference from other users.

To combat the frequency selectivity of the wireless channel, orthogonal frequency division multiplexing (OFDM) is considered a feasible option while to combat the inherent fading of the wireless channel, bit interleaved coded modulation (BICM) is considered a suitable choice. Since last decade,

research has focused on appending the spatial dimension to the communication systems in order to augment the classical communication resources of power and bandwidth. Multiple antennas at both the transmitter and the receiver play a significant role not only to enhance the spectral efficiency but also to increase the reliability of the wireless communication. Therefore a particularly promising candidate for next-generation fixed and mobile wireless systems is multiple input multiple output (MIMO) technology combined with OFDM and BICM. Recently the standardization of almost all the upcoming wireless standards have converged to these technologies which are briefly discussed below.

1.1.1 Multiple Input Multiple Output - MIMO

For a long time, power and bandwidth were treated as the classical communication resources hence time and frequency were the only available dimensions for user or data multiplexing until the discovery of a new spatial communication dimension. This dimension emerges when multiple antennas are employed both at the transmitting side and at the receiving side of a communication link. The proper exploitation of these extra spatial degrees of freedom brought by the use of multiple antennas promises huge gains without any extra investment of the classical communication resources [1] [2]. This spatial dimension can be used to get one or more of the following benefits depending upon the system/application requirements: a higher spectral efficiency, an increase in the communication reliability and spatial separation of the users. In cellular communications, these benefits of MIMO are particularly interesting for the downlink communication as compared to the uplink communication and the benefit of higher spectral efficiency is more attractive as compared to the advantage of reliability. This is indebted to the asymmetric nature of the predominant data traffic as compared to the symmetric nature of voice traffic. Enhanced spectral efficiency can be realized by multi-stream transmission which divides the incoming data into multiple parallel substreams and transmits each on a different spatial dimension (e.g. a different antenna). As long as there are at least as many (sufficiently spaced) receive antennas as the transmitted streams, multi-stream transmission increases the capacity linearly with the number of streams, i.e. if there are n_t transmit antennas at the base station (BS) and n_r receive antennas at the user (this system is generally termed as single-user MIMO), then the multiplexing gain of the system is $\min(n_t, n_r)$. Note that the presence of multiple antennas only at one end of the communication link may provide diversity/power/array gain or a combination thereof but not multiplexing

gain.

1.1.2 Orthogonal Frequency Division Multiplexing - OFDM

Recently, a worldwide convergence has occurred for the use of OFDM as an emerging technology for high data rates in wireless communications. The underlying reasons for this trend are the efficiency of OFDM to combat intersymbol interference (ISI) and its effectiveness as a multiple access scheme. In particular, many wireless standards (Wi-Max, Wireless LAN, LTE, LTE-Advanced, DVB, HDTV) have adopted the OFDM technology which is a particular form of multi-carrier transmission suited for wideband transmission. This transmission technique transforms a frequency selective wideband channel into a group of non-selective narrowband channels, which makes it robust against large delay spreads by preserving orthogonality in the frequency domain. Moreover, the ingenious introduction of cyclic redundancy at the transmitter reduces the complexity to only FFT processing and one tap scalar equalization at the receiver. The key idea of OFDM transmission is to make the symbol period longer with respect to the delay spread of the channel. In the frequency domain this can be viewed as the system bandwidth being split into a number of subcarriers, each featuring a bandwidth smaller than the system's coherence bandwidth. While the smaller bandwidth of the subcarrier and the resulting large OFDM symbol time reduces the effect of ISI, the orthogonality among the subcarriers mitigates the inter-carrier interference (ICI).

1.1.3 Bit Interleaved Coded Modulation - BICM

Modern wireless communication systems transmitting at high data rates need robust coding schemes for the reliability of the transmission and an appropriate solution in today's wireless world is BICM. Zehavi [3] and Caire [4] realized that the code diversity and therefore the reliability of coded modulation over a Rayleigh channel could be improved by using bit wise interleaving after the encoder rather than using symbol wise interleaving after the modulator. The order of diversity for any coded system with a symbol interleaver is the minimum number of distinct symbols between the codewords. Preventing parallel transitions (trellis based) and increasing the constraint length of the code are the only ways of increasing the code diversity. However, bit-wise interleaving results in the diversity dictated by the smallest number of distinct bits, rather than channel symbols, along any error event.

MIMO because of its enhanced spectral efficiency and reliability, OFDM due to its low complexity equalization and proficient multiplexing while BICM for the reason of its improved code diversity over fast fading channels, are all making their ways into the future and currently standardized wireless communication systems such as third generation partnership project (3GPP) long term evolution (LTE) [5], LTE-Advanced [6], IEEE 802.11n (Wireless LAN) [7] and IEEE 802.16m (WiMax) [8].

1.2 Challenges for Future Wireless Systems

Though current and ongoing wireless standardizations have converged to several state of the art technologies in the pursuit of higher data rates and enhanced quality of service (QoS), they still face many daunting challenges. The most significant challenge is the interference which affects the reusability of the spectrum and is therefore inherent in the high data rate communication systems. Another challenge emerges from the hardware constraints which restrict the implementation of sophisticated transceiver algorithms and necessitate low complexity solutions. One example is the difficulty of achieving requisite antenna spacing in the mobile handsets which severely limits the promised gains of MIMO systems. It has led to another application of the spatial dimension in terms of spatial separation of the users, i.e. multiuser (MU) MIMO. However, the efficient employment of MU MIMO due to the constraint of extensive feedback is not yet perceived in future wireless systems as 3GPP LTE [9]. We discuss some of these challenges in the following paragraphs.

1.2.1 Interference

In addition to the incorporation of spatial dimension in the pursuit of higher spectral efficiency, reusability of spectral resources will also play an important role in future wireless communication systems. Where complexity is the challenge in the integration of spatial dimension, interference restricts the spectrum reusability (e.g. tight frequency reuse). Interference handling can be broadly divided into five categories as avoidance, containment, rejection, coordination and exploitation. Interference avoidance refers to its orthogonalization (time, frequency, space, codes) which is based on the spatial reuse partitioning, i.e. preventing the reuse of any spectral resources within a certain cluster of cells. This approach leads to an *a priori* loss of degrees of freedom, no matter how weak the potential interference is. Interference containment refers to the strategies of leaking just enough interference to

meet a desired quality of service (QoS) constraint. Interference rejection implies advanced receiver processing based on beamforming in the spatial domain. Different rejection techniques have been proved to be instrumental in mitigating the detrimental interference by its cancellation or attenuation. Another area of interference handling is coordination and cooperation [10] which is a softer approach to reduce interference, i.e. non-zero interference is leaked from the transmitter but the level or dimension of the interference can be reduced by coordinating resource allocation, soft handover, interference alignment etc. This approach extends to the concept of Network MIMO [11] [12] (where neighboring BSs are connected to form an antenna array) which demands sharing of CSI and user data among the BSs thereby requiring tremendous backhaul capacity. Another category is interference suppression or exploitation where the interference structure is exploited at the receiver in mitigating its effects. Recently, the focus has shifted on how to intelligently exploit the knowledge and/or structure of the interference to achieve improved reliability and throughput in the wireless communication systems.

1.2.2 From Single-User MIMO to Multiuser MIMO

The spatial communication dimension emerges when multiple antennas are used at both ends of a transmission link. However, the exceptional benefits of SU MIMO are limited by the prerequisite of having independent channels between transmitting and receiving antennas, a requirement which is challenging to realize because of closely spaced antennas on the handset. Nevertheless, this spatial dimension also kicks in when there are multiple users (links) in the system. For the capacity growth to be linear with the number of streams, the restriction of the availability of “at least as many (sufficiently spaced) receive antennas as the transmitted streams” in SU MIMO systems relaxes to the availability of “at least as many single antenna users as the transmitted streams” in MU MIMO systems [13]. Therefore in MU MIMO communication system where a BS equipped with n_t antennas is communicating with n_r single-antenna users, the spectral efficiency gains of the order of $\min(n_t, n_r)$ are achievable as compared to a SISO system operating over the same amount of classical communication resources. In addition to providing user multiplexing and stream multiplexing, MU MIMO is also characterized by the selection possibility over surplus number of users, a gain coined as MU diversity [14].

1.3 Major Themes in the Thesis

The gains of MIMO proliferate with the expansion in the dimensionality of the system and so is the complexity. Thus the main challenge in a practical communication system is to choose the dimensionality of the system, for which the baseband algorithms can be implemented in the existing hardware. The intricacy of realizing the requisite antenna spacing of half the wavelength in the mobile handset combined with the added complexity of separate radio-frequency (RF) chains for each antenna and the corresponding cost considerations shall be restricting future MIMO wireless systems to lower dimensionality (especially in the number of receive antennas for the downlink channel). The maximum number of spatial streams being restricted to four in 3GPP LTE [5] and WiMax [8] substantiate this proposition. Therefore our focus in this thesis is on the low dimensional BICM MIMO OFDM systems. For these systems, we look at the low complexity detection in SU systems, interference suppression in cellular systems and the feasibility of MU MIMO in future wireless systems.

1.3.1 Low Complexity Detection for SU MIMO Systems

In the pursuit of higher spectral efficiency, rate oriented schemes as multi-stream transmission are getting more attention in the next generation wireless systems. In these transmission schemes, each spatial layer is independently encoded and interleaved before being transmitted. Shamaï [15] termed the approach of single code layer at each transmit antenna as *MAC-outage approach*. The reception is consequently based on successive interference cancellation (SIC), i.e. sequential decoding and subtraction (stripping) of spatial streams which introduces unequal error protection (UEP). This reception is plagued with the increased detection complexity which is exponential in the number of spatial streams and polynomial in the size of the constellation. Therefore the maximum likelihood (ML) detection in such systems is NP-hard [16] which implies that there are no known efficient (i.e. polynomial-time) solutions. A preprocessing technique to reduce the complexity is lattice reduction (LR) [17] [18], however, finding a new basis for each channel realization is itself a computationally intensive operation. Another alternative is Sphere Decoder of Fincke and Pohst [19] which is still characterized by exponential complexity in the worst case scenario. Naive suboptimal solutions, like linear minimum mean square error (MMSE) [20] and zero forcing (ZF) [21], in general work poorly as compared to the ML detectors especially at lower signal to noise ratios (SNRs) for low dimensional

systems. The degradation of the performance due to the sub-optimality combined with the complexity in the calculation of linear equalizers at each frequency tone (in OFDM based system) renders the real-time implementation of these algorithms challenging especially in the fast fading wideband environments. For the incorporation of MIMO technology in modern wireless systems, there is a dire need to develop low complexity detectors with improved performance which can be implemented in the existing hardware. It should be noted that the detector we refer to in this thesis (as in [22] and [23]) is a demodulator, rather than a full sequence detector.

1.3.2 Feasibility of MU MIMO for Future Wireless Systems

To offset the impediment of less number of sufficiently spaced receive antennas on the handsets (users), the spatial dimension is exploited in terms of spatial separation of the users, i.e. precoding in the downlink of MU cellular system, where spatial resources can be used to transmit data to multiple users simultaneously. Optimal precoding in MU MIMO Gaussian broadcast channel involves a theoretical pre-interference subtraction technique known as dirty paper coding (DPC) [24] combined with an implicit user scheduling and power loading algorithm. Amongst the linear precoding schemes, interference cancellation based schemes as channel inversion (CI) [21] and interference attenuation based schemes as regularized channel inversion (RCI) [25] are the focus of attention. These precoding strategies strive to transform the cross-coupled channels into parallel non interacting channels by pre-subtracting, canceling or attenuating the interference therefore leading to simplified receiver structures. However, they are void of exploiting the interference structure in mitigating its effects. This evasion is evident as these precoding strategies are based on the unrealistic Gaussian assumption for the interference which therefore encompasses no structure to be exploited. In practical systems, inputs must be drawn from discrete constellations (often with very limited peak-to-average power ratios) which may significantly depart from the Gaussian idealization.

Furthermore, above mentioned precoding strategies necessitate full channel state information at the transmitter (CSIT). It's acquisition in time division duplex (TDD) system and frequency division duplex (FDD) system is indebted to reciprocity in the former case and a dedicated feedback channel in the latter case. Full acquisition of the CSIT in a practical system is far from realizable. How much channel state information is available at the transmitter may limit the gains due to MU MIMO techniques. It has led to the precoding schemes based on partial CSIT or quantized CSIT [26]. For

MU MIMO mode, 3GPP LTE has focused on a low resolution precoder codebook [5] which is based on the principle of equal gain transmission (EGT). The efficient employment of these precoders for MU MIMO mode is not yet fully understood. This has led to the common perception that MU MIMO is not workable in LTE as is stated in [9] (page 244)

“Single-user MIMO techniques dominate the algorithms selected for LTE, with multiuser MIMO not being used to the maximum extent in the first version of LTE, despite its potential”

It was also shown in [27] that SU MIMO mode performs better than MU MIMO mode in LTE once the channel has no spatial correlation though MU MIMO gets benefit from the enhanced transmit correlation. So the uncertainty about the feasibility of MU MIMO in future wireless systems dominates ongoing standardizations. There is a need to devise strategies so that future wireless systems as LTE can exploit the advantages of MU MIMO in the presence of partial CSIT.

1.3.3 Interference Handling

To achieve higher spectral efficiency, frequency resources will be aggressively utilized in the future wireless systems thereby leading to interference limited systems. Interference avoidance and containment strategies which restrict the reusability of the spectral resources will not be feasible in these systems. On the other hand, the requisite of large backhaul capacity and intricacy in the synchronization shall restrict the role of coordination and cooperation strategies for interference mitigation. Therefore focus of the future systems shall be on the interference rejection and exploitation strategies.

Optimal strategy for treating the interference in the regime of very strong [28] (subtractive cancellation) and very weak interference (Gaussian assumption) is well known but if the interference is in the moderate region, no optimal strategy is known though it was shown in [29] that partial decoding of interference can significantly improve the performance. Handover algorithms impede the interferences to be strong in cellular scenario while weak interferences are merged in the noise. However, one or two dominant interferences (moderate regime) from the neighboring cells limit the capacity of the desired streams of the cell edge users. How to effectively handle these interferences is still an open question. Gaussian assumption for this moderate interference leads to a significant degradation in the performance while subtractive cancellation is plagued with the dilemma of error propagation. Moreover, signaling constraints for subtractive cancellation makes this approach unfeasible for future wireless systems. In this scenario, interference

rejection and exploitation strategies can be employed. Interference rejection techniques are based on interference cancellation or attenuation by exploiting the spatial dimension in the form of linear detectors as MMSE and ZF. The shortcoming of noise enhancement for the ill conditioned channels in the case of ZF detector instigates MMSE detector as the likely candidate for an interference limited system [30]. However, MMSE detection being based on interference attenuation is void of exploiting the interference structure in mitigating its effects. Moreover, Gaussian assumption of the post detection interference in MMSE is valid for asymptotic cases (large number of interferers) [31] but the fidelity of this approximation in a lower dimensional system is questionable. There is a dire need not only to study the effects of moderate interferences on the cell edge users but also to develop low complexity algorithms for the exploitation of these interferences. Frequency reuse schemes need to be defined in a way that with the enhancement of spectral efficiency, the ensuing interferences can be effectively handled thereby not degrading the system performance.

1.4 Thesis Outline and Contributions

We have generally focused in this thesis on the practical low dimensional MIMO systems. The research work conducted in this thesis can be divided in three different parts. Part I deals with the transmission and detection techniques in SU MIMO systems, part II focuses on the interference suppression in cellular systems while part III considers precoding in MU MIMO systems. Part I, comprising chapters 2 and 3, focuses on the low complexity detection in OFDM based BICM SISO and MIMO systems. Part II, comprising chapter 4 alone is the analysis of interference suppression where a novel fractional frequency reuse scheme is proposed. Part III, consisting of chapter 5 focuses on the precoding for MU MIMO with specific reference to 3GPP LTE. In the following paragraphs, we give a brief overview of the dissertation and describe the contributions on a per chapter basis.

Chapter 2 - Low Complexity Detection in BICM SISO System

In this chapter, we consider soft detection in BICM SISO OFDM system. ML computation of these soft decisions (log-likelihood ratios - LLRs) involve the summation of a number of terms exponential in the number of bits per modulation symbol. We show that these ML soft decision bit metrics can be significantly simplified to a scaled version of the matched filter (MF) output. This simplification is aided by the decoupling of real and imaginary parts of

the metric. The complexity is maintained at almost the same level for all constellations and the resulting metrics being based on the MF outputs are suitable for implementation in the hardware. This result has been published in:

- Rizwan Ghaffar and Raymond Knopp, “Low Complexity Metrics for BICM SISO and MIMO systems”, *Proceedings of IEEE 71-st Vehicular Technology Conference, VTC-Spring 2010*, Taipei, May, 2010.

Chapter 3 - Low Complexity Detection in BICM MIMO Systems

A dual stream BICM MIMO OFDM system is considered in this chapter. We propose a low complexity MF based near ML detector for SIC detection which successfully reduces one complex dimension of the MIMO system. The proposed detector therefore escapes the exponential complexity of MIMO detection for the considered dual stream system. We further carry out the performance analysis of the proposed detector and show that this detector has full diversity while MMSE detector loses one diversity order. We then extend low complexity detection to higher-dimensional systems by focusing on the uniform rate, nonuniform power distribution and uniform power, nonuniform rate distribution between the spatial streams.

The work in this chapter has been published in:

- Rizwan Ghaffar and Raymond Knopp, “Low complexity BICM demodulation for MIMO transmission”, *Proceedings of 9th IEEE Workshop on Signal Processing Advances for Wireless Communications, SPAWC 2008*, Recife, July, 2008.
- Rizwan Ghaffar and Raymond Knopp, “Low Complexity Soft Detection for Spatially Multiplexed BICM MIMO OFDM System”, *Proceedings of 10th IEEE Workshop on Signal Processing Advances for Wireless Communications, SPAWC 2009*, Perugia, June, 2009.
- Rizwan Ghaffar and Raymond Knopp, “Spatial Interference Cancellation and Pairwise Error Probability Analysis”, *Proceedings of IEEE International Conference on Communications, ICC 2009*, Dresden, June, 2009.

- Rizwan Ghaffar and Raymond Knopp, “Performance Analysis of Low Complexity Soft Detection for BICM MIMO System”, *Proceedings of IEEE 7th Intl. Symposium on Wireless Communication Systems, ISWCS 2010*, York, Sep, 2010.
- Florian Kaltenberger, Rizwan Ghaffar, Raymond Knopp et. al. “Design and Implementation of a Single-Frequency Mesh Network Using OpenAirInterface”, *EURASIP Journal on Wireless Communications and Networking*, 2010.

Chapter 4 - Interference Suppression in Future Cellular Systems

In this chapter, we study interference suppression in the future single frequency reuse cellular systems. We focus on the cell edge users and propose the employment of the earlier proposed low complexity MF based detector for interference suppression. Unlike linear detectors which are based on the unrealistic assumption of Gaussianity for interference, this detector considers interference to be from discrete constellations and subsequently exploits the structure of this interference in mitigating its effects. In the sequel, we further study the effect of the rate and the strength of interference on coded pairwise error probability (PEP) of the proposed detector. For this analysis, we look at the more realistic case of spatially correlated channel. In addition to the earlier derived result of full diversity of the MF based low complexity detector, we show that this detector exhibits a coding gain (the horizontal shift of the BER curve) as either the interference gets stronger or its rate trims down. We further show that MMSE detection, being independent of the interfering constellation, suffers from a coding loss as the interference gets stronger which is evident as this detection scheme does not exploit the interference structure in the detection process. Based on the characteristic of effective exploitation of the lower rate interference by the proposed detector, we further propose a novel fractional frequency reuse (FFR) which is more spectrally and energy efficient than the traditional FFR strategies.

The work in this chapter has been published in:

- Rizwan Ghaffar and Raymond Knopp, “Interference Suppression for Next Generation Wireless Systems”, *Proceedings of IEEE 69-th Vehicular Technology Conference VTC-Spring 2009*, Barcelona, April, 2009.

- Rizwan Ghaffar and Raymond Knopp, “Spatial Interference Cancellation Algorithm”, *Proceedings of IEEE Wireless Communications and Networking Conference WCNC 2009*, Budapest, April, 2009.
- Rizwan Ghaffar and Raymond Knopp, “Analysis of low complexity max log MAP detector and MMSE detector for Interference Suppression in Correlated Fading”, *Proceedings of IEEE Global Communications Conference, Globecom 2009*, Hawaii, Dec, 2009.
- Rizwan Ghaffar and Raymond Knopp, “Fractional Frequency Reuse and Interference Suppression for OFDMA Networks”, *Proceedings of IEEE 8th Intl. Symposium on Modeling and Optimization in Mobile, Ad Hoc, and Wireless Networks (WiOpt 2010)*, Avignon, June, 2010.

and submitted as:

- Rizwan Ghaffar and Raymond Knopp, “Interference Suppression for future wireless systems”, *IEEE transactions on wireless communications*.

The work in chapter 3 and chapter 4 has also been published in the form of a book chapter as

- Rizwan Ghaffar and Raymond Knopp, “Low dimensional MIMO systems with finite sized constellation inputs” *Radio Communications*, Alessandro Bazzi (Ed.), ISBN: 978-953-307-091-9, IN-TECH, April 2010

Chapter 5 - Making Multiuser MIMO work for LTE

The feasibility of MU MIMO for LTE is the subject investigated in this chapter for which the effectiveness of the low resolution LTE precoders is analyzed. We propose a precoding strategy based on the LTE precoders which encompasses geometrical interference alignment at the eNodeB (LTE notation for the BS) followed by the exploitation of the residual interference structure by the user equipment (UE). On one hand, this strategy relegates the interference seen by each UE by a geometric scheduling algorithm while on the other hand, UEs exploit the structure of residual interference by low complexity detectors. However, the prerequisite of this detection strategy

is the knowledge of the interference constellation. Downlink control information (DCI) formats in 3GPP LTE [32] do not allow the transmission of this information to the UE. Consequently we also look at the sensitivity of this detection scheme to the knowledge of the interfering constellation and propose a blind detector which is unaware of this information. However, the significance of this information motivates its consideration to be included in the ongoing standardization of LTE-Advanced [6]. We also propose in this chapter an algorithm for the employment of LTE precoders for SU MIMO mode. EGT being an important characteristic of LTE precoders, we look at the effects of this transmission strategy and show that EGT has full diversity in SU MIMO mode while it suffers from a loss of diversity in MU MIMO mode.

The work in this chapter has been published in:

- Rizwan Ghaffar and Raymond Knopp, “Channel Capacity for Linearly Precoded Multiuser MIMO for Discrete Constellations”, *Proceedings of IEEE 20-th International Symposium on Personal, Indoor and Mobile Radio Communications (PIMRC 2009)*, Tokyo, Sep, 2009.
- Rizwan Ghaffar and Raymond Knopp, “Linear Precoders for Multiuser MIMO for finite constellations and a simplified receiver structure under controlled interference”, *Proceedings of Asilomar Conference on Signals, Systems and Computers*, Pacific Grove, Nov, 2009.
- Rizwan Ghaffar and Raymond Knopp, “Near Optimal Linear Precoder for Multiuser MIMO for Discrete Alphabets”, *Proceedings of IEEE International Conference on Communications, ICC 2010*, Cape Town, June, 2010.
- Rizwan Ghaffar and Raymond Knopp, “Making Multiuser MIMO work for LTE”, *Proceedings of IEEE 21-st International Symposium on Personal, Indoor and Mobile Radio Communications (PIMRC 2010)*, Istanbul, Sep, 2010.
- Rizwan Ghaffar and Raymond Knopp, “Diversity Analysis of Equal Gain Transmission for Singleuser and Multiuser MIMO”, *Proceedings of IEEE Global Communications Conference, Globecom 2010*, Mi-

ami, Dec, 2010.

and being submitted to:

- Rizwan Ghaffar, Raymond Knopp et. al., “MU MIMO in 4G systems : from theory to practice”, *EURASIP Journal on Wireless Communications and Networking, MU-MIMO special issue*.

In thesis writing, there are two somewhat contradictory objectives that we like to achieve, i) avoiding repetition ii) having self-contained chapters. Although both of these conflicting themes have their own merits, we have certainly given preference to the second objective. Hence we have tried to make self-contained chapters with as little repetition as possible.

Part I

Single User MIMO

Chapter 2

Low Complexity Detection in BICM SISO System

2.1 Introduction

Enhanced reliability being one of the significant characteristics of future wireless communication systems, demands robust coding schemes. It was shown by Zehavi [3] and subsequently investigated by Caire *et al.* [4] that the code diversity could be improved by using bit-wise interleaving after the encoder rather than using symbol-wise interleaving after the modulator. The order of diversity for any coded system with a symbol interleaver is the minimum number of distinct symbols between codewords. Preventing parallel transitions (trellis based) and increasing the constraint length of the code are the only ways of increasing diversity. However bit-wise interleaving results in the diversity dictated by the smallest number of distinct bits, rather than channel symbols, along any error event. It therefore has the ability to provide large Hamming distances and is ideally suited to the fast fading channels. This coding technique was coined by Caire as BICM and its capacity was later shown in [33] to be close to that of the multilevel codes (MLC) if and only if Gray labeling is used. If set partition labeling or mixed labeling is used, then an iterative decoding approach (BICM-ID) [34] can be used to achieve high performance. Gray labeling on the other hand does not show any performance improvement with the iterative decoding [34] as

it allows parallel independent decoding of each bit [35] thereby reducing the detection complexity. BICM because of its improved code diversity over the fast fading channels has made its place in almost all the upcoming wireless communication standards as IEEE 802.11n [7], IEEE 802.16m [8] and 3GPP LTE [36].

This improved diversity of BICM comes at the cost of increased detection complexity even with Gray labeling. For SISO coded systems with symbol interleaving, the symbol metric for ML detection is based on the calculation of the minimum distance between the received symbol and M constellation points on the complex plane (M -ary QAM alphabet). However in the case of bit interleaving, same number of computations ($2^{\log M}$) are involved for each bit metric which is also called as LLR. This complexity renders the real time implementation of BICM based systems in the existing hardware quite challenging especially for large sized constellations.

Research community has been trying to find simplified receiver structures for BICM SISO systems in accordance with the existing hardware limitations. A set of approximated bit metrics for QAM16 and QAM64 constellations using the LLR for each bit are given in [37] for HIPERLAN/2 system. It was shown in [38] that for the Gray encoded BICM systems, the minimum distance calculation for each bit LLR can be reduced from M points on the complex constellation to \sqrt{M} points on the real line.

2.1.1 Contribution

Our contribution in this chapter is to show that the soft decision bit metrics for the ML detector for BICM SISO system can be significantly simplified to a scaled version of the matched filter (MF) output. This simplification is aided by the decoupling of the real and imaginary parts of the metric. Resultant bit metrics need no computation of the minimum distances and their subsequent comparisons. The complexity is maintained at almost the same level for all constellations as it involves only the computation of the MF output. This fundamentally reduces the number of calculations needed for each bit LLR without compromising the performance.

2.1.2 Organization

This chapter is divided into four sections. Section II defines the system model while in section III we derive the MF based low complexity metrics for different constellations. Section IV encompasses the simulation results which are followed by the conclusions.

2.2 System Model

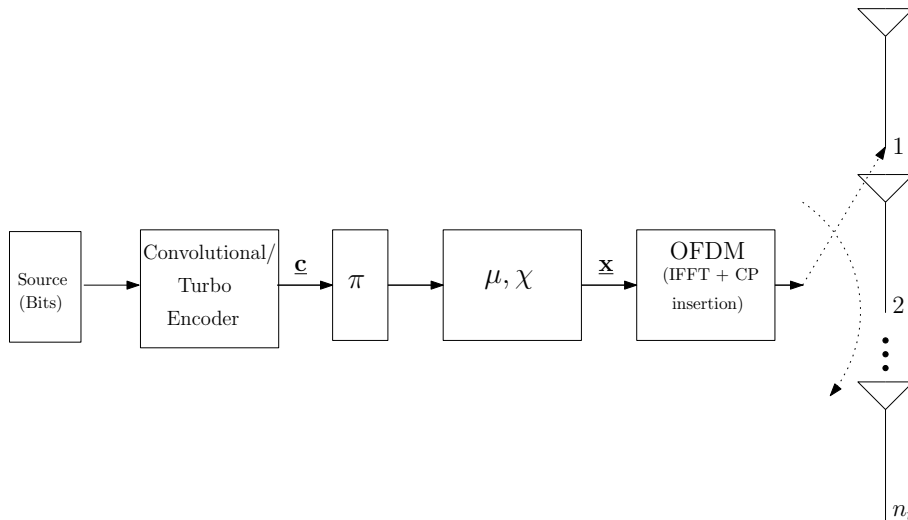


Figure 2.1: Block diagram of the transmitter. π indicates the interleaver while μ and χ indicate the labeling map and the constellation respectively.

We consider the downlink of a cellular system with n_t antennas at the BS and single antenna user/mobile station. Keeping in view the upcoming wireless standards as 802.16m [8] and 3GPP LTE [36], we assume that the BS uses BICM based OFDM system for the downlink transmission as shown in Fig. 2.1. We further assume antenna cycling at the BS [1] with each stream being transmitted by one antenna in any dimension. The antenna is randomly assigned per dimension so that the stream sees all the degrees of freedom of the channel. x is the symbol over a signal set $\chi \subseteq \mathcal{C}$ with a Gray labeling map $\mu : \{0, 1\}^{\log|\chi|} \rightarrow \chi$. During the transmission at the BS, the code sequence \underline{c} is interleaved by π and then is mapped onto the signal sequence \underline{x} . Bit interleaver can be modeled as $\pi : k' \rightarrow (k, i)$ where k' denotes the original ordering of the coded bits $c_{k'}$, k denotes the subcarrier index of the signal x_k and i indicates the position of the bit $c_{k'}$ in the symbol x_k . We assume that the cyclic prefix (CP) of appropriate length is added to the OFDM symbols at the BS. Cascading inverse fast Fourier transform (IFFT) at the BS and fast Fourier transform (FFT) at the user with CP extension, transmission at the k -th frequency tone can be expressed as

$$y_k = h_k x_k + z_k, \quad k = 1, 2, \dots, T \quad (2.1)$$

where h_k is the channel at the k -th frequency tone. Each subcarrier corresponds to a symbol from the constellation map χ . $y_k, z_k \in \mathcal{C}$ are the received symbols and circularly symmetric complex white Gaussian noise of double-sided power spectral density $N_0/2$. $h_k \in \mathcal{C}$ characterizes the flat fading channel response from the switched transmitting antenna to the user at the k -th subcarrier. The complex symbol x_k has the variance σ^2 .

Let $\chi_{c_{k'}}^i$ denotes the subset of all the signals $x \in \chi$ whose label has the value $c_{k'} \in \{0, 1\}$ in the position i . Then the ML bit metric can be given by

$$\begin{aligned}
\Lambda^i(y_k, c_{k'}) &= \log p(c_{k'}|y_k) \\
&\approx \log p(y_k|c_{k'}) \\
&= \log \sum_{x \in \chi_{c_{k'}}^i} p(y_k|x) \\
&= \log \sum_{x \in \chi_{c_{k'}}^i} \frac{1}{\pi N_0} \exp\left[-\frac{1}{N_0} |y_k - h_k x|^2\right] \\
&\approx \max_{x \in \chi_{c_{k'}}^i} \log \frac{1}{\pi N_0} \exp\left[-\frac{1}{N_0} |y_k - h_k x|^2\right] \\
&\approx \max_{x \in \chi_{c_{k'}}^i} \left[-\frac{1}{N_0} |y_k - h_k x|^2\right] \tag{2.2}
\end{aligned}$$

where we have used the log sum approximation [4], i.e. if $a > b$ then

$$\begin{aligned}
\log[\exp(a) + \exp(b)] &= \log[\exp(a)(1 + \exp(b-a))] \\
&= \log[\exp(a)] + \log[1 + \exp(b-a)] \\
&\approx \log[\exp(a)] \tag{2.3}
\end{aligned}$$

Metric (2.2) is commonly referred as the max log MAP metric. Note that the max log MAP approximation does not involve significant complexity reduction as the complexity lies in the computation of the terms in the metric rather than their summation or maximization. The ML decoder at the receiver can make decisions according to the rule

$$\hat{\underline{c}} = \arg \max_{\underline{c} \in \mathbb{C}} \sum_{k'} \Lambda^i(y_k, c_{k'}) \tag{2.4}$$

where \mathbb{C} defines the code book. In decoding, this metric incorporates different ordering of the bits before and after the interleaver at the transmitter,

by associating a contribution to the metric for each bit associated with the symbol received while that bit is transmitted. The bit LLR can be given as

$$\begin{aligned} \text{LLR}_i(y_k, c_{k'}) &\approx \Lambda^i(y_k, c_{k'} = 1) - \Lambda^i(y_k, c_{k'} = 0) \\ &= \max_{x \in \chi_{c_{k'}=1}^i} \left\{ \frac{-1}{N_0} |y_k - h_k x|^2 \right\} - \max_{x \in \chi_{c_{k'}=0}^i} \left\{ \frac{-1}{N_0} |y_k - h_k x|^2 \right\} \end{aligned} \quad (2.5)$$

2.3 Simplified Bit Metrics

In this section, we propose simplifications and approximations for (2.5) and state bit metrics for QPSK, QAM16 and QAM64 constellations. Using similar techniques, the simplified bit metrics can also be derived for larger sized constellations. Rewriting (2.5) by ignoring the scaling factor $1/N_0$, we get

$$\begin{aligned} \text{LLR}_i(y_k, c_{k'}) &\approx \max_{x \in \chi_{c_{k'}=1}^i} \left\{ 2(y_k(h_k x)^*)_R - |h_k x|^2 - |y_k|^2 \right\} \\ &\quad - \max_{x \in \chi_{c_{k'}=0}^i} \left\{ 2(y_k(h_k x)^*)_R - |h_k x|^2 - |y_k|^2 \right\} \end{aligned} \quad (2.6)$$

where $(\cdot)_R$ indicates the real part while $(\cdot)_I$ indicates the imaginary part. For the sake of brevity, we drop the frequency and interleaving indices. Writing in terms of the real and imaginary parts, we get

$$\begin{aligned} \text{LLR}_i &\approx \max_{x \in \chi_1^i} \left\{ 2\bar{y}_R x_R + 2\bar{y}_I x_I - |h|^2 x_R^2 - |h|^2 x_I^2 \right\} \\ &\quad - \max_{x \in \chi_0^i} \left\{ 2\bar{y}_R x_R + 2\bar{y}_I x_I - |h|^2 x_R^2 - |h|^2 x_I^2 \right\} \\ &= \max_{x_R \in \chi_1^i} \left\{ 2\bar{y}_R x_R - |h|^2 x_R^2 \right\} + \max_{x_I \in \chi_1^i} \left\{ 2\bar{y}_I x_I - |h|^2 x_I^2 \right\} \\ &\quad - \max_{x_R \in \chi_0^i} \left\{ 2\bar{y}_R x_R - |h|^2 x_R^2 \right\} - \max_{x_I \in \chi_0^i} \left\{ 2\bar{y}_I x_I - |h|^2 x_I^2 \right\} \end{aligned} \quad (2.7)$$

where $\bar{y} = h^* y$ is the MF output. x_R is the real and x_I is the imaginary part of x while \bar{y}_R and \bar{y}_I are the real and imaginary parts of \bar{y} . Note that $x_R \in \chi_1^i$ represent the real parts of those constellation points of χ where the bit at position i is 1. The metric (2.7) decouples the real and imaginary parts. Let $m = \log M$ be the number of bits per symbol. Then as per the Gray labeling shown in Fig. 2.2, $x_I \in \chi_1^i = x_I \in \chi_0^i$ for $i = 1, 2, \dots, m/2$, so the LLR is written as

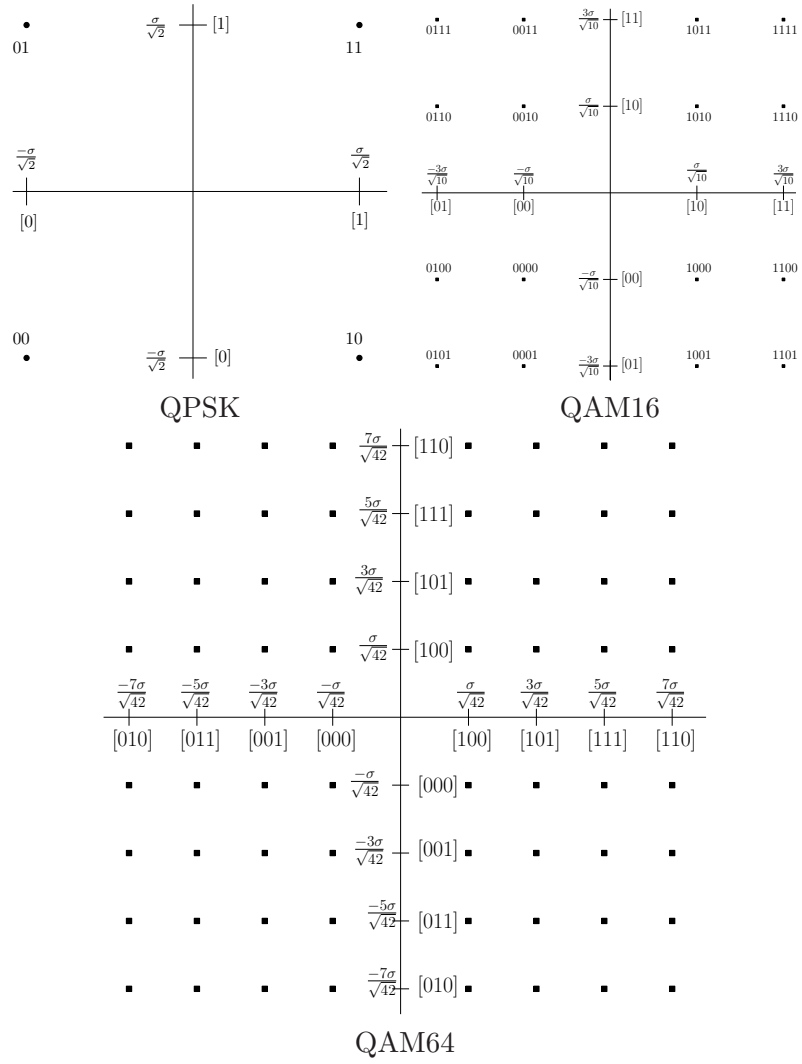


Figure 2.2: Normalized constellations of QPSK, QAM16 and QAM64 with Gray mapping.

$$\text{LLR}_i \approx \max_{x_R \in \chi_1^i} \left\{ 2\bar{y}_R x_R - |h|^2 x_R^2 \right\} - \max_{x_R \in \chi_0^i} \left\{ 2\bar{y}_R x_R - |h|^2 x_R^2 \right\} \quad (2.8)$$

whereas for $i = m/2 + 1, \dots, m$, $x_R \in \chi_1^i = x_R \in \chi_0^i$, so the LLR can be written as

$$\text{LLR}_i \approx \max_{x_I \in \chi_1^i} \left\{ 2\bar{y}_I x_I - |h|^2 x_I^2 \right\} - \max_{x_I \in \chi_0^i} \left\{ 2\bar{y}_I x_I - |h|^2 x_I^2 \right\} \quad (2.9)$$

2.3.1 QPSK

QPSK being equal energy alphabets, $|h|^2 x_R^2$ will be canceled in (2.8) while $|h|^2 x_I^2$ will be canceled in (2.9). LLR for the first bit of QPSK is given as

$$\begin{aligned} \text{LLR}_1 &\approx \max_{x_R = \frac{\sigma}{\sqrt{2}}} \left\{ \bar{y}_R x_R \right\} - \max_{x_R = -\frac{\sigma}{\sqrt{2}}} \left\{ \bar{y}_R x_R \right\} \\ &= \sqrt{2} \sigma \bar{y}_R \end{aligned} \quad (2.10)$$

whereas for the second bit, LLR is given as

$$\begin{aligned} \text{LLR}_2 &\approx \max_{x_I = \frac{\sigma}{\sqrt{2}}} \left\{ \bar{y}_I x_I \right\} - \max_{x_I = -\frac{\sigma}{\sqrt{2}}} \left\{ \bar{y}_I x_I \right\} \\ &= \sqrt{2} \sigma \bar{y}_I \end{aligned} \quad (2.11)$$

2.3.2 QAM16

QAM16 being nonequal energy alphabet, LLR for the first bit is written as

$$\begin{aligned} \text{LLR}_1 &\approx \max_{x_R = \frac{\sigma}{\sqrt{10}}, \frac{3\sigma}{\sqrt{10}}} \left\{ 2\bar{y}_R x_R - |h|^2 x_R^2 \right\} - \max_{x_R = -\frac{\sigma}{\sqrt{10}}, -\frac{3\sigma}{\sqrt{10}}} \left\{ 2\bar{y}_R x_R - |h|^2 x_R^2 \right\} \\ &= \max \left\{ \frac{-|h|^2 \sigma^2}{10} + \frac{2\bar{y}_R \sigma}{\sqrt{10}}, \frac{-9|h|^2 \sigma^2}{10} + \frac{6\bar{y}_R \sigma}{\sqrt{10}} \right\} \\ &\quad - \max \left\{ \frac{-|h|^2 \sigma^2}{10} - \frac{2\bar{y}_R \sigma}{\sqrt{10}}, \frac{-9|h|^2 \sigma^2}{10} - \frac{6\bar{y}_R \sigma}{\sqrt{10}} \right\} \\ &\stackrel{(i)}{=} \begin{cases} \frac{8\sigma}{\sqrt{10}} \bar{y}_R + \frac{8|h|^2 \sigma^2}{10} & \text{if } \bar{y}_R < -\frac{2\sigma|h|^2}{\sqrt{10}} \\ \frac{4\sigma}{\sqrt{10}} \bar{y}_R & \text{if } -\frac{2\sigma|h|^2}{\sqrt{10}} \leq \bar{y}_R < \frac{2\sigma|h|^2}{\sqrt{10}} \\ \frac{8\sigma}{\sqrt{10}} \bar{y}_R - \frac{8|h|^2 \sigma^2}{10} & \text{if } \bar{y}_R \geq \frac{2\sigma|h|^2}{\sqrt{10}} \end{cases} \\ &\stackrel{(ii)}{\approx} \frac{20\sigma}{3\sqrt{10}} \bar{y}_R \end{aligned} \quad (2.12)$$

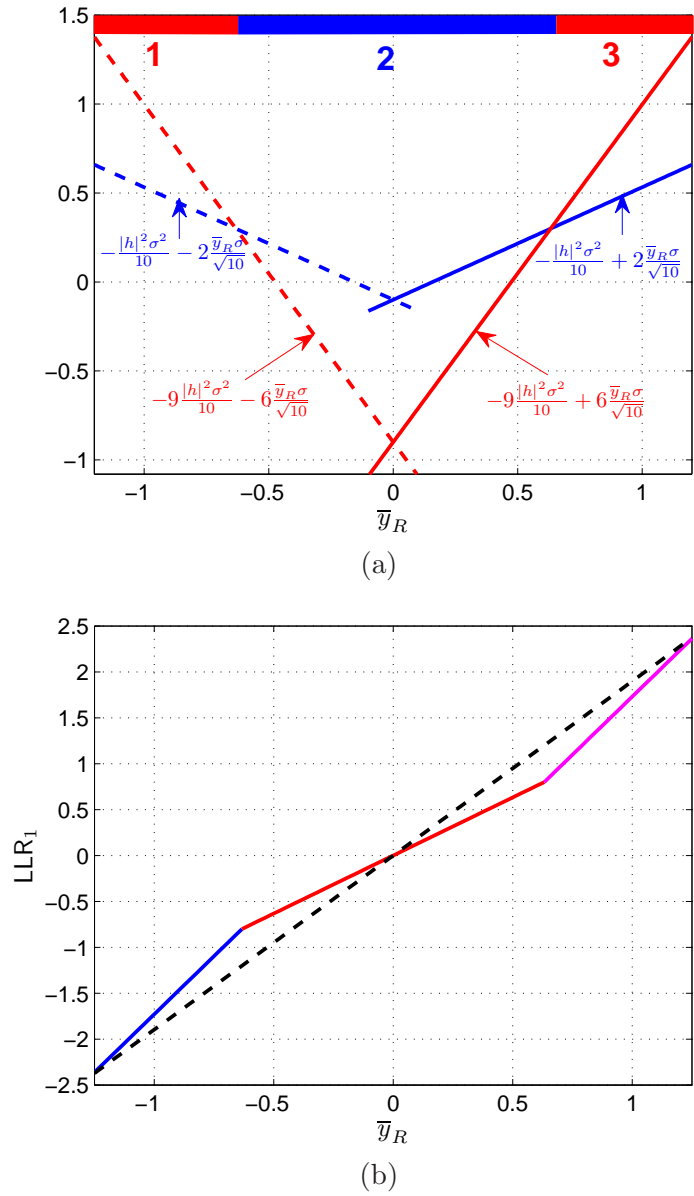


Figure 2.3: Metric for the first bit of QAM16. (a) shows 3 regions for the LLR where (b) shows the exact and approximated bit metric. In (b), continuous line indicates the exact bit metric while the dashed line indicates the approximated bit metric. Note that $|h|$ and σ are taken as 1.

where we have introduced a little suboptimality in the last step by averaging over three possible bit metrics. Fig. 2.3(a) shows three regions as defined by (i) while Fig. 2.3(b) shows the approximated bit metric in the dotted line as indicated in (ii). The LLR for the second bit is written as

$$\begin{aligned}
\text{LLR}_2 &\approx \max_{x_R = \frac{3\sigma}{\sqrt{10}}, \frac{-3\sigma}{\sqrt{10}}} \left\{ 2\bar{y}_R x_R - |h|^2 x_R^2 \right\} - \max_{x_R = \frac{\sigma}{\sqrt{10}}, \frac{-\sigma}{\sqrt{10}}} \left\{ 2\bar{y}_R x_R - |h|^2 x_R^2 \right\} \\
&= \max \left\{ \frac{-9|h|^2 \sigma^2}{10} + \frac{6\bar{y}_R \sigma}{\sqrt{10}}, \frac{-9|h|^2 \sigma^2}{10} - \frac{6\bar{y}_R \sigma}{\sqrt{10}} \right\} \\
&\quad - \max \left\{ \frac{-|h|^2 \sigma^2}{10} + \frac{2\bar{y}_R \sigma}{\sqrt{10}}, \frac{-|h|^2 \sigma^2}{10} - \frac{2\bar{y}_R \sigma}{\sqrt{10}} \right\} \\
&= \left\{ \frac{-9|h|^2 \sigma^2}{10} + \frac{6\sigma}{\sqrt{10}} |\bar{y}_R| \right\} - \left\{ \frac{-|h|^2 \sigma^2}{10} + \frac{2\sigma}{\sqrt{10}} |\bar{y}_R| \right\} \\
&= \frac{4\sigma}{\sqrt{10}} |\bar{y}_R| - \frac{8|h|^2 \sigma^2}{10} \tag{2.13}
\end{aligned}$$

LLRs of the third and the fourth bit are similar to the LLRs of the first and the second bit except that \bar{y}_R is replaced by \bar{y}_I .

2.3.3 QAM64

For QAM64, LLR for the first bit is given as

$$\begin{aligned}
\text{LLR}_1 &\approx \max_{x_R = \frac{\sigma}{\sqrt{42}}, \frac{3\sigma}{\sqrt{42}}, \frac{5\sigma}{\sqrt{42}}, \frac{7\sigma}{\sqrt{42}}} \left\{ 2\bar{y}_R x_R - |h|^2 x_R^2 \right\} - \max_{x_R = \frac{-\sigma}{\sqrt{42}}, \frac{-3\sigma}{\sqrt{42}}, \frac{-5\sigma}{\sqrt{42}}, \frac{-7\sigma}{\sqrt{42}}} \left\{ 2\bar{y}_R x_R - |h|^2 x_R^2 \right\} \\
&= \begin{cases} \frac{16\sigma}{\sqrt{42}} \bar{y}_R + \frac{48|h|^2 \sigma^2}{42} & \text{if } \bar{y}_R < -\frac{6\sigma|h|^2}{\sqrt{42}} \\ \frac{12\sigma}{\sqrt{42}} \bar{y}_R + \frac{24|h|^2 \sigma^2}{42} & \text{if } -\frac{6\sigma|h|^2}{\sqrt{42}} \leq \bar{y}_R < -\frac{4\sigma|h|^2}{\sqrt{42}} \\ \frac{8\sigma}{\sqrt{42}} \bar{y}_R + \frac{8|h|^2 \sigma^2}{42} & \text{if } -\frac{4\sigma|h|^2}{\sqrt{42}} \leq \bar{y}_R < -\frac{2\sigma|h|^2}{\sqrt{42}} \\ \frac{4\sigma}{\sqrt{42}} \bar{y}_R & \text{if } -\frac{2\sigma|h|^2}{\sqrt{42}} \leq \bar{y}_R < \frac{2\sigma|h|^2}{\sqrt{42}} \\ \frac{8\sigma}{\sqrt{42}} \bar{y}_R - \frac{8|h|^2 \sigma^2}{42} & \text{if } \frac{2\sigma|h|^2}{\sqrt{42}} \leq \bar{y}_R < \frac{4\sigma|h|^2}{\sqrt{42}} \\ \frac{12\sigma}{\sqrt{42}} \bar{y}_R - \frac{24|h|^2 \sigma^2}{42} & \text{if } \frac{4\sigma|h|^2}{\sqrt{42}} \leq \bar{y}_R < \frac{6\sigma|h|^2}{\sqrt{42}} \\ \frac{16\sigma}{\sqrt{42}} \bar{y}_R - \frac{48|h|^2 \sigma^2}{42} & \text{if } \frac{6\sigma|h|^2}{\sqrt{42}} \leq \bar{y}_R \end{cases} \\
&\approx \frac{76\sigma}{7\sqrt{42}} \bar{y}_R \tag{2.14}
\end{aligned}$$

Again we have introduced a slight suboptimality in the last step by averaging over seven possible bit metrics as shown in Fig. 2.4. Similarly for the second bit, LLR is written as

$$\begin{aligned}
 \text{LLR}_2 &\approx \max_{x_R = \frac{5\sigma}{\sqrt{42}}, \frac{7\sigma}{\sqrt{42}}, \frac{-5\sigma}{\sqrt{42}}, \frac{-7\sigma}{\sqrt{42}}} \left\{ 2\bar{y}_R x_R - |h|^2 x_R^2 \right\} - \max_{x_R = \frac{\sigma}{\sqrt{42}}, \frac{3\sigma}{\sqrt{42}}, \frac{-\sigma}{\sqrt{42}}, \frac{-3\sigma}{\sqrt{42}}} \left\{ 2\bar{y}_R x_R - |h|^2 x_R^2 \right\} \\
 &= \max_{x_R = \frac{5\sigma}{\sqrt{42}}, \frac{7\sigma}{\sqrt{42}}} \left\{ 2|\bar{y}_R| x_R - |h|^2 x_R^2 \right\} - \max_{x_R = \frac{\sigma}{\sqrt{42}}, \frac{3\sigma}{\sqrt{42}}} \left\{ 2|\bar{y}_R| x_R - |h|^2 x_R^2 \right\} \\
 &= \begin{cases} \frac{8\sigma}{\sqrt{42}} |\bar{y}_R| - \frac{24|h|^2 \sigma^2}{42} & \text{if } |\bar{y}_R| < \frac{2\sigma|h|^2}{\sqrt{42}} \\ \frac{4\sigma}{\sqrt{42}} |\bar{y}_R| - \frac{16|h|^2 \sigma^2}{42} & \text{if } \frac{2\sigma|h|^2}{\sqrt{42}} \leq |\bar{y}_R| < \frac{6\sigma|h|^2}{\sqrt{42}} \\ \frac{8\sigma}{\sqrt{42}} |\bar{y}_R| - \frac{40|h|^2 \sigma^2}{42} & \text{if } \frac{6\sigma|h|^2}{\sqrt{42}} \leq |\bar{y}_R| \end{cases} \\
 &\approx \frac{20\sigma}{3\sqrt{42}} |\bar{y}_R| - \frac{80|h|^2 \sigma^2}{3 \times 42} \tag{2.15}
 \end{aligned}$$

The suboptimality introduced in the last step is shown in Fig. 2.5. For the third bit, LLR is given as

$$\begin{aligned}
 \text{LLR}_3 &\approx \max_{x_R = \frac{\sigma}{\sqrt{42}}, \frac{7\sigma}{\sqrt{42}}, \frac{-\sigma}{\sqrt{42}}, \frac{-7\sigma}{\sqrt{42}}} \left\{ 2\bar{y}_R x_R - |h|^2 x_R^2 \right\} - \max_{x_R = \frac{3\sigma}{\sqrt{42}}, \frac{5\sigma}{\sqrt{42}}, \frac{-3\sigma}{\sqrt{42}}, \frac{-5\sigma}{\sqrt{42}}} \left\{ 2\bar{y}_R x_R - |h|^2 x_R^2 \right\} \\
 &= \begin{cases} \frac{-4\sigma}{\sqrt{42}} |\bar{y}_R| + \frac{8|h|^2 \sigma^2}{42} & \text{if } |\bar{y}_R| < \frac{4\sigma|h|^2}{\sqrt{42}} \\ \frac{4\sigma}{\sqrt{42}} |\bar{y}_R| - \frac{24|h|^2 \sigma^2}{42} & \text{if } |\bar{y}_R| > \frac{4\sigma|h|^2}{\sqrt{42}} \end{cases} \tag{2.16} \\
 &= \left| \frac{4\sigma}{\sqrt{42}} |\bar{y}_R| - \frac{16|h|^2 \sigma^2}{42} \right| - \frac{8|h|^2 \sigma^2}{42}
 \end{aligned}$$

LLRs for the fourth, fifth and sixth bits are similar to the LLRs of the first, second and third bits with \bar{y}_R being replaced by \bar{y}_I . Using the same procedure, the LLRs for higher sized constellations can be easily derived.

The complexity analysis of these bit metrics in terms of the complex operations (complex multiplications, complex additions) is tabulated in Table.2.1. Number of complex multiplications for the simplified metrics result from the computation of the MF output and the channel norm. Note that where the complexity of original metrics increases exponentially in m , the complexity of simplified metrics is maintained at almost the same level for all constellations.

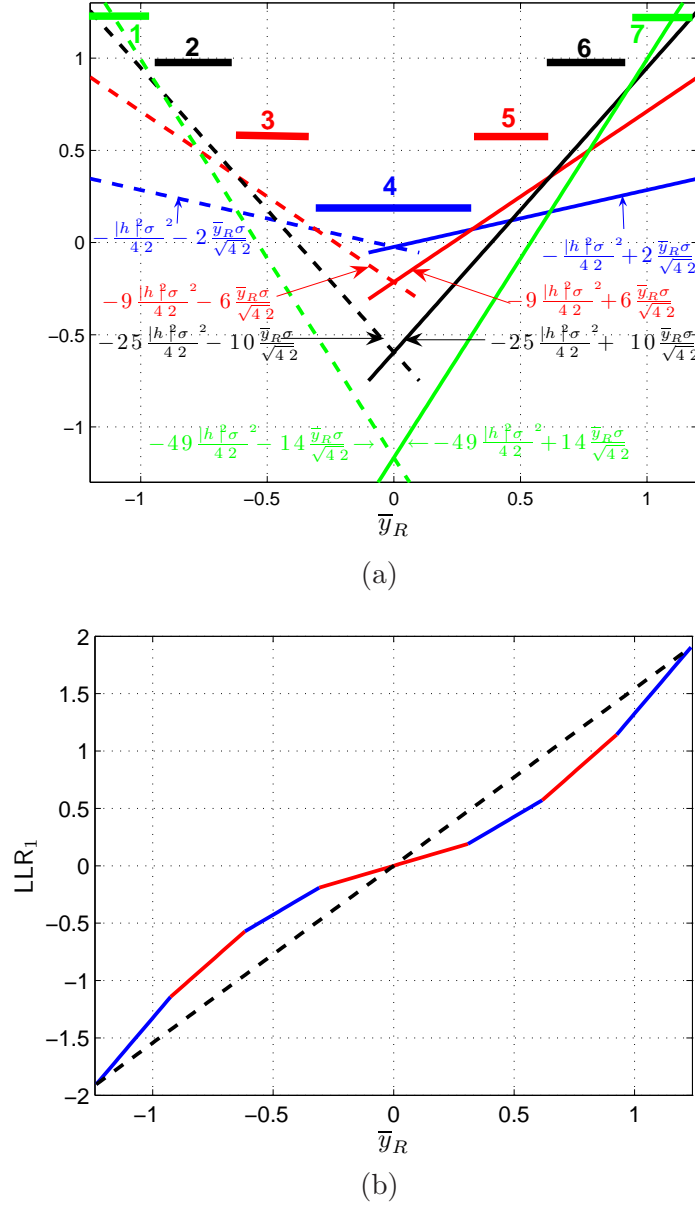


Figure 2.4: Metric for the first bit of QAM64. (a) shows 7 regions for the LLR where (b) shows the exact and the approximated bit metric.

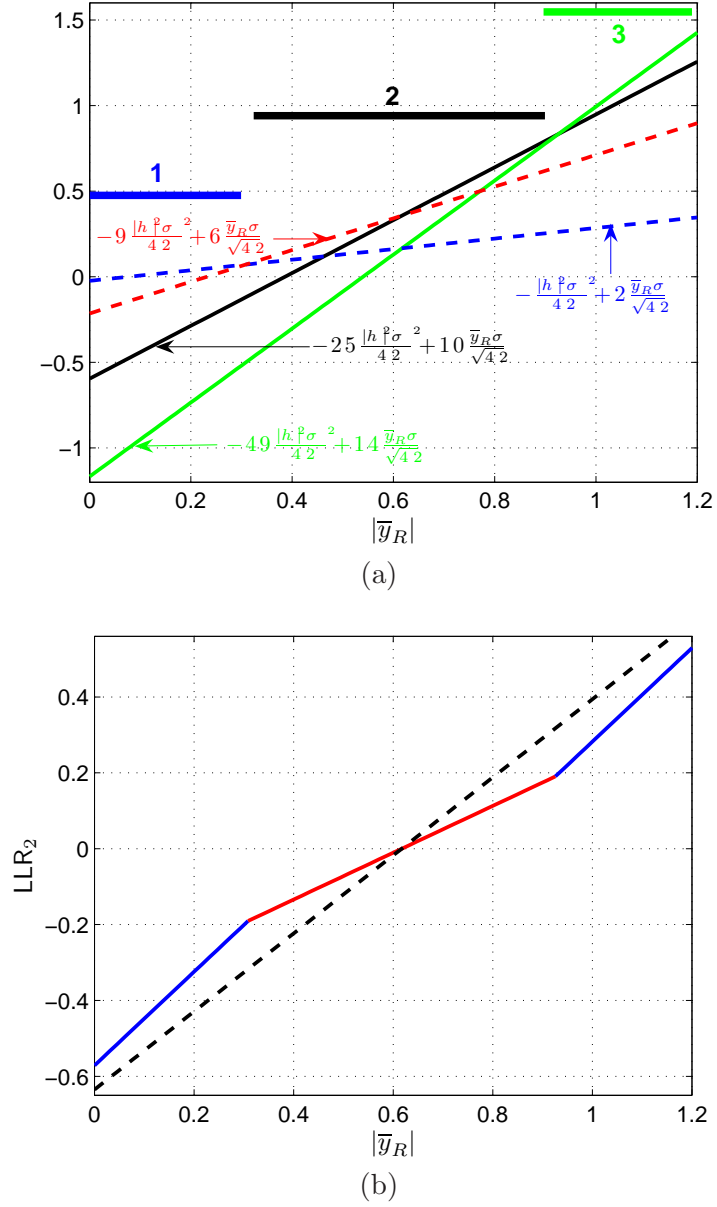


Figure 2.5: Metric for the second bit of QAM64. (a) shows 3 regions for the LLR where (b) shows the exact and the approximated bit metric.

Table 2.1: Computational complexity for the calculation of LLRs for one symbol in the SISO system

M -ary	Multiplications		Additions		Comparisons	
	original	simplified	original	simplified	original	simplified
4	16	1	8	0	8	0
16	128	2	64	0	64	0
64	768	2	384	0	384	0

2.4 Simulation Results

We consider a BICM SISO OFDM system using the rate-1/2 punctured turbo code¹ of 3GPP LTE [36] and analyze the system in the frequency domain. The channel has iid Gaussian matrix entries with unit variance and the effect of antenna cycling is simulated by independent generation of the channel for each channel use. Perfect CSI at the receiver is assumed. We consider the original max log MAP bit metrics (ML) and the simplified metrics. Due to the approximations involved, we call the simplified bit metric approach as Quasi-ML approach. We focus on the frame error rates (FER) where the frame length is fixed to 1056 information bits. Note that for QPSK constellation, the simplified bit metrics are same as the ML metrics. Fig. 2.6 shows that there is negligible degradation in the performance with the simplified bit metrics for QAM16. It is attributed to the fact that in the Quasi-ML approach for QAM16, two LLRs have slight suboptimality while two LLRS are exact. There is a slight degradation in the performance for QAM64 for the Quasi-ML approach which is attributed to the fact that four bits have the approximated LLRs whereas two bits have the exact LLRs.

2.5 Conclusions

In this chapter, we have proposed the low complexity MF based bit metrics for the BICM SISO system. These proposed metrics are merely scaled versions of the MF outputs and involve no distance computations and comparisons. These low complexity bit metrics being based on the MF outputs and devoid of any division operation can be easily implemented in the receiver structures for forthcoming wireless systems taking into account the existing hardware limitations.

¹The LTE turbo decoder design was performed using the coded modulation library www.iterativesolutions.com

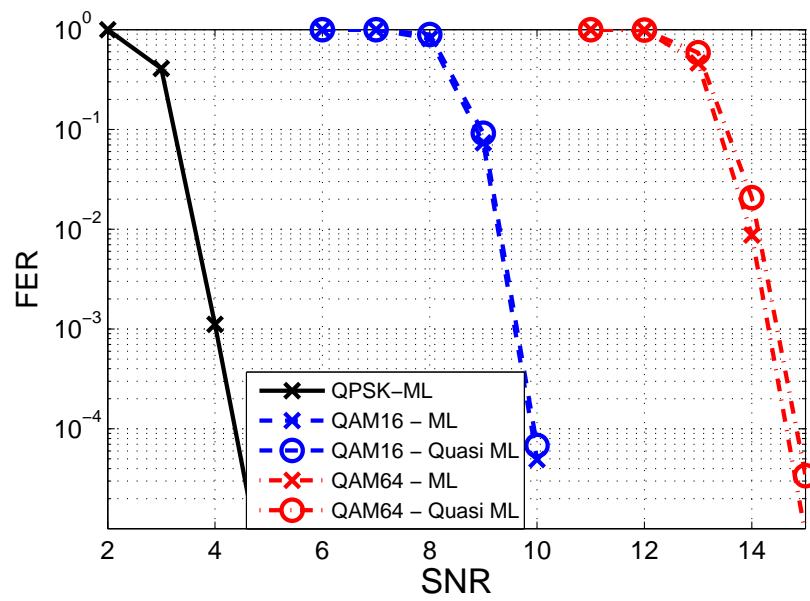


Figure 2.6: SISO System using punctured rate 1/2 turbo code of 3GPP LTE. Decoding iterations are 5.

Chapter 3

Low Complexity Detection in BICM MIMO Systems

3.1 Introduction

Point-to-point SU MIMO communication promises large gains for both channel capacity and reliability [1] [2], essentially via the use of space-time codes (diversity gain oriented) combined with the multi-stream transmission (rate maximization oriented) [39]. Diversity increases the robustness of the system by eliminating fades; channel-aware diversity also raises the average received SNR in proportion to the number of transmit and/or receive antennas. If the channel is not known, then diversity hardens the SNR to the mean SNR rather than increasing it, i.e. it converts a fading channel to a non-fading channel as the number of antennas grows large. Even if the average SNR increases linearly with the number of antennas, capacity growth is logarithmic, easily verified with Shannon's formula $C = B \log_2(1 + \text{SNR})$ where B is the bandwidth. Multi-stream transmission, on the other hand, divides the incoming data into multiple parallel substreams and transmits each on a different spatial dimension (e.g. a different antenna). As long as there are at least as many (sufficiently spaced) receive antennas as the transmitted streams, multi-stream transmission increases the capacity linearly with the number of streams. The consequential high data rates are particularly interesting for the downlink communication as compared to the

uplink communication due to the dominance of asymmetric data traffic as compared to the symmetric voice traffic. However, the intricacy of realizing requisite antenna spacing in the user/mobile station combined with the hardware complexity and the cost considerations shall be restricting future MIMO systems to low dimensionality (in the number of receive antennas for the downlink channel). It can be reasonably assumed that the number of transmit antennas n_t (at the BS) will be larger than the number of receive antennas n_r thereby resulting into the transmission of n_r data streams to the user and leaving $(n_t - n_r)$ degrees of freedom. In the absence of CSIT, these degrees of freedom can be used to achieve transmit diversity by using space time coding (STC) [40] or antenna cycling [1]. It was shown in [41] that remarkable coding and diversity gains can be obtained if capacity achieving temporal encoders, such as turbo or Low-Density Parity-Check (LDPC) codes are used in concatenation with a STC. Multi-stream transmission combined with a standard outer error-correcting code is a strong concatenated STC scheme where the space dimension is multiplexing. Bit interleaving combined with an error correcting code, i.e. BICM [4] improves the code diversity, ideally suited to the fast fading wireless channels. Frequency selectivity of the wireless channel leads to enhanced detection complexity and OFDM is considered to be a suitable choice for low complexity equalization due to its ability to convert frequency selective channels to a number of flat fading channels.

These arguments underline that low dimensional stream multiplexed BICM MIMO OFDM systems provide a promising choice for the next-generation wireless networks. Advanced and upcoming wireless standards such as 3GPP LTE [36], LTE-Advanced [6], IEEE 802.11n (Wireless LAN) [7] and IEEE 802.16m (WiMax) [8] substantiate this proposition. Of particular interest in mobile applications are MIMO systems with two transmit and two receive antennas (baseline configuration in 3GPP LTE [36]) as this configuration is able to provide both the diversity and multiplexing gains while keeping costs at a minimum. Due to the transmission strategy of stream multiplexing, the receiver views a multiple access channel (MAC) and the reception is consequently based on SIC, i.e. sequential decoding and subtraction (stripping) of the spatial streams. The design of low complexity detectors for such systems which can be implemented in the existing hardware is a key problem. Therefore our main focus in this chapter is on the low complexity SIC based detection in such systems.

3.1.1 The state of the Art

Shamai [15] termed the approach of single code layer at each transmit antenna as *MAC-outage approach*. For decoding, it is important to obtain the reliability information (soft decisions) for each bit. ML computation of such soft decisions (LLRs) involves the summation of a number of terms that grows exponentially with the number of spatial streams and the number of bits per modulation symbol, i.e. $2^{\log|\chi|n_t}$ where $|\chi|$ is the constellation size and n_t is the number of spatial streams/transmit antennas. In many cases of practical interest, one resorts to the approximation of replacing the sums with the largest term commonly termed as the max log MAP approximation [4]. Unfortunately this problem is NP-hard [16] which implies that there are no known efficient (i.e. polynomial-time) solutions. An alternative is Sphere Decoder of Fincke and Pohst [19] which has expected complexity to be polynomial (for small noise variance) but it still has exponential complexity in the worst case. Another preprocessing technique to reduce the complexity is lattice reduction (LR) [17] [18] which is generally referred as lattice-reduction-aided detection. Channel realization is regarded as a basis of the lattice, and LR changes the generating matrix of the lattice to obtain a “nicer” (more orthogonal) basis of the same lattice. Finding new basis for each channel realization is a computationally intensive operation and furthermore, this method leads to non-negligible increase in the error rates with respect to non-lattice-reduction-aided detectors for low SNRs. Some modified low-complexity ML detectors have also been proposed in the literature as [23].

Naive suboptimal solutions, like neglecting the integer constraint coupled with the Gaussian assumption for the alphabets and then subsequently projecting the so-obtained solution onto the finite set of permissible transmit symbols (linear receivers as MMSE and zero forcing - ZF [20]), in general work poorly as compared to ML detectors especially at lower SNRs for low dimensional systems. For example, V-BLAST [42] uses linear MMSE filters against yet undecoded streams at each successive cancellation stage which is optimum for power constrained Gaussian inputs case [43] but shows degraded performance in low dimensional practical systems which make use of discrete modulation alphabets. The degradation of the performance due to the sub-optimality combined with the complexity in calculation of linear equalizers at each frequency tone (in OFDM based system) renders the real-time implementation of these algorithms difficult especially in fast fading wideband environments. Literature also discusses SIC and parallel interference cancellation (PIC) detection schemes for CDMA systems in reference

to different powers of the received signals in the multiuser context [44].

3.1.2 Contribution

We propose in this chapter a low complexity matched filter (MF) based near ML detector for SIC based detection which successfully reduces one complex dimension of the system, i.e. the complexity of detection reduces from $\mathcal{O}(|\chi|^2)$ to $\mathcal{O}(|\chi|^1)$ in the dual stream scenario. The proposed detector is a low complexity adaptation of the max log MAP detector (practical version of the ML detector) which successfully escapes the exponential complexity of MIMO detection for the considered $2 \times n_r$ system. While decoding the first stream, this detector takes into account yet undecoded second stream instead of using a linear filter (MMSE or ZF) against it. This leads to a performance (error rate) better than the standard linear detector based approaches coupled with a significant reduction in the complexity. Though in this chapter we discuss the proposed detector for the dual stream scenario, it remains valid to the general multi-stream (spatially multiplexed) MIMO systems where this detector reduces the complexity of ML detection from $\mathcal{O}(|\chi|^{n_t})$ to $\mathcal{O}(|\chi|^{n_t-1})$. Reduction of one complex dimension is a fundamental result as space and technology constraints shall be restricting future MIMO systems to low dimensionality.

A natural question concerns the achievable performance of this detector. In the sequel, we further study coded pairwise error probability (PEP) of the proposed detector using *moment generating function* (MGF) based approach associated with the quadratic form of a complex Gaussian random variable [45] and show that the proposed detector has full diversity. For comparison purposes, we also include the analysis of MMSE detector and show yet again the well known result that MMSE detection loses one diversity order in dual stream scenario [46]. The analysis also shows that the proposed detector has better coding gain than MMSE detector. We then extend the low complexity detection to higher-dimensional systems by focusing on uniform rate, nonuniform power distribution and uniform power, nonuniform rate distribution between the spatial streams. The performance slightly degrades for higher dimensional systems but it is concurrently matched with a boost in the complexity savings. Power or rate distribution between the spatial streams combined with independent coding on each stream introduces UEP which adds flexibility to the system. We also propose a broadcast strategy based on the UEP (rate distribution) which helps the system to gear up to a higher data rate as the channel conditions improve without any adjustment at the transmitter.

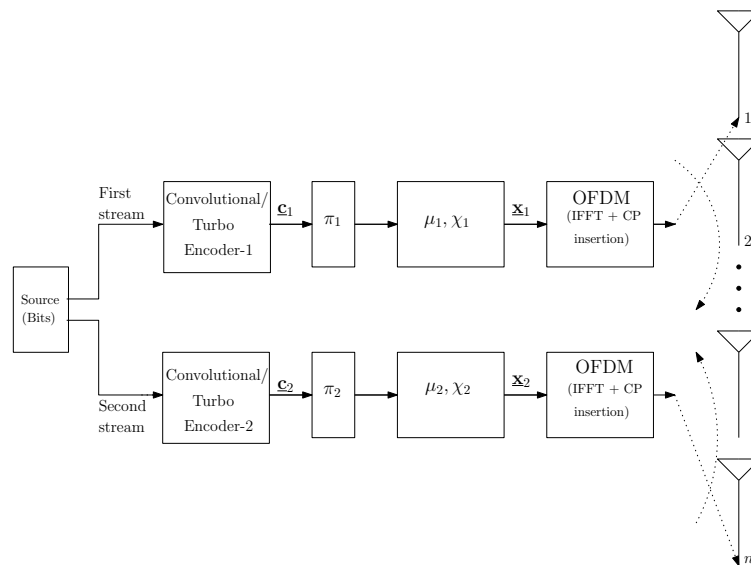


Figure 3.1: Block diagram of the transmitter of dual stream BICM MIMO OFDM system. π_1 denotes the random interleaver, μ_1 the labeling map and χ_1 the signal set for the first stream.

3.1.3 Organization

This chapter is divided into nine sections. In section II we define the system model while section III gives insight into the mutual information of the system. In section IV, we give an overview of the state of the art detectors coupled with their performance analysis. In section V, we propose the low complexity MF based detectors and carry out their performance analysis. Section VI and VII encompass the proposed broadcast strategy and the extension of the proposed low complexity detection to higher dimensional systems. Section VIII contains the simulation results which are followed by the conclusions.

3.2 System Model

We consider a MIMO system which is $n_t \times n_r$ ($n_t \geq 2$, $n_r \geq 2$) BICM MIMO OFDM system with two spatial streams. We effectively reduce this to $2 \times n_r$ system by antenna cycling [1] at the transmitter with each stream being transmitted by one antenna in any dimension as shown in Fig. 3.1. The

antenna used by a particular stream is randomly assigned per dimension so that each stream sees all the degrees of freedom of the channel. We assume that the two spatial streams are $\underline{\mathbf{x}}_1$ and $\underline{\mathbf{x}}_2$. x_1 is the symbol of $\underline{\mathbf{x}}_1$ over a signal set $\chi_1 \subseteq \mathcal{C}$ with a Gray labeling map $\mu_1 : \{0, 1\}^{\log|\chi_1|} \rightarrow \chi_1$ where $|\chi_1| = M_1$ and x_2 is the symbol of $\underline{\mathbf{x}}_2$ over a signal set χ_2 where $|\chi_2| = M_2$. During the transmission, the code sequence $\underline{\mathbf{c}}_1$ is interleaved by π_1 and then is mapped onto the signal sequence $\underline{\mathbf{x}}_1$. Bit interleaver for the first stream can be modeled as $\pi_1 : k' \rightarrow (k, i)$ where k' denotes the original ordering of the coded bits $c_{k'}$ of the first stream, k denotes the subcarrier index of the signal $x_{1,k}$ and i indicates the position of the bit $c_{k'}$ in the symbol $x_{1,k}$. Assuming that the cyclic prefix (CP) of appropriate length is added to the OFDM symbols, transmission at the k -th frequency tone after cascading IFFT at the transmitter and FFT at the receiver is given as

$$\begin{aligned} \mathbf{y}_k &= \mathbf{h}_{1,k}x_{1,k} + \mathbf{h}_{2,k}x_{2,k} + \mathbf{z}_k, \quad k = 1, 2, \dots, T \\ &= \mathbf{H}_k \mathbf{x}_k + \mathbf{z}_k \end{aligned} \quad (3.1)$$

where T is the total number of frequency tones and $\mathbf{H}_k = [\mathbf{h}_{1,k} \ \mathbf{h}_{2,k}]$ is the channel at the k -th frequency tone and $\mathbf{x}_k = [x_{1,k} \ x_{2,k}]^T$. Each subcarrier corresponds to a symbol from the constellation map χ_1 for the first stream and χ_2 for the second stream. $\mathbf{y}_k, \mathbf{z}_k \in \mathbb{C}^{n_r}$ are the vectors of the received symbols and circularly symmetric complex white Gaussian noise of double-sided power spectral density $N_0/2$ at n_r receive antennas. $\mathbf{h}_{1,k} \in \mathbb{C}^{n_r}$ is the vector characterizing the flat fading channel response from the first transmitting antenna to n_r receive antennas at the k -th subcarrier. This vector has complex-valued multivariate Gaussian distribution with $\mathcal{CN}(\mathbf{0}, \mathbf{I}_{n_r})$. The complex symbols $x_{1,k}$ and $x_{2,k}$ of two streams are assumed to be independent with the variances σ_1^2 and σ_2^2 respectively. The channels at different subcarriers are also assumed to be independent.

Fig. 3.2 shows the receiver which is based on SIC principle. Firstly, the receiver detects the first stream using the proposed low complexity MF based detector (to be discussed in section 3.5) and then strips it out. Second stream is then detected using the standard SIMO detector. In the figure, $\overline{\mathbf{H}}_1$ denotes the channel (comprising of N channel vectors $\mathbf{h}_{1,k}$) to transmit the first codeword $\underline{\mathbf{c}}_1$ while the corresponding received signal at the user is denoted as $\overline{\mathbf{Y}}$. π_1^{-1} and π_2^{-1} denote deinterleavers for the first and the second stream respectively. Note that under the power constraint P_T , the average SNR at each receiver branch is $\frac{P_T}{N_0}$.

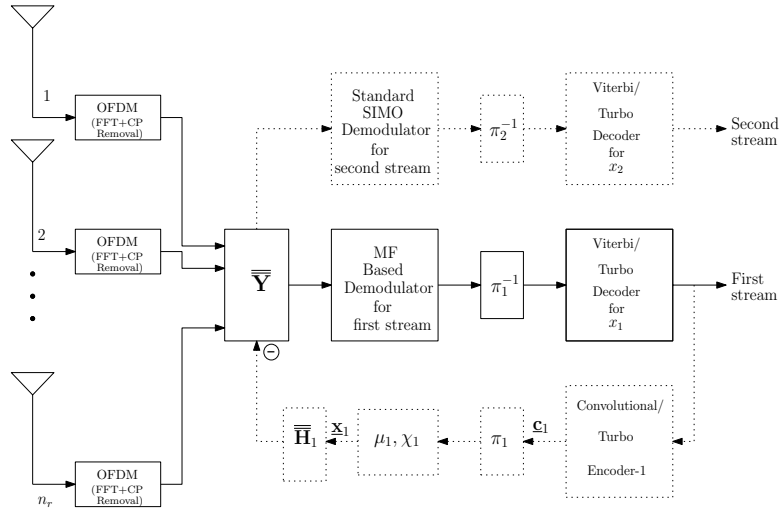


Figure 3.2: Block diagram of the SIC receiver of dual stream BICM MIMO OFDM system.

3.3 An Information Theoretic View

In this section, we focus on the information theoretic analysis of the system while assuming perfect CSI at the receiver. Capacity of the dual stream scenario from the chain rule [1] is given as

$$I(\mathbf{Y}; X_1, X_2 | \mathbf{H}) = I(\mathbf{Y}; X_1 | \mathbf{H}) + I(\mathbf{Y}; X_2 | X_1, \mathbf{H}) \quad (3.2)$$

where $\mathbf{H} = [\mathbf{h}_1 \ \mathbf{h}_2]$, \mathbf{Y} is the received symbol vector whereas X_1 and X_2 are the two symbols transmitted by the transmitter. Assuming alphabets to be Gaussian which are entropy maximizers [47], the mutual information expressions have been derived in Appendix 3A and are given as

$$I(\mathbf{Y}; X_1 | \mathbf{H}) = E_{\mathbf{H}} \left(\log_2 \left[\det \left\{ \mathbf{I} + \sigma_1^2 \mathbf{h}_1 \mathbf{h}_1^\dagger \left(N_0 \mathbf{I} + \sigma_2^2 \mathbf{h}_2 \mathbf{h}_2^\dagger \right)^{-1} \right\} \right] \right) \quad (3.3)$$

$$I(\mathbf{Y}; X_2 | X_1, \mathbf{H}) = E_{\mathbf{H}} \left(\log_2 \left(1 + \frac{\sigma_2^2}{N_0} \|\mathbf{h}_2\|^2 \right) \right) \quad (3.4)$$

Note that these expressions already exist in the literature [47] and have been rederived for the sake of completeness. Key to the optimality of

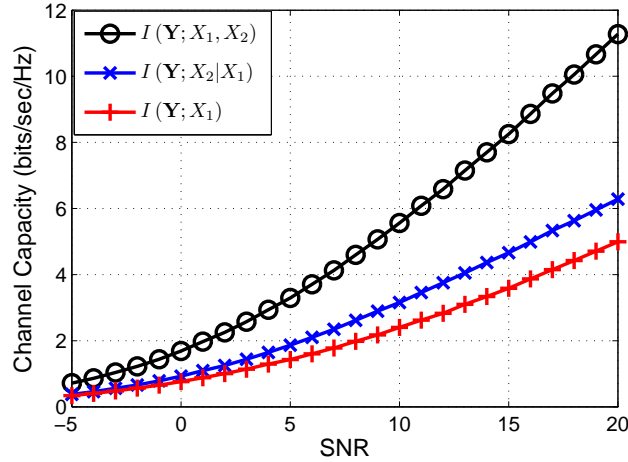


Figure 3.3: Capacity of the dual stream system for Gaussian alphabets once the channel is known at the receiver. Both streams have equal power i.e. $\sigma_1^2 = \sigma_2^2$ in (3.3) and (3.4). Note that SNR is $(\sigma_1^2 + \sigma_2^2)/N_0$

the stripping is the use of Gaussian inputs as long as the stripping decoders incorporate MMSE filters against yet undecoded streams at each successive cancellation stage. Successive stripping requires that each stream must be transmitted at a different rate with equal power thereby leading to $I(\mathbf{Y}; X_1|\mathbf{H}) < I(\mathbf{Y}; X_2|X_1, \mathbf{H})$ as shown in Fig. 3.3. We now investigate a slightly suboptimal solution where we guarantee equal rate on each stream with nonuniform power distribution between the streams for 2×2 (two streams) and 3×3 (three streams) systems. Numerical optimization revealed that equal rate, nonuniform power distribution leads to negligible suboptimality as compared to the equal power case as shown in Fig. 3.4. Fig. 3.5 shows optimal power distribution between the spatial streams with the objective of equating their rates in the successive stripping scenario. In 2×2 system, as the first stream sees interference from the second stream whereas the second stream sees no interference, so power share of the first stream increases whereas that of the second stream decreases with the increase in SNR so as to equate the rates of both the streams at each SNR value.

We now depart from the idealized Gaussian assumption and look at the effect of practical discrete constellations on the mutual information of the system. The mutual information expressions for the dual stream scenario

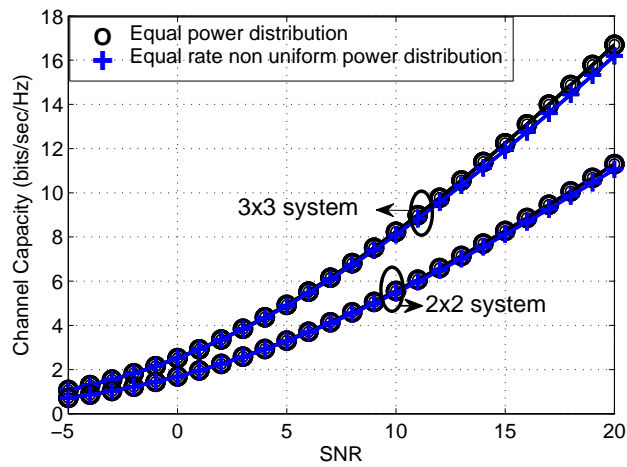


Figure 3.4: Capacity of the 2×2 and 3×3 systems for Gaussian alphabets once the channel is known at the receiver. There are two scenarios of equal power with nonuniform rate distribution between the streams and equal rate with nonuniform power distribution between the streams. Note that for the case of equal power with nonuniform rate distribution for 2×2 system, $\sigma_1^2 = \sigma_2^2$ where for the case of equal rate with nonuniform power distribution, total power is optimally divided in σ_1^2 and σ_2^2 to equate $I(\mathbf{Y}; X_1 | \mathbf{H})$ and $I(\mathbf{Y}; X_2 | X_1, \mathbf{H})$. This optimal power distribution is shown in the next figure.

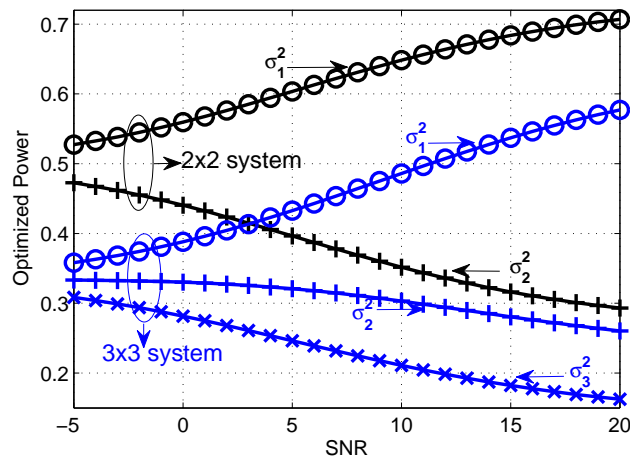


Figure 3.5: Optimized power distribution between the spatial streams. The objective is to equate their rates at each SNR value. Total power is normalized to 1.

(discrete alphabets) have been derived in Appendix 4A (in chapter 4 where two streams are assumed to be coming from two different BSs). The mutual information of the first stream is given by (4.12) while that of the second stream is given by (4.14) by interchanging the roles of X_1 and X_2 . Fig. 3.6 shows the mutual information of the first stream once the second stream is not yet decoded for different combinations of finite constellation alphabets while Fig. 3.7 shows the mutual information of the second stream once the first stream has been stripped off. Note that both the streams have equal power in these simulations. For moderate values of SNR, the mutual information of the first stream is a function of the yet undecoded second stream and this mutual information decreases as the rate (constellation size) of the second stream increases. This degradation is not observed at the low and high values of the SNR as at low SNR, both the streams are noise limited while at high SNR, the second stream can be perfectly stripped off leading to the detection of the first stream. In the moderate SNR regime, the rate of the first stream being a function of the rate of the second stream leads to nonuniform rates in the uniform power dual stream scenario thereby introducing UEP.

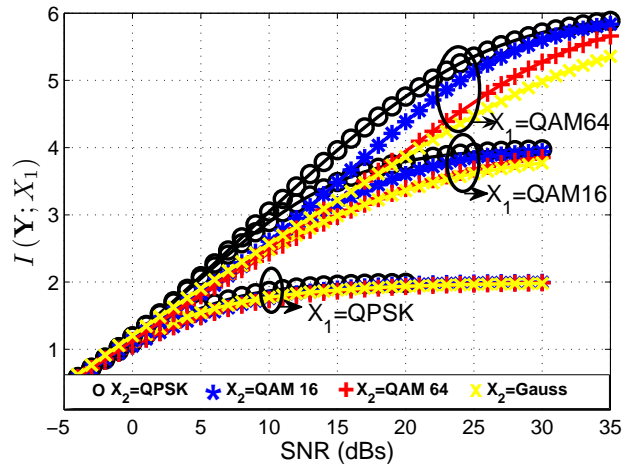


Figure 3.6: Capacity of the first stream in the dual stream scenario for finite size alphabets once the channel is known at the receiver. Both the streams have equal power. Note that SNR includes the power of both the streams.

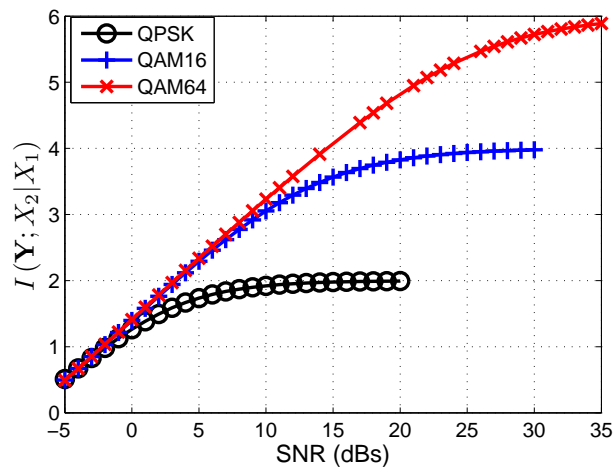


Figure 3.7: Capacity of the second stream in the dual stream scenario for finite size alphabets once the channel is known at the receiver. First stream has already been stripped off.

3.4 State of the Art Detection Schemes

In this section, we look at some of the standard off-the-shelf detectors for the multi-stream coded transmission systems. Note that most of the derivations in this section already exist in literature [43] [46] and have been reproduced here for the sake of completeness.

3.4.1 Linear MMSE Detector for SIC

MMSE criteria is a desirable criteria but the resulting Bayes estimator $E[\mathbf{x}_k|\mathbf{y}_k]$, the mean of the a posteriori distribution $p(\mathbf{x}_k|\mathbf{y}_k)$, is complicated to derive. In practice, one often resorts to low complexity estimators and the natural choice for a low complexity estimator is to restrict the estimator to be a linear function of the data which is called as linear MMSE [43]. So we shall call $\mathbf{G}_k^{MMSE}\mathbf{y}_k$ to be the linear estimate of \mathbf{x}_k where \mathbf{G}_k^{MMSE} is a $n_t \times n_r$ matrix of parameters. The MSE risk function is $E|\mathbf{x}_k - \mathbf{G}_k^{MMSE}\mathbf{y}_k|^2$. Setting the gradient equal to zero leads to

$$\begin{aligned} \nabla_{\mathbf{G}_k^{MMSE}} E|\mathbf{x}_k - \mathbf{G}_k^{MMSE}\mathbf{y}_k|^2 &= 0 \\ \nabla_{\mathbf{G}_k^{MMSE}} E\left(\mathbf{x}_k^\dagger\mathbf{x}_k - \mathbf{x}_k^\dagger\mathbf{G}_k^{MMSE}\mathbf{y}_k - \mathbf{y}_k^\dagger\mathbf{G}_k^{MMSE\dagger}\mathbf{x}_k + \mathbf{y}_k^\dagger\mathbf{G}_k^{MMSE\dagger}\mathbf{G}_k^{MMSE}\mathbf{y}_k\right) &= 0 \\ E\left(-\mathbf{x}_k\mathbf{y}_k^\dagger + \mathbf{G}_k^{MMSE}\mathbf{y}_k\mathbf{y}_k^\dagger\right) &= 0 \\ \mathbf{G}_k^{MMSE} &= \mathbf{R}_{\mathbf{x}_k\mathbf{y}_k}\mathbf{R}_{\mathbf{y}_k\mathbf{y}_k}^{-1} \end{aligned} \quad (3.5)$$

where $\nabla_{\mathbf{G}_k^{MMSE}} = \frac{\partial}{\partial(\mathbf{G}_k^{MMSE})^*}$. Note that $\mathbf{R}_{\mathbf{x}_k\mathbf{y}_k}$ indicates the correlation between \mathbf{x}_k and \mathbf{y}_k . Here we have used the relation $\nabla_{\mathbf{B}}\mathbf{a}^\dagger\mathbf{B}^\dagger\mathbf{c} = \mathbf{c}\mathbf{a}^\dagger$.

V-BLAST systems employ linear MMSE detectors [48] which are based on the same stripping and decoding principle which would be optimal for Gaussian inputs. A specific ordering for stripping needs to be enforced. Spatial streams are ordered based on their decreasing received power levels (induced by the channel or the nonuniform transmit power). Contribution of the strongest stream is detected and is subsequently subtracted leading to the detection of residual streams. In almost all the modern communication systems as 3GPP LTE [36], there is a feedback for per stream power control to achieve the performance goals. An analysis of MMSE SIC with different user power levels in the multi user context for CDMA system can be found in [37]. For the dual stream scenario, linear MMSE filter [43] based on the system equation (3.1) to detect $x_{1,k}$ from \mathbf{y}_k is given as

$$\mathbf{g}_{1,k}^{MMSE} = \mathbf{R}_{x_{1,k}\mathbf{y}_k}\mathbf{R}_{\mathbf{y}_k\mathbf{y}_k}^{-1} \quad (3.6)$$

The MMSE filter is therefore given as

$$\begin{aligned}\mathbf{g}_{1,k}^{MMSE} &= \sigma_1^2 \mathbf{h}_{1,k}^\dagger \left(\sigma_1^2 \mathbf{h}_{1,k} \mathbf{h}_{1,k}^\dagger + \sigma_2^2 \mathbf{h}_{2,k} \mathbf{h}_{2,k}^\dagger + N_0 \mathbf{I} \right)^{-1} \\ &= \sigma_1^2 \mathbf{h}_{1,k}^\dagger \left(\sigma_1^2 \mathbf{h}_{1,k} \mathbf{h}_{1,k}^\dagger + \mathbf{R}_{2,k} \right)^{-1}\end{aligned}\quad (3.7)$$

where we have defined the covariance of the second stream plus noise as $\mathbf{R}_{2,k} = \sigma_2^2 \mathbf{h}_{2,k} \mathbf{h}_{2,k}^\dagger + N_0 \mathbf{I}$. Using the matrix inversion lemma, $\mathbf{D} (\mathbf{A} + \mathbf{BCD})^{-1} = \mathbf{C}^{-1} (\mathbf{DA}^{-1} \mathbf{B} + \mathbf{C}^{-1})^{-1} \mathbf{DA}^{-1}$ [49], we get

$$\mathbf{g}_{1,k}^{MMSE} = \left(\mathbf{h}_{1,k}^\dagger \mathbf{R}_{2,k}^{-1} \mathbf{h}_{1,k} + \sigma_1^{-2} \right)^{-1} \mathbf{h}_{1,k}^\dagger \mathbf{R}_{2,k}^{-1} \quad (3.8)$$

Note that if there are n_t streams, then the MMSE filter to detect $x_{1,k}$ is same as in (3.8) with $\mathbf{R}_{2,k} = \sigma_2^2 \mathbf{h}_{2,k} \mathbf{h}_{2,k}^\dagger + \sigma_3^2 \mathbf{h}_{3,k} \mathbf{h}_{3,k}^\dagger + \cdots + \sigma_{n_t}^2 \mathbf{h}_{n_t,k} \mathbf{h}_{n_t,k}^\dagger + N_0 \mathbf{I}$. MMSE includes the noise power in the filter calculations and instead of nulling other streams, it attenuates them to the noise level and in this way controls the noise enhancement problem encountered in ZF. This technique can be interpreted as an extension of the ZF-equalization based detection to the correlated post detection interference. After the application of MMSE filter we get

$$\mathbf{g}_{1,k}^{MMSE} \mathbf{y}_k = y_k = \alpha_k x_{1,k} + z_k \quad (3.9)$$

where z_k is assumed to be zero mean Gaussian random variable with variance $N_k = \sigma_2^2 \mathbf{g}_{1,k}^{MMSE} \mathbf{h}_{2,k} \mathbf{h}_{2,k}^\dagger \mathbf{g}_{1,k}^{MMSE} + N_0 \mathbf{g}_{1,k}^{MMSE} \mathbf{g}_{1,k}^{MMSE} = \mathbf{g}_{1,k}^{MMSE} \mathbf{R}_{2,k} \mathbf{g}_{1,k}^{MMSE}$ and $\alpha_k = \mathbf{g}_{1,k}^{MMSE} \mathbf{h}_{1,k}$. As $\mathbf{R}_{2,k}$ is a positive semidefinite matrix so α_k is a positive scalar. Gaussianity has been assumed for the post detection interference (second stream) which increases the suboptimality of MMSE, notably in the case of less number of interferers. Bit metric for the i -th bit for the bit value $c_{k'}$ on the first stream is given as

$$\Lambda_1^i(\mathbf{y}_k, c_{k'}) \approx \min_{x_1 \in \chi_{1,c_{k'}}^i} \left[\frac{1}{N_k} |y_k - \alpha_k x_1|^2 \right] \quad (3.10)$$

where $\chi_{1,c_{k'}}^i$ denotes the subset of the signal set $x_1 \in \chi_1$ whose labels have the value $c_{k'} \in \{0, 1\}$ in the position i . Note that the bit LLR for the i -th bit is given as

$$\text{LLR}_1^i = \Lambda_1^i(\mathbf{y}_k, c_{k'} = 1) - \Lambda_1^i(\mathbf{y}_k, c_{k'} = 0) \quad (3.11)$$

3.4.2 Linear MMSE Detector for PIC

Instead of successive stripping, the spatial streams can be detected in parallel thereby leading to PIC. Linear MMSE filter for the PIC detection is given as [20]

$$\mathbf{G}_k^{MMSE} = \left(N_0 \mathbf{P}^{-1} + \mathbf{H}_k^\dagger \mathbf{H}_k \right)^{-1} \mathbf{H}_k^\dagger \quad (3.12)$$

where \mathbf{P} is the diagonal power distribution matrix with the diagonal as $[\sigma_1^2, \sigma_2^2]$. Application of the MMSE filter on the received signal \mathbf{y}_k leads to the biased estimate of \mathbf{x}_k , i.e. $\tilde{\mathbf{x}}_k = \mathbf{G}_k^{MMSE} \mathbf{y}_k$. It is followed by an unbiaseding operation, i.e. $\hat{\mathbf{x}}_k = \Gamma_k^{-1} \tilde{\mathbf{x}}_k$ where $\Gamma_k = \text{diag}(\mathbf{G}_k^{MMSE} \mathbf{H}_k)$. Based on the Gaussian assumption of the post detection interference, MMSE preprocessing decouples the spatial streams thereby reducing the detection complexity. The bit metric for the i -th bit for the bit value $c_{k'}$ of the symbol x_j on the j -th stream is given as

$$\Lambda_j^i(\mathbf{y}_k, c_{k'}) \approx \min_{x_j \in \chi_{j,c_{k'}}^i} \left[\frac{\gamma_j^2}{N_0} |\hat{x}_j - x_j|^2 \right] \quad (3.13)$$

for $j = 1, 2$ where γ_j is the j -th diagonal element of Γ . Note that $\mathbf{g}_{1,k}^{MMSE}$ in the previous subsection is the first row of \mathbf{G}_k^{MMSE} .

3.4.3 PEP Analysis

We now look at the performance analysis of MMSE detectors. The PEP expressions for the dual stream system and the general $n_t \times n_r$ MIMO system have been derived in Appendix 3C. The PEP between the correct codeword $\underline{\mathbf{c}}_1$ and the error codeword $\hat{\underline{\mathbf{c}}}_1$ for the dual stream case, is upper bounded as

$$\mathcal{P}_{\underline{\mathbf{c}}_1}^{\hat{\underline{\mathbf{c}}}_1} \leq \frac{1}{2} \left(\frac{4N_0}{\sigma_1^2 \check{d}_{1,\min}^2} \right)^{d_{free}(n_r-1)} \left(\frac{4}{\sigma_1^2 \check{d}_{1,\min}^2} \right)^{d_{free}} (n_r \sigma_2^2 + N_0)^{d_{free}} \quad (3.14)$$

where d_{free} is the minimum Hamming distance of the code and $d_{1,\min}^2 = \sigma_1^2 \check{d}_{1,\min}^2$ with $\check{d}_{1,\min}^2$ being the normalized minimum distance of the constellation χ_1 . (3.14) shows the diversity of $d_{free}(n_r - 1)$ which indicates the loss of one diversity order by MMSE detection in the presence of one interference (undetected stream).

For the general case of $n_t \times n_r$ MIMO system ($n_r \geq n_t$) with n_t uniform power spatial streams, the PEP of the j -th stream is upper bounded as

$$\mathcal{P}_{\mathbf{c}_j}^{\hat{\mathbf{c}}_j} \leq \frac{1}{2} \left(\frac{4N_0}{\sigma_j^2 \check{d}_{j,\min}^2} \right)^{d_{free}(n_r - n_t + 1)} \prod_{l=n_r - n_t + 2}^{n_r} \left(\frac{4\bar{\lambda}_{j,l}}{\sigma_j^2 \check{d}_{j,\min}^2} \right)^{d_{free}} \quad (3.15)$$

where $\bar{\lambda}_{j,l} = E[\lambda_{j,k,l}]$ (see eq.3.70) and σ^2 is the power of the j -th stream. This PEP upperbound demonstrates the well known result of the loss of diversity order in MMSE detection [46]. Order of the loss of diversity due to undetected streams can be interpreted as precisely the number of interferers needed to be canceled. For slow fading channels, i.e. assuming one channel realization per codeword, (3.15) is modified as

$$\mathcal{P}_{\mathbf{c}_j}^{\hat{\mathbf{c}}_j} \leq \frac{1}{2} \left(\frac{4N_0}{\sigma_j^2 \check{d}_{j,\min}^2} \right)^{n_r - n_t + 1} \prod_{l=n_r - n_t + 2}^{n_r} \frac{4\bar{\lambda}_{j,l}}{\sigma_j^2 \check{d}_{j,\min}^2} \quad (3.16)$$

3.5 Proposed Low Complexity MF Based Detection Schemes

In this section, we propose low complexity MF based detectors for the multi-stream coded systems.

3.5.1 First Approach - Dual Stream Scenario

We first consider the dual stream scenario. For the ML soft detection of the first stream x_1 , the detector calculates LLRs for all the bits that constitute x_1 by summing the Euclidean distances for the values of x_1 and x_2 for which that particular bit of x_1 is one and zero. The ML bit metric for the bit $c_{k'}$ on the first stream at the k -th subcarrier and its max log MAP approximation [4] is given as

$$\begin{aligned} \Lambda_1^i(\mathbf{y}_k, c_{k'}) &= \log p(c_{k'} | \mathbf{y}_k) \\ &\propto \log \sum_{x_1 \in \mathcal{X}_{1,c_{k'}}^i} \sum_{x_2 \in \mathcal{X}_2} p(\mathbf{y}_k | x_1, x_2) \\ &\approx \max_{x_1 \in \mathcal{X}_{1,c_{k'}}^i, x_2 \in \mathcal{X}_2} \log \frac{1}{\pi^2 N_0^2} \exp \left[-\frac{1}{N_0} \|\mathbf{y}_k - \mathbf{h}_{1,k}x_1 - \mathbf{h}_{2,k}x_2\|^2 \right] \\ &\approx \min_{x_1 \in \mathcal{X}_{1,c_{k'}}^i, x_2 \in \mathcal{X}_2} \frac{1}{N_0} \|\mathbf{y}_k - \mathbf{h}_{1,k}x_1 - \mathbf{h}_{2,k}x_2\|^2 \end{aligned} \quad (3.17)$$

(3.17) has the computational complexity of $\mathcal{O}(|\chi_1||\chi_2|)$ which can be reduced if x_1 and x_2 can be decoupled. Ignoring $\|\mathbf{y}_k\|^2$ and adding $\left| \frac{\mathbf{h}_{1,k}^\dagger \mathbf{y}_k}{\|\mathbf{h}_{1,k}\|} \right|^2$, the bit metric can be written as

$$\Lambda_1^i(\mathbf{y}_k, c_{k'}) \approx \min_{x_1 \in \chi_{1,c_{k'}}^i, x_2 \in \chi_2} \left[\left| \frac{\mathbf{h}_{1,k}^\dagger \mathbf{y}_k}{\|\mathbf{h}_{1,k}\|} \right|^2 + \|\mathbf{h}_{1,k} x_1\|^2 + \|\mathbf{h}_{2,k} x_2\|^2 - 2 \left(\frac{\mathbf{h}_{1,k}^\dagger \mathbf{y}_k x_1^*}{R} - 2 \left(x_2^* \left(\frac{\mathbf{h}_{2,k}^\dagger \mathbf{y}_k - \mathbf{h}_{2,k}^\dagger \mathbf{h}_{1,k} x_1}{R} \right) \right) \right) \right] \quad (3.18)$$

where subscript $(\cdot)_R$ indicates the real part. Let the normalized MF outputs of the first and second stream be $\bar{y}_{1,k}^N = \frac{\mathbf{h}_{1,k}^\dagger \mathbf{y}_k}{\|\mathbf{h}_{1,k}\|}$ and $\bar{y}_{2,k}^N = \frac{\mathbf{h}_{2,k}^\dagger \mathbf{y}_k}{\|\mathbf{h}_{2,k}\|}$ while $p_{21,k}^N = \frac{\mathbf{h}_{2,k}^\dagger \mathbf{h}_{1,k}}{\|\mathbf{h}_{2,k}\|}$ indicates the normalized cross correlation between the two channels. So (3.18) takes the form

$$\begin{aligned} \Lambda_1^i(\mathbf{y}_k, c_{k'}) &\approx \min_{x_1 \in \chi_{1,c_{k'}}^i, x_2 \in \chi_2} \left[\left| \bar{y}_{1,k}^N \right|^2 + \|\mathbf{h}_{1,k} x_1\|^2 - 2 \|\mathbf{h}_{1,k}\| (\bar{y}_{1,k}^N x_1^*)_R \right. \\ &\quad \left. - 2 \|\mathbf{h}_{2,k}\| (x_2^* (\bar{y}_{2,k}^N - p_{21,k}^N x_1))_R + \|\mathbf{h}_{2,k} x_2\|^2 \right] \\ &= \min_{x_1 \in \chi_{1,c_{k'}}^i} \left[\left| \bar{y}_{1,k}^N - \|\mathbf{h}_{1,k}\| x_1 \right|^2 \right. \\ &\quad \left. + \min_{x_2 \in \chi_2} \left\{ -2 \|\mathbf{h}_{2,k}\| (x_2^* (\bar{y}_{2,k}^N - p_{21,k}^N x_1))_R + \|\mathbf{h}_{2,k} x_2\|^2 \right\} \right] \quad (3.19) \end{aligned}$$

Let $\bar{y}'_{2,k}(x_1) = \bar{y}_{2,k}^N - p_{21,k}^N x_1$, which is the MF output of the second stream after removing the contribution of the first stream. Adding and subtracting $\left| \bar{y}'_{2,k}(x_1) \right|^2$, we get

$$\Lambda_1^i(\mathbf{y}_k, c_{k'}) \approx \min_{x_1 \in \chi_{1,c_{k'}}^i} \left[\left| \bar{y}_{1,k}^N - \|\mathbf{h}_{1,k}\| x_1 \right|^2 - \left| \bar{y}'_{2,k}(x_1) \right|^2 + \min_{x_2 \in \chi_2} \left\{ \left| \bar{y}'_{2,k}(x_1) - \|\mathbf{h}_{2,k}\| x_2 \right|^2 \right\} \right] \quad (3.20)$$

This metric reduces the computational complexity by marginally decoupling the two streams x_1 and x_2 . For each value of $x_1 \in \chi_{1,c_{k'}}^i$, we need to find the constellation point x_2 which minimizes (3.20). To reduce the computational complexity of finding this point, we decouple x_2 into its real and imaginary parts, i.e.

$$\left| \bar{y}'_{2,k}(x_1) - \|\mathbf{h}_{2,k}\| x_2 \right|^2 = \left(\bar{y}'_{2,k}(x_1) - \|\mathbf{h}_{2,k}\| x_2 \right)_R^2 + \left(\bar{y}'_{2,k}(x_1) - \|\mathbf{h}_{2,k}\| x_2 \right)_I^2 \quad (3.21)$$

where subscript $(\cdot)_I$ indicates the imaginary part of a complex number. Note that $\left| \bar{y}'_{2,k}(x_1) - \|\mathbf{h}_{2,k}\| x_2 \right|^2$ is the MF based metric for the second stream for a particular symbol x_1 on the first stream. The decoupling of x_2 into its real and imaginary parts reduces the search space for $x_2 \in \chi_2$ while quantization further trims down the complexity. The minimum of (3.21) can be found by much fewer operations (comparisons) as compared to the constellation size of x_2 . This complexity reduction is realized by quantizing the constellation $\|\mathbf{h}_{2,k}\| x_2$. The signs of real and imaginary parts of $\bar{y}'_{2,k}(x_1)$ specify the quadrant in which it lies thereby reducing the search space. Moreover the quantized regions of $\|\mathbf{h}_{2,k}\| x_2$ further simplify the operation of finding the minimum. For example, once x_2 belongs to QPSK, only the quadrant information of $\bar{y}'_{2,k}(x_1)$ is sufficient to find the minimum of (3.21). In case x_2 belongs to QAM16, only two comparisons of real and imaginary parts is required once the quadrant information of $\bar{y}'_{2,k}(x_1)$ is obtained by looking at the signs of its real and imaginary parts. The quantization of $\|\mathbf{h}_{2,k}\| x_2$ may even avoid these two comparisons by finding the quantized regions of the real and imaginary parts of $\|\mathbf{h}_{2,k}\| x_2$ where the real and imaginary parts of $\bar{y}'_{2,k}(x_1)$ lie.

In (3.20), $\left| \bar{y}_{1,k}^N - \|\mathbf{h}_{1,k}\| x_1 \right|^2$ is the metric for the MF output for x_1 ignoring x_2 , $\left| \bar{y}'_{2,k}(x_1) - \|\mathbf{h}_{2,k}\| x_2 \right|^2$ is the metric for the MF output for x_2 taking into account x_1 and $\left| \bar{y}'_{2,k}(x_1) \right|^2$ can be termed as the correction factor. This not only implies the reduction in complexity from $\mathcal{O}(|\chi_1| |\chi_2|)$ to $\mathcal{O}(|\chi_1|)$ but the metric being based on MF outputs is easy to compute and implement in practical systems. In the case of uniform power and nonuniform rate streams, second stream x_2 is the higher rate stream which implies substantial reduction in the complexity. Note that the employment of this low complexity MF based bit metric is limited to the dual stream scenario.

3.5.2 Second Approach - General Scenario

We now consider the general case where n_t spatial streams are transmitted in $n_t \times n_r$ system. The max log MAP bit metric for the bit $c_{k'}$ on the first stream at the k -th subcarrier is given as

$$\Lambda_1^i(\mathbf{y}_k, c_{k'}) \approx \min_{x_1 \in \chi_{1,c_{k'}}, x_2 \in \chi_2, \dots, x_{n_t} \in \chi_{n_t}} \|\mathbf{y}_k - \mathbf{h}_{1,k}x_1 - \dots - \mathbf{h}_{n_t,k}x_{n_t}\|^2 \quad (3.22)$$

(3.22) has the computational complexity of $\mathcal{O}(|\chi_1| \cdots |\chi_{n_t}|)$. Expanding further the bit metric and grouping the terms containing x_{n_t} , we get

$$\begin{aligned} \Lambda_1^i(\mathbf{y}_k, c_{k'}) &\approx \min_{x_1 \in \chi_{1,c_{k'}}, x_2 \in \chi_2, \dots, x_{n_t} \in \chi_{n_t}} \left\{ \|\mathbf{y}_k\|^2 + \sum_{j=1}^{n_t} \|\mathbf{h}_{j,k} x_j\|^2 - 2 \sum_{j=1}^{n_t} (\mathbf{y}_k^\dagger \mathbf{h}_{j,k} x_j)_R \right. \\ &\quad \left. + 2 \sum_{j=1}^{n_t-1} \sum_{l=j+1}^{n_t} (\mathbf{h}_{j,k}^\dagger \mathbf{h}_{l,k} x_j^* x_l)_R \right\} \\ &= \min_{x_1 \in \chi_{1,c_{k'}}, x_2 \in \chi_2, \dots, x_{n_t} \in \chi_{n_t}} \left\{ \|\mathbf{y}_k\|^2 + \sum_{j=1}^{n_t-1} \|\mathbf{h}_{j,k} x_j\|^2 + 2 \sum_{j=1}^{n_t-1} \sum_{l=j+1}^{n_t-1} (p_{jl,k} x_j^* x_l)_R \right. \\ &\quad \left. - 2 \sum_{j=1}^{n_t-1} (\bar{y}_{j,k}^* x_j)_R + 2 \sum_{j=1}^{n_t-1} (p_{jn_t,k} x_j^* x_{n_t})_R - 2 (\bar{y}_{n_t,k}^* x_{n_t})_R + \|\mathbf{h}_{n_t,k} x_{n_t}\|^2 \right\} \quad (3.23) \end{aligned}$$

where $\bar{y}_{j,k} = \mathbf{h}_{j,k}^\dagger \mathbf{y}_k$ is the MF output for the j -th stream and $p_{jl,k} = \mathbf{h}_{j,k}^\dagger \mathbf{h}_{l,k}$ is the cross correlation between the channels of the j -th and l -th streams at the k -th subcarrier. Breaking some of the terms in their real and imaginary parts, we have

$$\begin{aligned} \Lambda_1^i(\mathbf{y}_k, c_{k'}) &\approx \min_{x_1 \in \chi_{1,c_{k'}}, \dots, x_{n_t} \in \chi_{n_t}} \left\{ \sum_{j=1}^{n_t-1} \|\mathbf{h}_{j,k} x_j\|^2 + 2 \sum_{j=1}^{n_t-1} \sum_{l=j+1}^{n_t-1} (p_{jl,k} x_j^* x_l)_R - 2 \sum_{j=1}^{n_t-1} (\bar{y}_{j,k}^* x_j)_R \right. \\ &\quad \left. + 2 \left(\sum_{j=1}^{n_t-1} (p_{jn_t,k,R} x_{j,R} + p_{jn_t,k,I} x_{j,I}) - \bar{y}_{n_t,k,R} \right) x_{n_t,R} + \|\mathbf{h}_{n_t,k}\|^2 x_{n_t,R}^2 \right. \\ &\quad \left. + 2 \left(\sum_{j=1}^{n_t-1} (p_{jn_t,k,R} x_{j,I} - p_{jn_t,k,I} x_{j,R}) - \bar{y}_{n_t,k,I} \right) x_{n_t,I} + \|\mathbf{h}_{n_t,k}\|^2 x_{n_t,I}^2 \right\} \quad (3.24) \end{aligned}$$

For x_{n_t} belonging to **equal energy alphabets**, $\|\mathbf{h}_{n_t,k}\|^2 x_{n_t,R}^2$ and $\|\mathbf{h}_{n_t,k}\|^2 x_{n_t,I}^2$ can be ignored and the values of $x_{n_t,R}$ and $x_{n_t,I}$ which minimize (3.24) need to be in the opposite directions of $\left(\sum_{j=1}^{n_t-1} (p_{jn_t,k,R} x_{j,R} + p_{jn_t,k,I} x_{j,I}) - \bar{y}_{n_t,k,R} \right)$ and $\left(\sum_{j=1}^{n_t-1} (p_{jn_t,k,R} x_{j,I} - p_{jn_t,k,I} x_{j,R}) - \bar{y}_{n_t,k,I} \right)$ respectively thereby evading search on the alphabets of x_{n_t} and reducing one complex dimension of the system,

i.e.

$$\Lambda_1^i(\mathbf{y}_k, c_k) \approx \min_{x_1 \in \chi_{1,c_k}^i, \dots, x_{n_t-1} \in \chi_{n_t-1}} \left\{ \sum_{j=1}^{n_t-1} \|\mathbf{h}_{j,k} x_j\|^2 + 2 \sum_{j=1}^{n_t-1} \sum_{l=j+1}^{n_t-1} (p_{jl,k} x_j^* x_l)_R - 2 \sum_{j=1}^{n_t-1} (\bar{y}_{j,k}^* x_j)_R \right. \\ \left. - 2 \left| \sum_{j=1}^{n_t-1} (p_{jn_t,k,R} x_{j,R} + p_{jn_t,k,I} x_{j,I}) - \bar{y}_{n_t,k,R} \right| |x_{n_t,R}| \right. \\ \left. - 2 \left| \sum_{j=1}^{n_t-1} (p_{jn_t,k,R} x_{j,I} - p_{jn_t,k,I} x_{j,R}) - \bar{y}_{n_t,k,I} \right| |x_{n_t,I}| \right\} \quad (3.25)$$

For x_{n_t} belonging to **non equal energy alphabets**, the bit metric is same as (3.25) but $\|\mathbf{h}_{n_t,k}\|^2 |x_{n_t,R}|^2$ and $\|\mathbf{h}_{n_t,k}\|^2 |x_{n_t,I}|^2$ can no longer be ignored. The decision regarding the signs of $x_{n_t,R}$ and $x_{n_t,I}$ will be taken in the same manner as for the case of equal energy alphabets. For finding their magnitudes which minimize (3.24), it is the minimization problem of a quadratic function and these are given as

$$|x_{n_t,R}| \rightarrow \left| \frac{\sum_{j=1}^{n_t-1} (p_{jn_t,k,R} x_{j,R} + p_{jn_t,k,I} x_{j,I}) - \bar{y}_{n_t,k,R}}{\|\mathbf{h}_{n_t,k}\|^2} \right| \\ |x_{n_t,I}| \rightarrow \left| \frac{\sum_{j=1}^{n_t-1} (p_{jn_t,k,R} x_{j,I} - p_{jn_t,k,I} x_{j,R}) - \bar{y}_{n_t,k,I}}{\|\mathbf{h}_{n_t,k}\|^2} \right| \quad (3.26)$$

where \rightarrow indicates the quantization process in which amongst the finite available points, the point closest to the calculated continuous value is selected. So if x_{n_t} belongs to QAM256, then instead of searching 256 constellation points for the minimization of (3.24), the metric (3.26) reduces it to merely two operations thereby trimming down one complex dimension. This bit metric implies the reduction of one complex dimension, i.e. it reduces the complexity to $\mathcal{O}(|\chi_1| \cdots |\chi_{n_t-1}|)$. The detector of the previous subsection was limited to the dual stream scenario however this metric can be employed for any dimensionality. This reduction of complexity without any additional processing is a fundamental result of significant importance for lower dimensional systems. The intricacy in the practical implementation of a higher dimensional MIMO system due to the space (requisite antenna spacing) and technology constraints underlines the significance of complexity reduction algorithms for lower dimensional systems. Additionally this bit metric being based on the MF outputs and channel correlations imply it's straightforward hardware implementation. Using this approach, the bit metrics for different combinations of constellations for the dual stream case have been derived in Appendix 3B.

3.5.3 PEP Analysis

We now carry out the performance analysis of the proposed low complexity MF based detector. The PEP for the dual stream case has been derived in Appendix 3D and is given as

$$\mathcal{P}_{\underline{\mathbf{c}}_1}^{\hat{\mathbf{c}}_1} \leq \frac{1}{2} \left(\frac{4N_0}{\sigma_1^2 d_{1,\min}^2} \right)^{n_r d_{free}} \left(\sum_{j=0}^{d_{free}} C_j^{d_{free}} \frac{(P(\hat{x}_{2,k} \neq x_{2,k}))^j (1 - P(\hat{x}_{2,k} \neq x_{2,k}))^{d_{free}-j}}{\left(1 + \frac{\sigma_2^2 d_{2,\min}^2}{\sigma_1^2 d_{1,\min}^2}\right)^{j n_r}} \right) \quad (3.27)$$

where $C_j^{d_{free}}$ is the binomial coefficient and $P(\hat{x}_{2,k} \neq x_{2,k})$ is the uncoded probability that the output of the max log MAP detector $\hat{x}_{2,k}$ is not equal to the actual transmitted symbol $x_{2,k}$. This upper bound shows that the MF based detector achieves full diversity of the system, i.e. $n_r d_{free}$. The complexity of both the MMSE and MF based detectors is $\mathcal{O}|\chi_1|$ in the dual stream scenario, but the MF based detector is characterized by full diversity while MMSE detector loses one order of diversity. Moreover, MF based detector is based on simple MF outputs while MMSE filter calculation involves complex matrix inversion operations and it needs additional knowledge of the noise variance.

3.6 Dual Stream Broadcast Strategy

The broadcast approach in the dual stream scenario is based on UEP (*MAC-outage* [15]) and is motivated by the capacity of Gaussian broadcast channel with two users, i.e.

$$C = I(\mathbf{Y}_1; X_1) + I(\mathbf{Y}_2; X_2 | X_1) \quad (3.28)$$

where \mathbf{Y}_1 is the signal received by user-1 while \mathbf{Y}_2 is the signal received by user-2 who sees a better channel and so is able to decode and strip off the interference.

The proposed broadcast strategy incorporates the transmission of two spatial streams of uniform power and nonuniform rate and incorporates two levels of performance. The reliably decoded information rate depends on the state of the channel which is determined by monitoring the received SNR being above or below a certain threshold. The transmitter is operating at a constant power and data rate but the limited adaptability of the system

helps the users to gear up to a higher data rate as the channel conditions improve. The low priority/quality users are able to decode the low rate stream $\underline{\mathbf{x}}_1$ while the high priority/quality users are able to decode both the low and high rate streams $\underline{\mathbf{x}}_1$ and $\underline{\mathbf{x}}_2$ by successive stripping. The rates of two streams are

$$R_1 \leq I(\mathbf{Y}_1; X_1) \quad (3.29)$$

and

$$R_2 \leq I(\mathbf{Y}_2; X_2|X_1) \quad (3.30)$$

The notion of priority/quality is typically the received SNR and/or stream decoupling. Users are divided into two groups, i.e. near-in users and far-out users based on their received SNR. The lower rate stream $\underline{\mathbf{x}}_1$ is designed for lower value of SNR, i.e. SNR_1 while the higher rate stream $\underline{\mathbf{x}}_2$ is designed for higher value of SNR, i.e. SNR_2 . The received SNR of a particular user dictates two decoding options.

1. If $\text{SNR}_2 > \text{SNR} \geq \text{SNR}_1$, the user decodes $\underline{\mathbf{x}}_1$.
2. If $\text{SNR} \geq \text{SNR}_2$, the user decodes both streams, i.e. $\underline{\mathbf{x}}_1$ and $\underline{\mathbf{x}}_2$. The user first decodes low rate stream $\underline{\mathbf{x}}_1$, strips it out and then decodes high rate stream $\underline{\mathbf{x}}_2$.

This broadcast strategy can be exploited for having prioritized users or advanced services in MIMO broadcast systems and in multimedia broadcast multicast services (MBMS). For instance it can be the broadcast of 2 multimedia streams with different rates (quality) of the same data and users decoding the lower or higher rate stream depending on the received SNR. It can also be the broadcast of low and high rate streams (as audio and video) with the prioritized or high SNR users decoding both the streams while the low SNR users decoding only the low rate stream. It is also applicable to high-definition TV (HDTV) scenario where low priority/quality users are able to receive standard-definition TV (SDTV) transmission while high priority/quality users access HDTV. This idea has limited similarity to the superposition codes [50] whose signal space has a cloud/satellite topology. Cloud centers because of relatively higher distance amongst them carry information for the low quality receiver whereas better receivers having larger noise tolerance can resolve up to the actual transmitted satellite symbol within the cloud.

3.7 Extension to Higher Dimensions

We now consider a higher dimensional system which after antenna cycling transforms to $n_t \times n_r$ system. The system equation at the k -th frequency tone is written as

$$\begin{aligned} \mathbf{y}_k &= \mathbf{h}_{1,k}x_{1,k} + \mathbf{h}_{2,k}x_{2,k} + \cdots + \mathbf{h}_{n_t,k}x_{n_t,k} + \mathbf{z}_k \\ \mathbf{y}_k &= \mathbf{H}_k\mathbf{x}_k + \mathbf{z}_k \end{aligned} \quad (3.31)$$

The detection complexity in the case of MMSE detector is $\mathcal{O}(|\chi|)$. However, MMSE detector suffers from a loss of diversity order which is dictated by the number of interferers (undetected streams). On the other hand, MF based detector has a complexity of $\mathcal{O}(|\chi|^{n_t-1})$ while it is characterized by full diversity. We now propose a hybrid detection algorithm which exploits the full diversity of MF based detector and the low complexity of MMSE detector. The key idea is to lower the detection complexity at the cost of reduced diversity order for good streams and to enhance the diversity order at the cost of increased detection complexity for poor streams. Good streams are those spatial streams which have either been imparted higher power or lower rate at the transmitter or they have benefited from good channel realizations thereby resulting into higher SNRs. On the other hand, poor streams are those spatial streams which have either been imparted lower power or higher rates at the transmitter or they have suffered from poor channel realizations and consequently have lower SNRs. The maximum number of spatial streams being restricted to four in future wireless systems as 3GPP LTE [5] and WiMax [8] allows to use a hybrid combination of MMSE and MF based detector without increasing the complexity of detection beyond $\mathcal{O}(|\chi|)$. Basis of the algorithm is to use MMSE detectors for good streams followed by the stripping so as to reduce the dimensionality of the system to $(2 \times n_r)$ and then use the low complexity MF based detector for comparatively poor streams. In the system with n_t spatial streams ($n_t \leq 4$ in view of 3GPP LTE), $(n_t - 2)$ streams at the receiver will be detected by MMSE based SIC detection. These detected streams after being stripped off will reduce the system dimensionality to $2 \times n_r$ for which low complexity MF based detector will be employed. We now look at the two cases of fast and slow fading channels.

3.7.1 Fast Fading Channel

In the fast fading environment, MF based detector will have a diversity of $d_{free}n_r$ while MMSE detection will have reduced diversity of $d_{free}(n_r - n_t + 1)$.

As each spatial stream sees multiple realizations of the channel, so categorization of good and bad streams as per channel realization is not feasible. Consequently the classification of good and bad streams is based on the nonuniform power or rate distribution between the spatial streams at the transmitter. The spatial streams being detected by the MMSE detectors are detected first and are characterized by lower diversity order. Therefore these streams will be imparted either higher powers or lower rates as compared to the streams which will be subsequently detected by the MF based detector and will enjoy higher diversity order. Power or rate distribution between the streams is optimized to equate the error rates on the spatial streams at all decoding levels. The algorithm therefore successfully escapes the exponential complexity of MIMO detection and the degraded performance of MMSE detectors.

3.7.2 Slow Fading Channels

In a slow fading channel where each codeword spans one realization of the channel, MMSE detection will have a diversity of $(n_r - n_t + 1)$ while MF based detector will have a diversity of n_r . As each spatial stream sees one realization of the channel, so the categorization of good and bad streams as per channel realization is feasible. We consider V-BLAST criteria [48] by simply ordering the streams as per the decreasing post detection SNR. This approach is termed as the “best first” cancellation approach within the multiuser community. The spatial streams to be detected by the MMSE filter are decided by choosing the rows of MMSE filter with the smallest norms. Depending on the system parameters, a threshold for the row norm of the MMSE filter can be decided as a criteria for the detection using MMSE filters. These streams after being detected are stripped off leading to the detection by the MF based detector.

3.8 Simulations

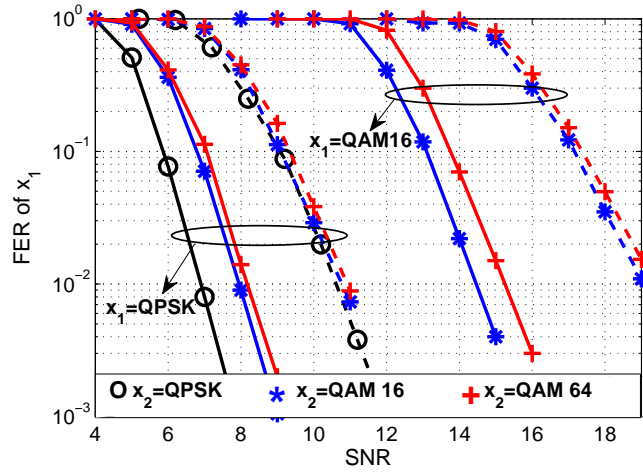
We consider a BICM MIMO OFDM system using the *de facto* standard, 64 state rate-1/2 convolutional encoder of 802.11n standard [7] and rate-1/3 punctured turbo code of 3GPP LTE¹ [36]. The MIMO channel has iid Gaussian matrix entries with unit variance while perfect CSI at the receiver is assumed. Furthermore, all mappings of the coded bits to QAM symbols

¹The LTE turbo decoder design was performed using the coded modulation library www.iterativesolutions.com

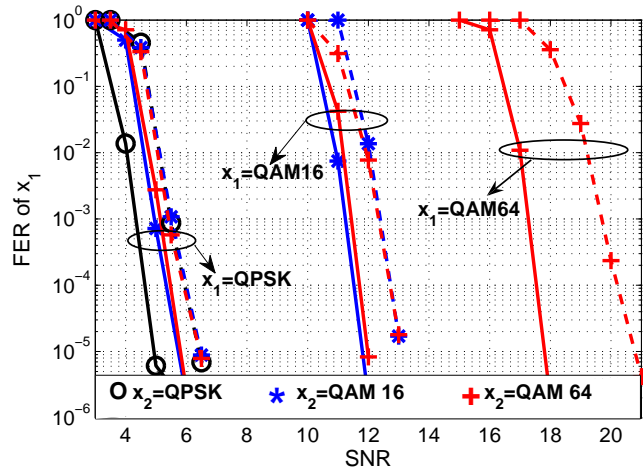
use Gray encoding. The upcoming WLAN standard 802.11n [7] supports the codeword sizes of 648, 1296, and 1944 bits. For our purposes, we selected the codeword size of 1296 bits for the first stream and the coding schemes of convolutional coding of 802.11n [7] and turbo coding of 3GPP LTE [36]. We consider three scenarios. First scenario is of the spatial streams characterized by uniform power and nonuniform rate while second scenario concerns the spatial streams characterized by nonuniform power and uniform rate. Both of these scenarios focus on the fast fading environment. Third scenario is about the spatial streams with uniform power and uniform rate in the slow fading environment.

In the first scenario, two spatial streams of uniform power and nonuniform rate are transmitted in 2×2 MIMO system. The channel is fast fading and is independently generated for each channel use. For detection, we consider SIC based detection in which the lower rate stream is detected first and is subsequently stripped off leading to the detection of the higher rate stream while for detectors, we consider the low complexity MF based detector and the MMSE detector. We focus on the frame error rate (FER) of the first stream as subsequent to stripping, the detection of the second stream is trivial (using SIMO detectors). Fig. 3.8 shows the improved performance of the MF based detector as compared to the MMSE detector. Degradation of the performance of the first stream as the rate (constellation size) of the second stream increases confirms the earlier result of section 3.3 that the rate of the first stream is a function of the rate of the second stream (for finite alphabets). The improvement in the performance for MF based detector is attributed to the partial decoding of the second stream [29]. The performance gap with respect to the MMSE detector decreases as the second stream grows in the constellation size. This trend can be attributed to the proximity of the behavior of these larger constellations to Gaussianity due to their high peak to average power ratio and further to the optimality of MMSE detection for Gaussian alphabets. The simulation results also show that MMSE detection is independent of the rate of the second stream. These results confirm the earlier findings of PEP analysis.

In the second scenario, the spatial streams of uniform rate and nonuniform power are transmitted in 2×2 and 3×3 MIMO systems. The channel is fast fading and is independently generated for each channel use. We focus on the FER of the system which is based on successive stripping. We again consider the low complexity MF based detector and MMSE detector. With P_T being the total power available, the power distribution between the streams is optimized to equate their rates in the desired SNR region where SNR is defined as the received SNR per antenna, i.e. $\frac{P_T}{N_0}$. In 2×2 system,



(a)

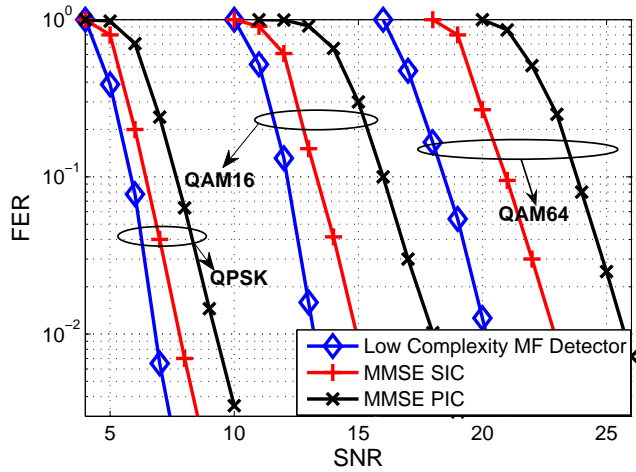


(b)

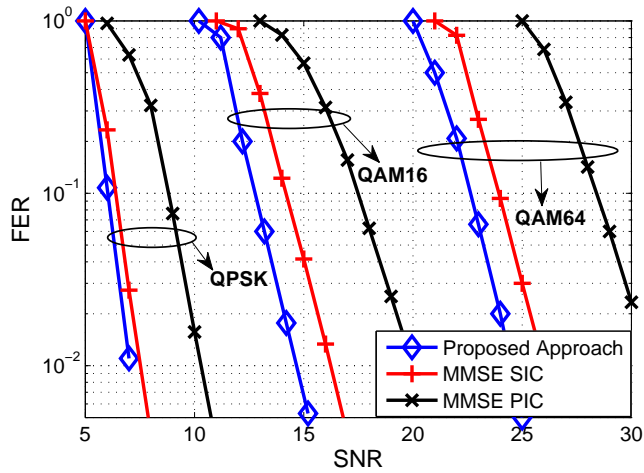
Figure 3.8: Performance of the first stream in 2×2 system. The channel is fast fading. Continuous lines indicate low complexity MF based detector while dashed lines indicate MMSE detector. Fig.(a) uses convolutional code while Fig.(b) employs 3GPP LTE turbo code.

the higher power stream is detected first and is subsequently stripped off leading to the detection of the lower power stream. In a 3×3 system, the proposed hybrid approach is based on the detection of the first stream by the MMSE filter which is then subsequently stripped off thereby reducing the dimensionality of the system to 2×3 . Then the low complexity MF based detector is used to detect the second stream while the last stream is detected by the standard SIMO detector. In MMSE SIC approach, first and second streams are successively detected and stripped off by MMSE filters leading to the detection of third stream by the SIMO detectors. As a reference, MMSE PIC has also been considered in which uniform power spatial streams are independently detected using MMSE filters. Fig. 3.9 shows the improved performance of the low complexity MF based detector (Fig.a) and the proposed hybrid approach (Fig.b) with respect to both MMSE SIC and MMSE PIC approaches. The proposed approach not only has higher coding gain but is also characterized by higher diversity as compared to the MMSE based approaches. Gains of the proposed hybrid approach with respect to MMSE SIC detection will keep reducing as the dimensionality of the system proliferates due to the detection of more streams by MMSE filters in the proposed approach.

In the third scenario, we consider uniform power and uniform rate streams transmitted in 4×4 MIMO system. The channel is slow fading, i.e. it remains constant for the duration of one codeword while it changes independently between the codewords. Different spatial streams therefore experience different SNRs as each stream sees a different realization of the channel. As per the hybrid approach, the two spatial streams to be detected by the MMSE filter are decided by choosing the rows of the MMSE filter with the smallest norms. These two streams after being detected are stripped off leading to the detection of the third stream by the MF based detector. Last stream is detected by the standard SIMO detector. Fig. 3.10 indicates the improved performance both in terms of FER and diversity of the proposed approach with respect to that of MMSE based approaches. MF based detector indicates that all streams are detected by MF based detector while MMSE detector indicates that all streams are detected by MMSE detector. The proposed approach being the fusion of the MMSE and the MF based detector, has improved diversity than that of MMSE detector while diversity order is less than that of MF based detector.

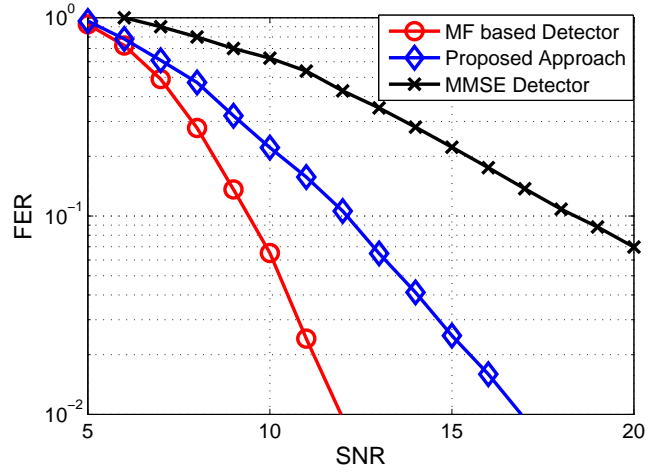


(a)

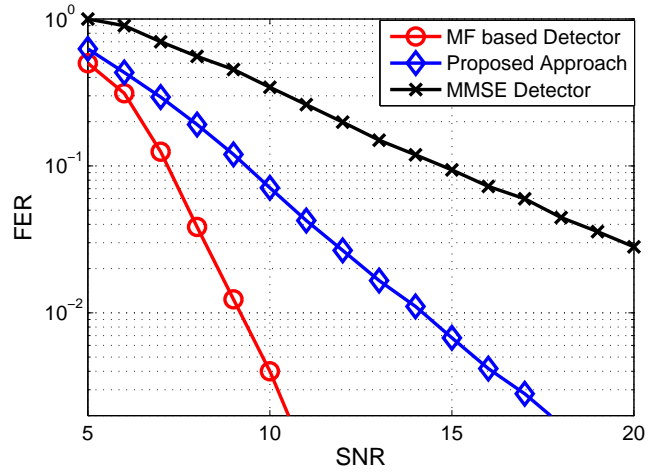


(b)

Figure 3.9: 2×2 and 3×3 systems with uniform rate and nonuniform power spatial streams. The channel is fast fading while convolutional code is used. Fig.(a) shows the performance in 2×2 system while Fig.(b) shows the performance in 3×3 system.



(a)



(b)

Figure 3.10: 4×4 MIMO system with four spatial streams using QPSK. The channel is slow fading. Fig.(a) uses convolutional code while Fig.(b) employs 3GPP LTE turbo code.

3.9 Conclusions

In this chapter, we have primarily focused on the dual stream scenario in SU MIMO systems. We have presented a novel low complexity MF based detector which successfully reduces one complex dimension of the system. The proposed detector is based on the MF outputs and is therefore suitable for the hardware implementation. This detector is characterized by full diversity and higher coding gain as compared to the standard linear equalizer based solutions as MMSE detector which has lower diversity and coding gain. Exploiting the UEP of the dual stream scenario, a broadcast strategy has also been proposed to prioritize different data streams to different users. We have further extended the low complexity detection to higher dimensional systems by a hybrid detection approach encompassing the MF based detector and the MMSE detector. This approach is based on the nonuniform power or rate distribution between the spatial streams so as to equate error rates on each decoding level.

3.A Mutual Information for Dual Stream Scenario

Considering alphabets to be Gaussian, the explicit expressions of the mutual information in (3.2) are

$$\begin{aligned}
I(\mathbf{Y}; X_1 | \mathbf{H}) &= \mathcal{H}(\mathbf{Y} | \mathbf{H}) - \mathcal{H}(\mathbf{Y} | X_1, \mathbf{H}) \\
&= \mathcal{H}(\mathbf{h}_1 x_1 + \mathbf{h}_2 x_2 + \mathbf{z} | \mathbf{H}) - \mathcal{H}(\mathbf{h}_2 x_2 + \mathbf{z} | \mathbf{H}) \\
&= \log_2 \left[\frac{\det(\sigma_1^2 \mathbf{h}_1 \mathbf{h}_1^\dagger + \sigma_2^2 \mathbf{h}_2 \mathbf{h}_2^\dagger + N_0 \mathbf{I})}{\det(\sigma_2^2 \mathbf{h}_2 \mathbf{h}_2^\dagger + N_0 \mathbf{I})} \right] \\
&= E_{\mathbf{H}} \left(\log_2 \left[\det \left\{ \mathbf{I} + \sigma_1^2 \mathbf{h}_1 \mathbf{h}_1^\dagger \left(N_0 \mathbf{I} + \sigma_2^2 \mathbf{h}_2 \mathbf{h}_2^\dagger \right)^{-1} \right\} \right] \right) \quad (3.32)
\end{aligned}$$

where \dagger indicates conjugate transpose while $\mathcal{H}(\cdot) = -E \log p(\cdot)$ is the entropy function. Note that the entropy of a complex multivariate Gaussian random variable with covariance matrix \mathbf{Q} is $\log_2 [(2\pi e)^n \det(\mathbf{Q})]$. In (3.32), we have used the relation $\det(\mathbf{C} + \mathbf{A}\mathbf{B}) = \det(\mathbf{C})\det(\mathbf{I} + \mathbf{B}\mathbf{C}^{-1}\mathbf{A})$. Simi-

larly

$$\begin{aligned}
I(\mathbf{Y}; X_2 | X_1, \mathbf{H}) &= \mathcal{H}(\mathbf{Y} | X_1, \mathbf{H}) - \mathcal{H}(\mathbf{Y} | X_1, X_2, \mathbf{H}) \\
&= \mathcal{H}(\mathbf{h}_2 x_2 + \mathbf{z} | \mathbf{H}) - \mathcal{H}(\mathbf{z} | \mathbf{H}) \\
&= \log_2 \left[\frac{\det(\sigma_2^2 \mathbf{h}_2 \mathbf{h}_2^\dagger + N_0 \mathbf{I})}{\det(N_0 \mathbf{I})} \right] \\
&= E_{\mathbf{h}_2} \left(\log_2 \left(1 + \frac{\sigma_2^2}{N_0} \|\mathbf{h}_2\|^2 \right) \right) \tag{3.33}
\end{aligned}$$

where we have used the fact that the eigenvalues of $(\sigma_2^2 \mathbf{h}_2 \mathbf{h}_2^\dagger + N_0 \mathbf{I})$ are

$$\lambda_j(\sigma_2^2 \mathbf{h}_2 \mathbf{h}_2^\dagger + N_0 \mathbf{I}) = \begin{cases} (\sigma_2^2 \|\mathbf{h}_2\|^2 + N_0), & j = 1 \\ N_0, & j = 2, \dots, n_r \end{cases} \tag{3.34}$$

while $\det(N_0 \mathbf{I}) = N_0^{n_r}$.

3.B Low Complexity Bit Metrics

For the dual stream scenario, the max log MAP bit metric for the bit $c_{k'}$ of the first stream x_1 is given as

$$\begin{aligned}
\Lambda_1^i(\mathbf{y}_k, c_{k'}) &\approx \min_{x_1 \in \mathcal{X}_{1,c_{k'}}^i, x_2 \in \mathcal{X}_2} \left\{ \|\mathbf{h}_{1,k} x_1\|^2 + \|\mathbf{h}_{2,k}\|^2 x_{2,R}^2 + \|\mathbf{h}_{2,k}\|^2 x_{2,I}^2 - 2(\bar{y}_{1,k}^* x_1)_R \right. \\
&\quad \left. + 2(p_{12,k,R} x_{1,R} + p_{12,k,I} x_{1,I} - \bar{y}_{2,k,R}) x_{2,R} + 2(p_{12,k,R} x_{1,I} - p_{12,k,I} x_{1,R} - \bar{y}_{2,k,I}) x_{2,I} \right\} \tag{3.35}
\end{aligned}$$

where $\bar{y}_{1,k} = \mathbf{h}_{1,k}^\dagger \mathbf{y}_k$ and $p_{12,k} = \mathbf{h}_{1,k}^\dagger \mathbf{h}_{2,k}$. For x_2 belonging to **equal energy alphabets**, the bit metric is given as

$$\begin{aligned}
\Lambda_1^i(\mathbf{y}_k, c_{k'}) &\approx \min_{x_1 \in \mathcal{X}_{1,c_{k'}}^i} \left\{ \|\mathbf{h}_{1,k} x_1\|^2 - 2|p_{12,k,R} x_{1,R} + p_{12,k,I} x_{1,I} - \bar{y}_{2,k,R}| |x_{2,R}| \right. \\
&\quad \left. - 2(\bar{y}_{1,k}^* x_1)_R - 2|p_{12,k,R} x_{1,I} - p_{12,k,I} x_{1,R} - \bar{y}_{2,k,I}| |x_{2,I}| \right\} \tag{3.36}
\end{aligned}$$

whereas for x_2 belonging to **non equal energy alphabets**, the magnitudes of its real and imaginary parts which minimize the bit metric are given as

$$\begin{aligned} |x_{2,R}| &\rightarrow \left| \frac{p_{12,k,R}x_{1,R} + p_{12,k,I}x_{1,I} - \bar{y}_{2,k,R}}{\|\mathbf{h}_{2,k}\|^2} \right| \\ |x_{2,I}| &\rightarrow \left| \frac{p_{12,k,R}x_{1,I} - p_{12,k,I}x_{1,R} - \bar{y}_{2,k,I}}{\|\mathbf{h}_{2,k}\|^2} \right| \end{aligned} \quad (3.37)$$

We now derive the low complexity bit metrics for different combinations of constellations (Fig. 2.2) basing on the equations (3.35), (3.36) and (3.37). Note that these bit metrics are based on the MF outputs and are devoid of any division operation and therefore can be easily implemented in the hardware. For the ease of notation, we drop the subcarrier index. Let

$$\psi_A = p_{12,R}x_{1,R} + p_{12,I}x_{1,I} - \bar{y}_{2,R} \quad (3.38)$$

$$\psi_B = p_{12,R}x_{1,I} - p_{12,I}x_{1,R} - \bar{y}_{2,I} \quad (3.39)$$

3.B.1 QPSK-QPSK

QPSK being equal energy alphabets, LLR for the first bit of the first stream is written as

$$\begin{aligned} \text{LLR}_1^1 &\approx \min_{\substack{x_{1,R} = \frac{\sigma_1}{\sqrt{2}} \\ x_{1,I}}} \{-\bar{y}_{1,I}x_{1,I} - |\psi_A| |x_{2,R}| - |\psi_B| |x_{2,I}|\} - \min_{\substack{x_{1,R} = \frac{-\sigma_1}{\sqrt{2}} \\ x_{1,I}}} \{-\bar{y}_{1,I}x_{1,I} - |\psi_A| |x_{2,R}| - |\psi_B| |x_{2,I}|\} \\ &\quad - \sqrt{2}\sigma_1 y_{1,R} \end{aligned} \quad (3.40)$$

LLR for the second bit of the first stream is written as

$$\begin{aligned} \text{LLR}_1^2 &\approx \min_{\substack{x_{1,I} = \frac{\sigma_1}{\sqrt{2}} \\ x_{1,R}}} \{-\bar{y}_{1,R}x_{1,R} - |\psi_A| |x_{2,R}| - |\psi_B| |x_{2,I}|\} - \min_{\substack{x_{1,I} = \frac{-\sigma_1}{\sqrt{2}} \\ x_{1,R}}} \{-\bar{y}_{1,R}x_{1,R} - |\psi_A| |x_{2,R}| - |\psi_B| |x_{2,I}|\} \\ &\quad - \sqrt{2}\sigma_1 y_{1,I} \end{aligned} \quad (3.41)$$

3.B.2 QAM16-QAM16

The values of $x_{2,R}$ and $x_{2,I}$ for the case of QAM16 are $\left[\frac{\sigma_2}{\sqrt{10}}, \frac{-\sigma_2}{\sqrt{10}}, \frac{3\sigma_2}{\sqrt{10}}, \frac{-3\sigma_2}{\sqrt{10}} \right]$. So the magnitudes of $x_{2,R}$ and $x_{2,I}$ which minimize the bit metric for the

first stream are given as

$$\begin{aligned} |x_{2,R}| &= \sigma_2 \frac{1}{\sqrt{10}} \left(2 + (-1)^{I\left(|\psi_A| < \sigma_2 \frac{2\|\mathbf{h}_2\|^2}{\sqrt{10}}\right)} \right) \\ |x_{2,I}| &= \sigma_2 \frac{1}{\sqrt{10}} \left(2 + (-1)^{I\left(|\psi_B| < \sigma_2 \frac{2\|\mathbf{h}_2\|^2}{\sqrt{10}}\right)} \right) \end{aligned} \quad (3.42)$$

where $I(\cdot)$ is the indicator function defined as

$$I(a < b) = \begin{cases} 1 & \text{if } a < b \\ 0 & \text{otherwise} \end{cases} \quad (3.43)$$

Let us denote

$$A_m = \|\mathbf{h}_1\|^2 x_{1,m}^2 - 2\bar{y}_{1,R}x_{1,R} - 2\bar{y}_{1,I}x_{1,I} - 2|\psi_A||x_{2,R}| - 2|\psi_B||x_{2,I}| + \|\mathbf{h}_2\|^2|x_2|^2$$

where $m = R$ or I .

LLR for the first bit of the first stream is given as

$$\text{LLR}_1^1 \approx \min_{\substack{x_{1,R} = \frac{\sigma_1}{\sqrt{10}}, \frac{3\sigma_1}{\sqrt{10}} \\ x_{1,I}}} \left\{ A_R + \|\mathbf{h}_1\|^2 x_{1,I}^2 \right\} - \min_{\substack{x_{1,R} = \frac{-\sigma_1}{\sqrt{10}}, \frac{-3\sigma_1}{\sqrt{10}} \\ x_{1,I}}} \left\{ A_R + \|\mathbf{h}_1\|^2 x_{1,I}^2 \right\} \quad (3.44)$$

LLR for the second bit is

$$\text{LLR}_1^2 \approx \min_{\substack{x_{1,R} = \frac{3\sigma_1}{\sqrt{10}}, \frac{-3\sigma_1}{\sqrt{10}} \\ x_{1,I}}} \left\{ A_I \right\} - \min_{\substack{x_{1,R} = \frac{\sigma_1}{\sqrt{10}}, \frac{-\sigma_1}{\sqrt{10}} \\ x_{1,I}}} \left\{ A_I \right\} + \frac{8\|\mathbf{h}_1\|^2\sigma_1^2}{10} \quad (3.45)$$

LLR for the third bit is given as

$$\text{LLR}_1^3 \approx \min_{\substack{x_{1,I} = \frac{\sigma_1}{\sqrt{10}}, \frac{3\sigma_1}{\sqrt{10}} \\ x_{1,R}}} \left\{ A_I + \|\mathbf{h}_1\|^2 x_{1,R}^2 \right\} - \min_{\substack{x_{1,I} = \frac{-\sigma_1}{\sqrt{10}}, \frac{-3\sigma_1}{\sqrt{10}} \\ x_{1,R}}} \left\{ A_I + \|\mathbf{h}_1\|^2 x_{1,R}^2 \right\} \quad (3.46)$$

LLR for the fourth bit is given as

$$\text{LLR}_1^4 \approx \min_{\substack{x_{1,I} = \frac{3\sigma_1}{\sqrt{10}}, \frac{-3\sigma_1}{\sqrt{10}} \\ x_{1,R}}} \left\{ A_R \right\} - \min_{\substack{x_{1,I} = \frac{\sigma_1}{\sqrt{10}}, \frac{-\sigma_1}{\sqrt{10}} \\ x_{1,R}}} \left\{ A_R \right\} + \frac{8\|\mathbf{h}_1\|^2\sigma_1^2}{10} \quad (3.47)$$

3.B.3 QAM64-QAM64

For QAM64 case, the derivation of bit metric is on similar lines as that of QAM16 however the magnitudes of $x_{2,R}$ and $x_{2,I}$ which minimize the bit metric (3.35) are given as

$$|x_{2,R}| = \sigma_2 \frac{1}{\sqrt{42}} \left\{ 4 + (-1)^{I\left(|\psi_A| < \sigma_2 \frac{4\|\mathbf{h}_2\|^2}{\sqrt{42}}\right)} + 2(-1)^{I\left(|\psi_A| < \sigma_2 \frac{2\|\mathbf{h}_2\|^2}{\sqrt{42}}\right)} \right. \\ \left. \times \left[I\left(|\psi_A| < \sigma_2 \frac{2\|\mathbf{h}_2\|^2}{\sqrt{42}}\right) \parallel I\left(|\psi_A| > \sigma_2 \frac{6\|\mathbf{h}_2\|^2}{\sqrt{42}}\right) \right] \right\} \\ |x_{2,I}| = \sigma_2 \frac{1}{\sqrt{42}} \left\{ 4 + (-1)^{I\left(|\psi_B| < \sigma_2 \frac{4\|\mathbf{h}_2\|^2}{\sqrt{42}}\right)} + 2(-1)^{I\left(|\psi_B| < \sigma_2 \frac{2\|\mathbf{h}_2\|^2}{\sqrt{42}}\right)} \right. \\ \left. \times \left[I\left(|\psi_B| < \sigma_2 \frac{2\|\mathbf{h}_2\|^2}{\sqrt{42}}\right) \parallel I\left(|\psi_B| > \sigma_2 \frac{6\|\mathbf{h}_2\|^2}{\sqrt{42}}\right) \right] \right\}$$

where $I(\cdot)$ is the indicator function defined by (3.43) and \parallel indicates OR operation.

3.B.4 QAM16-QPSK

x_2 being from equal energy alphabet, we can ignore $\|\mathbf{h}_2 x_2\|^2$. Let us denote

$$B_m = \|\mathbf{h}_1\|^2 x_{1,m}^2 - 2\bar{y}_{1,R} x_{1,R} - 2\bar{y}_{1,I} x_{1,I} - 2|\psi_A| |x_{2,R}| - 2|\psi_B| |x_{2,I}|$$

where $m = R$ or I .

LLR for the first bit of the first stream (QAM16) is then given as

$$\text{LLR}_1^1 \approx \min_{\substack{x_{1,R} = \frac{\sigma_1}{\sqrt{10}}, \frac{3\sigma_1}{\sqrt{10}} \\ x_{1,I}}} \left\{ B_R + \|\mathbf{h}_1\|^2 x_{1,R}^2 \right\} - \min_{\substack{x_{1,R} = \frac{\sigma_1}{\sqrt{10}}, \frac{3\sigma_1}{\sqrt{10}} \\ x_{1,I}}} \left\{ B_R + \|\mathbf{h}_1\|^2 x_{1,I}^2 \right\} \quad (3.48)$$

LLR for the second bit is given as

$$\text{LLR}_1^2 \approx \min_{\substack{x_{1,R} = \frac{3\sigma_1}{\sqrt{10}}, \frac{-3\sigma_1}{\sqrt{10}} \\ x_{1,I}}} \{B_I\} - \min_{\substack{x_{1,R} = \frac{\sigma_1}{\sqrt{10}}, \frac{-\sigma_1}{\sqrt{10}} \\ x_{1,I}}} \{B_I\} + \frac{8\sigma_1^2 \|\mathbf{h}_1\|^2}{10} \quad (3.49)$$

LLR for the third bit is given as

$$\text{LLR}_1^3 \approx \min_{\substack{x_{1,I} = \frac{\sigma_1}{\sqrt{10}}, \frac{3\sigma_1}{\sqrt{10}} \\ x_{1,R}}} \left\{ B_I + \|\mathbf{h}_1\|^2 x_{1,R}^2 \right\} - \min_{\substack{x_{1,I} = \frac{\sigma_1}{\sqrt{10}}, \frac{3\sigma_1}{\sqrt{10}} \\ x_{1,R}}} \left\{ B_I + \|\mathbf{h}_1\|^2 x_{1,R}^2 \right\} \quad (3.50)$$

LLR for the fourth bit is given as

$$\text{LLR}_1^4 \approx \min_{\substack{x_{1,I} = \frac{3\sigma_1}{\sqrt{10}}, \frac{-3\sigma_1}{\sqrt{10}} \\ x_{1,R}}} \{B_R\} - \min_{\substack{x_{1,I} = \frac{\sigma_1}{\sqrt{10}}, \frac{-\sigma_1}{\sqrt{10}} \\ x_{1,R}}} \{B_R\} + \frac{8\sigma_1^2 \|\mathbf{h}_1\|^2}{10} \quad (3.51)$$

Now we consider the case of QPSK (Note that $x_1 = \text{QAM16}$ and $x_2 = \text{QPSK}$). For the sake of brevity, let us define

$$\psi_C = p_{12,R}x_{2,R} - p_{12,I}x_{2,I} - \bar{y}_{1,R} \quad (3.52)$$

$$\psi_D = p_{12,R}x_{2,I} + p_{12,I}x_{2,R} - \bar{y}_{1,I} \quad (3.53)$$

The values of $|x_{1,R}|$ and $|x_{1,I}|$ which minimize the bit metric for the second stream are given as

$$\begin{aligned} |x_{1,R}| &= \sigma_1 \frac{1}{\sqrt{10}} \left(2 + (-1)^I \left(|\psi_C| < \sigma_1 \frac{2\|\mathbf{h}_1\|^2}{\sqrt{10}} \right) \right) \\ |x_{1,I}| &= \sigma_1 \frac{1}{\sqrt{10}} \left(2 + (-1)^I \left(|\psi_D| < \sigma_1 \frac{2\|\mathbf{h}_1\|^2}{\sqrt{10}} \right) \right) \end{aligned} \quad (3.54)$$

Let us denote

$$C_m = \|\mathbf{h}_1\|^2 |x_{1,R}|^2 + \|\mathbf{h}_1\|^2 |x_{1,I}|^2 - 2\bar{y}_{2,m}x_{2,m} - 2|\psi_C| |x_{1,R}| - 2|\psi_D| |x_{1,I}| \quad (3.55)$$

where $m = R$ or I .

So LLR for the first bit of the second stream (QPSK) is given as

$$\text{LLR}_2^1 \approx \min_{\substack{x_{2,R} = \frac{\sigma_2}{\sqrt{2}} \\ x_{2,I}}} \{C_I\} - \min_{\substack{x_{2,R} = \frac{-\sigma_2}{\sqrt{2}} \\ x_{2,I}}} \{C_I\} - 2\sqrt{2}\sigma_2\bar{y}_{2,R} \quad (3.56)$$

LLR for the second bit is given as

$$\text{LLR}_2^2 \approx \min_{\substack{x_{2,I} = \frac{\sigma_2}{\sqrt{2}} \\ x_{2,R}}} \{C_R\} - \min_{\substack{x_{2,I} = \frac{-\sigma_2}{\sqrt{2}} \\ x_{2,R}}} \{C_R\} - 2\sqrt{2}\sigma_2\bar{y}_{2,I} \quad (3.57)$$

3.C PEP Analysis of MMSE Detector

We first consider the performance analysis of the MMSE detector for the dual stream scenario. This analysis is based on the Gaussian assumption of the post detection interference. Bit metric for the bit $c_{k'}$ on the first stream as in (3.10) is given as

$$\Lambda_1^i(\mathbf{y}_k, c_{k'}) \approx \min_{x_1 \in \chi_{1,c_{k'}}^i} \left[\frac{1}{N_k} |y_k - \alpha_k x_1|^2 \right] \quad (3.58)$$

The conditional PEP between the correct codeword $\underline{\mathbf{c}}_1$ and the error codeword $\hat{\underline{\mathbf{c}}}_1$, i.e. $P(\underline{\mathbf{c}}_1 \rightarrow \hat{\underline{\mathbf{c}}}_1 | \overline{\overline{\mathbf{H}}}) = \mathcal{P}_{\underline{\mathbf{c}}_1 | \overline{\overline{\mathbf{H}}}}^{\hat{\underline{\mathbf{c}}}_1}$ is given as

$$\mathcal{P}_{\underline{\mathbf{c}}_1 | \overline{\overline{\mathbf{H}}}}^{\hat{\underline{\mathbf{c}}}_1} = P \left(\sum_{k'} \min_{x_1 \in \mathcal{X}_{1,c_{k'}}^i} \frac{1}{N_k} |y_k - \alpha_k x_1|^2 \geq \sum_{k'} \min_{x_1 \in \mathcal{X}_{1,\hat{c}_{k'}}^i} \frac{1}{N_k} |y_k - \alpha_k x_1|^2 \right) \quad (3.59)$$

where $\overline{\overline{\mathbf{H}}} = [\mathbf{H}_1 \cdots \mathbf{H}_N]$ is the channel for the transmission of the codeword $\underline{\mathbf{c}}_1$. Assume $d(\underline{\mathbf{c}}_1 - \hat{\underline{\mathbf{c}}}_1) = d_{free}$ for $\underline{\mathbf{c}}_1$ and $\hat{\underline{\mathbf{c}}}_1$ under consideration for PEP analysis, which is the worst case scenario between any two codewords as d_{free} is the minimum Hamming distance of the code. Therefore, inequality in (3.59) shares the same terms on all but d_{free} summation points for which $\hat{c}_{k'} = \bar{c}_{k'}$ where (\cdot) denotes the binary complement. Let

$$\tilde{x}_{1,k} = \arg \min_{x_1 \in \mathcal{X}_{1,c_{k'}}^i} \frac{1}{N_k} |y_k - \alpha_k x_1|^2, \quad \hat{x}_{1,k} = \arg \min_{x_1 \in \mathcal{X}_{1,\bar{c}_{k'}}^i} \frac{1}{N_k} |y_k - \alpha_k x_1|^2$$

Using the fact that $\frac{1}{N_k} |y_k - \alpha_k x_{1,k}|^2 \geq \frac{1}{N_k} |y_k - \alpha_k \tilde{x}_{1,k}|^2$, the conditional PEP is upper bounded as

$$\begin{aligned} \mathcal{P}_{\underline{\mathbf{c}}_1 | \overline{\overline{\mathbf{H}}}}^{\hat{\underline{\mathbf{c}}}_1} &\leq P \left(\sum_{k,d_{free}} \frac{1}{N_k} |y_k - \alpha_k x_{1,k}|^2 \geq \sum_{k,d_{free}} \frac{1}{N_k} |y_k - \alpha_k \hat{x}_{1,k}|^2 \right) \\ &= P \left(\sum_{k,d_{free}} \frac{1}{N_k} 2\alpha_k (z_k^* (\hat{x}_{1,k} - x_{1,k}))_R \geq \sum_{k,d_{free}} \frac{\alpha_k^2}{N_k} |\hat{x}_{1,k} - x_{1,k}|^2 \right) \\ &= Q \left(\sqrt{\sum_{k,d_{free}} \frac{\alpha_k^2}{2N_k} |\hat{x}_{1,k} - x_{1,k}|^2} \right) \end{aligned} \quad (3.60)$$

where $\overline{\overline{\mathbf{H}}} = [\mathbf{H}_1 \cdots \mathbf{H}_{d_{free}}]$. In (3.60) we have used the Gaussian Q function, i.e. for a Gaussian random variable m with mean μ and variance σ^2 , $P(m \geq d) = Q\left(\frac{d-\mu}{\sigma}\right)$ where $Q(x) = \frac{1}{\sqrt{2\pi}} \int_x^\infty e^{-t^2/2} dt$. Simplifying $\frac{\alpha_k^2}{N_k}$

$$\frac{S_{1,k}^{-1} \mathbf{h}_{1,k}^\dagger \mathbf{R}_{2,k}^{-1} \mathbf{h}_{1,k} \mathbf{h}_{1,k}^\dagger \mathbf{R}_{2,k}^{-1} \mathbf{h}_{1,k} S_{1,k}^{-1}}{S_{1,k}^{-1} \mathbf{h}_{1,k}^\dagger \mathbf{R}_{2,k}^{-1} \mathbf{R}_{2,k} \mathbf{R}_{2,k}^{-1} \mathbf{h}_{1,k} S_{1,k}^{-1}} = \mathbf{h}_{1,k}^\dagger \mathbf{R}_{2,k}^{-1} \mathbf{h}_{1,k} \quad (3.61)$$

where $S_{1,k} = (\mathbf{h}_{1,k}^\dagger \mathbf{R}_{2,k}^{-1} \mathbf{h}_{1,k} + \sigma_1^{-2})$ and $\mathbf{R}_{2,k} = \sigma_2^2 \mathbf{h}_{2,k} \mathbf{h}_{2,k}^\dagger + N_0 \mathbf{I}$. Bounding $|\hat{x}_{1,k} - x_{1,k}|^2 \geq d_{1,\min}^2$ and using the Chernoff bound $Q(x) \leq \frac{1}{2} \exp\left(\frac{-x^2}{2}\right)$

[46], the conditional PEP can be written as

$$\begin{aligned} \mathcal{P}_{\mathbf{c}_1|\bar{\mathbf{H}}}^{\hat{\mathbf{c}}_1} &\leq \frac{1}{2} \exp \left(-\frac{d_{1,\min}^2}{4} \sum_{k,d_{free}} \mathbf{h}_{1,k}^\dagger \mathbf{R}_{2,k}^{-1} \mathbf{h}_{1,k} \right) \\ &= \frac{1}{2} \exp \left(-\frac{d_{1,\min}^2}{4} \left[\mathbf{h}_{1,1}^\dagger \cdots \mathbf{h}_{1,d_{free}}^\dagger \right] \text{diag} \left[\mathbf{R}_{2,1}^{-1}, \dots, \mathbf{R}_{2,d_{free}}^{-1} \right] \left[\mathbf{h}_{1,1}^T \cdots \mathbf{h}_{1,d_{free}}^T \right]^T \right) \end{aligned} \quad (3.62)$$

For a Hermitian quadratic form in complex Gaussian random variable $q = \mathbf{m}^\dagger \mathbf{A} \mathbf{m}$ where \mathbf{A} is a Hermitian matrix and column vector \mathbf{m} is a circularly symmetric complex Gaussian vector, i.e. $\mathbf{m} \sim \mathcal{NC}(\boldsymbol{\mu}, \boldsymbol{\Sigma})$ with $\boldsymbol{\mu} = E[\mathbf{m}]$ and $\boldsymbol{\Sigma} = E[\mathbf{m}\mathbf{m}^\dagger] - \boldsymbol{\mu}\boldsymbol{\mu}^\dagger$, the MGF is [45]

$$E \left[\exp \left(-t\mathbf{m}^\dagger \mathbf{A} \mathbf{m} \right) \right] = \frac{\exp \left[-t\boldsymbol{\mu}^\dagger \mathbf{A} (\mathbf{I} + t\boldsymbol{\Sigma}\mathbf{A})^{-1} \boldsymbol{\mu} \right]}{\det(\mathbf{I} + t\boldsymbol{\Sigma}\mathbf{A})} \quad (3.63)$$

Therefore the conditional PEP conditioned on $\mathbf{h}_2 = [\mathbf{h}_{2,1}, \dots, \mathbf{h}_{2,d_{free}}]$ is upper bounded as

$$\begin{aligned} \mathcal{P}_{\mathbf{c}_1|\mathbf{h}_2}^{\hat{\mathbf{c}}_1} &\leq \frac{1}{2\det \left(\mathbf{I}_{n_r d_{free}} + \frac{d_{1,\min}^2}{4} \text{diag} \left[\mathbf{R}_{2,1}^{-1}, \dots, \mathbf{R}_{2,d_{free}}^{-1} \right] \right)} \\ &= \frac{1}{2 \prod_{i=1}^{n_r d_{free}} \left(1 + \frac{d_{1,\min}^2}{4} \lambda_i \left(\text{diag} \left[\mathbf{R}_{2,1}^{-1}, \dots, \mathbf{R}_{2,d_{free}}^{-1} \right] \right) \right)} \\ &\leq \frac{1}{2 \prod_{i=1}^{n_r d_{free}} \left(\frac{d_{1,\min}^2}{4} \lambda_i \left(\text{diag} \left[\mathbf{R}_{2,1}^{-1}, \dots, \mathbf{R}_{2,d_{free}}^{-1} \right] \right) \right)} \end{aligned} \quad (3.64)$$

where we have used the identity $\det(\mathbf{I} + \mathbf{A}) = \prod_i (1 + \lambda_i(\mathbf{A}))$. Note that the eigenvalues of $\mathbf{R}_{2,k}^{-1}$ are

$$\lambda_j \left(\mathbf{R}_{2,k}^{-1} \right) = \begin{cases} \left(\sigma_2^2 \|\mathbf{h}_{2,k}\|^2 + N_0 \right)^{-1}, & j = 1 \\ N_0^{-1}, & j = 2, \dots, n_r \end{cases} \quad (3.65)$$

So the conditional PEP is upper bounded as

$$\begin{aligned} \mathcal{P}_{\mathbf{c}_1|\mathbf{h}_2}^{\hat{\mathbf{c}}_1} &\leq \frac{1}{2 \left(\frac{d_{1,\min}^2}{4} \right)^{d_{free} n_r} (N_0^{-1})^{d_{free}(n_r-1)} \prod_{l=1}^{d_{free}} \left(\sigma_2^2 \|\mathbf{h}_{2,l}\|^2 + N_0 \right)^{-1}} \\ &= \frac{1}{2} \left(\frac{4N_0}{d_{1,\min}^2} \right)^{d_{free}(n_r-1)} \left(\frac{4}{d_{1,\min}^2} \right)^{d_{free}} \prod_{l=1}^{d_{free}} \left(\frac{\sigma_2^2}{2} \left\| \sqrt{2}\mathbf{h}_{2,l} \right\|^2 + N_0 \right) \end{aligned}$$

Channel independence at each subcarrier yields

$$\begin{aligned} \mathcal{P}_{\underline{\mathbf{c}}_1}^{\hat{\mathbf{c}}_1} &\leq \frac{1}{2} \left(\frac{4N_0}{d_{1,\min}^2} \right)^{d_{free}(n_r-1)} \left(\frac{4}{d_{1,\min}^2} \right)^{d_{free}} (n_r\sigma_2^2 + N_0)^{d_{free}} \\ &= \frac{1}{2} \left(\frac{4N_0}{\sigma_1^2 \check{d}_{1,\min}^2} \right)^{d_{free}(n_r-1)} \left(\frac{4}{\sigma_1^2 \check{d}_{1,\min}^2} \right)^{d_{free}} (n_r\sigma_2^2 + N_0)^{d_{free}} \end{aligned} \quad (3.66)$$

where we have used the fact that $\|\sqrt{2}\mathbf{h}_{2,l}\|^2$ is a chi square distributed random variable with $2n_r$ degrees of freedom.

Now we consider a general $n_t \times n_r$ MIMO system ($n_r \geq n_t$) with n_t spatial streams. We consider the detection of the j -th stream by the MMSE detector. Analysis is same as in the case of dual stream scenario till (3.62) where conditional PEP is given as

$$\begin{aligned} \mathcal{P}_{\underline{\mathbf{c}}_j|\bar{\mathbf{H}}}^{\hat{\mathbf{c}}_j} &\leq \frac{1}{2} \exp \left(-\frac{d_{j,\min}^2}{4} \sum_{k,d_{free}} \mathbf{h}_{j,k}^\dagger \mathbf{R}_{j,k}^{-1} \mathbf{h}_{j,k} \right) \\ &= \frac{1}{2} \prod_{k,d_{free}} \exp \left(-\frac{d_{j,\min}^2}{4} \mathbf{h}_{j,k}^\dagger \mathbf{R}_{j,k}^{-1} \mathbf{h}_{j,k} \right) \end{aligned} \quad (3.67)$$

where

$$\begin{aligned} \mathbf{R}_{j,k} &= \sigma_1^2 \mathbf{h}_{1,k} \mathbf{h}_{1,k}^\dagger + \dots + \sigma_{j-1}^2 \mathbf{h}_{j-1,k} \mathbf{h}_{j-1,k}^\dagger + \sigma_{j+1}^2 \mathbf{h}_{j+1,k} \mathbf{h}_{j+1,k}^\dagger + \dots + \sigma_{n_t}^2 \mathbf{h}_{n_t,k} \mathbf{h}_{n_t,k}^\dagger + N_0 \mathbf{I} \\ &= \mathbf{H}_{j,k} \sqrt{\mathbf{P}_j} \sqrt{\mathbf{P}_j} \mathbf{H}_{j,k}^\dagger + N_0 \mathbf{I} \end{aligned}$$

where $\mathbf{H}_{j,k} = [\mathbf{h}_{1,k} \dots \mathbf{h}_{j-1,k} \mathbf{h}_{j+1,k} \dots \mathbf{h}_{n_t,k}]$, i.e. a submatrix of \mathbf{H}_k formed by deleting the j -th column and $\mathbf{P}_j = \text{Diag} \left([\sigma_1^2 \dots \sigma_{j-1}^2 \sigma_{j+1}^2 \dots \sigma_{n_t}^2] \right)$. Using unitary transformation \mathbf{U}_j , the covariance matrix $\mathbf{R}_{j,k}$ can be written as

$$\mathbf{R}_{j,k} = \mathbf{U}_{j,k}^\dagger (\mathbf{\Lambda}_{j,k} + N_0 \mathbf{I}) \mathbf{U}_{j,k} \quad (3.68)$$

where $\mathbf{\Lambda}_{j,k} = \text{Diag}([\lambda_{j,k,1}, \lambda_{j,k,2}, \dots, \lambda_{j,k,n_r}])$ is the diagonal matrix containing the eigenvalues (sorted in the ascending order) of $\mathbf{H}_{j,k} \mathbf{P}_j \mathbf{H}_{j,k}^\dagger$. So PEP can be written as

$$\mathcal{P}_{\underline{\mathbf{c}}_j|\bar{\mathbf{H}}}^{\hat{\mathbf{c}}_j} \leq \frac{1}{2} \prod_{k,d_{free}} \exp \left(-\frac{d_{j,\min}^2}{4} \left(\mathbf{h}_{j,k}^\dagger \mathbf{U}_{j,k} (\mathbf{\Lambda}_{j,k} + N_0 \mathbf{I})^{-1} \mathbf{U}_{j,k}^\dagger \mathbf{h}_{j,k} \right) \right) \quad (3.69)$$

As unitary transformation preserves the distribution so $\mathbf{U}_{j,k}^\dagger \mathbf{h}_{j,k} \sim \mathcal{CN}(\mathbf{0}, \mathbf{I})$. Using the MGF of Hermitian quadratic form of complex Gaussian random variable (3.63), the conditional PEP conditioned on $\underline{\mathbf{H}}_j = [\mathbf{H}_{j,1}, \dots, \mathbf{H}_{j,d_{free}}]$ is upper bounded as

$$\begin{aligned} \mathcal{P}_{\underline{\mathbf{c}}_j | \underline{\mathbf{H}}_j}^{\hat{\mathbf{c}}_j} &\leq \frac{1}{2 \prod_{k,d_{free}} \det \left(\mathbf{I}_{n_r} + \frac{d_{j,\min}^2}{4} (\mathbf{A}_{j,k} + N_0 \mathbf{I})^{-1} \right)} \\ &= \frac{1}{2 \prod_{k,d_{free}} \prod_{l=1}^{n_r} \left(1 + \frac{d_{j,\min}^2}{4} (\lambda_{j,k,l} + N_0)^{-1} \right)} \end{aligned} \quad (3.70)$$

where we have assumed channel independence at each subcarrier. As $n_r \geq n_t$, it can be seen that out of the n_r eigenvalues of $\mathbf{H}_{j,k} \mathbf{P}_j \mathbf{H}_{j,k}^\dagger$, $(n_r - n_t + 1)$ eigenvalues would be zero as $\mathbf{H}_{j,k}$ is a full column rank matrix of dimension $n_r \times n_t - 1$. Taking expectation w.r.t the eigenvalues while assuming channel to be iid, PEP is then further written as

$$\mathcal{P}_{\underline{\mathbf{c}}_j}^{\hat{\mathbf{c}}_j} \leq \frac{1}{2 \left(1 + \frac{\sigma_j^2 \check{d}_{j,\min}^2}{4N_0} \right)^{d_{free}(n_r - n_t + 1)} \prod_{l=n_r - n_t + 2}^{n_r} \left(1 + \frac{\sigma_j^2 \check{d}_{j,\min}^2}{4(\bar{\lambda}_{j,l} + N_0)} \right)^{d_{free}}} \quad (3.71)$$

where $\bar{\lambda}_{j,l} = E[\lambda_{j,k,l}]$ and $\bar{\lambda}_{j,l}$ can be found via closed form solutions in some cases. At high SNR when $\sigma^2 \bar{\lambda}_{j,k,l} \gg N_0$, so PEP is upper bounded as

$$\mathcal{P}_{\underline{\mathbf{c}}_j}^{\hat{\mathbf{c}}_j} \leq \frac{1}{2} \left(\frac{4N_0}{\sigma_j^2 \check{d}_{j,\min}^2} \right)^{d_{free}(n_r - n_t + 1)} \prod_{l=n_r - n_t + 2}^{n_r} \left(\frac{4\bar{\lambda}_{j,l}}{\sigma_j^2 \check{d}_{j,\min}^2} \right)^{d_{free}} \quad (3.72)$$

3.D PEP Analysis of the MF Based Detector

As the proposed MF based detector is a low complexity version of the max log MAP detector, so the conditional PEP is given as

$$\begin{aligned} \mathcal{P}_{\underline{\mathbf{c}}_1 | \bar{\mathbf{H}}}^{\hat{\mathbf{c}}_1} &= P \left(\sum_{k'} \min_{x_1 \in \chi_{1,c_{k'}^i}, x_2 \in \chi_2} \frac{1}{N_0} \|\mathbf{y}_k - \mathbf{h}_{1,k} x_1 - \mathbf{h}_{2,k} x_2\|^2 \right. \\ &\quad \left. \geq \sum_{k'} \min_{x_1 \in \chi_{1,\hat{c}_{k'}^i}, x_2 \in \chi_2} \frac{1}{N_0} \|\mathbf{y}_k - \mathbf{h}_{1,k} x_1 - \mathbf{h}_{2,k} x_2\|^2 \right) \end{aligned} \quad (3.73)$$

We consider the worst case scenario between the two codewords i.e. $d(\underline{\mathbf{c}}_1 - \hat{\underline{\mathbf{c}}}_1) = d_{free}$. Let

$$\begin{aligned}\tilde{x}_{1,k}, \tilde{x}_{2,k} &= \arg \min_{x_1 \in \chi_{1,c'_k}^i, x_2 \in \chi_2} \frac{1}{N_0} \|\mathbf{y}_k - \mathbf{h}_{1,k}x_1 - \mathbf{h}_{2,k}x_2\|^2 \\ \hat{x}_{1,k}, \hat{x}_{2,k} &= \arg \min_{x_1 \in \chi_{1,\hat{c}_k}^i, x_2 \in \chi_2} \frac{1}{N_0} \|\mathbf{y}_k - \mathbf{h}_{1,k}x_1 - \mathbf{h}_{2,k}x_2\|^2\end{aligned}\quad (3.74)$$

As $x_{1,k}$ and $x_{2,k}$ are the transmitted symbols so $\|\mathbf{y}_k - \mathbf{h}_{1,k}x_{1,k} - \mathbf{h}_{2,k}x_{2,k}\|^2 \geq \|\mathbf{y}_k - \mathbf{h}_{1,k}\tilde{x}_{1,k} - \mathbf{h}_{2,k}\tilde{x}_{2,k}\|^2$. The conditional PEP is given as

$$\begin{aligned}\mathcal{P}_{\underline{\mathbf{c}}_1|\bar{\mathbf{H}}}^{\hat{\underline{\mathbf{c}}}_1} &\leq P\left(\sum_{k,d_{free}} \frac{1}{N_0} \|\mathbf{y}_k - \mathbf{h}_{1,k}x_{1,k} - \mathbf{h}_{2,k}x_{2,k}\|^2 \geq \sum_{k,d_{free}} \frac{1}{N_0} \|\mathbf{y}_k - \mathbf{h}_{1,k}\hat{x}_{1,k} - \mathbf{h}_{2,k}\hat{x}_{2,k}\|^2\right) \\ &= P\left(\sum_{k,d_{free}} \frac{1}{N_0} 2\left(\mathbf{z}_k^\dagger \mathbf{H}_k (\hat{\mathbf{x}}_k - \mathbf{x}_k)\right)_R \geq \sum_{k,d_{free}} \frac{1}{N_0} \|\mathbf{H}_k \mathbf{x}_k - \mathbf{H}_k \hat{\mathbf{x}}_k\|^2\right) \\ &= Q\left(\sqrt{\sum_{k,d_{free}} \frac{1}{2N_0} \|\mathbf{H}_k (\hat{\mathbf{x}}_k - \mathbf{x}_k)\|^2}\right) \\ &= Q\left(\sqrt{\frac{1}{2N_0} \text{vec}(\bar{\mathbf{H}}^\dagger)^\dagger (\mathbf{I}_{n_r} \otimes \mathbf{D}\mathbf{D}^\dagger) \text{vec}(\bar{\mathbf{H}}^\dagger)}\right)\end{aligned}\quad (3.75)$$

where $\mathbf{D}_{2d_{free} \times d_{free}} = \text{Diag}([\hat{\mathbf{x}}_1 - \mathbf{x}_1, \hat{\mathbf{x}}_2 - \mathbf{x}_2, \dots, \hat{\mathbf{x}}_{k,d_{free}} - \mathbf{x}_{k,d_{free}}])$. Note that $\mathbf{D}\mathbf{D}^\dagger$ is a block diagonal matrix with real entries on the main diagonal. Using the Chernoff bound, we get

$$\mathcal{P}_{\underline{\mathbf{c}}_1|\bar{\mathbf{H}}}^{\hat{\underline{\mathbf{c}}}_1} \leq \frac{1}{2} \exp\left(-\frac{1}{4N_0} \text{vec}(\bar{\mathbf{H}}^\dagger)^\dagger (\mathbf{I}_{n_r} \otimes \mathbf{D}\mathbf{D}^\dagger) \text{vec}(\bar{\mathbf{H}}^\dagger)\right)\quad (3.76)$$

The eigenvalues of $(\mathbf{D}\mathbf{D}^\dagger)$ are

$$\lambda_k(\mathbf{D}\mathbf{D}^\dagger) = \begin{cases} \|\hat{\mathbf{x}}_k - \mathbf{x}_k\|^2 & \text{for } k = 1, \dots, d_{free} \\ 0 & \text{for } k = d_{free} + 1, \dots, 2d_{free} \end{cases}$$

As the argument of exponential in (3.76) is the Hermitian quadratic form of a Gaussian random variable so using the MGF (3.63) and using the identity

$\text{eig}(\mathbf{A} \otimes \mathbf{B}) = \text{eig}(\mathbf{A}) \otimes \text{eig}(\mathbf{B})$, we get

$$\begin{aligned} \mathcal{P}_{\mathbf{e}_1}^{\hat{\mathbf{c}}_1} &\leq \frac{1}{2 \det \left(\mathbf{I} + \frac{1}{4N_0} \mathbf{I}_{n_r} \otimes \mathbf{D}\mathbf{D}^\dagger \right)} \\ &= \frac{1}{2 \prod_{k=1}^{d_{free}} \prod_{l=1}^{n_r} \left(1 + \frac{1}{4N_0} \|\hat{\mathbf{x}}_k - \mathbf{x}_k\|^2 \right)} \\ &\leq \frac{1}{2} \prod_{k=1}^{d_{free}} \prod_{l=1}^{n_r} \frac{4N_0}{\left(\|\hat{\mathbf{x}}_k - \mathbf{x}_k\|^2 \right)} \end{aligned} \quad (3.77)$$

Note that $\|\hat{\mathbf{x}}_k - \mathbf{x}_k\|^2 \geq d_{1,\min}^2 + d_{2,\min}^2$ if $\hat{x}_{2,k} \neq x_{2,k}$ and $\|\hat{\mathbf{x}}_k - \mathbf{x}_k\|^2 \geq d_{1,\min}^2$ if $\hat{x}_{2,k} = x_{2,k}$. There exists $2^{d_{free}}$ possible vectors of $[\hat{x}_{2,1}, \dots, \hat{x}_{2,d_{free}}]^T$ basing on the binary criteria that $\hat{x}_{2,k}$ is equal or not equal to $x_{2,k}$. We call these events as ξ_i where $i = 1, \dots, 2^{d_{free}}$. Consider a particular event ξ_m where amongst d_{free} terms of $\|\hat{\mathbf{x}}_k - \mathbf{x}_k\|^2$, m terms have $\hat{x}_{2,k} \neq x_{2,k}$. Conditioned on this event ξ_m , we have

$$\prod_{k=1}^{d_{free}} \prod_{l=1}^{n_r} \frac{\|\hat{\mathbf{x}}_k - \mathbf{x}_k\|^2}{4N_0} \geq ((d_{1,\min}^2 + d_{2,\min}^2)^m)^{n_r} \left((d_{1,\min}^2)^{(d_{free}-m)} \right)^{n_r} \left(\frac{1}{4N_0} \right)^{n_r d_{free}}$$

So conditional PEP is given as

$$\mathcal{P}_{\mathbf{e}_1}^{\hat{\mathbf{c}}_1} | \xi_m \leq \frac{1}{2} \left(\frac{4N_0}{d_{1,\min}^2} \right)^{n_r d_{free}} \frac{1}{\left(1 + \frac{d_{2,\min}^2}{d_{1,\min}^2} \right)^{mn_r}} \quad (3.78)$$

The probability of this event ξ_m is given as

$$P(\xi_m) = (P(\hat{x}_{2,k} \neq x_{2,k}))^m (1 - P(\hat{x}_{2,k} \neq x_{2,k}))^{d_{free}-m} \quad (3.79)$$

$P(\hat{x}_{2,k} \neq x_{2,k})$ is the uncoded probability that the output of max log MAP detector $\hat{x}_{2,k}$ is not equal to the actual transmitted symbol $x_{2,k}$ and has been derived in Appendix 3E. Considering all possible events ξ_s , the PEP is upper bounded as

$$\mathcal{P}_{\mathbf{e}_1}^{\hat{\mathbf{c}}_1} \leq \frac{1}{2} \left(\frac{4N_0}{\sigma_1^2 \check{d}_{1,\min}^2} \right)^{n_r d_{free}} \left(\sum_{j=0}^{d_{free}} C_j^{d_{free}} \frac{(P(\hat{x}_{2,k} \neq x_{2,k}))^j (1 - P(\hat{x}_{2,k} \neq x_{2,k}))^{d_{free}-j}}{\left(1 + \frac{\sigma_2^2 \check{d}_{2,\min}^2}{\sigma_1^2 \check{d}_{1,\min}^2} \right)^{jn_r}} \right) \quad (3.80)$$

It has been shown in Appendix 3E that $P(\hat{x}_{2,k} \neq x_{2,k})$ depends on the strength and rates of the first and the second streams.

3.E $P(\hat{x}_{2,k} \neq x_{2,k})$

We look at the uncoded probability that interfering symbol $\hat{x}_{2,k}$ being detected by (3.74) is not equal to the actual transmitted symbol $x_{2,k}$. Considering the definition of $\hat{x}_{2,k}$ in (3.74), it can be expanded as

$$\begin{aligned} \hat{x}_{1,k}, \hat{x}_{2,k} = \arg \min_{x_1 \in \chi_{1,\bar{c}_k}, x_2 \in \chi_{2,N_0}} \frac{1}{N_0} \left\{ \|\mathbf{h}_{1,k}(x_{1,k} - x_1) + \mathbf{z}_k\|^2 + \|\mathbf{h}_{2,k}(x_{2,k} - x_2)\|^2 \right. \\ \left. + 2 \left((\mathbf{h}_{1,k}(x_{1,k} - x_1) + \mathbf{z}_k)^\dagger \mathbf{h}_{2,k}(x_{2,k} - x_2) \right)_R \right\} \end{aligned} \quad (3.81)$$

Note that the first term in (3.81) is positive and the second and third term will go to zero if $\hat{x}_{2,k} = x_{2,k}$ thereby implying that $\hat{x}_{2,k}$ is not equal to $x_{2,k}$ only if the sum of the second and third term is negative. So this probability $P(\hat{x}_{2,k} \neq x_{2,k} | \mathbf{h}_{1,k}, \mathbf{h}_{2,k}, x_1) = \mathcal{P}_{x_2 | \mathbf{H}_k, x_1}^{\hat{x}_2}$ is given as

$$\begin{aligned} \mathcal{P}_{x_2 | \mathbf{H}_k, x_1}^{\hat{x}_2} &= P \left(-2 \left((\mathbf{h}_{1,k}(x_{1,k} - x_1) + \mathbf{z}_k)^\dagger \mathbf{h}_{2,k}(x_{2,k} - x_2) \right)_R \geq \|\mathbf{h}_{2,k}(x_{2,k} - x_2)\|^2 \right) \\ &= P \left(-2 \left(\mathbf{z}_k^\dagger \mathbf{h}_{2,k}(x_{2,k} - x_2) \right)_R \geq \|\mathbf{h}_{2,k}(x_{2,k} - x_2)\|^2 + 2 \left((\mathbf{h}_{1,k}(x_{1,k} - x_1))^\dagger \mathbf{h}_{2,k}(x_{2,k} - x_2) \right)_R \right) \\ &= Q \left(\sqrt{\frac{\|\mathbf{h}_{2,k}(x_{2,k} - x_2)\|^2}{2N_0}} + \sqrt{\frac{2}{N_0}} \left(\frac{(\mathbf{h}_{1,k}(x_{1,k} - x_1))^\dagger \mathbf{h}_{2,k}(x_{2,k} - x_2)}{\sqrt{\|\mathbf{h}_{2,k}(x_{2,k} - x_2)\|^2}} \right)_R \right) \end{aligned}$$

Now we use the bound $Q(a+b) \leq Q(a_{\min} - |b_{\max}|)$. First term is minimized by the bound $|x_{2,k} - x_2|^2 \geq d_{2,\min}^2$ while the magnitude of the second term is $\sqrt{\frac{2}{N_0}} \|\mathbf{h}_{1,k}\| |x_{1,k} - x_1|$. For the second term, we use the bound $(\mathbf{a}^\dagger \hat{\mathbf{b}})_R \leq \|\mathbf{a}\|$ where $\hat{\mathbf{b}}$ is the unit vector. So we get

$$\begin{aligned} \mathcal{P}_{x_2 | \mathbf{H}_k}^{\hat{x}_2} &\leq Q \left(\sqrt{\frac{\|\mathbf{h}_{2,k}\|^2 d_{2,\min}^2}{2N_0}} - \sqrt{\frac{2 \|\mathbf{h}_{1,k}\|^2 d_{1,\max}^2}{N_0}} \right) \\ &\leq \frac{1}{2} \exp \left(-\frac{\|\mathbf{h}_{2,k}\|^2 d_{2,\min}^2}{4N_0} - \frac{\|\mathbf{h}_{1,k}\|^2 d_{1,\max}^2}{N_0} + \frac{\|\mathbf{h}_{2,k}\| \|\mathbf{h}_{1,k}\| d_{2,\min} d_{1,\max}}{N_0} \right) \end{aligned}$$

where we have used the Chernoff bound while $d_{1,\max}$ is the maximum distance of the constellation χ_1 .

Considering the norms of $\mathbf{h}_{1,k}$ and $\mathbf{h}_{2,k}$, we make two non-overlapping regions as $(\|\mathbf{h}_{2,k}\| \geq \|\mathbf{h}_{1,k}\|)$ and $(\|\mathbf{h}_{2,k}\| < \|\mathbf{h}_{1,k}\|)$ with the corresponding probabilities as $\mathcal{P}_{\mathbf{h}_1}^< = P(\|\mathbf{h}_{1,k}\| \leq \|\mathbf{h}_{2,k}\| | \mathbf{h}_{1,k})$ and $\mathcal{P}_{\mathbf{h}_1}^> = P(\|\mathbf{h}_{1,k}\| > \|\mathbf{h}_{2,k}\| | \mathbf{h}_{1,k})$.

Note that in the first region $\|\mathbf{h}_{2,k}\|\|\mathbf{h}_{1,k}\| \leq \|\mathbf{h}_{2,k}\|^2$ while for second region $\|\mathbf{h}_{2,k}\|\|\mathbf{h}_{1,k}\| < \|\mathbf{h}_{1,k}\|^2$. So

$$\begin{aligned}
\mathcal{P}_{x_2|\mathbf{H}_k}^{\hat{x}_2} &\leq \left[\frac{1}{2} \exp\left(-\frac{\|\mathbf{h}_{2,k}\|^2 d_{2,\min}^2}{4N_0} - \frac{\|\mathbf{h}_{1,k}\|^2 d_{1,\max}^2}{N_0} + \frac{\|\mathbf{h}_{2,k}\|^2 d_{2,\min} d_{1,\max}}{N_0}\right) \mathcal{P}_{\mathbf{h}_1}^{\leq} + \right. \\
&\quad \left. \frac{1}{2} \exp\left(-\frac{\|\mathbf{h}_{2,k}\|^2 d_{2,\min}^2}{4N_0} - \frac{\|\mathbf{h}_{1,k}\|^2 d_{1,\max}^2}{N_0} + \frac{\|\mathbf{h}_{1,k}\|^2 d_{2,\min} d_{1,\max}}{N_0}\right) \mathcal{P}_{\mathbf{h}_1}^{\geq} \right] \\
&= \frac{1}{2} \left[\exp\left(-\|\mathbf{h}_{2,k}\|^2 \frac{d_{2,\min}^2 - 4d_{2,\min} d_{1,\max}}{4N_0}\right) \exp\left(-\frac{\|\mathbf{h}_{1,k}\|^2 d_{1,\max}^2}{N_0}\right) \mathcal{P}_{\mathbf{h}_1}^{\leq} \right. \\
&\quad \left. + \exp\left(-\frac{\|\mathbf{h}_{2,k}\|^2 d_{2,\min}^2}{4N_0}\right) \exp\left(-\|\mathbf{h}_{1,k}\|^2 \frac{d_{1,\max}^2 - d_{2,\min} d_{1,\max}}{N_0}\right) \mathcal{P}_{\mathbf{h}_1}^{\geq} \right] \tag{3.82}
\end{aligned}$$

We upperbound both the probabilities, i.e. $P\left(\|\mathbf{h}_{1,k}\| \leq \|\mathbf{h}_{2,k}\| \mid \mathbf{h}_{1,k}\right)$ and $P\left(\|\mathbf{h}_{1,k}\| > \|\mathbf{h}_{2,k}\| \mid \mathbf{h}_{1,k}\right)$ by 1. Taking expectation over $\mathbf{h}_{2,k}$ conditioned on $\mathbf{h}_{1,k}$ and then subsequently taking expectation over $\mathbf{h}_{1,k}$ yields

$$\begin{aligned}
\mathcal{P}_{x_2}^{\hat{x}_2} &\leq \frac{1}{2} \left[\left(\frac{4N_0}{d_{2,\min}^2 - 4d_{2,\min} d_{1,\max}} \right)^{n_r} E_{\mathbf{h}_{1,k}} \exp\left(-\frac{\|\mathbf{h}_{1,k}\|^2 d_{1,\max}^2}{N_0}\right) \right. \\
&\quad \left. + \left(\frac{4N_0}{d_{2,\min}^2} \right)^{n_r} E_{\mathbf{h}_{1,k}} \exp\left(-\|\mathbf{h}_{1,k}\|^2 \frac{d_{1,\max}^2 - d_{2,\min} d_{1,\max}}{N_0}\right) \right] \\
&\leq \frac{1}{2} \left(\frac{4N_0}{\sigma_2^2 \check{d}_{2,\min}^2} \right)^{n_r} \left(\frac{N_0}{\sigma_1^2 \check{d}_{1,\max}^2} \right)^{n_r} \left(\frac{1}{\left(1 - \frac{4\sigma_1 \check{d}_{1,\max}}{\sigma_2 \check{d}_{2,\min}}\right)^{n_r}} + \frac{1}{\left(1 - \frac{\sigma_2 \check{d}_{2,\min}}{\sigma_1 \check{d}_{1,\max}}\right)^{n_r}} \right)
\end{aligned}$$

where we have used the MGF of Hermitian quadratic form of a Gaussian random variable by writing $\|\mathbf{h}_{j,k}\|^2 = \mathbf{h}_{j,k}^\dagger \mathbf{I}_{n_r} \mathbf{h}_{j,k}$ where $\mathbf{h}_{j,k} \sim \mathcal{CN}(\mathbf{0}, \mathbf{I}_{n_r})$. This expression shows the dependence of $P(\hat{x}_{2,k} \neq x_{2,k})$ on the strength of the first and the second stream.

Part II

Interference Suppression

Chapter 4

Interference Suppression in Future Cellular Systems

4.1 Introduction

Wireless communication is plagued by three impediments as noise, fading and interference. While noise affects the quality of communication, fading puts limits on the coverage and reliability of the wireless connection. Interference on the other hand restricts the reusability of spectral resources (time, frequency, codes) in space thereby limiting the overall spectral efficiency. Where noise can be effectively dealt by increasing the transmit power, the detrimental effects of fading can be minimized by exploiting the diversity in time, space, frequency or users. However, interference remains a dilemma in high data rate systems as it substantially limits the reliability and the throughput of a wireless communication system.

Modern wireless communication systems are characterized by the ever-increasing demands of higher spectral efficiency thereby leading to a tight frequency reuse (closer to 1) as in 3GPP LTE [5], LTE-Advanced [6] and IEEE 802.16m (WiMax) [8]. These systems have chosen OFDMA technology for the downlink in order to provide multiple access and eliminate the intracell interference. A key issue with OFDMA, employing reusability of the spectrum, is the co-channel interference (CCI) or inter-cell interference: especially the terminals located at the cell border largely suffer from the power

radiated by the base stations (BSs) of neighboring cells in their communication band. Adaptive modulation and coding schemes employed by these BSs combined with the diversified data services lead to variable transmission rate streams. These system characteristics overall effectuate an interference-limited system where one or two dominant interferences of variable rates are limiting the capacity of the cell-edge users. Gaussian assumption for this moderate interference leads to significant degradation in the performance while the subtractive cancellation is plagued with the predicament of error propagation. Moreover, signaling constraints for the subtractive cancellation make this approach unfeasible for future wireless systems. Recently, the paradigm has shifted to focus on how to intelligently exploit the knowledge and/or the structure of interference to achieve improved reliability and throughput in wireless communication systems.

4.1.1 The state of the Art

Most state of the art wireless systems deal with interference either by orthogonalizing the communication links in time or frequency (interference avoidance) [51] or by allowing the communication links to share the same degrees of freedom but modeling the interference as additive Gaussian random process (interference containment) [52]. Both of these approaches may be suboptimal as the first approach entails an *a priori* loss of the degrees of freedom in both links, no matter how weak the potential interference is while the second approach treats interference as pure noise while it actually carries information and has the structure that can be potentially exploited in mitigating its effect. A fascinating technique to completely eliminate the inter-cell interference and increase the overall spectral efficiency is through cooperation and coordination between the BSs, commonly termed as network MIMO or distributed MIMO [53] [10]. However, the requisite of high capacity backhaul and intricacy in the synchronization renders this approach far from realizable for modern wireless systems. These systems are focusing on interference rejection techniques for which different detector structures based on the combinations of interference cancellation and diversity have been proposed in the literature [54] [55]. Amongst them, linear detectors as MMSE [20] and ZF [56] are the focus of attention to minimize the level of interference in the former case while nulling out the interference in the latter case. The shortcoming of noise enhancement for ill conditioned channels in the case of ZF detector instigates MMSE detector as the likely candidate for future wireless system [30]. However, MMSE detection being based on interference attenuation is void of exploiting the interference structure in

mitigating its effects. Moreover, Gaussian assumption of the post detection interference (PDI) in MMSE is valid for asymptotic cases (large number of interferers) [31] but the fidelity of this approximation in a lower dimensional system is questionable.

In the realm of interference avoidance, OFDMA facilitates the orthogonalization of communication links as it provides the ability for each BS to selectively allocate frequency subbands, rates and power to the users depending on their location in the cell. To this effect, there are three major frequency reuse patterns for mitigating the inter-cell interference: hard frequency reuse (HFR), fractional frequency reuse (FFR) and soft frequency reuse (SFR). HFR splits the system bandwidth into a number of distinct subbands according to a chosen reuse factor and lets neighboring cells transmit on different subbands. HFR though simple in implementation suffers from quite reduced spectral efficiency. In SFR [57] [58], the overall bandwidth is shared by all the BSs (i.e. a reuse factor of one is applied), but for the transmission on each sub-carrier, the BSs are restricted to a certain power bound. It is characterized by full frequency reuse and is a strong tool for inter-cell interference mitigation [59] [60]. But as it implies centralized, coordinated resource allocation, such a system can be impractical in realistic settings involving a large number of BSs, random traffic and realistic path-loss models. However, an encouraging result is that by using even limited (yet practical) levels of coordination, significant performance benefits can still be obtained over a conventional cellular architecture [61]. To this end, FFR [62] plays a significant role. It splits the given bandwidth into an inner and an outer part, allocating the inner part to the *near* users (located close to the BS in terms of path loss) with reduced power applying a frequency reuse factor of one, i.e. the inner part is completely reused by all the BSs. For users closer to the cell edge (*far* users), a fraction of the outer part of bandwidth is dedicated with the frequency reuse factor greater than one. FFR is considered as a compromise between HFR and SFR and is therefore an attractive option for future wireless systems. Consequently it has been discussed in cellular network standardization as 3GPP and 3GPP2 [62]. The notions of FFR and interference avoidance also appear in [63].

4.1.2 Contribution

Interference avoidance, rejection, containment and even coordination are all based on the notion of killing the interference either at the receiver or at the transmitter or even before the transmission. This notion stems from the fact that these strategies are based on the unrealistic assumption of

Gaussianity for the interference whose presence can only degrade the performance. However, in practical systems, interference comes from discrete constellations and possesses structure that can be exploited in the detection process. Consequently we focus in this chapter on the scenario of interference exploitation. To this end, we propose the employment of the previously proposed low complexity matched filter (MF) based detector for interference suppression as this detector is characterized by the exploitation of interference structure in mitigating its effects. In the sequel, we further study the effect of the rate and the strength of the interference on the coded PEP of the proposed detector. For this analysis, we look at the more realistic case of the spatially correlated channel as inadequate antenna separation at the mobile station (MS) and the lack of scatterers around the elevated BS antennas will lead to both transmit and receive correlation. In addition to the earlier derived result of full diversity of the MF based low complexity detector, we show that the proposed detector exhibits a coding gain (the horizontal shift of the BER curve) as either the interference gets stronger or the rate of interference declines. We further show that MMSE detection, being independent of the interfering constellation, suffers from a coding loss as the interference gets stronger which is evident as this detection is based on the Gaussian assumption of the post detection interference. As the prerequisite of the proposed detector is interference constellation so we also look at the significance of this information and propose a MF based blind detector which is unaware of this constellation information. We further propose a novel FFR scheme characterized by higher spectral efficiency as compared to the traditional FFR. Basing on the characteristic of effective exploitation of lower rate interference by the proposed detector, we then propose a strategy in the novel FFR which significantly reduces the power consumption at the BSs for satisfying a predefined QoS constraint.

4.1.3 Organization

The chapter is divided into seven sections. In section II we define the system model while section III gives insight into the mutual information analysis of the desired stream in the presence of interfering stream. Section IV encompasses the PEP analysis of the detectors which is followed by the simulation results. Section VI discusses some relevant applications of interference suppression and the chapter is subsequently concluded.

4.2 System Model

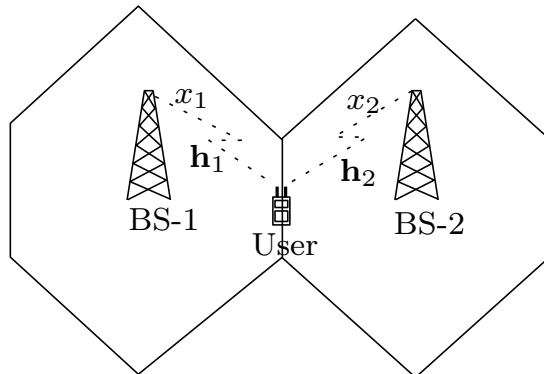


Figure 4.1: Interference in single frequency reuse cellular network. x_1 is the desired signal while x_2 is the interfering signal.

We consider the downlink of a single frequency reuse cellular system (as shown in Fig. 4.1) with n_r antennas at the user and two BSs each using antenna cycling [1] for the transmission. We assume that both the BSs use BICM based OFDM system for the downlink transmission. Two spatial streams which arrive at the user are denoted as $\underline{\mathbf{x}}_1$ (desired stream) and $\underline{\mathbf{x}}_2$ (interference stream). x_1 is the symbol of $\underline{\mathbf{x}}_1$ over a signal set $\chi_1 \subseteq \mathcal{C}$ with a Gray labeling map $\mu_1 : \{0, 1\}^{\log|\chi_1|} \rightarrow \chi_1$ where $|\chi_1| = M_1$ and x_2 is the symbol of $\underline{\mathbf{x}}_2$ over signal set χ_2 where $|\chi_2| = M_2$. During the transmission at BS-1, code sequence $\underline{\mathbf{c}}_1$ is interleaved by π_1 and then is mapped onto the signal sequence $\underline{\mathbf{x}}_1$. Bit interleaver for the desired stream can be modeled as $\pi_1 : k' \rightarrow (k, i)$ where k' denotes the original ordering of the coded bits $c_{k'}$ of the desired stream, k denotes the subcarrier index of the signal $x_{1,k}$ and i indicates the position of the bit $c_{k'}$ in the symbol $x_{1,k}$. Based on the assumption that cyclic prefix (CP) of appropriate length is added to the OFDM symbols, transmission at the k -th frequency tone after cascading IFFT at the BS and FFT at the user is given as

$$\begin{aligned} \mathbf{y}_k &= \mathbf{h}_{1,k}x_{1,k} + \mathbf{h}_{2,k}x_{2,k} + \mathbf{z}_k, & k = 1, 2, \dots, T \\ &= \mathbf{H}_k\mathbf{x}_k + \mathbf{z}_k \end{aligned} \quad (4.1)$$

where T is the total number of frequency tones and $\mathbf{H}_k = [\mathbf{h}_{1,k} \ \mathbf{h}_{2,k}]$ is the channel at the k -th frequency tone and $\mathbf{x}_k = [x_{1,k} \ x_{2,k}]^T$. Each subcarrier

corresponds to a symbol from a constellation map χ_1 for the desired stream and χ_2 for the interference stream. $\mathbf{y}_k, \mathbf{z}_k \in \mathbb{C}^{n_r}$ are the vectors of the received symbols and circularly symmetric complex white Gaussian noise of double-sided power spectral density $N_0/2$ at n_r receive antennas. $\mathbf{h}_{1,k} \in \mathbb{C}^{n_r}$ is the vector characterizing flat fading channel response from BS-1 to n_r receive antennas at the k -th subcarrier. This vector has complex-valued multivariate Gaussian distribution with $E[\mathbf{h}_{1,k}] = \mathbf{0}$ and is correlated in spatial domain. The complex symbols $x_{1,k}$ and $x_{2,k}$ of the two streams are assumed to be independent with variances σ_1^2 and σ_2^2 respectively. The channels at different subcarriers are also assumed to be independent.

4.2.1 Spatial Correlation Model

As entries of the channel matrix are assumed to be circularly symmetric complex Gaussian random variables with zero-mean and unit variance so their magnitudes exhibit Rayleigh distribution. The average Frobenius norm is equal to $n_r \times n_t$ (this is not the case for the instantaneous Frobenius norm). $\mathbf{H}_k(i, j)$ is the complex path gain between j -th BS and i -th antenna of the user at k -th frequency tone and has the following covariance structure:

$$E[\mathbf{H}_k(p, j) \mathbf{H}_k(q, l)^*] = \Psi_T(j, l) \Psi_R(p, q) \quad (4.2)$$

where Ψ_R and Ψ_T are $n_r \times n_r$ receive and $n_t \times n_t$ transmit correlation matrices. The correlation matrix being Hermitian leads to orthogonal eigenvectors and being positive semidefinite leads to non-negative eigenvalues. So square root of the correlation matrix can be found by the eigenvalue decomposition of the matrix, i.e. $\Psi_R = \mathbf{E}\mathbf{\Xi}\mathbf{E}^{-1}$ where \mathbf{E} is the matrix of eigenvectors and $\mathbf{\Xi}$ is the diagonal matrix with the eigenvalues on the diagonal. Eigenvectors being orthogonal leads to $\Psi_R = \mathbf{E}\mathbf{\Xi}\mathbf{E}^\dagger$ and accordingly the square root of the correlation matrix is

$$\Psi_R^{1/2} = \mathbf{E}\sqrt{\mathbf{\Xi}}\mathbf{E}^\dagger \quad (4.3)$$

Note that $\Psi_R = \Psi_R^{1/2}\Psi_R^{1/2} = \Psi_R^{\dagger/2}\Psi_R^{1/2} = \Psi_R^{1/2}\Psi_R^{\dagger/2}$. This fading model embodies following assumptions:

- The correlation between the fading from a BS to the j -th and l -th receive antenna is $\Psi_R(j, l)$ and does not depend on the BS. Ψ_R is equal to the correlation of $n_r \times 1$ vector channel when excited by any BS and is therefore same for all the BSs, i.e. $\Psi_R = \frac{1}{n_t} E[\mathbf{H}_k \mathbf{H}_k^\dagger]$.

- The correlation between fading from the BSs p and q to the same receive antenna at the user is $\Psi_T(p, q)$ and does not depend on the receive antenna. The transmit correlation matrix is given as $\Psi_T = \frac{1}{n_r} E [\mathbf{H}_k^\dagger \mathbf{H}_k]$.
- The correlation between the fading of 2 distinct antennas pairs is the product of the corresponding transmit correlation and receive correlation.
- The correlation is independent of the frequency tone.

Since for Rayleigh fading, second-order statistics fully describe the multi-antenna channel, a general model is

$$\text{vec}(\mathbf{H}_k) = \Psi^{1/2} \text{vec}(\mathbf{W}_k) \quad (4.4)$$

where \mathbf{W}_k is the spatially white (Rayleigh iid) MIMO channel; Ψ is the covariance matrix defined as $\Psi = E \left\{ \text{vec}(\mathbf{H}_k) \text{vec}(\mathbf{H}_k)^\dagger \right\}$. For a user with 2 receive antennas, the covariance matrix is defined as

$$\Psi = \begin{bmatrix} 1 & r_1 & t_1^* & s_1 \\ r_1^* & 1 & s_2^* & t_2^* \\ t_1 & s_2 & 1 & r_2 \\ s_1^* & t_2 & r_2^* & 1 \end{bmatrix} \quad (4.5)$$

The parameters r_1, r_2, t_1, t_2 represent the correlations between channels at two receive (resp. transmit) antennas at one side, but originating from (resp. impinging on) the same transmit (resp. receive) antenna at the other side of the link. They are the classical correlation coefficients of diversity-based systems (MISO and SIMO). Two remaining parameters s_1 and s_2 are defined as the diagonal correlations, or cross-correlations. They represent the correlations between channels originating from and impinging on different antennas at each side of the link.

Basing on the assumptions of receive correlation being independent of the BS and transmit correlation being independent of the receive antenna, it is possible to decompose any MIMO system into two “interconnected”

MISO/SIMO subsystems, i.e.

$$\begin{aligned}
\mathbf{\Psi} &= \mathbf{\Psi}_T^T \otimes \mathbf{\Psi}_R \\
&= \begin{bmatrix} 1 & t^* \\ t & 1 \end{bmatrix} \otimes \begin{bmatrix} 1 & r \\ r^* & 1 \end{bmatrix} \\
&= \begin{bmatrix} 1 & r & t^* & t^*r \\ r^* & 1 & t^*r^* & t^* \\ t & tr & 1 & r \\ tr^* & t & r^* & 1 \end{bmatrix} \tag{4.6}
\end{aligned}$$

As stated in the above declared assumptions, the conditions for (4.5) and (4.6) to be equivalent are that the transmit (respectively receive) correlation coefficients are (in magnitude) independent from the considered receive (respectively transmit) antenna, so that $r_1 = r_2$ and $t_1 = t_2$. Second condition is that the cross correlations must be equal to the product of transmit and receive correlations, i.e. $s_1 = t^*r$ and $s_2 = rt$. \mathbf{H}_k can therefore be factorized in the form

$$\mathbf{H}_k = \mathbf{\Psi}_R^{1/2} \mathbf{W}_k \mathbf{\Psi}_T^{1/2} \tag{4.7}$$

This channel matrix represents the *Kronecker correlation model* [64] since the correlation of the vectorized channel matrix can be written as the Kronecker product of transmit and receive correlation.

4.2.2 Correlation Structure

Let us now focus on the structure of the correlation matrix. We consider a simple single-parameter exponential correlation matrix model [65]. For this model, the components of $\mathbf{\Psi}_R$ are given by

$$\begin{aligned}
\mathbf{\Psi}_R(p, q) &= \rho^{|q-p|}, & p \leq q \\
&= \left(\rho^{|q-p|}\right)^*, & p > q
\end{aligned}$$

where ρ is the (complex) correlation coefficient of the neighboring receive branches with $|\rho| \leq 1$. Similarly the components of $\mathbf{\Psi}_T$ are given by

$$\begin{aligned}
\mathbf{\Psi}_T(j, l) &= \tau^{|l-j|}, & j \leq l \\
&= \left(\tau^{|l-j|}\right)^*, & j > l
\end{aligned}$$

where τ is the (complex) correlation coefficient of two BSs with $|\tau| \leq 1$.

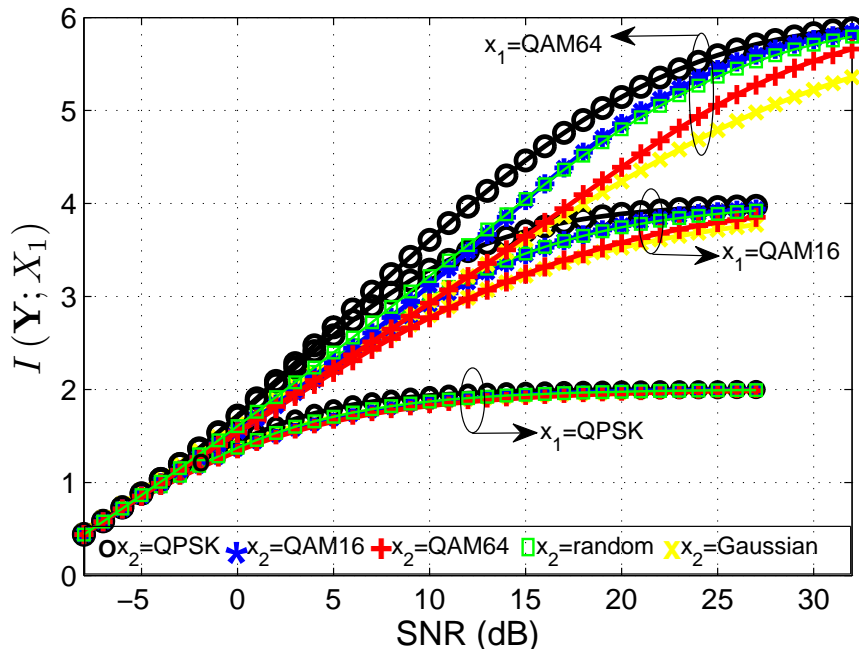


Figure 4.2: Effect of the rate of interference stream x_2 on the mutual information of the desired stream x_1 . Interference strength is of the same strength as the desired stream, i.e. $\sigma_2^2/\sigma_1^2 = 1$. Random interference refers to the case once interference is not static but changes randomly between QPSK, QAM16 and QAM64.

4.3 An Information Theoretic View

In this section, we focus on the mutual information of the desired stream in the presence of one interfering stream and investigate the effects of the strength and the rate of the interference stream. In this information theoretic analysis, we do not resort to the classical assumption of Gaussianity for the alphabets but rather consider them to be from discrete alphabets. This analysis is motivated by the fact that Gaussian alphabets are entropy maximizers [47] but the same is not true for Gaussian interference. Assuming interference to be Gaussian may not give real insight into the effects of the interference on the system capacity.

For this analysis, we assume perfect CSI at the receiver. The mutual

information expressions have been derived in Appendix 4A. Fig. 4.2 shows the effects of the rate (constellation size) of the interference stream on the mutual information of the desired stream where strength of the interfering stream is kept constant. It clearly illustrates that there is a significant boost in the mutual information of the desired stream once interference stream is from discrete alphabets as compared to the case when it belongs to Gaussian alphabets. It confirms that Gaussian interference is not entropy maximizer, which is otherwise the case for Gaussian alphabets [47]. Discrete interference possesses structure that can be exploited in the detection of the desired stream. However, if the interference is Gaussian, it is void of any structure and therefore can not facilitate the detection of desired stream. Note that the gap between the mutual information of Gaussian and discrete interference shrinks as the rate of the interference stream increases. This diminution of gap may be related to the proximity of the behavior of higher rate (large constellation) interference to Gaussianity as both are characterized by high peak to average power ratios. In a more realistic scenario, the allocation of subcarriers to the users in the neighboring cell may not coincide with the subcarrier allocation to users in the cell under consideration thereby resulting into different interfering constellations on different subcarriers. To take into account this case, we have also considered the case of random interference arising due to different multiuser allocations in the interfering cell. Notably mutual information in the presence of random interference is also much improved compared to the case of Gaussian interference. Fig. 4.3 shows the effect of the strength of the interference on the mutual information of the desired stream once the SNR (of the desired stream) is kept constant. For the case of interference belonging to discrete alphabets, the mutual information of the desired stream first declines and then improves as the interference gets stronger. This point of transformation depends on the relative strength and the rate of the interference stream as compared to those of the desired stream. This behavior is due to the partial decoding of the interference stream, i.e. as the strength of the interference relative to the SNR allows its partial decoding, the mutual information of the desired stream starts improving with the interference strength. So as the interference gets stronger, its structure can be more effectively exploited thereby improving the mutual information of the desired stream. However, contrary is the case for Gaussian interference where the mutual information of the desired stream decreases as the interference stream gets stronger.

This analysis underlines the possible gains of exploiting the interference structure rather than assuming it to be Gaussian thereby signifying interference suppression strategies. To this end, we propose the employment

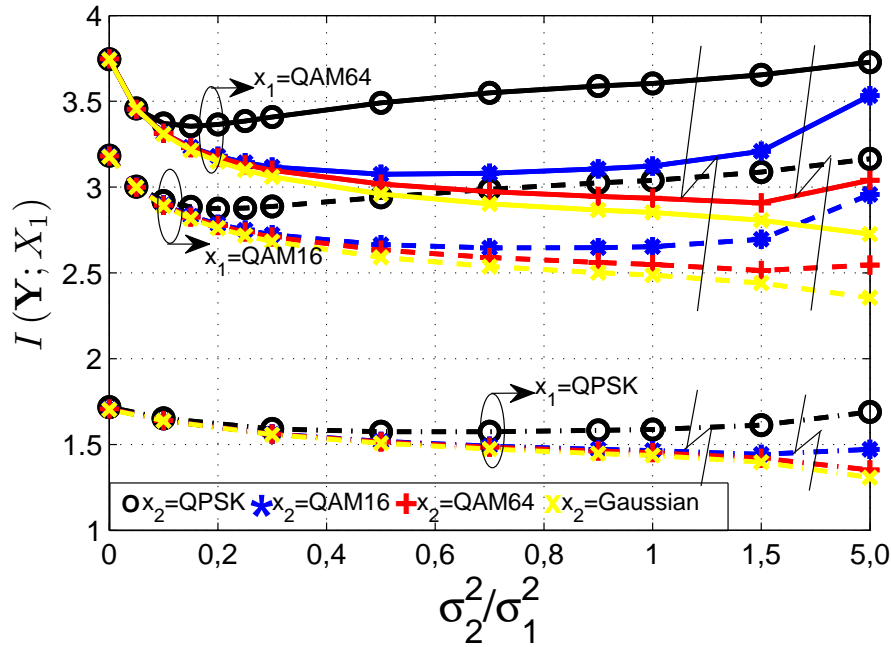


Figure 4.3: Effect of the strength of interference stream x_2 on the mutual information of the desired stream x_1 . SNR is 4.5 dB for x_1 =QPSK, 11 dB for x_1 =QAM16 and 13 dB for x_1 =QAM64

of low complexity MF based detector proposed in the subsection 3.5.2 for interference suppression in cellular systems.

4.4 PEP Analysis

In this section we carry out the PEP analysis of the proposed low complexity MF based detector and the MMSE detector for interference suppression.

4.4.1 Low Complexity MF Based Detector

The PEP between the correct codeword $\underline{\mathbf{c}}_1$ and the error codeword $\hat{\underline{\mathbf{c}}}_1$ has been derived in Appendix 4B and is given as

$$\mathcal{P}_{\underline{\mathbf{c}}_1}^{\hat{\underline{\mathbf{c}}}_1} \leq \frac{1}{2} \left(\frac{4N_0}{\sigma_1^2 \check{d}_{1,\min}^2} \right)^{\kappa d_{free}} \left(\prod_{l=1}^{\kappa} \frac{1}{(\lambda_l(\Psi_R))^{d_{free}}} \right) \left(\frac{1}{[\theta]^{d_{free}}} \right)^{\kappa} \\ \times \left(\sum_{j=0}^{d_{free}} C_j^{d_{free}} \frac{(P(\hat{x}_{2,k} \neq x_{2,k}))^j (1 - P(\hat{x}_{2,k} \neq x_{2,k}))^{d_{free}-j}}{\left(1 + \frac{\sigma_2^2 \check{d}_{2,\min}^2}{\sigma_1^2 \check{d}_{1,\min}^2}\right)^{j\kappa}} \right) \quad (4.8)$$

where $d_{j,\min}^2 = \sigma_j^2 \check{d}_{j,\min}^2$ with $\check{d}_{j,\min}^2$ being the normalized minimum distance of the constellation χ_j for $j = \{1, 2\}$ and $\kappa = \text{rank}(\Psi_R)$. d_{free} is the minimum Hamming distance of the code. $[\theta]^{d_{free}}$ indicates the product $\theta_1 \theta_2 \cdots \theta_{d_{free}}$ where θ s are related to the eigenvalues of transmit correlation matrix and are given by (4.22) in Appendix 4B. $C_j^{d_{free}}$ is the binomial coefficient while $P(\hat{x}_{2,k} \neq x_{2,k})$ is the uncoded probability that the output of max log MAP detector $\hat{x}_{2,k}$ is not equal to the actual transmitted symbol $x_{2,k}$ and has been derived in Appendix 4D.

Note that for the case of no transmit but only receive correlation, the PEP is upper bounded as

$$\mathcal{P}_{\underline{\mathbf{c}}_1}^{\hat{\underline{\mathbf{c}}}_1} \leq \frac{1}{2} \left(\frac{4N_0}{\sigma_1^2 \check{d}_{1,\min}^2} \right)^{\kappa d_{free}} \left(\prod_{l=1}^{\kappa} \frac{1}{(\lambda_l(\Psi_R))^{d_{free}}} \right) \\ \times \left(\sum_{j=0}^{d_{free}} C_j^{d_{free}} \frac{(P(\hat{x}_{2,k} \neq x_{2,k}))^j (1 - P(\hat{x}_{2,k} \neq x_{2,k}))^{d_{free}-j}}{\left(1 + \frac{\sigma_2^2 \check{d}_{2,\min}^2}{\sigma_1^2 \check{d}_{1,\min}^2}\right)^{j\kappa}} \right) \quad (4.9)$$

while for the case of iid fading, PEP is upperbounded as

$$\mathcal{P}_{\underline{\mathbf{c}}_1}^{\hat{\underline{\mathbf{c}}}_1} \leq \frac{1}{2} \left(\frac{4N_0}{\sigma_1^2 \check{d}_{1,\min}^2} \right)^{n_r d_{free}} \left(\sum_{j=0}^{d_{free}} C_j^{d_{free}} \frac{(P(\hat{x}_{2,k} \neq x_{2,k}))^j (1 - P(\hat{x}_{2,k} \neq x_{2,k}))^{d_{free}-j}}{\left(1 + \frac{\sigma_2^2 \check{d}_{2,\min}^2}{\sigma_1^2 \check{d}_{1,\min}^2}\right)^{j n_r}} \right)$$

which is in line with (3.80). These expressions validate the earlier derived result that MF based detector achieves full diversity of the system, i.e. $n_r d_{free}$.

Rank of the receive correlation matrix affects the diversity order while eigenvalues of the transmit and receive correlation matrices affect the coding gain. Another interesting result is that the coding gain of the MF based detector increases as the interference gets stronger relative to the desired stream, i.e. $\sigma_2^2 > \sigma_1^2$ or the rate of interference (constellation size) decreases relative to the desired stream, i.e. $\check{d}_{2,\min}^2 > \check{d}_{1,\min}^2$. Note that as the size of constellation increases, \check{d}_{\min}^2 decreases. It has been shown in Appendix 4D that $P(\hat{x}_{2,k} \neq x_{2,k})$ depends on the eigenvalues of receive correlation matrix in addition to its dependence on the strength of the desired and interference streams.

4.4.2 MMSE Detector

PEP for the MMSE detector for the case of receive correlation matrix to be full rank has been derived in Appendix 4C and is given as

$$\mathcal{P}_{\mathbf{c}_1}^{\hat{\mathbf{c}}_1} \leq \frac{1}{2} \left(\frac{4N_0}{\sigma_1^2 \check{d}_{1,\min}^2} \right)^{d_{free}(n_r-1)} \left(\frac{4}{\sigma_1^2 \check{d}_{1,\min}^2} \right)^{d_{free}} (n_r \sigma_2^2 + N_0)^{d_{free}} \prod_{i=1}^{n_r} \frac{1}{\lambda_i(\mathbf{\Psi}_R)^{d_{free}}} \quad (4.10)$$

thereby indicating the diversity order of $d_{free}(n_r - 1)$. (4.10) not only demonstrates the well known result of the loss of one diversity order in MMSE detection in the presence of one interferer [66] but also exhibits a coding loss as the interference gets stronger which is contrary to the case of MF based detector. Interestingly, the performance of the MMSE detector is not dependent on the rate of interference (constellation size) which is again divergent from the MF based detector.

4.5 Simulation Results

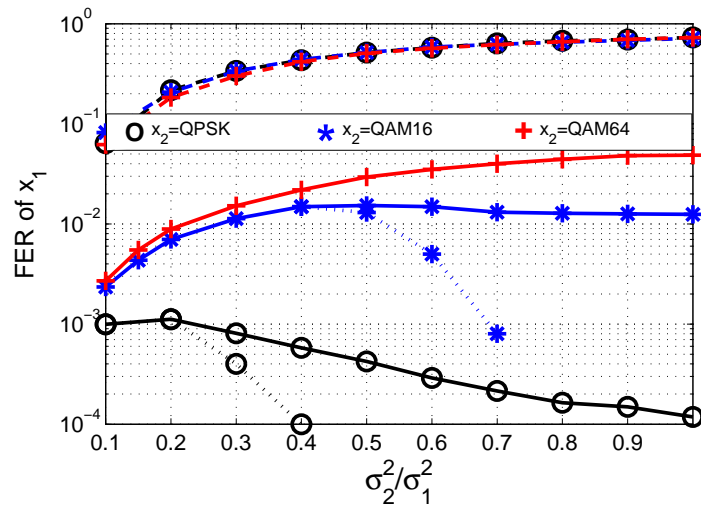
We carry out three sets of simulations and compare the performance of the low complexity MF based detector with that of the linear MMSE detector in the interference limited system. In the first set of simulations, we consider the effects of the strength and the rate of the interference on both the detectors while the second set reflects on the significance of the knowledge of interfering constellation for MF based detector. Third set focuses on the degrading effects of the receive and transmit correlation on these detectors. In the simulation setup, we consider two BSs each using BICM OFDM system for the downlink transmission using the *de facto* standard, 64 state

(133, 171) rate-1/2 convolutional encoder of 802.11n standard and the punctured rate 1/2 turbo code¹ of 3GPP LTE [32]. We consider an ideal OFDM based system (no ISI) and analyze the system in the frequency domain. We further assume antenna cycling at the BS and receive diversity at the user with two antennas. We assume a fully interleaved channel with perfect CSI at the user and no CSI at the BSs. Furthermore, all mappings of the coded bits to QAM symbols use Gray encoding. In the simulations, we look at the FER of the desired stream with the frame length of 1056 information bits.

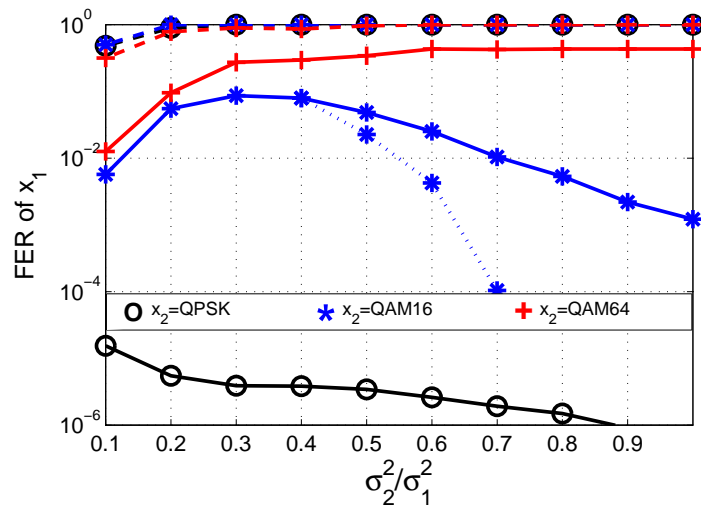
To segregate the effects of the strength and the rate of interference stream in the first set of simulations, SNR (of desired stream) is kept constant as the interference gets stronger while the channel is considered to have iid Gaussian matrix entries. Fig. 4.4 shows that the performance of MMSE detection is independent of the rate of the interference stream (constellation size) but its dependence on the interference strength is considerable. The performance substantially degrades as the interference gets stronger which is in line with the PEP analysis of Section.4.4. Contrary is the case for low complexity MF based detector, where once interference has lower or comparable rate as compared to the desired stream, a significant improvement is observed in the performance as the interference gets stronger. In such a case, we have also considered successive interference cancellation (SIC) based detection, i.e. once interference strength allows its detection, user first detects interference by the MF based detector, strips it out and then detects the desired stream. Once interference has a higher rate as compared to the desired stream, performance of the MF based detector would improve once interference stream is substantially stronger than the desired stream, a case unlikely to occur in the cellular scenario due to handover algorithms. Consequently SIC based detection would not be possible in this scenario. Improvement in the performance for MF based detector as interference gets stronger, is attributed to the partial decoding of interference [29]. It is also observed that for a given interference level, the performance is generally degraded as the rate of the interfering stream increases. Performance gap with respect to MMSE decreases as the desired and interference streams grow in the constellation size. This trend can be attributed to the proximity of the behavior of these larger constellations to Gaussianity due to their high peak to average power ratio and further to the optimality of MMSE detection for Gaussian alphabets.

Prerequisites of the MF based detector are the knowledge of interference

¹The LTE turbo decoder design was performed using the coded modulation library www.iterativesolutions.com



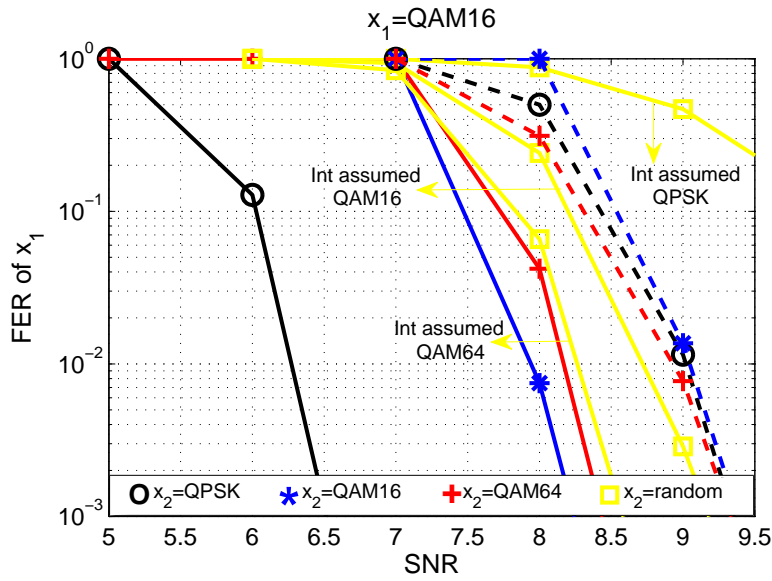
(a)



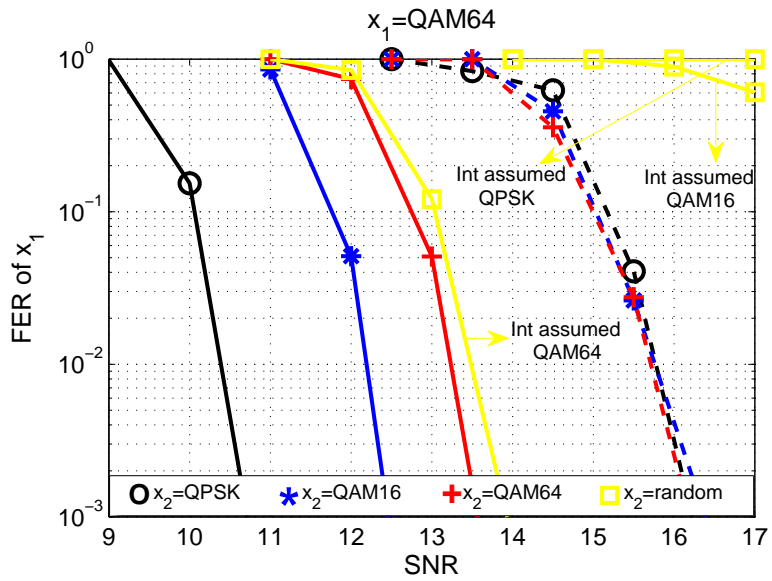
(b)

Figure 4.4: Effect of the strength and the rate of interference stream x_2 on the detection of desired stream x_1 . Continuous lines indicate low complexity MF based detection while dashed lines indicate linear MMSE detection. In Fig.(a), x_1 is QAM16, SNR is 11 dB while 64-state, rate 1/2 convolutional code is used. In Fig.(b), x_1 is QAM64, SNR is 13 dB while LTE turbo code (rate 1/2) is used.

channel and its constellation. Moreover, BSs need to be synchronized in the time division duplex (TDD) mode however, this constraint is not compelling in the frequency division duplex (FDD) mode. Transmission of orthogonal pilot signals by the neighboring BSs is a requisite to enable the users to estimate their interference channels. As an example, we consider how these prerequisites can be met in 3GPP LTE. The orthogonality among pilot signals can be achieved as 3GPP LTE considers three non-overlapping formats of pilot signals [5]. However, pilot signals of one BS would interfere with the control information or data of the neighboring BS. The downlink control information (DCI) is heavily protected (coded) [32] so user after decoding its control information can strip it off thereby leading to clean pilot signals of the interfering BS. As the DCI in 3GPP LTE does not include the information of interfering constellation, we now look at the significance of this information. In a more realistic scenario, the allocation of subcarriers to users in the neighboring cell may not coincide with the subcarrier allocation to users in the cell under consideration thereby resulting into different interfering constellations on different subcarriers. To take into account this case, we consider a more realistic case of non-static interference which is randomly generated from QPSK, QAM16 and QAM64. Fig. 4.5 considers the case once the interference has same strength as the desired stream (cell edge scenario, i.e. $\sigma_2^2/\sigma_1^2 = 1$). Here we consider the additional case of a MF based blind detector which does not know the constellation of interference. This MF based blind detector always assumes interference to be from the highest possible constellation (QAM64) and is based on the metrics (3.36) and (3.37). As the complexity of this detector is independent of the interfering constellation, so this assumption does not lead to added complexity. For comparison purposes, we also consider the cases once blind detector assumes interference to be from QPSK and QAM16. Continuous lines indicate MF based detection while dashed lines indicate MMSE approach. LTE turbo code (rate 1/2) is used. Results show that the best assumption for the unknown interfering stream is QAM64 (highest modulation format among possible constellations). Though the blind detector is not able to effectively exploit the structure of lower rate interference but its performance is still better than that of MMSE detector. These results also underline the significance of the transmission of interfering constellation to the user for its subsequent effective exploitation. Third set of simulations looks at the degrading effects of the receive and transmit correlation. For the structure of correlation matrix, we consider exponential correlation matrix model [65]. To isolate the effects of receive correlation in Fig. 4.6, strengths of the desired and interference streams are kept same (Cell Edge case) while FERs

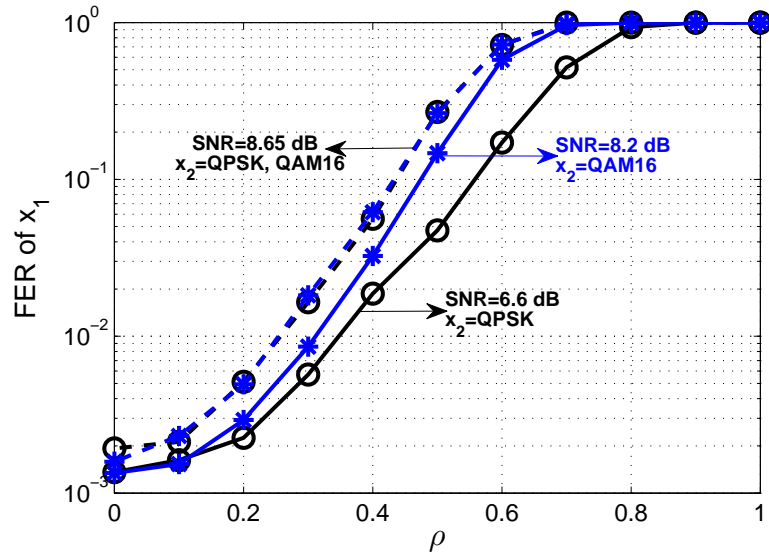


(a)

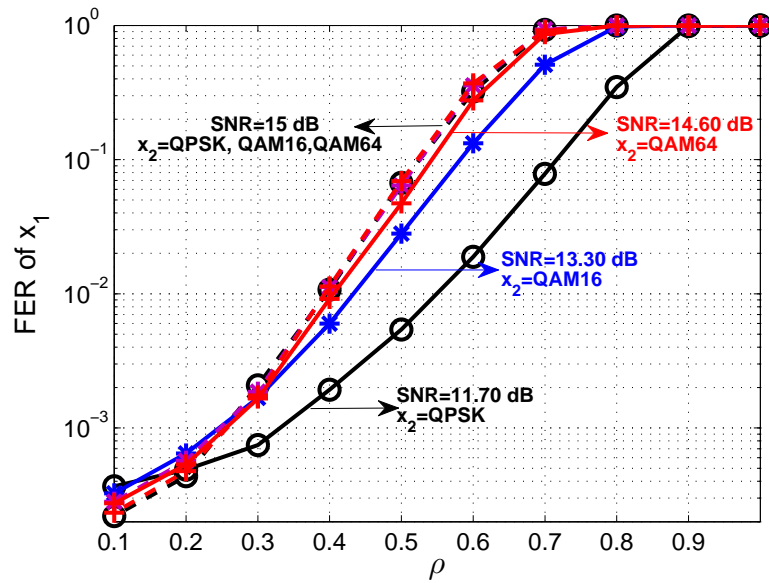


(b)

Figure 4.5: Blind detection and random interference. Random interference indicates that interference is randomly generated from all three constellations.



(a)



(b)

Figure 4.6: Effect of receive correlation. x_1 is QAM16 in (a) and QAM64 in (b).

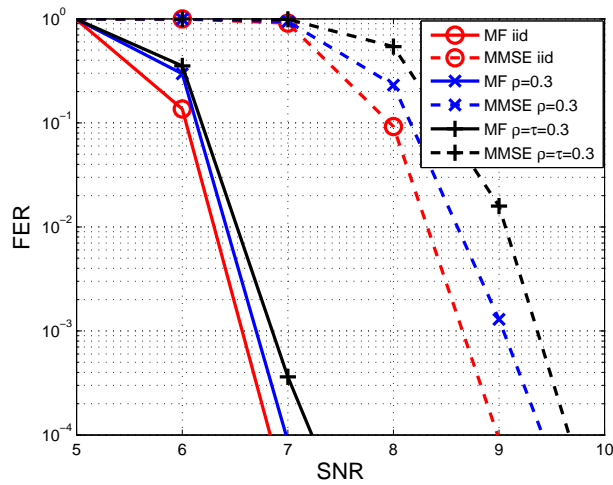


Figure 4.7: Effect of transmit and receive correlation. Desired stream x_1 is QAM16 while interference stream x_2 is QPSK. Settings are same as in Fig. 4.6.

of the desired stream in the presence of different interference streams have been approximately equated once there is no correlation. Then as the receive correlation gets stronger, degrading effect on the performance of both the detectors in the presence of different interferences is compared. Note that continuous lines indicate low complexity MF based detection and dashed lines indicate MMSE based detection while LTE turbo code (rate 1/2) is used. Results show that in the case of equal rate streams, degrading effect of the correlation on both MMSE and MF based detection is approximately same. However, less degradation in the performance of MF based detector with enhanced correlation is observed as the rate of interference decreases relative to that of the desired stream. Due to the partial decoding capability of the MF based detector, the SNR gap between MF based detection and MMSE detection for the same FER (at zero correlation) widens as the rate of interference stream decreases relative to the desired stream. Degradation of MMSE performance with the increase in correlation is independent of the rate of interference which is evident as MMSE detection does not benefit from exploiting the interference structure. Fig. 4.7 shows the combined effects of transmit and receive correlation along with the rate of interference stream. It shows that the degrading effect of correlation is more pronounced

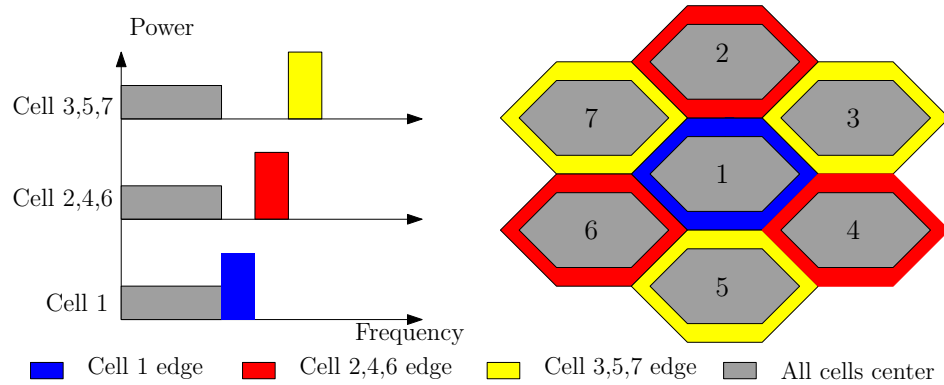


Figure 4.8: FFR in LTE. Frequency reuse factor for cell edge users is 3.

on MMSE detection as compared to MF based detection. PEP analysis of MMSE detection in Section.4.4 does not explain this behavior as this analysis is based on the Gaussian assumption of interference. Note that we have not plotted the upper bounds of error probability in these simulation results to avoid congested figures. These PEP bounds in fact give us an understanding of the behavior of the desired stream in the presence of interference stream under different scenarios and the simulation results have verified the findings of PEP analysis.

4.6 Novel Fractional Frequency Reuse Scheme

Based on the analytical and simulation results of interference suppression by employing low complexity MF based detector, we now propose a novel FFR scheme for cellular systems. As already mentioned that there are three major frequency reuse patterns for mitigating inter-cell interference: HFR, FFR and SFR [67]. We focus on FFR which splits the given bandwidth into an inner and an outer part as shown in Fig. 4.8. It allocates the inner part to the *near* users (located close to the BS in terms of path loss) with reduced power applying a frequency reuse factor of one, i.e. the inner part is completely reused by all the BSs. For users closer to the cell edge (*far* users), a fraction of the outer part of bandwidth is dedicated orthogonally in the neighboring cells with the frequency reuse factor of 3 which leads from the simple calculation $1 / [(3 (\frac{1}{3}) + 3 (\frac{1}{3}) + \frac{1}{3}) / 7]$. Focusing on the cell edge users, we propose a novel FFR scheme that improves the spectral efficiency by allowing one out-of-cell interference as shown in Fig. 4.9. The proposed

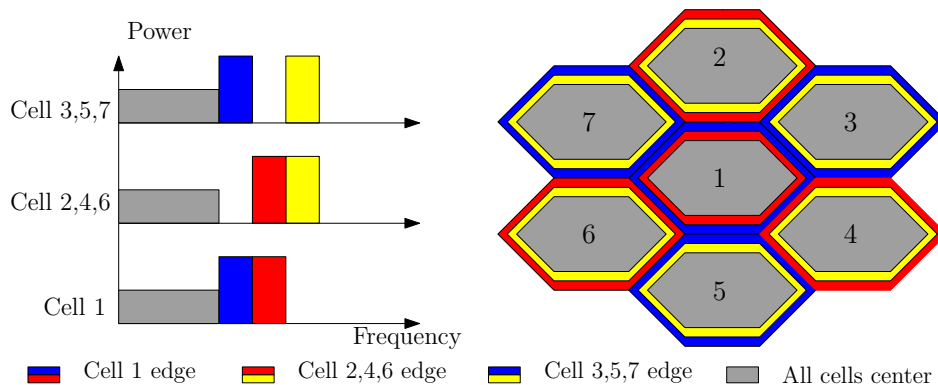


Figure 4.9: Proposed FFR in LTE. Only one interference is ensured in the worst case scenario. Frequency reuse factor for cell edge users is 1.5.

FFR ensures maximum of one interference for the cell edge users and the frequency reuse factor subsequently reduces to 1.5 leading from the calculation $1 / [(3(\frac{2}{3}) + 3(\frac{2}{3}) + \frac{2}{3}) / 7]$. This leads to significant improvement in the spectral efficiency but at the cost of one interference. However, employment of the proposed MF based detectors by the users do not increase the complexity of detection. The question is how to efficiently allocate subcarriers to the users so that the resulting interference can be effectively exploited. We know that a good user-to-subcarrier assignment strategy, from the overall system performance point of view, would be the one allowing system to support the required/requested data rates with minimum transmitted power. Here we propose a strategy of combining subcarrier allocation with the rate allocation. Key idea of the proposed strategy is the exploitation of lower rate interference stream in the decoding of higher rate desired stream. It is based on coordinating the inter-cell interferences while satisfying the requested data rates of the users in such a way that the structures of resulting interferences can be efficiently exploited by the users. This exploitation leads to the reduction of required SNRs at the users while ensuring a predefined quality of service (QoS) which subsequently leads to the minimization of transmitted power at the BSs.

For further illustration, we consider the scenario of two neighboring cells and focus on two cell edge users in each cell as shown in Fig. 4.10. Blue users are high data rate users while red users are low data rate users. Two different rate allocation schemes have been shown. Left figure shows the case once the same rates are allocated to the same subcarrier in both the cells. In this

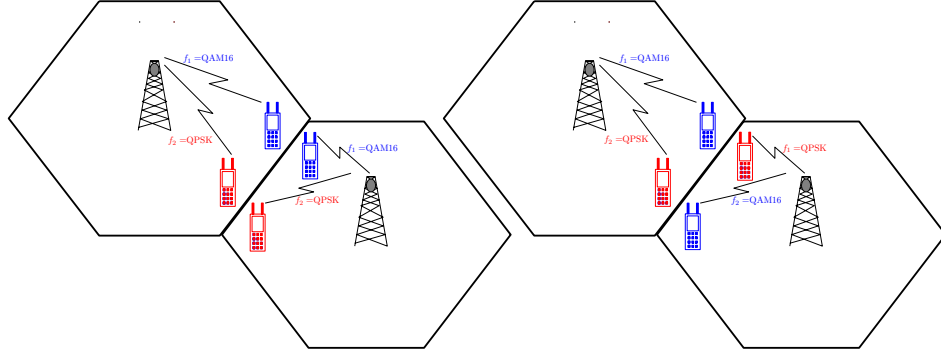
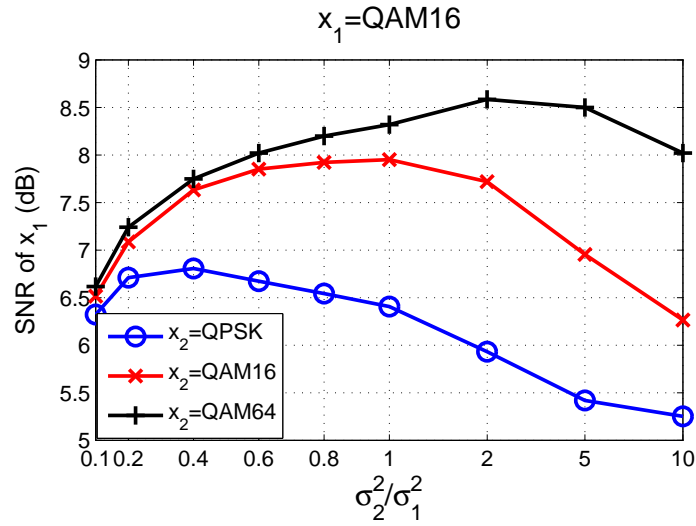
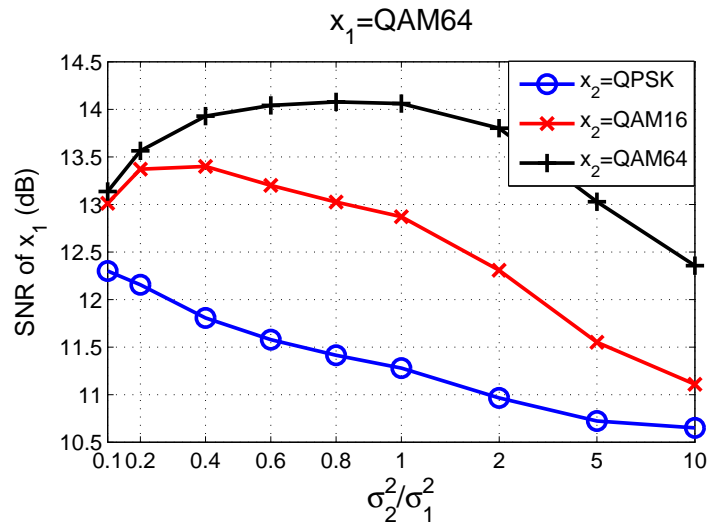


Figure 4.10: Two ways of subcarrier assignment to the cell edge users. Blue users are high data rate while red users are low data rate users. Left figure shows the case of uniform rate streams while right figure shows the case of nonuniform rate streams.

case of uniform rate streams, each cell edge user sees interference from the same constellation as its desired stream. Right figure shows the case once different rates are allocated to the same subcarrier in the neighboring cells. So in this case of nonuniform rate streams, two users being served on the same subcarrier in the neighboring cells see interference from either a lower or a higher rate stream. To substantiate the difference in the performance of these two schemes, we consider the required SNR to achieve a desired FER for the case of uniform rate and non uniform rate interference. The simulation settings are same as for Fig. 4.5, i.e. BICM based transmission, dual antenna UEs, fully interleaved iid channel and 3GPP LTE rate 1/2 turbo code. We focus on the required SNR for each value of σ_2^2/σ_1^2 to achieve the desired FER of 10^{-2} . Fig. 4.11 shows that once the interference x_2 has a lower rate as compared to the desired stream x_1 , the required SNR of x_1 decreases with the increase of interference strength. In the case once interference and desired streams have same rates, decoding of x_1 starts getting benefit from x_2 once interference starts getting stronger than the desired stream, a case which is not relevant in cellular scenario due to handover algorithms. So if both the interference and desired streams are from the same constellation, then users can not efficiently exploit interference structure in the decoding of desired stream. Fig. 4.12 shows that how the desired FER of 10^{-2} can be achieved on both the streams x_1 and x_2 once these streams



(a)



(b)

Figure 4.11: Required SNR for the desired stream x_1 for different constellations of interference x_2 for the target FER of 10^{-2} .

Constellation combinations	Desired Parameters			
	σ_2^2/σ_1^2	SNR $_{x_1}$ (dBs)	SNR $_{x_2}$ (dBs)	$\frac{\sigma_1^2+\sigma_2^2}{N_0}$
x_1 =QAM64, x_2 =QPSK	0.117	12.22	2.90	18.62
x_1 =QAM64, x_2 =QAM16	0.329	13.38	8.55	28.94
x_1 =QAM16, x_2 =QPSK	0.347	6.75	2.15	6.37
x_1 =QPSK, x_2 =QPSK	1.0	1.13	1.13	2.59
x_1 =QAM16, x_2 =QAM16	1.0	7.95	7.95	12.47
x_1 =QAM64, x_2 =QAM64	1.0	14.06	14.06	50.94

Table 4.1: Optimized values of σ_2^2/σ_1^2 and SNR of x_1 and x_2 to achieve the desired FER of 10^{-2} on both streams. Note that $\frac{\sigma_1^2+\sigma_2^2}{N_0}$ is not in dB

Cell Edge Users		Uniform rate streams	Nonuniform rate streams	Power savings
Cell 1	Cell 2	$\frac{\sigma_1^2}{N_0} + \frac{\sigma_2^2}{N_0}$	$\frac{\sigma_1^2}{N_0} + \frac{\sigma_2^2}{N_0}$	%
1×QAM64, 1×QPSK	1×QAM64, 1×QPSK	50.94+2.59	18.62+18.62	30.43%
1×QAM16, 1×QPSK	1×QAM16, 1×QPSK	12.47+2.59	6.37+6.37	15.41%
1×QAM64, 1×QAM16	1×QAM64, 1×QAM16	50.94+12.47	28.94+28.94	8.72%

Table 4.2: Power savings of nonuniform rate streams over uniform rate streams. Note that $\frac{\sigma_1^2}{N_0} + \frac{\sigma_2^2}{N_0}$ is not in dB.

are of different rates. Using this technique, the required SNRs with the corresponding σ_2^2/σ_1^2 values for different combinations of constellations are shown in Table (4.1).

Table (4.2) demonstrates the gains in terms of power savings of nonuniform rate streams with reference to uniform rate streams. Two cell edge users are considered in two neighboring cells with different data requirements. In uniform rate streams, the same subcarrier in both the cells have the same rates whereas in nonuniform rate streams, same subcarrier in both the cells have different rates thereby enabling some users to exploit the lower rate interference streams in the decoding process. The power indicated is the sum power of both the cells required to achieve the FER of 10^{-2} for the users. Note that the power savings decline as the difference between the rates of two streams decreases which can be attributed to the reduction in the ability of exploiting interference structure. The proposed FFR can also be extended to satellite communications via spot beams where different antenna groups on a satellite have different non-overlapping coverage areas. The idea of effective exploitation of lower rate interference can also be extended to cellular networks with frequency reuse of one or to SFR. In cellular scenario, *near* users enjoying a higher SNR have higher rates as compared to the *far* users suffering from the path loss. Allotment of the same frequency subbands to the near users of one cell as the frequency subbands allotted to

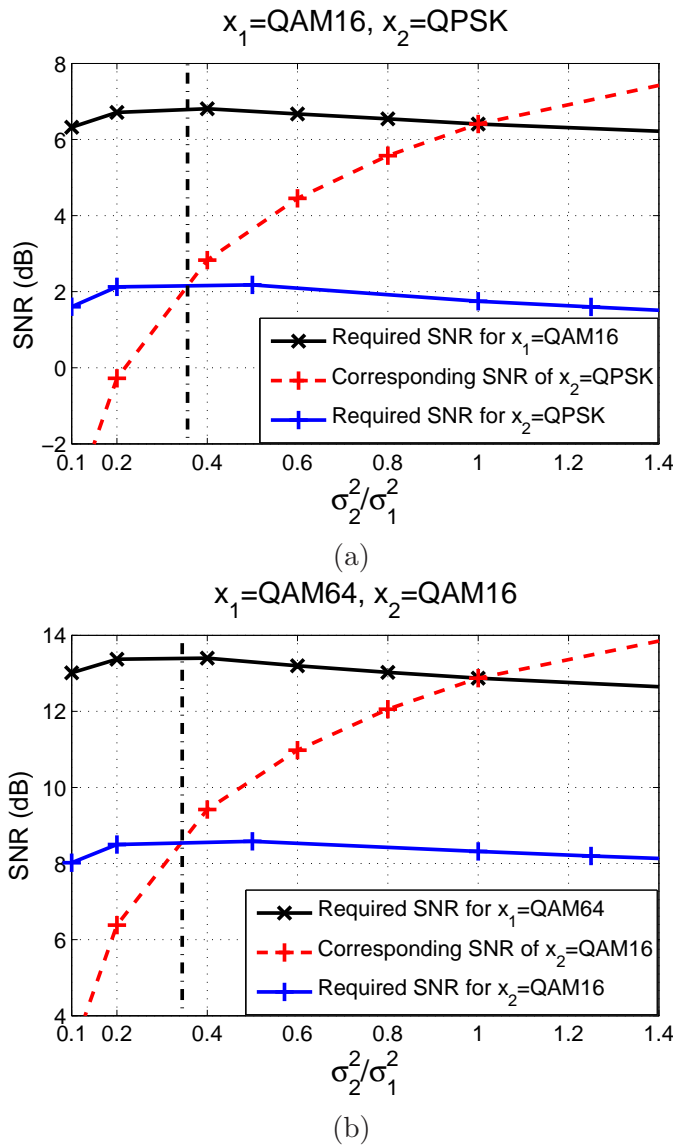


Figure 4.12: Optimizing required SNRs to achieve the desired FER on both streams. Continuous lines indicate the required SNRs to achieve the desired FER both for x_1 and x_2 while dashed line indicates the corresponding SNR of x_2 for the required SNR of x_1 for that particular value of σ_2^2/σ_1^2 . Dashed-dotted line indicates the point where both streams achieve the desired FER of 10^{-2} with minimum SNRs

the far users of the neighboring cell shall enable higher rate users to exploit lower rate interferences.

4.7 Conclusions

We have focused in this chapter on the scenario of interference suppression and to this end, we have proposed the employment of low complexity MF based detector. This detector effectively exploits the structure of interference in mitigating its effects. We have studied the effects of the strength and the rate of interference on the performance of the MF based detector and linear MMSE detector. In addition to the full diversity of MF based detector, we have shown that as the interference gets stronger, the proposed detector has a coding gain. MMSE detector not only loses one diversity order but also suffers from a coding loss as the interference gets stronger. We have further shown that where MMSE detection is independent of the rate of interference stream, the proposed detector benefits from a coding gain as the rate of interference trims down. The degrading effect of correlation is less pronounced for MF based detector as compared to MMSE detector, especially in the cases when interference because of its relative rate or strength allows its partial decoding. The idea of effective exploitation of the lower rate interference led to the proposition of a novel FFR scheme. In the perspective of 3GPP LTE, we have also considered the case of random interference and have proposed a blind detector (unaware of interfering constellation) for this scenario.

4.A Mutual Information for Discrete Alphabets

For notational convenience, we drop the frequency index. Assuming perfect CSI at the receiver, the mutual information of desired stream is given as

$$\begin{aligned}
I(\mathbf{Y}; X_1 | \mathbf{H}) &= \mathcal{H}(X_1 | \mathbf{H}) - \mathcal{H}(X_1 | \mathbf{Y}, \mathbf{H}) \\
&= \log M_1 - \sum_{x_1} \int_{\mathbf{y}} \int_{\mathbf{H}} p(\mathbf{y}, \mathbf{H}, x_1) \log \frac{1}{p(x_1 | \mathbf{y}, \mathbf{H})} d\mathbf{y} d\mathbf{H} \\
&= \log M_1 - \sum_{x_1} \int_{\mathbf{y}} \int_{\mathbf{H}} p(\mathbf{y}, \mathbf{H}, x_1) \log \frac{p(\mathbf{y} | \mathbf{H})}{p(\mathbf{y}, x_1 | \mathbf{H})} d\mathbf{y} d\mathbf{H} \\
&= \log M_1 - \sum_{x_1} \sum_{x_2} \int_{\mathbf{y}} \int_{\mathbf{H}} p(\mathbf{y}, \mathbf{H}, x_1, x_2) \log \frac{\sum_{x'_1} \sum_{x'_2} p(\mathbf{y}, x'_1, x'_2 | \mathbf{H})}{\sum_{x'_2} p(\mathbf{y}, x_1, x'_2 | \mathbf{H})} d\mathbf{y} d\mathbf{H} \\
&= \log M_1 - \frac{1}{M_1 M_2} \sum_{x_1} \sum_{x_2} \int_{\mathbf{y}} \int_{\mathbf{H}} p(\mathbf{y}, \mathbf{H} | x_1, x_2) \log \frac{\sum_{x'_1} \sum_{x'_2} p(\mathbf{y} | \mathbf{H}, x'_1, x'_2)}{\sum_{x'_2} p(\mathbf{y} | \mathbf{H}, x_1, x'_2)} d\mathbf{y} d\mathbf{H}
\end{aligned} \tag{4.11}$$

where $\mathcal{H}(\cdot) = -E \log p(\cdot)$ is the entropy function and $\mathbf{H} = [\mathbf{h}_1 \ \mathbf{h}_2]$ is the channel matrix. Note that $x'_1 \in \chi_1$ and $x'_2 \in \chi_2$. (4.11) is characterized by two random variables, i.e. channel and noise, and apparently it does not have closed form solution. However, (4.11) can be approximated numerically using sampling (Monte-Carlo) methods with N_z realizations of noise and N_H realizations of channel, i.e.

$$\begin{aligned}
I(\mathbf{Y}; X_1 | \mathbf{H}) &= \log M_1 \\
&- \frac{1}{M_1 M_2 N_z N_H} \left(\sum_{x_1} \sum_{x_2} \sum_{\mathbf{H}} \sum_{\mathbf{z}}^{N_H N_z} \log \frac{\sum_{x'_1} \sum_{x'_2} \exp \left[-\frac{1}{N_0} \|\mathbf{y} - \mathbf{h}_1 x'_1 - \mathbf{h}_2 x'_2\|^2 \right]}{\sum_{x'_2} \exp \left[-\frac{1}{N_0} \|\mathbf{y} - \mathbf{h}_1 x_1 - \mathbf{h}_2 x'_2\|^2 \right]} \right)
\end{aligned} \tag{4.12}$$

If the interference stream x_2 due to its relative strength allows its decoding, then it can be detected and stripped off leading to the detection of the desired stream x_1 . The mutual information of desired stream when

interference has been detected is given by

$$\begin{aligned}
I(\mathbf{Y}; X_1|X_2, \mathbf{H}) &= \mathcal{H}(X_1|X_2, \mathbf{H}) - \mathcal{H}(X_1|\mathbf{Y}, X_2, \mathbf{H}) \\
&= \log M_1 - \sum_{x_1} \sum_{x_2} \int_{\mathbf{y}} \int_{\mathbf{H}} p(\mathbf{y}, \mathbf{H}, x_1, x_2) \log \frac{1}{p(x_1|\mathbf{y}, x_2, \mathbf{H})} d\mathbf{y} d\mathbf{H} \\
&= \log M_1 - \sum_{x_1} \sum_{x_2} \int_{\mathbf{y}} \int_{\mathbf{H}} p(\mathbf{y}, \mathbf{H}, x_1, x_2) \log \frac{p(\mathbf{y}, x_2|\mathbf{H})}{p(\mathbf{y}, x_1, x_2|\mathbf{H})} d\mathbf{y} d\mathbf{H} \\
&= \log M_1 - \sum_{x_1} \sum_{x_2} \int_{\mathbf{y}} \int_{\mathbf{H}} p(\mathbf{y}, \mathbf{H}, x_1, x_2) \log \frac{\sum_{x'_1} p(\mathbf{y}, x'_1, x_2|\mathbf{H})}{p(\mathbf{y}, x_1, x_2|\mathbf{H})} d\mathbf{y} d\mathbf{H} \\
&= \log M_1 - \frac{1}{M_1 M_2} \sum_{x_1} \sum_{x_2} \int_{\mathbf{y}} \int_{\mathbf{H}} p(\mathbf{y}, \mathbf{H}|x_1, x_2) \log \frac{\sum_{x'_1} p(\mathbf{y}|\mathbf{H}, x'_1, x_2)}{p(\mathbf{y}|\mathbf{H}, x_1, x_2)} d\mathbf{y} d\mathbf{H}
\end{aligned} \tag{4.13}$$

Estimation of this quantity using Monte-Carlo simulation

$$\begin{aligned}
I(\mathbf{Y}; X_1|X_2, \mathbf{H}) &= \log M_1 \\
&- \frac{1}{M_1 M_2 N_z N_H} \left(\sum_{x_1} \sum_{x_2} \sum_{\mathbf{H}} \sum_{\mathbf{z}}^{N_H N_z} \log \frac{\sum_{x'_1} \exp \left[-\frac{1}{N_0} \|\mathbf{y} - \mathbf{h}_1 x'_1 - \mathbf{h}_2 x_2\|^2 \right]}{\exp \left[-\frac{1}{N_0} \|\mathbf{y} - \mathbf{h}_1 x_1 - \mathbf{h}_2 x_2\|^2 \right]} \right)
\end{aligned} \tag{4.14}$$

For comparison purposes, we consider the case when the desired stream x_1 belongs to finite alphabet ($x_1 \in M_1$) but the interference stream x_2 is Gaussian. Mutual information of the desired stream in this case is given as

$$\begin{aligned}
I(\mathbf{Y}; X_1|\mathbf{H}) &= \log M_1 - \sum_{x_1} \int_{\mathbf{y}} \int_{\mathbf{H}} p(\mathbf{y}, x_1, \mathbf{H}) \log \frac{p(\mathbf{y}|\mathbf{H})}{p(x_1, \mathbf{y}|\mathbf{H})} d\mathbf{y} d\mathbf{H} \\
&= \log M_1 - \sum_{x_1} \int_{x_2} \int_{\mathbf{y}} \int_{\mathbf{H}} p(\mathbf{y}, \mathbf{H}, x_2, x_1) \log \frac{\sum_{x'_1} p(\mathbf{y}|\mathbf{H}, x'_1)}{p(\mathbf{y}|\mathbf{H}, x_1)} d\mathbf{y} d\mathbf{H}
\end{aligned}$$

Estimation of this quantity using Monte-Carlo simulations with N_{x_2} realizations of x_2 , N_z realizations of noise and N_H realizations of the channel

is

$$I(\mathbf{Y}; X_1 | \mathbf{H}) = \log M_1 - \frac{1}{M_1 N_{x_2} N_z N_H} \times \left(\sum_{x_1} \sum_{x_2} \sum_{\mathbf{H}} \sum_{\mathbf{z}} \log \frac{\sum_{x'_1} \exp \left\{ - [\mathbf{y} - \mathbf{h}_1 x'_1]^\dagger (\sigma_2^2 \mathbf{h}_2 \mathbf{h}_2^\dagger + N_0 \mathbf{I})^{-1} [\mathbf{y} - \mathbf{h}_1 x'_1] \right\}}{\exp \left\{ - [\mathbf{y} - \mathbf{h}_1 x_1]^\dagger (\sigma_2^2 \mathbf{h}_2 \mathbf{h}_2^\dagger + N_0 \mathbf{I})^{-1} [\mathbf{y} - \mathbf{h}_1 x_1] \right\}} \right)$$

4.B PEP Analysis of MF Based Detector

The conditional PEP between the correct codeword $\underline{\mathbf{c}}_1$ and the error codeword $\hat{\underline{\mathbf{c}}}_1$, i.e. $P(\underline{\mathbf{c}}_1 \rightarrow \hat{\underline{\mathbf{c}}}_1 | \bar{\mathbf{H}}) = \mathcal{P}_{\underline{\mathbf{c}}_1 | \bar{\mathbf{H}}}^{\hat{\underline{\mathbf{c}}}_1}$ as per (3.76) is given as

$$\mathcal{P}_{\underline{\mathbf{c}}_1 | \bar{\mathbf{H}}}^{\hat{\underline{\mathbf{c}}}_1} \leq \frac{1}{2} \exp \left(-\frac{1}{4N_0} \text{vec}(\bar{\mathbf{H}}^\dagger)^\dagger \Delta \text{vec}(\bar{\mathbf{H}}^\dagger) \right) \quad (4.15)$$

Note that $\bar{\mathbf{H}} = \Psi_R^{1/2} [\mathbf{W}_1 \cdots \mathbf{W}_{d_{free}}] (\mathbf{I}_{d_{free}} \otimes \Psi_T^{1/2}) = \Psi_R^{1/2} \bar{\mathbf{W}}_{n_r \times 2d_{free}} (\mathbf{I}_{d_{free}} \otimes \Psi_T^{1/2})$. Using the Kronecker product identity $\text{vec}(\mathbf{A}\mathbf{X}\mathbf{B}) = (\mathbf{B}^T \otimes \mathbf{A}) \text{vec}(\mathbf{X})$ [49], we get

$$\begin{aligned} \text{vec}(\bar{\mathbf{H}}^\dagger) &= \text{vec} \left((\mathbf{I}_{d_{free}} \otimes \Psi_T^{\dagger/2}) \bar{\mathbf{W}}^\dagger \Psi_R^{\dagger/2} \right) \\ &= (\Psi_R^{*/2} \otimes (\mathbf{I}_{d_{free}} \otimes \Psi_T^{\dagger/2})) \text{vec}(\bar{\mathbf{W}}^\dagger) \end{aligned} \quad (4.16)$$

Developing (4.15) further on the lines of [68], the conditional PEP is given as

$$\begin{aligned} \mathcal{P}_{\underline{\mathbf{c}}_1 | \bar{\mathbf{H}}}^{\hat{\underline{\mathbf{c}}}_1} &\leq \frac{1}{2} \exp \left(-\frac{1}{4N_0} \text{vec}(\bar{\mathbf{H}}^\dagger)^\dagger \Delta \text{vec}(\bar{\mathbf{H}}^\dagger) \right) \\ &\stackrel{a}{=} \frac{1}{2} \exp \left(\frac{-1}{4N_0} \text{vec}(\bar{\mathbf{W}}^\dagger)^\dagger (\Psi_R^{T/2} \otimes \mathbf{I}_{d_{free}} \otimes \Psi_T^{1/2}) (\mathbf{I}_{n_r} \otimes \mathbf{D}\mathbf{D}^\dagger) (\Psi_R^{*/2} \otimes \mathbf{I}_{d_{free}} \otimes \Psi_T^{\dagger/2}) \text{vec}(\bar{\mathbf{W}}^\dagger) \right) \\ &\stackrel{b}{=} \frac{1}{2} \exp \left(\frac{-1}{4N_0} \text{vec}(\bar{\mathbf{W}}^\dagger)^\dagger (\Psi_R^{T/2} \otimes \mathbf{I}_{d_{free}} \otimes \Psi_T^{1/2}) (\Psi_R^{*/2} \otimes \mathbf{D}\mathbf{D}^\dagger (\mathbf{I}_{d_{free}} \otimes \Psi_T^{\dagger/2})) \text{vec}(\bar{\mathbf{W}}^\dagger) \right) \\ &\stackrel{c}{=} \frac{1}{2} \exp \left(\frac{-1}{4N_0} \text{vec}(\bar{\mathbf{W}}^\dagger)^\dagger (\Psi_R^{T/2} \Psi_R^{*/2}) \otimes (\mathbf{I}_{d_{free}} \otimes \Psi_T^{1/2}) \mathbf{D}\mathbf{D}^\dagger (\mathbf{I}_{d_{free}} \otimes \Psi_T^{\dagger/2}) \text{vec}(\bar{\mathbf{W}}^\dagger) \right) \\ &\stackrel{d}{=} \frac{1}{2} \exp \left(\frac{-1}{4N_0} \text{vec}(\bar{\mathbf{W}}^\dagger)^\dagger (\Psi_R)^T \otimes (\mathbf{I}_{d_{free}} \otimes \Psi_T^{1/2}) \mathbf{D}\mathbf{D}^\dagger (\mathbf{I}_{d_{free}} \otimes \Psi_T^{\dagger/2}) \text{vec}(\bar{\mathbf{W}}^\dagger) \right) \end{aligned} \quad (4.17)$$

where in (a) we have used the identity $(A \otimes B)^\dagger = A^\dagger \otimes B^\dagger$, in (b) and (c) we have used the identity $(A \otimes C)(B \otimes D) = AB \otimes CD$. In (d) we have used the relation $\Psi_R^{T/2} \Psi_R^{*/2} = \left(\Psi_R^{\dagger/2} \Psi_R^{1/2} \right)^T = \Psi_R^T$. Based on the fact that for two Hermitian matrices \mathbf{A} and \mathbf{B} , $\mathbf{A} \otimes \mathbf{B}$ and $\mathbf{A}\mathbf{B}\mathbf{A}^\dagger$ are Hermitian matrices, the argument of exponential in (4.17) is the Hermitian quadratic form of a Gaussian random variable. So using the MGF (3.63), we get

$$\begin{aligned} \mathcal{P}_{\hat{\mathbf{c}}_1}^{\hat{\mathbf{c}}_1} &\leq \frac{1}{2 \det \left(\mathbf{I} + \frac{1}{4N_0} (\Psi_R)^T \otimes \left(\mathbf{I}_{d_{free}} \otimes \Psi_T^{1/2} \right) \mathbf{D}\mathbf{D}^\dagger \left(\mathbf{I}_{d_{free}} \otimes \Psi_T^{\dagger/2} \right) \right)} \\ &= \frac{1}{2 \det \left(\mathbf{I} + \frac{1}{4N_0} (\Psi_R)^T \otimes \mathbf{D}\mathbf{D}^\dagger \left(\mathbf{I}_{d_{free}} \otimes \Psi_T \right) \right)} \end{aligned} \quad (4.18)$$

which involves the identity $\det(\mathbf{I} + \mathbf{A} \otimes \mathbf{B}\mathbf{C}) = \det(\mathbf{I} + \mathbf{A} \otimes \mathbf{C}\mathbf{B})$. This identity can be proved as

$$\begin{aligned} \det(\mathbf{I} + \mathbf{A} \otimes \mathbf{B}\mathbf{C}) &= \det(\mathbf{I} + \mathbf{A}\mathbf{I} \otimes \mathbf{B}\mathbf{C}) \\ &\stackrel{\text{i}}{=} \det(\mathbf{I} + (\mathbf{A} \otimes \mathbf{B})(\mathbf{I} \otimes \mathbf{C})) \\ &\stackrel{\text{ii}}{=} \det(\mathbf{I} + (\mathbf{I} \otimes \mathbf{C})(\mathbf{A} \otimes \mathbf{B})) \\ &\stackrel{\text{iii}}{=} \det(\mathbf{I} + \mathbf{A} \otimes \mathbf{C}\mathbf{B}) \end{aligned} \quad (4.19)$$

where in (i) and (iii) we have used the identity $(\mathbf{A} \otimes \mathbf{C})(\mathbf{B} \otimes \mathbf{D}) = \mathbf{A}\mathbf{B} \otimes \mathbf{C}\mathbf{D}$, while in (ii) we have used the identity $\det(\mathbf{I} + \mathbf{A}\mathbf{B}) = \det(\mathbf{I} + \mathbf{B}\mathbf{A})$. Now we further use two identities, i.e. $\det(\mathbf{I} + \mathbf{A}) = \prod_i (1 + \lambda_i(\mathbf{A}))$ and $\lambda(\mathbf{A} \otimes \mathbf{B}) = \lambda(\mathbf{A}) \otimes \lambda(\mathbf{B})$. To be precise for the latter identity, the eigenvalues of $\mathbf{A} \otimes \mathbf{B}$, where \mathbf{A} and \mathbf{B} are square matrices of size m and n , are given as

$$\lambda_l(\mathbf{A}) \lambda_k(\mathbf{B}) \quad l = 1, \dots, m, \quad k = 1, \dots, n. \quad (4.20)$$

(4.18) is therefore developed as

$$\begin{aligned} \mathcal{P}_{\hat{\mathbf{c}}_1}^{\hat{\mathbf{c}}_1} &\leq \frac{1}{2 \prod_{k=1}^{2d_{free}} \prod_{l=1}^{n_r} \left(1 + \frac{1}{4N_0} \lambda_l(\Psi_R) \lambda_k(\mathbf{D}\mathbf{D}^\dagger (\mathbf{I}_{d_{free}} \otimes \Psi_T)) \right)} \\ &\stackrel{a}{\leq} \frac{1}{2} \prod_{k=1}^{d_{free}} \prod_{l=1}^{\kappa} \frac{4N_0}{\lambda_l(\Psi_R) \lambda_k(\mathbf{D}\mathbf{D}^\dagger (\mathbf{I}_{d_{free}} \otimes \Psi_T))} \\ &\stackrel{b}{=} \frac{1}{2} \prod_{k=1}^{d_{free}} \prod_{l=1}^{\kappa} \frac{4N_0}{\lambda_l(\Psi_R) \theta_k \|\hat{\mathbf{x}}_k - \mathbf{x}_k\|^2} \end{aligned} \quad (4.21)$$

For (a) we have considered $\kappa = \text{rank}(\Psi_R)$. More facts are needed in (a). Let \mathbf{A} be a $m \times n$ matrix, \mathbf{B} be a $n \times k$ with rank n and \mathbf{C} be a $l \times m$ with rank m , then as per [49]

$$\begin{aligned}\text{rank}(\mathbf{AB}) &= \text{rank}(\mathbf{A}) \\ \text{rank}(\mathbf{CA}) &= \text{rank}(\mathbf{A})\end{aligned}$$

The eigenvalues of $(\mathbf{DD}^\dagger)_{2d_{free} \times 2d_{free}}$ are

$$\lambda_k(\mathbf{DD}^\dagger) = \begin{cases} \|\hat{\mathbf{x}}_k - \mathbf{x}_k\|^2 & \text{for } k = 1, \dots, d_{free} \\ 0 & \text{for } k = d_{free} + 1, \dots, 2d_{free} \end{cases}$$

Assuming transmit correlation matrix to be full rank, the eigenvalues of $\mathbf{I}_{d_{free}} \otimes \Psi_T$ in the increasing order are

$$\lambda_k(\mathbf{I}_{d_{free}} \otimes \Psi_T) = \begin{cases} \lambda_1(\Psi_T) & \text{for } k = 1, \dots, d_{free} \\ \lambda_2(\Psi_T) & \text{for } k = d_{free} + 1, \dots, 2d_{free} \end{cases}$$

In (b), we have used the lemma 1 of [69], i.e.

$$\lambda_k(\mathbf{DD}^\dagger (\mathbf{I}_{d_{free}} \otimes \Psi_T)) = \theta_k \lambda_k(\mathbf{DD}^\dagger) \quad (4.22)$$

such that for each k , there exists a positive real number θ_k such that $\lambda_1(\Psi_T) \leq \theta_k \leq \lambda_2(\Psi_T)$. So

$$\lambda_k(\mathbf{DD}^\dagger (\mathbf{I}_{d_{free}} \otimes \Psi_T)) = \begin{cases} \theta_k \|\hat{\mathbf{x}}_k - \mathbf{x}_k\|^2 & \text{for } k = 1, \dots, d_{free} \\ 0 & \text{for } k = d_{free} + 1, \dots, 2d_{free} \end{cases}$$

Note that $\|\hat{\mathbf{x}}_k - \mathbf{x}_k\|^2 \geq d_{1,\min}^2 + d_{2,\min}^2$ if $\hat{x}_{2,k} \neq x_{2,k}$ and $\|\hat{\mathbf{x}}_k - \mathbf{x}_k\|^2 \geq d_{1,\min}^2$ if $\hat{x}_{2,k} = x_{2,k}$. There exist $2^{d_{free}}$ possible vectors of $[\hat{x}_{2,1}, \dots, \hat{x}_{2,d_{free}}]^T$ based on the binary criteria that $\hat{x}_{2,k}$ is equal or not equal to $x_{2,k}$. We call these events as ξ_i where $i = 1, \dots, 2^{d_{free}}$. Consider a particular event ξ_m where amongst d_{free} terms of $\|\hat{\mathbf{x}}_k - \mathbf{x}_k\|^2$, m terms have $\hat{x}_{2,k} \neq x_{2,k}$. Let the product of θ s for these m terms be denoted as $[\theta]^m$ and the product of θ s for the remaining $(d_{free} - m)$ terms be denoted as $[\theta]^{m'}$. Conditioned on this event ξ_m , we have

$$\begin{aligned} & \prod_{k=1}^{d_{free}} \prod_{l=1}^{\kappa} \frac{\lambda_l(\Psi_R) \theta_k \|\hat{\mathbf{x}}_k - \mathbf{x}_k\|^2}{4N_0} \\ & \geq \prod_{l=1}^{\kappa} \left[\left(\frac{\lambda_l(\Psi_R)}{4N_0} \right)^m (d_{1,\min}^2 + d_{2,\min}^2)^m [\theta]^m \right] \prod_{l=1}^{\kappa} \left[\left(\frac{\lambda_l(\Psi_R)}{4N_0} \right)^{d_{free}-m} (d_{1,\min}^2)^{d_{free}-m} [\theta]^{m'} \right] \\ & = ((d_{1,\min}^2 + d_{2,\min}^2)^m [\theta]^m)^\kappa \left((d_{1,\min}^2)^{d_{free}-m} [\theta]^{m'} \right)^\kappa \left(\prod_{l=1}^{\kappa} (\lambda_l(\Psi_R))^{d_{free}} \right) \left(\frac{1}{4N_0} \right)^{\kappa d_{free}} \end{aligned}$$

So conditional PEP for the correlated case is given as

$$\begin{aligned}
 \mathcal{P}_{\xi_1}^{\hat{\xi}_1} | \xi_m &\leq \frac{1}{2} \left(\frac{(4N_0)^{d_{free}}}{(d_{1,\min}^2 + d_{2,\min}^2)^m [\theta]^m (d_{1,\min}^2)^{d_{free}-m} [\theta]^{m'}} \right)^\kappa \left(\prod_{l=1}^{\kappa} \frac{1}{(\lambda_l(\Psi_R))^{d_{free}}} \right) \\
 &= \frac{1}{2} \left(\frac{4N_0}{d_{1,\min}^2} \right)^{\kappa d_{free}} \left(\prod_{l=1}^{\kappa} \frac{1}{(\lambda_l(\Psi_R))^{d_{free}}} \right) \left(\frac{1}{[\theta]^{d_{free}}} \right)^\kappa \frac{1}{\left(1 + \frac{d_{2,\min}^2}{d_{1,\min}^2}\right)^{m\kappa}} \quad (4.23)
 \end{aligned}$$

where $[\theta]^{d_{free}}$ indicates the product $\theta_1 \theta_2 \cdots \theta_{d_{free}}$. The probability of this event ξ_m is given as

$$P(\xi_m) = (P(\hat{x}_{2,k} \neq x_{2,k}))^m (1 - P(\hat{x}_{2,k} \neq x_{2,k}))^{d_{free}-m} \quad (4.24)$$

$P(\hat{x}_{2,k} \neq x_{2,k})$ is the uncoded probability that the output of max log MAP detector $\hat{x}_{2,k}$ is not equal to the actual transmitted symbol $x_{2,k}$ and has been derived in Appendix 4D. Considering all possible events ξ_i s, the PEP is upper bounded as

$$\begin{aligned}
 \mathcal{P}_{\xi_1}^{\hat{\xi}_1} &\leq \frac{1}{2} \left(\frac{4N_0}{\sigma_1^2 d_{1,\min}^2} \right)^{\kappa d_{free}} \left(\prod_{l=1}^{\kappa} \frac{1}{(\lambda_l(\Psi_R))^{d_{free}}} \right) \left(\frac{1}{[\theta]^{d_{free}}} \right)^\kappa \\
 &\quad \times \left(\sum_{j=0}^{d_{free}} C_j^{d_{free}} \frac{(P(\hat{x}_{2,k} \neq x_{2,k}))^j (1 - P(\hat{x}_{2,k} \neq x_{2,k}))^{d_{free}-j}}{\left(1 + \frac{\sigma_2^2 d_{2,\min}^2}{\sigma_1^2 d_{1,\min}^2}\right)^{j\kappa}} \right) \quad (4.25)
 \end{aligned}$$

where $d_{j,\min}^2 = \sigma_j^2 \check{d}_{j,\min}^2$ with $\check{d}_{j,\min}^2$ being the normalized minimum distance of the constellation χ_j for $j = \{1, 2\}$ and $C_j^{d_{free}}$ is the binomial coefficient.

4.C PEP Analysis of MMSE Detector

Developing from (3.60) while noting that $\frac{\alpha_k^2}{N_k} = \mathbf{h}_{1,k}^\dagger \mathbf{R}_{2,k}^{-1} \mathbf{h}_{1,k}$ and using the Chernoff bound coupled with the bound $|\hat{x}_{1,k} - x_{1,k}|^2 \geq d_{1,\min}^2$, we get

$$\begin{aligned}
\mathcal{P}_{\mathbf{c}_1|\mathbf{H}}^{\hat{\mathbf{c}}_1} &\leq \frac{1}{2} \exp \left(-\frac{d_{1,\min}^2}{4} \sum_{k,d_{free}} \mathbf{h}_{1,k}^\dagger \mathbf{R}_{2,k}^{-1} \mathbf{h}_{1,k} \right) \\
&= \frac{1}{2} \exp \left(-\frac{d_{1,\min}^2}{4} \left[\mathbf{h}_{1,1}^\dagger \cdots \mathbf{h}_{1,d_{free}}^\dagger \right] \text{diag} \left[\mathbf{R}_{2,1}^{-1} \cdots \mathbf{R}_{2,d_{free}}^{-1} \right] \left[\mathbf{h}_{1,1}^T \cdots \mathbf{h}_{1,d_{free}}^T \right]^T \right) \\
&= \frac{1}{2} \exp \left(-\frac{d_{1,\min}^2}{4} \left[\mathbf{w}_{1,1}^\dagger \cdots \mathbf{w}_{1,d_{free}}^\dagger \right] \left(\mathbf{I}_{d_{free}} \otimes \Psi_R^{\frac{1}{2}} \right) \text{diag} \left[\mathbf{R}_{2,1}^{-1} \cdots \mathbf{R}_{2,d_{free}}^{-1} \right] \right. \\
&\quad \left. \times \left(\mathbf{I}_{d_{free}} \otimes \Psi_R^{\frac{1}{2}} \right) \left[\mathbf{w}_{1,1}^T \cdots \mathbf{w}_{1,d_{free}}^T \right]^T \right)
\end{aligned}$$

Using the MGF (3.63), conditional PEP conditioned on $\mathbf{h}_2 = [\mathbf{h}_{2,1}, \dots, \mathbf{h}_{2,d_{free}}]$ is upper bounded as

$$\begin{aligned}
\mathcal{P}_{\mathbf{c}_1|\mathbf{h}_2}^{\hat{\mathbf{c}}_1} &\leq \frac{1}{2 \det \left(\mathbf{I}_{n_r d_{free}} + \frac{d_{1,\min}^2}{4} \left(\mathbf{I}_{d_{free}} \otimes \Psi_R^{\frac{1}{2}} \right) \text{diag} \left[\mathbf{R}_{2,1}^{-1} \cdots \mathbf{R}_{2,d_{free}}^{-1} \right] \left(\mathbf{I}_{d_{free}} \otimes \Psi_R^{\frac{1}{2}} \right) \right)} \\
&\stackrel{a}{=} \frac{1}{2 \det \left(\mathbf{I}_{n_r d_{free}} + \frac{d_{1,\min}^2}{4} \left(\mathbf{I}_{d_{free}} \otimes \Psi_R^{\frac{1}{2}} \right) \left(\mathbf{I}_{d_{free}} \otimes \Psi_R^{\frac{1}{2}} \right) \text{diag} \left[\mathbf{R}_{2,1}^{-1} \cdots \mathbf{R}_{2,d_{free}}^{-1} \right] \right)} \\
&\stackrel{b}{=} \frac{1}{2 \det \left(\mathbf{I}_{n_r d_{free}} + \frac{d_{1,\min}^2}{4} \left(\mathbf{I}_{d_{free}} \otimes \Psi_R \right) \text{diag} \left[\mathbf{R}_{2,1}^{-1} \cdots \mathbf{R}_{2,d_{free}}^{-1} \right] \right)} \\
&\stackrel{c}{=} \frac{1}{2 \prod_{i=1}^{n_r d_{free}} \left(1 + \frac{d_{1,\min}^2}{4} \lambda_i \left(\left(\mathbf{I}_{d_{free}} \otimes \Psi_R \right) \text{diag} \left[\mathbf{R}_{2,1}^{-1} \cdots \mathbf{R}_{2,d_{free}}^{-1} \right] \right) \right)} \\
&\leq \frac{1}{2 \prod_{i=1}^{n_r d_{free}} \left(\frac{d_{1,\min}^2}{4} \lambda_i \left(\left(\mathbf{I}_{d_{free}} \otimes \Psi_R \right) \text{diag} \left[\mathbf{R}_{2,1}^{-1} \cdots \mathbf{R}_{2,d_{free}}^{-1} \right] \right) \right)} \quad (4.26)
\end{aligned}$$

where in (a), we have used the identity $\det(\mathbf{I} + \mathbf{AB}) = \det(\mathbf{I} + \mathbf{BA})$ and in (b), we have used the identity $(\mathbf{A} \otimes \mathbf{B})(\mathbf{C} \otimes \mathbf{D}) = \mathbf{AC} \otimes \mathbf{BD}$. In (c), we have used the identity $\det(\mathbf{I} + \mathbf{A}) = \prod_i (1 + \lambda_i(\mathbf{A}))$ assuming that the receive correlation matrix Ψ_R has full rank.

Using the identity that for full rank square matrices $\det(\mathbf{AB}) = \det\mathbf{A}\det\mathbf{B}$ thereby leading to $\prod_i \lambda_i(\mathbf{AB}) = \prod_i \lambda_i(\mathbf{A}) \prod_l \lambda_l(\mathbf{B})$, we can rewrite (4.26) as

$$\begin{aligned} \mathcal{P}_{\mathbf{c}_1|\mathbf{h}_2}^{\hat{\mathbf{c}}_1} &\leq \frac{1}{2 \left(\frac{d_{1,\min}^2}{4}\right)^{d_{free} n_r} \prod_{i=1}^{n_r d_{free}} \lambda_i(\mathbf{I}_{d_{free}} \otimes \mathbf{\Psi}_R) \prod_{l=1}^{n_r d_{free}} \lambda_l(\text{diag}[\mathbf{R}_{2,1}^{-1}, \dots, \mathbf{R}_{2,d_{free}}^{-1}])} \\ &= \frac{1}{2 \left(\frac{d_{1,\min}^2}{4}\right)^{d_{free} n_r} \prod_{i=1}^{n_r} \lambda_i(\mathbf{\Psi}_R)^{d_{free}} (N_0^{-1})^{d_{free}(n_r-1)} \prod_{l=1}^{d_{free}} (\sigma_2^2 \|\mathbf{h}_{2,l}\|^2 + N_0)^{-1}} \end{aligned}$$

where we have considered the fact that the eigenvalues of $\mathbf{R}_{2,k}^{-1}$ are

$$\lambda_j(\mathbf{R}_{2,k}^{-1}) = \begin{cases} (\sigma_2^2 \|\mathbf{h}_{2,k}\|^2 + N_0)^{-1}, & j = 1 \\ N_0^{-1}, & j = 2, \dots, n_r \end{cases} \quad (4.27)$$

So the conditional PEP is upper bounded as

$$\mathcal{P}_{\mathbf{c}_1|\mathbf{h}_2}^{\hat{\mathbf{c}}_1} \leq \frac{1}{2} \left(\frac{4N_0}{d_{1,\min}^2}\right)^{d_{free}(n_r-1)} \left(\frac{4}{d_{1,\min}^2}\right)^{d_{free}} \prod_{i=1}^{n_r} \frac{1}{\lambda_i(\mathbf{\Psi}_R)^{d_{free}}} \prod_{l=1}^{d_{free}} (\sigma_2^2 \|\mathbf{h}_{2,l}\|^2 + N_0) \quad (4.28)$$

Averaging over \mathbf{h}_2 leads to PEP being upper bounded as

$$\mathcal{P}_{\mathbf{c}_1}^{\hat{\mathbf{c}}_1} \leq \frac{1}{2} \left(\frac{4N_0}{\sigma_1^2 \check{d}_{1,\min}^2}\right)^{d_{free}(n_r-1)} \left(\frac{4}{\sigma_1^2 \check{d}_{1,\min}^2}\right)^{d_{free}} (n_r \sigma_2^2 + N_0)^{d_{free}} \prod_{i=1}^{n_r} \frac{1}{\lambda_i(\mathbf{\Psi}_R)^{d_{free}}} \quad (4.29)$$

4.D $P(\hat{x}_{2,k} \neq x_{2,k})$

Derivation of $P(\hat{x}_{2,k} \neq x_{2,k})$ in the case of correlated channel follows the same line as uncorrelated case till (3.82). Then we upperbound both the probabilities, i.e. $P(\|\mathbf{h}_{1,k}\| \leq \|\mathbf{h}_{2,k}\| \mid \mathbf{h}_{1,k})$ and $P(\|\mathbf{h}_{1,k}\| > \|\mathbf{h}_{2,k}\| \mid \mathbf{h}_{1,k})$. Taking expectation over $\mathbf{h}_{2,k}$ conditioned on $\mathbf{h}_{1,k}$ and then subsequently

taking expectation over $\mathbf{h}_{1,k}$ yields:-

$$\begin{aligned}
\mathcal{P}_{x_2}^{\hat{x}_2} &\leq \frac{1}{2} \left[\left(\frac{4N_0}{d_{2,\min}^2 - 4d_{2,\min}d_{1,\max}} \right) \prod_{l=1}^{\kappa} \frac{1}{\lambda_l(\Psi_R)} E_{\mathbf{h}_{1,k}} \exp \left(-\frac{\|\mathbf{h}_{1,k}\|^2 d_{1,\max}^2}{N_0} \right) \right. \\
&\quad \left. + \left(\frac{4N_0}{d_{2,\min}^2} \right) \prod_{l=1}^{\kappa} \frac{1}{\lambda_l(\Psi_R)} E_{\mathbf{h}_{1,k}} \exp \left(-\|\mathbf{h}_{1,k}\|^2 \frac{d_{1,\max}^2 - d_{2,\min}d_{1,\max}}{N_0} \right) \right] \\
&\leq \frac{1}{2} \left(\frac{4N_0}{\sigma_2^2 \check{d}_{2,\min}^2} \right) \left(\frac{N_0}{\sigma_1^2 \check{d}_{1,\max}^2} \right) \prod_{l=1}^{\kappa} \frac{1}{(\lambda_l(\Psi_R))^2} \left(\frac{1}{\left(1 - \frac{4\sigma_1 \check{d}_{1,\max}}{\sigma_2 \check{d}_{2,\min}}\right)^\kappa} + \frac{1}{\left(1 - \frac{\sigma_2 \check{d}_{2,\min}}{\sigma_1 \check{d}_{1,\max}}\right)^\kappa} \right)
\end{aligned} \tag{4.30}$$

where we have used the MGF of Hermitian quadratic form of a Gaussian random variable while writing $\|\mathbf{h}_{j,k}\|^2 = \mathbf{h}_{j,k}^\dagger \mathbf{I}_{n_r} \mathbf{h}_{j,k}$ where $\mathbf{h}_{j,k} \sim \mathcal{CN}(\mathbf{0}, \Psi_R)$. This expression shows the dependence of $P(\hat{x}_{2,k} \neq x_{2,k})$ on the interference strength, SNR and the receive correlation. Interestingly there is no dependence on the transmit correlation.

Part III

Multuser MIMO

Chapter 5

Making Multiuser MIMO Work for LTE

5.1 Introduction

The spatial dimension arising from the usage of multiple antennas promises improved reliability and higher spectral efficiency [2]. These extra spatial degrees of freedom can be advantageously exploited to enhance the system capacity by spatial separation of the co-scheduled users. This spatial sharing of the channel (spatial multiple access) without any bandwidth expansion entails a fundamental paradigm shift from single user (SU) communications. Some of the key advantages of multiuser (MU) MIMO communications over SU MIMO communications are as follows:

- MU MIMO is more immune to most of the propagation limitations plaguing SU MIMO communications such as channel rank loss or antenna correlation as it provides decorrelation of the spatial signatures of the users.
- Line of sight propagation (low rank channels), which causes severe degradation in SU multi-stream transmission schemes, is no longer a problem in MU setting.
- MU MIMO allows user multiplexing in addition to stream multiplexing, i.e. it allows the spatial multiplexing gain at the BS to be obtained

without the need for multiple antenna terminals, thereby allowing the development of small and cheap terminals while intelligence and cost is kept on the infrastructure side.

- MU MIMO adds another dimension to the diversity, i.e. MU diversity [14].

These advantages unfortunately come at a price. Perhaps the most substantial cost is due to the fact that MU MIMO requires (although benefits from) CSIT to properly serve the spatially multiplexed users [13]. CSIT, while not essential in SU MIMO communication channels, is of critical importance to most downlink MU precoding techniques. The need for CSIT feedback places a significant burden on the uplink capacity in most systems, exacerbated in modern wireless systems which are characterized by wideband (OFDM) and high mobility (such as 3GPP-LTE, WiMax, etc.). Intricacy in the acquisition of CSIT combined with the complexity of scheduling algorithms render the feasibility of MU MIMO for future wireless systems in question.

5.1.1 The State of the Art

Optimal precoding in MU MIMO Gaussian broadcast channel involves a theoretical pre-interference subtraction technique known as dirty paper coding (DPC) [24] combined with an implicit user scheduling and power loading algorithm. Due to the highly nonlinear nature of signal processing involved in DPC, its practical implementation is far from realizable and moreover, its optimality is constrained to idealistic Gaussian alphabets. Another nonlinear transmit processing technique is Tomlinson-Harashima precoding (THP) [70] [71] which is closely related to the decision feedback equalizers (DFEs). Whereas DFE feeds back already quantized symbols, the already transmitted symbols are fed back in a THP system and modulo operations are applied at the transmitter and the receiver(s). Still being nonlinear, its hardware implementation is quite challenging. Linear precoding provides an alternative approach trading off a reduction in the precoder complexity for suboptimal performance. Interference cancellation based schemes such as channel inversion (CI) [21] and interference attenuation based schemes such as regularized channel inversion (RCI) [25] transform the MU downlink into parallel SU systems.

5.1.2 Motivation

Precoding strategies, both in SU MIMO and MU MIMO systems, strive to transform the cross-coupled channels into parallel noninteracting channels therefore leading to simplified receiver structures. However, they are void of exploiting the interference structure in mitigating its effect. This evasion is evident as these precoding strategies are based on the Gaussian assumption for interference which encompasses no structure to be manipulated. In the real world, inputs must be drawn from discrete constellations (often with very limited peak-to-average ratios) which may significantly depart from the Gaussian idealization. The ensuing interferences have structures that can be exploited in the detection process. Precoders can therefore be designed to manage the interference in a way that this interference can be effectively exploited in the detection process at the receivers.

Modern wireless systems characterized by a large number of users are considering different precoding strategies to transmit spatial streams to multiple users sharing the same time-frequency resources in order to achieve high capacity gains. In 3GPP LTE system [72], several MIMO modes of operation including precoding for SU MIMO and MU MIMO are considered. The precoders defined in LTE [5] are low resolution and are based on the principle of equal gain transmission (EGT). This transmission strategy has more modest transmit amplifier requirements as compared to the other precoding strategies since it does not require antenna amplifiers to modify the amplitudes of the transmitted signals. This property therefore allows inexpensive amplifiers to be used at each antenna as long as the gains are carefully matched. However, the efficient employment of these precoders for MU MIMO mode is not yet fully understood. This has led to the common perception that MU MIMO is not workable in LTE [9] (page 244).

5.1.3 Contribution

In this chapter, we look into the viability of MU MIMO for LTE by investigating the effectiveness of the low resolution LTE precoders. We propose a precoding strategy based on the LTE precoders which encompasses geometrical interference alignment at the eNodeB (LTE notation for the base station) followed by the exploitation of the residual interference structure by the user equipments (UEs). On one hand, this strategy reduces the interference seen by each UE by a geometric scheduling algorithm while on the other hand, UEs exploit the structure of the residual interference in the detection process. To this end, we propose an extension of the previously

proposed low complexity matched filter (MF) based detector (chapter 3) in this scenario. This low complexity detector not only reduces one complex dimension of the system but also exploits the interference structure in the detection process at no additional cost of complexity (in two users case). However, the prerequisites of the MF based detector are the knowledge of the precoder of interference (other co-scheduled user) and its constellation. Though the proposed scheduling strategy enables the UE to find the precoder of interference but the information regarding its constellation is still eluded as downlink control information (DCI) formats in 3GPP LTE [32] do not allow the transmission of this information to the UE. Consequently we also look at the sensitivity of the proposed detector to the knowledge of the interfering constellation and propose a MF based blind detector. However, the significance of this information motivates its consideration to be included in the ongoing standardization of LTE-Advanced [6]. We also propose an algorithm for the employment of LTE precoders for SU MIMO mode and we further look at the performance analysis of EGT precoders for SU MIMO. We show that EGT has full diversity in SU MIMO mode (a result earlier derived for equal gain combining for BPSK in [73] and for EGT in MIMO systems in [74]). Analysis of EGT in MU MIMO mode seems to be intractable so we show by simulations that EGT in MU MIMO mode suffers from a loss of diversity.

5.1.4 Organization

This chapter is divided into six sections. In section II, we give a brief overview of LTE and define the system model. In section III, we propose a strategy for MU MIMO mode in LTE and look at the information theoretic perspective of this strategy. We also extend the low complexity MF based detectors (proposed in chapter 3) to this scenario for single and dual antenna UEs. Section IV is dedicated to the performance analysis of EGT precoders. Section V comprises of simulation results which are followed by the conclusions.

5.2 LTE System Model

5.2.1 LTE - A Brief Overview

In 3GPP LTE, a 2×2 configuration for MIMO is assumed as the baseline configuration however, configurations with four transmit or receive antennas are also foreseen and reflected in the specifications [72]. LTE restricts

transmission of maximum of two codewords in the downlink which can be mapped onto different layers where one codeword represents an output from the channel encoder. Number of layers available for transmission is equal to the rank of the channel matrix (maximum four). In this chapter, we restrict ourselves to the baseline configuration with eNodeB equipped with two antennas while we consider single and dual antenna UEs. Physical layer technology employed for the downlink in LTE is OFDMA combined with BICM [4]. Several different transmission bandwidths are possible, ranging from 1.08 MHz to 19.8 MHz with the constraint of being a multiple of 180 kHz. Resource Blocks (RBs) are defined as groups of 12 consecutive resource elements (REs - LTE notation for subcarriers) with a bandwidth of 180 kHz thereby leading to the constant RE spacing of 15 kHz. For 5 MHz bandwidth, it is divided into 25 RBs. Approximately 4 RBs form a subband and the feedback is generally done on subband basis. Minimum allocation in time domain is a subframe or transmission time interval (TTI), which has a duration of 1 ms and consists of two slots. One TTI consists of 12 or 14 OFDM symbols depending on normal or extended cyclic prefix. Seven operation modes are specified in LTE downlink, however, we focus on the following modes.

- Transmission mode 2. Fall back transmit diversity. Transmission rank is one. Employs Alamouti scheme [40].
- Transmission mode 4. Closed-loop spatial multiplexing. Transmission rank is two. SU MIMO mode.
- Transmission mode 5. MU MIMO mode. Supports only rank one transmission.
- Transmission mode 6. Closed-loop precoding for rank one transmission. SU MIMO mode.

In the case of transmit diversity and closed loop precoding, one data stream is transmitted to each UE using Alamouti code in the former case and LTE precoders in the latter case. In closed-loop spatial multiplexing, two data streams are transmitted to each UE using LTE precoders. The UE needs to have minimum of two antennas for transmission mode 4. Time-frequency resources are orthogonal to different UEs in these modes thereby avoiding interference in the system. However, in MU MIMO mode, parallel data streams are transmitted simultaneously, one for each UE, sharing the same time-frequency resources. Note that LTE restricts transmission of one

stream to each UE in MU MIMO mode. Here we do not consider transmission mode 1 (single-antenna transmission), transmission mode 3 (open-loop spatial multiplexing employing cyclic delay diversity when transmission rank is greater than 1) and transmission mode 7 (beamforming based on direction of arrival estimations).

Transmission modes 4, 5 and 6 are closed loop, i.e. they are based on the UE feedback which is crucial in order to select precoders taking into account current state of the channel. There are three types of feedback: the precoding matrix indication (PMI), the channel quality indication (CQI) and the rank indication (RI). PMI is an index in the codebook for the preferred precoder to be used by the eNodeB. The granularity for computation and signaling of the precoding index can range from a couple of RBs to the full bandwidth. For transmission mode 5, the eNodeB selects the precoding matrix to induce high orthogonality between the streams so that interference between data streams is minimized. In transmission modes 4 and 6, the eNodeB selects the precoding vector/matrix such that data streams are transmitted to the corresponding UEs with maximum throughput. RI is wideband, i.e. one value is fed back for the entire bandwidth. CQI can be on wideband or on subband basis. For wideband CQI, one CQI value is fed back for the whole system bandwidth while for subband CQI, in addition to one wideband value, a CQI value for each subband is fed back based on differential encoding.

In LTE, it is assumed that the UEs are semi-statically allocated in MU MIMO mode, implying that it is not allowed for a UE to be scheduled in one subframe in MU MIMO mode and in the next subframe in SU MIMO mode. For each resource allocation, the scheduler has to decide between single-stream SU transmission or MU-MIMO transmission. For transmission modes 4, 5 and 6, low resolution precoders are employed which are based on the principle of EGT. For the case of eNodeB with two antennas, LTE proposes the use of following four precoders for transmission mode 5 basing on two bits feedback from the UEs:

$$\mathbf{p} = \frac{1}{\sqrt{4}} \begin{bmatrix} 1 \\ 1 \end{bmatrix}, \frac{1}{\sqrt{4}} \begin{bmatrix} 1 \\ -1 \end{bmatrix}, \frac{1}{\sqrt{4}} \begin{bmatrix} 1 \\ j \end{bmatrix}, \frac{1}{\sqrt{4}} \begin{bmatrix} 1 \\ -j \end{bmatrix} \quad (5.1)$$

The number of precoders increases to sixteen in the case of four transmit antennas however in this chapter we restrict to the case of two transmit antennas. The precoders remain same for transmission mode 6 except with

a change of scaling factor for normalizing the power, i.e.

$$\mathbf{P} = \frac{1}{\sqrt{2}} \begin{bmatrix} 1 \\ 1 \end{bmatrix}, \frac{1}{\sqrt{2}} \begin{bmatrix} 1 \\ -1 \end{bmatrix}, \frac{1}{\sqrt{2}} \begin{bmatrix} 1 \\ j \end{bmatrix}, \frac{1}{\sqrt{2}} \begin{bmatrix} 1 \\ -j \end{bmatrix} \quad (5.2)$$

For transmission mode 4, LTE proposes the use of following two precoder matrices on subband basis.

$$\mathbf{P} = \frac{1}{\sqrt{4}} \begin{bmatrix} 1 & 1 \\ 1 & -1 \end{bmatrix}, \frac{1}{\sqrt{4}} \begin{bmatrix} 1 & 1 \\ j & -j \end{bmatrix} \quad (5.3)$$

Note that there is a possibility of swapping the columns in \mathbf{P} but the swap must occur over the entire band.

5.2.2 System Model

We first consider the system model for transmission mode 5, i.e. MU MIMO mode in which the eNodeB transmits one stream each to two single antenna UEs using the same time-frequency resources. During the transmission for UE-1, the code sequence $\underline{\mathbf{c}}_1$ is interleaved by π_1 and then is mapped onto the signal sequence $\underline{\mathbf{x}}_1$. x_1 is the symbol of $\underline{\mathbf{x}}_1$ over a signal set $\chi_1 \subseteq \mathcal{C}$ with a Gray labeling map where $|\chi_1| = M_1$ and x_2 is the symbol of $\underline{\mathbf{x}}_2$ over signal set χ_2 where $|\chi_2| = M_2$. The bit interleaver for UE-1 can be modeled as $\pi_1 : k' \rightarrow (k, i)$ where k' denotes the original ordering of the coded bits $c_{k'}$, k denotes the RE of the symbol $x_{1,k}$ and i indicates the position of the bit $c_{k'}$ in the symbol $x_{1,k}$. Note that each RE corresponds to a symbol from a constellation map χ_1 for UE-1 and χ_2 for UE-2. Selection of the normal or extended cyclic prefix (CP) for each OFDM symbol converts the downlink frequency selective channel into parallel flat fading channels. Cascading IFFT at the eNodeB and FFT at the UE with cyclic prefix extension, transmission at the k -th RE for UE-1 in mode 5 can be expressed as

$$y_{1,k} = \mathbf{h}_{1,k}^\dagger \mathbf{p}_{1,k} x_{1,k} + \mathbf{h}_{1,k}^\dagger \mathbf{p}_{2,k} x_{2,k} + z_{1,k}$$

where $y_{1,k}$ is the received symbol at UE-1 and $z_{1,k}$ is the zero mean circularly symmetric complex white Gaussian noise of variance N_0 . $x_{1,k}$ is the complex symbol for UE-1 with the variance σ_1^2 and $x_{2,k}$ is the symbol for UE-2 with the variance σ_2^2 . $\mathbf{h}_{n,k}^\dagger \in \mathbb{C}^{1 \times 2}$ symbolizes the spatially uncorrelated flat Rayleigh fading MISO channel from the eNodeB to the n -th UE ($n = 1, 2$) at the k -th RE. Its elements can therefore be modeled as independent and identically distributed (iid) zero mean circularly symmetric complex Gaussian random variables with a variance of 0.5 per dimension. Note that $\mathbb{C}^{1 \times 2}$

denotes a two dimensional complex space. $\mathbf{p}_{n,k}$ denotes the precoding vector for the n -th UE at the k -th RE and is given by (5.1). For the dual antenna UEs, the system equation for mode 5 is modified as

$$\mathbf{y}_{1,k} = \mathbf{H}_{1,k} [\mathbf{p}_{1,k}x_{1,k} + \mathbf{p}_{2,k}x_{2,k}] + \mathbf{z}_{1,k}$$

where $\mathbf{y}_{1,k}, \mathbf{z}_{1,k} \in \mathbb{C}^{2 \times 1}$ are the vectors of the received symbols and circularly symmetric complex white Gaussian noise of double-sided power spectral density $N_0/2$ at 2 receive antennas of UE-1 while $\mathbf{H}_{1,k} \in \mathbb{C}^{2 \times 2}$.

As in transmission mode 6 only one UE will be served in one time-frequency resource, the system equation for single antenna UE at the k -th RE is given as

$$y_k = \mathbf{h}_k^\dagger \mathbf{p}_k x_k + z_k$$

where \mathbf{p}_k is given by (5.2). For the dual antenna UEs, the system equation for mode 6 is modified as

$$\mathbf{y}_k = \mathbf{H}_k \mathbf{p}_k x_k + \mathbf{z}_k$$

The system equation for mode 4 in the case of dual antenna UE is written as

$$\mathbf{y}_k = \mathbf{H}_k \mathbf{P}_k \mathbf{x}_k + \mathbf{z}_k$$

where \mathbf{P}_k is the precoding matrix employed by the eNodeB at k -th RE and is given by (5.3). $\mathbf{x}_k \in \mathbb{C}^{2 \times 1}$ is the vector of two complex symbols.

5.3 MU MIMO Mode

We now look at the effectiveness of low resolution LTE precoders for MU MIMO mode and propose a strategy for their effectual utilization. We consider both single and dual antenna UEs.

5.3.1 Single Antenna UEs

As the processing at the UE is performed on a RE basis for each received OFDM symbol, the dependency on RE index can be ignored for notational convenience thereby leading to the system equation for mode 5 as

$$y_1 = \mathbf{h}_1^\dagger \mathbf{p}_1 x_1 + \mathbf{h}_1^\dagger \mathbf{p}_2 x_2 + z_1$$

Our proposed precoding strategy involves the computation of low complexity MF precoders at the UEs. Having channel knowledge, this computation

involves merely a conjugate operation while the computation of other precoders like CI [21] or RCI [25] involve complex matrix inversions. As the decision to schedule a UE in SU MIMO, MU MIMO or transmit diversity mode will be made by the eNodeB, each UE is expected to feedback the precoder which maximizes its received signal strength. Therefore, in accordance with the low resolution LTE precoders as given in (5.2), the UEs compute quantized versions of their respective MF precoders, i.e. the UE first measures its channel $\mathbf{h}_1^\dagger = [h_{11}^* \quad h_{21}^*]$ from the eNodeB and consequently computes the MF precoder $[h_{11} \quad h_{21}]^T$ (the normalized version involves a division by $\|\mathbf{h}_1\|$). As LTE precoders are characterized by unit coefficients (see (5.1)), UE normalizes the first coefficient of the MF precoder so that

$$\mathbf{p}_{MF} = \frac{h_{11}^*}{|h_{11}|^2} \begin{bmatrix} h_{11} \\ h_{21} \end{bmatrix} = \begin{bmatrix} 1 \\ h_{11}^* h_{21} / |h_{11}|^2 \end{bmatrix} \quad (5.4)$$

The second coefficient indicates the phase between the two channel coefficients. Now basing on the minimum distance between \mathbf{p}_{MF} and \mathbf{p} , one of the four precoders is selected by the UE and the index of that precoder is fed back to the eNodeB. Let that precoder be $\mathbf{p}_1 = \frac{1}{\sqrt{2}} \begin{bmatrix} 1 \\ q \end{bmatrix}$, $q \in [\pm 1, \pm j]$. From the geometrical perspective, this precoder once employed by the eNodeB would try to align h_{21}^* with h_{11}^* in the complex plane so as to maximize the received signal power, i.e. $|h_{11}^* + qh_{21}^*|^2$ subject to the constraint that the precoder allows rotation of h_{21}^* by $0^\circ, \pm 90^\circ$ or 180° . Therefore this precoding ensures that h_{11}^* and h_{21}^* lie in the same quadrant as shown in fig. 5.1(b). These requested precoders may be employed by the eNodeB if it decides to serve the UEs in SU MIMO mode (transmission mode 6).

In MU MIMO mode, two UEs can be served by the eNodeB on the same time-frequency resources. We assume a densely populated cell where the eNodeB has the requested precoders of most of the UEs in the cell. Here we propose a scheduling algorithm for MU MIMO mode where the eNodeB schedules two UEs on the same RBs which have requested opposite precoders, i.e. the eNodeB selects as the second UE to be served in each group of allocatable RBs one of the UEs whose requested precoder \mathbf{p}_2 is 180° out of phase from the precoder \mathbf{p}_1 of the first UE to be served on the same RBs. The precoder matrix is therefore given as $\mathbf{P} = \frac{1}{\sqrt{4}} \begin{bmatrix} 1 & 1 \\ q & -q \end{bmatrix}$. So the signal received by UE-1 is given as

$$y_1 = \frac{1}{\sqrt{4}} (h_{11}^* + qh_{21}^*) x_1 + \frac{1}{\sqrt{4}} (h_{11}^* - qh_{21}^*) x_2 + z_1 \quad (5.5)$$

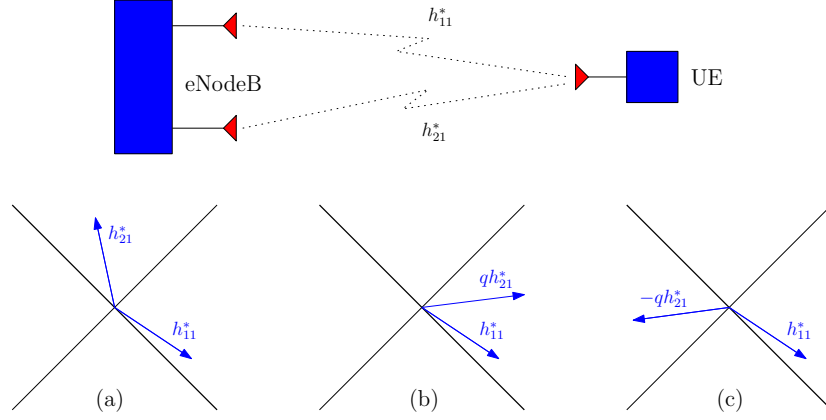


Figure 5.1: Geometric alignment of interference. (a) shows the original channel from the eNodeB to the UE while (b) shows the effective channel of the desired signal while (c) shows the effective channel of the interference.

where the selection of the precoder for each UE would ensure maximization of its desired signal strength, i.e. $|\mathbf{h}_1^\dagger \mathbf{p}_1|^2$ for the first UE and $|\mathbf{h}_2^\dagger \mathbf{p}_2|^2$ for the second UE while selection of the UE pairs with out of phase precoders would ensure minimization of the interference strength seen by each UE, i.e. $|\mathbf{h}_1^\dagger \mathbf{p}_2|^2$ for the first UE and $|\mathbf{h}_2^\dagger \mathbf{p}_1|^2$ for the second UE. Note that these maximizations and minimizations are subject to the constraint of the utilization of low resolution LTE precoders. This scheduling strategy would ensure that the UEs selected to be served in MU MIMO mode on same time-frequency resources have good channel separation.

Let θ be the angle between h_{11}^* and h_{21}^* which can be calculated as $\theta = \cos^{-1} \left(\frac{(h_{11} h_{21}^*)_R}{|h_{11}| |h_{21}|} \right)$ where $(\cdot)_R$ indicates the real part. Conditioned on the use of the proposed precoding and scheduling strategy, the strength of the desired signal for UE-1 is given as

$$\begin{aligned} |\mathbf{h}_1^\dagger \mathbf{p}_1|^2 &= \sigma_1^2 |h_{11}^* + qh_{21}^*|^2 / 4 \\ &= \sigma_1^2 \left(|h_{11}|^2 + |h_{21}|^2 + 2|h_{11}| |h_{21}| \max(|\cos \theta|, |\sin \theta|) \right) / 4 \end{aligned}$$

where

$$\max(|\cos \theta|, |\sin \theta|) = \max(\cos(\theta), \cos(\theta \pm 90^\circ), \cos(\theta + 180^\circ))$$

The strength of the interference signal seen by UE-1 is given as

$$\begin{aligned} \left| \mathbf{h}_1^\dagger \mathbf{p}_2 \right|^2 &= \sigma_2^2 |h_{11}^* - qh_{21}^*|^2 / 4 \\ &= \sigma_2^2 \left(|h_{11}|^2 + |h_{21}|^2 - 2|h_{11}||h_{21}|\max(|\cos \theta|, |\sin \theta|) \right) / 4 \end{aligned}$$

Though this precoding and scheduling strategy would ensure minimization of interference under the constraint of low resolution LTE precoders, the residual interference would still be significant. This interference belongs to a finite alphabet and its structure can be exploited in the detection process however this exploitation comes at the cost of enhanced complexity. Here we propose an extension of the earlier proposed low complexity MF based detector which on one hand reduces one complex dimension of the system while on the other, exploits the interference structure in the detection of the desired stream.

Low Complexity MF Based Detector

The max log MAP bit metric for the bit $c_{k'}$ of x_1 is given as [4]

$$\begin{aligned} \Lambda_1^i(y_1, c_{k'}) &\approx \min_{x_1 \in \chi_{1,c_{k'}}^i, x_2 \in \chi_2} \left| y_1 - \mathbf{h}_1^\dagger \mathbf{p}_1 x_1 - \mathbf{h}_1^\dagger \mathbf{p}_2 x_2 \right|^2 \\ &= \min_{x_1 \in \chi_{1,c_{k'}}^i, x_2 \in \chi_2} \left\{ |y_1|^2 + \left| \mathbf{h}_1^\dagger \mathbf{p}_1 x_1 \right|^2 - 2 \left(\mathbf{h}_1^\dagger \mathbf{p}_1 x_1 y_1^* \right)_R + 2 (\rho_{12} x_1^* x_2)_R \right. \\ &\quad \left. - 2 \left(\mathbf{h}_1^\dagger \mathbf{p}_2 x_2 y_1^* \right)_R + \left| \mathbf{h}_1^\dagger \mathbf{p}_2 x_2 \right|^2 \right\} \end{aligned} \quad (5.6)$$

where $\chi_{1,c_{k'}}^i$ denotes the subset of the signal set $x_1 \in \chi_1$ whose labels have the value $c_{k'} \in \{0, 1\}$ in the position i and $p_{12} = \left(\mathbf{h}_1^\dagger \mathbf{p}_1 \right)^* \mathbf{h}_1^\dagger \mathbf{p}_2$ indicates the cross correlation between the two coefficients. The complexity of detection is $\mathcal{O}(|\chi_1||\chi_2|)$. Proceeding on lines similar to section 3.4.1, we introduce two terms as outputs of MF, i.e. $\bar{y}_1 = \left(\mathbf{h}_1^\dagger \mathbf{p}_1 \right)^* y_1$ and $\bar{y}_2 = \left(\mathbf{h}_1^\dagger \mathbf{p}_2 \right)^* y_1$. Ignoring $|y_1|^2$ and writing the terms involving interference (x_2) in their real and imaginary parts, we have

$$\begin{aligned} \Lambda_1^i(y_1, c_{k'}) &\approx \min_{x_1 \in \chi_{1,c_{k'}}^i, x_2 \in \chi_2} \left\{ \left| \mathbf{h}_1^\dagger \mathbf{p}_1 x_1 \right|^2 - 2(\bar{y}_1^* x_1)_R + \left| \mathbf{h}_1^\dagger \mathbf{p}_2 \right|^2 x_{2,R}^2 + \left| \mathbf{h}_1^\dagger \mathbf{p}_2 \right|^2 x_{2,I}^2 \right. \\ &\quad \left. + 2(p_{12,R} x_{1,R} + p_{12,I} x_{1,I} - \bar{y}_{2,R}) x_{2,R} + 2(p_{12,R} x_{1,I} - p_{12,I} x_{1,R} - \bar{y}_{2,I}) x_{2,I} \right\} \end{aligned} \quad (5.7)$$

where $(\cdot)_I$ indicates the imaginary part. For x_2 belonging to equal energy alphabets, the bit metric is

$$\Lambda_1^i(y_1, c_{k'}) \approx \min_{x_1 \in \chi_{1,c_{k'}}^i} \left\{ \left| \mathbf{h}_1^\dagger \mathbf{p}_1 x_1 \right|^2 - 2 (\bar{y}_1^* x_1)_R - 2 |p_{12,R} x_{1,R} + p_{12,I} x_{1,I} - \bar{y}_{2,R}| |x_{2,R}| \right. \\ \left. - 2 |p_{12,R} x_{1,I} - p_{12,I} x_{1,R} - \bar{y}_{2,I}| |x_{2,I}| \right\} \quad (5.8)$$

which is on similar lines as (3.25). If x_2 belongs to QPSK for which the values of $x_{2,R}$ and $x_{2,I}$ are $\left[\pm \frac{\sigma_2}{\sqrt{2}} \right]$, then the bit metric is written as

$$\Lambda_1^i(y_1, c_{k'}) \approx \min_{x_1 \in \chi_{1,c_{k'}}^i} \left\{ \left| \mathbf{h}_1^\dagger \mathbf{p}_1 x_1 \right|^2 - 2 (\bar{y}_1^* x_1)_R - \sqrt{2} \sigma_2 |p_{12,R} x_{1,R} + p_{12,I} x_{1,I} - \bar{y}_{2,R}| \right. \\ \left. - \sqrt{2} \sigma_2 |p_{12,R} x_{1,I} - p_{12,I} x_{1,R} - \bar{y}_{2,I}| \right\} \quad (5.9)$$

For x_2 belonging to non equal energy alphabets, the bit metric is written as

$$\Lambda_1^i(y_1, c_{k'}) \approx \min_{x_1 \in \chi_{1,c_{k'}}^i} \left\{ \left| \mathbf{h}_1^\dagger \mathbf{p}_1 x_1 \right|^2 - 2 (\bar{y}_1^* x_1)_R + \left| \mathbf{h}_1^\dagger \mathbf{p}_2 \right|^2 |x_{2,R}|^2 + \left| \mathbf{h}_1^\dagger \mathbf{p}_2 \right|^2 |x_{2,I}|^2 \right. \\ \left. - 2 |p_{12,R} x_{1,R} + p_{12,I} x_{1,I} - \bar{y}_{2,R}| |x_{2,R}| - 2 |p_{12,R} x_{1,I} - p_{12,I} x_{1,R} - \bar{y}_{2,I}| |x_{2,I}| \right\} \quad (5.10)$$

where in this metric, $x_{2,R}$ and $x_{2,I}$ are the discrete optimal values of $x_2 \in \chi_2$ minimizing (5.10). Their continuous counterparts (see 3.26)) can be found as

$$|x_{2,R}| = \left| \frac{p_{12,R} x_{1,R} + p_{12,I} x_{1,I} - \bar{y}_{2,R}}{\left| \mathbf{h}_1^\dagger \mathbf{p}_2 \right|^2} \right| \\ |x_{2,I}| = \left| \frac{p_{12,R} x_{1,I} - p_{12,I} x_{1,R} - \bar{y}_{2,I}}{\left| \mathbf{h}_1^\dagger \mathbf{p}_2 \right|^2} \right| \quad (5.11)$$

We consider the cases of x_2 belonging to QAM16 and QAM64 for the discretization of these continuous values. As the values of $x_{2,R}$ and $x_{2,I}$ for the case of QAM16 are $\left[\pm \frac{\sigma_2}{\sqrt{10}}, \pm \frac{3\sigma_2}{\sqrt{10}} \right]$ so their magnitudes in (5.10) are given

as

$$|x_{2,R}| = \sigma_2 \frac{1}{\sqrt{10}} \left(2 + (-1)^{I\left(|\psi_A| < \sigma_2 \frac{2|\mathbf{h}_1^\dagger \mathbf{p}_2|^2}{\sqrt{10}}\right)} \right)$$

$$|x_{2,I}| = \sigma_2 \frac{1}{\sqrt{10}} \left(2 + (-1)^{I\left(|\psi_B| < \sigma_2 \frac{2|\mathbf{h}_1^\dagger \mathbf{p}_2|^2}{\sqrt{10}}\right)} \right)$$

where

$$\psi_A = p_{12,R}x_{1,R} + p_{12,I}x_{1,I} - \bar{y}_{2,R}$$

$$\psi_B = p_{12,R}x_{1,I} - p_{12,I}x_{1,R} - \bar{y}_{2,I}$$

and $I(\cdot)$ is the indicator function defined as

$$I(a < b) = \begin{cases} 1 & \text{if } a < b \\ 0 & \text{otherwise} \end{cases}$$

For the case of x_2 belonging to QAM64, the values of $x_{2,R}$ and $x_{2,I}$ are $\left[\pm \frac{\sigma_2}{\sqrt{42}}, \pm \frac{3\sigma_2}{\sqrt{42}}, \pm \frac{\sigma_2}{5\sqrt{42}}, \pm \frac{\sigma_2}{7\sqrt{42}}\right]$. So the magnitudes of $x_{2,R}$ and $x_{2,I}$ in (5.10) are given as

$$|x_{2,R}| = \frac{\sigma_2}{\sqrt{42}} \left\{ 4 + (-1)^{I\left(|\psi_A| < \sigma_2 \frac{4|\mathbf{h}_1^\dagger \mathbf{p}_2|^2}{\sqrt{42}}\right)} + 2(-1)^{I\left(|\psi_A| < \sigma_2 \frac{2|\mathbf{h}_1^\dagger \mathbf{p}_2|^2}{\sqrt{42}}\right)} \right.$$

$$\left. \times \left[I\left(|\psi_A| < \sigma_2 \frac{2|\mathbf{h}_1^\dagger \mathbf{p}_2|^2}{\sqrt{42}}\right) \parallel I\left(|\psi_A| > \sigma_2 \frac{6|\mathbf{h}_1^\dagger \mathbf{p}_2|^2}{\sqrt{42}}\right) \right] \right\}$$

$$|x_{2,I}| = \frac{\sigma_2}{\sqrt{42}} \left\{ 4 + (-1)^{I\left(|\psi_B| < \sigma_2 \frac{4|\mathbf{h}_1^\dagger \mathbf{p}_2|^2}{\sqrt{42}}\right)} + 2(-1)^{I\left(|\psi_B| < \sigma_2 \frac{2|\mathbf{h}_1^\dagger \mathbf{p}_2|^2}{\sqrt{42}}\right)} \right.$$

$$\left. \times \left[I\left(|\psi_B| < \sigma_2 \frac{2|\mathbf{h}_1^\dagger \mathbf{p}_2|^2}{\sqrt{42}}\right) \parallel I\left(|\psi_B| > \sigma_2 \frac{6|\mathbf{h}_1^\dagger \mathbf{p}_2|^2}{\sqrt{42}}\right) \right] \right\}$$

where \parallel indicates OR operation. So the complexity of detection system reduces to $\mathcal{O}(|\mathcal{X}_1|)$ thereby trimming down one complex dimension of the system. The

proposed detector not only has complexity equivalent to that of a detector confronting no interference but has the ability to exploit the structure of the interference in detecting the desired signal. As the UE already knows its own channel and the requested precoder, it can determine the effective channel of the interference basing on the above mentioned scheduling algorithm, i.e. the precoder of the interference is 180° out of phase of the precoder of the desired signal. Consequently there is no additional complexity in utilizing this detector as compared to using SU detectors except that the UE needs to know the interference constellation.

Information Theoretic Perspective

In this section, we look at the information theoretic analysis of the system while restricting ourselves to the case of finite alphabets. We analyze the degradation caused by the low level quantization and EGT of LTE precoders with reference to the unquantized precoders and optimal linear precoders. The sum rate of the downlink channel (MU MIMO) with two UEs for a given precoder \mathbf{P} is given as

$$I = I(Y_1; X_1 | \mathbf{H}, \mathbf{P}) + I(Y_2; X_2 | \mathbf{H}, \mathbf{P}) \quad (5.12)$$

where $\mathbf{P} = [\mathbf{p}_1 \ \mathbf{p}_2]$ is the precoder matrix and $I(Y_1; X_1 | \mathbf{H}, \mathbf{P})$ is the mutual information of UE-1 once the channel is known at the receiver. Y_1 is the received signal by single-antenna UE-1 whereas X_1 is the signal transmitted by the eNodeB for UE-1. Note that the precoder \mathbf{P} is employed by the transmitter and is the function of the channel. How much channel information is available at the transmitter and which types of receivers are being employed by the users dictate different options for the precoder \mathbf{P} . As per 3GPP LTE, we assume equal power distribution between the two UEs. The above mutual information expressions for the case of finite alphabets have been derived in Appendix 5A. For the choice of the precoder, we look at the following different possible choices of linear precoders.

CI precoding matrix [75] can be found by the Moore-Penrose pseudoinverse which is given as

$$\mathbf{W} = \ddot{\mathbf{H}}^\dagger \left(\ddot{\mathbf{H}} \ddot{\mathbf{H}}^\dagger \right)^{-1} \quad (5.13)$$

where $\ddot{\mathbf{H}}^\dagger = [\mathbf{h}_1 \ \mathbf{h}_2]$. The CI precoding matrix \mathbf{P} can be obtained from \mathbf{W} by normalizing all of its columns. For rank-deficient channels, the performance of CI precoding can be improved by a regularization of the pseudo-inverse

as mentioned in [25], i.e. RCI, which can be expressed as

$$\mathbf{P} = \ddot{\mathbf{H}}^\dagger \left(\ddot{\mathbf{H}}\ddot{\mathbf{H}}^\dagger + \frac{n_t N_0}{\sigma^2} \mathbf{I}_2 \right)^{-1} \quad (5.14)$$

where n_t is the number of transmit antennas which is 2 in this case. Moreover, it is assumed that $\sigma_1^2 = \sigma_2^2 = \sigma^2$. The precoder is normalized as $\mathbf{P}/\sqrt{\text{tr}(\mathbf{P}^\dagger\mathbf{P})}$. The MF precoder [75] is given as

$$\mathbf{p}_1 = \frac{1}{\sqrt{|h_{11}|^2 + |h_{21}|^2}} \begin{bmatrix} h_{11} \\ h_{21} \end{bmatrix}, \quad \mathbf{p}_2 = \frac{1}{\sqrt{|h_{12}|^2 + |h_{22}|^2}} \begin{bmatrix} h_{12} \\ h_{22} \end{bmatrix} \quad (5.15)$$

For EGT, the unquantized MF precoder is given as

$$\mathbf{p}_1 = \frac{1}{\sqrt{2}} \begin{bmatrix} 1 \\ h_{11}^* h_{21} / |h_{11}| |h_{21}| \end{bmatrix}, \quad \mathbf{p}_2 = \frac{1}{\sqrt{2}} \begin{bmatrix} 1 \\ h_{12}^* h_{22} / |h_{12}| |h_{22}| \end{bmatrix} \quad (5.16)$$

For comparison purposes, we also look at an optimal linear precoder that maximizes the sum rate. Under the power constraint P_t , the optimal linear precoder will be the solution to the following equation.

$$\mathbf{P}_{OPT} = \arg \max_{\mathbf{P}} \left\{ I(Y_1; X_1 | \mathbf{H}, \mathbf{P}) + I(Y_2; X_2 | \mathbf{H}, \mathbf{P}) + \mathcal{L} \left[\text{Tr}(\mathbf{P}\mathbf{P}^\dagger) - P_t \right] \right\} \quad (5.17)$$

where \mathcal{L} is the Lagrange multiplier which is chosen to satisfy the power constraint. In Appendix 5B, we have developed an iterative algorithm to find the near optimal linear precoder (finding optimal linear precoder is a non-convex problem). This algorithm is based on the gradient descent method for finding local optimum. It's performance is dependent on the initial guess for which we used three precoders, i.e. MF, CI and RCI precoders. For a given channel realization, both initializations of CI and RCI precoders converged to the same local optimal linear precoder. However, considering MF precoder as the initial guess, it generally converged to different local optimal precoders with comparatively higher sum rates.

To be fair in comparison with the proposed scheduling algorithm for MU MIMO in LTE, we introduce a geometric scheduling algorithm for unquantized precoders. We divide the spatial space into 4 quadrants according to the spatial angle between \mathbf{h}_1^\dagger and \mathbf{h}_2^\dagger which is given as

$$\phi = \cos^{-1} \left(\frac{|\mathbf{h}_1^\dagger \mathbf{h}_2|}{\|\mathbf{h}_1\| \|\mathbf{h}_2\|} \right) \quad 0^\circ \leq \phi \leq 90^\circ \quad (5.18)$$

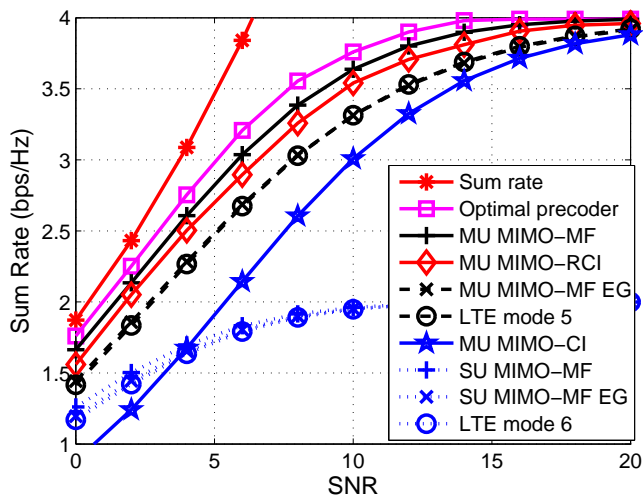


Figure 5.2: Sum rates of different precoding strategies. The eNodeB has two antennas while we consider two single antenna UEs. Both the UEs belong to QPSK constellations.

The scheduling algorithm ensures that for a given UE, i.e. UE-1, the eNodeB chooses the second UE to be served on the same RE such that \mathbf{h}_1^\dagger and \mathbf{h}_2^\dagger lie in the opposite quadrants. Fig. 5.2 shows the sum rates of a broadcast channel with 2 transmit antennas and 2 single antenna UEs for QPSK. SNR is the transmit SNR, i.e. $\frac{\sigma_1^2 \|\mathbf{p}_1\|^2 + \sigma_2^2 \|\mathbf{p}_2\|^2}{N_0}$ for MU MIMO modes where two streams are transmitted to two UEs and SNR is $\frac{\sigma_1^2 \|\mathbf{p}_1\|^2}{N_0}$ for SU MIMO modes where one stream is transmitted to one UE. Geometric scheduling has been used in the MU MIMO modes where two UEs have equal power distribution, i.e. $\sigma_1^2 = \sigma_2^2$. CI, RCI, MF and MF EGT are unquantized precoders while LTE modes use the low resolution LTE precoders. Sum rate capacity (Gaussian broadcast channel) [24], sum rate for near optimal linear precoder and sum rates of unquantized precoders along with those of LTE quantized precoders are shown. An interesting result is the nearness of the sum rate of MF precoder to that of near optimal linear precoder in the low SNR regime. The sum rates of MF EGT precoders and LTE mode 5 precoders are approximately same which shows that the loss in spectral efficiency with respect to the unquantized MF precoders is attributed to the EGT rather than to the low resolution or quantization of LTE precoders.

The results also show significant degradation in the sum rate for CI precoder as compared to the other considered precoding strategies.

5.3.2 Dual Antenna UEs

Now we consider dual antenna UEs with the eNodeB also equipped with two antennas. The earlier proposed transmission strategies for single antenna UEs also remain valid in this case. UEs feedback the indices of precoding vectors which maximize the strength of their desired signals, i.e. $\|\mathbf{H}\mathbf{p}\|^2$. For MU MIMO mode (transmission mode 5), the eNodeB schedules two UEs on the same RE which have requested opposite precoders (precoders being 180 degrees out of phase), i.e. if $\mathbf{p}_1 = \frac{1}{2} \begin{bmatrix} 1 \\ q \end{bmatrix}$ then $\mathbf{p}_2 = \frac{1}{2} \begin{bmatrix} 1 \\ -q \end{bmatrix}$. This strategy ensures the maximization of the desired signal strength and the minimization of the interference strength subject to the constraint of the employment of LTE precoders. For transmission mode 6, the eNodeB employs the requested precoders of the UEs thereby maximizing the strength of their desired signals.

For dual antenna UEs, transmission mode 4 (closed loop spatial multiplexing) can also be employed by the eNodeB if the UE has fed back the RI as 2. As already mentioned in Section 5.2.2, there are two possible choices of precoding matrices (subband basis) in transmission mode 4, with the possibility of swapping the columns on complete band. Here we propose an algorithm based on successive interference cancellation (SIC), i.e. firstly the UE detects the first stream, strips it off and then subsequently detects the second stream. As the detection of the first stream suffers from interference of the second stream while second stream enjoys higher diversity as first stream has already been stripped off, so the UE selects the precoding matrix which enhances the strength of the first stream relative to that of the second stream. The choice of precoding matrices on subband basis leads to the following post processing ratios of the strength of the first stream to that of the second stream.

$$\left(\frac{\|\mathbf{h}_1 + \mathbf{h}_2\|^2}{\|\mathbf{h}_1 - \mathbf{h}_2\|^2}, \frac{\|\mathbf{h}_1 + j\mathbf{h}_2\|^2}{\|\mathbf{h}_1 - j\mathbf{h}_2\|^2} \right)$$

If the RI is 2, the UE selects the maximum of the two which ensures first stream to be stronger than the second stream. The precoding matrix related to this selection is fed back to the eNodeB.

Low Complexity MF Based Detector

This detector is based on the same underlying principle as the detector for single antenna UEs. This detector can be used both for transmission modes 4 and 5. Ignoring the RE index, the system equation can be rewritten as

$$\mathbf{y} = \mathbf{H} [\mathbf{p}_1 x_1 + \mathbf{p}_2 x_2] + \mathbf{z}$$

In transmission mode 4, the detector firstly needs to detect x_1 , then strip it out leading to the detection of x_2 while in transmission mode 5, the detector needs to only detect x_1 as x_2 is the interference symbol. The max log MAP bit metric for the bit $c_{k'}$ of the desired stream x_1 is given as [4]

$$\begin{aligned} \Lambda_1^i(\mathbf{y}, c_{k'}) &\approx \min_{x_1 \in \mathcal{X}_{1,c_{k'}}^i, x_2 \in \mathcal{X}_2} \|\mathbf{y} - \mathbf{H}\mathbf{p}_1 x_1 - \mathbf{H}\mathbf{p}_2 x_2\|^2 \\ &= \min_{x_1 \in \mathcal{X}_{1,c_{k'}}^i, x_2 \in \mathcal{X}_2} \left\{ \|\mathbf{y}\|^2 + \|\mathbf{H}\mathbf{p}_1 x_1\|^2 - 2(\bar{y}_1^* x_1)_R + 2(p_{12} x_1^* x_2)_R - 2(\bar{y}_2^* x_2)_R + \|\mathbf{H}\mathbf{p}_2 x_2\|^2 \right\} \end{aligned} \quad (5.19)$$

where $\bar{y}_1 = (\mathbf{H}\mathbf{p}_1)^\dagger \mathbf{y}$, $\bar{y}_2 = (\mathbf{H}\mathbf{p}_2)^\dagger \mathbf{y}$ and $p_{12} = (\mathbf{H}\mathbf{p}_1)^\dagger \mathbf{H}\mathbf{p}_2$. Writing terms in their real and imaginary parts, we have

$$\begin{aligned} \Lambda_1^i(\mathbf{y}, c_{k'}) &\approx \min_{x_1 \in \mathcal{X}_{1,c_{k'}}^i, x_2 \in \mathcal{X}_2} \left\{ \|\mathbf{H}\mathbf{p}_1 x_1\|^2 - (2\bar{y}_1^* x_1)_R + \|\mathbf{H}\mathbf{p}_2\|^2 x_{2,I}^2 + \|\mathbf{H}\mathbf{p}_2\|^2 x_{2,R}^2 \right. \\ &\quad \left. + 2(p_{12,R} x_{1,R} + p_{12,I} x_{1,I} - \bar{y}_{2,R}) x_{2,R} + 2(p_{12,R} x_{1,I} - p_{12,I} x_{1,R} - \bar{y}_{2,I}) x_{2,I} \right\} \end{aligned} \quad (5.20)$$

For x_2 belonging to the equal energy alphabets, the bit metric is written as

$$\begin{aligned} \Lambda_1^i(\mathbf{y}, c_{k'}) &\approx \min_{x_1 \in \mathcal{X}_{1,c_{k'}}^i, x_2 \in \mathcal{X}_2} \left\{ \|\mathbf{H}\mathbf{p}_1 x_1\|^2 - (2\bar{y}_1^* x_1)_R - 2|p_{12,R} x_{1,R} + p_{12,I} x_{1,I} - \bar{y}_{2,R}| |x_{2,R}| \right. \\ &\quad \left. - 2|p_{12,R} x_{1,I} - p_{12,I} x_{1,R} - \bar{y}_{2,I}| |x_{2,I}| \right\} \end{aligned} \quad (5.21)$$

For non equal energy alphabets, the continuous values of the real and imaginary parts of x_2 which minimize (5.20) are given as

$$\begin{aligned} x_{2,R} &= -\frac{p_{12,R} x_{1,R} + p_{12,I} x_{1,I} - \bar{y}_{2,R}}{\|\mathbf{H}\mathbf{p}_2\|^2} \\ x_{2,I} &= -\frac{p_{12,R} x_{1,I} - p_{12,I} x_{1,R} - \bar{y}_{2,I}}{\|\mathbf{H}\mathbf{p}_2\|^2} \end{aligned} \quad (5.22)$$

Their discrete counterparts can be found in the similar manner as discussed in section 5.3.1.

5.4 Performance Analysis

As LTE precoders are characterized by EGT, so we carry out the performance analysis of EGT in SU MIMO systems by restricting ourselves to single antenna UEs while the eNodeB has two antennas. Analysis for EGT in MU MIMO system seems to be intractable so we restrict our analysis to SU systems where the received signal at k -th RE is given by

$$y_{1,k} = \mathbf{h}_{1,k}^\dagger \mathbf{p}_{1,k} x_{1,k} + z_{1,k}$$

For EGT, precoder vector is given by $\mathbf{p}_{1,k} = \frac{1}{\sqrt{2}} \begin{bmatrix} 1 & \frac{h_{21,k} h_{11,k}^*}{|h_{21,k}| |h_{11,k}|} \end{bmatrix}^T$. So the received signal after normalization by $\frac{h_{11,k}}{|h_{11,k}|}$ is given by

$$y_{1,k} = \frac{1}{\sqrt{2}} (|h_{11,k}| + |h_{21,k}|) x_{1,k} + \frac{h_{11,k}}{|h_{11,k}|} z_{1,k}$$

where for the ease of notation, we have redefined $\frac{h_{11,k}}{|h_{11,k}|} y_{1,k} = y_{1,k}$. The PEP has been derived in Appendix 5C and is given as

$$P(\underline{\mathbf{c}}_1 \rightarrow \hat{\underline{\mathbf{c}}}_1) \leq \frac{1}{2} \prod_{d_{free}} \left(\frac{48}{\left(\check{d}_{1,\min}^2 \left(\frac{\sigma_1^2}{N_0} \right) \right)^2} \right) \quad (5.23)$$

where $\check{d}_{1,\min}^2$ is the normalized minimum distance of the constellation χ_1 . (5.23) clearly shows full diversity of EGT, a result which was earlier derived for equal gain combining for BPSK in [73]. The same result was derived in [74] for EGT in MIMO systems using the approach of metrics of diversity order. Analysis of EGT for MU MIMO system seemingly does not have closed form solution so we shall resort to the simulations for its analysis in the next section.

5.5 Simulation Results

Simulations are divided into 3 parts. In the first part, we look at the performance of the proposed algorithm for MU MIMO mode in LTE while the second part is dedicated to the sensitivity analysis of the proposed algorithm to the knowledge of interference constellation. This sensitivity analysis is motivated by the fact that DCI formats in LTE MU MIMO mode do not

include the information of interfering constellation. Third part looks at the diversity order of EGT in SU MIMO and MU MIMO modes in LTE.

For the first part, we consider the downlink of 3GPP LTE which is based on BICM OFDM transmission from the eNodeB equipped with two antennas using rate-1/3 LTE turbo code¹ [32] with rate matching to rate 1/2 and 1/4. We deliberate on both the cases of single and dual antenna UEs. We consider an ideal OFDM system (no ISI) and analyze it in the frequency domain where the channel has iid Gaussian matrix entries with unit variance and is independently generated for each channel use. We assume no power control in MU MIMO mode so two UEs have equal power distribution. Furthermore, all mappings of the coded bits to QAM symbols use Gray encoding. We focus on the frame error rates (FER) while the frame length is fixed to 1056 information bits. As a reference, we consider fallback transmit diversity scheme (LTE mode 2 - Alamouti code) and compare it with the SU MIMO and MU MIMO modes employing LTE low resolution precoders. To analyze the degradation caused by the low resolution and EGT of LTE precoders, we also look at the system performance employing unquantized MF and unquantized MF EGT precoders. To be fair in the comparison of the LTE MU MIMO mode (mode 5) employing the proposed geometric scheduling algorithm with MU MIMO mode employing unquantized MF and MF EGT precoders, we consider the earlier discussed scheduling algorithm (Section 5.3.1) based on the spatial angle between the two channels (5.18). Perfect CSIT is assumed for the case of MF and MF EGT precoding while error free feedback of 2 bits is assumed for LTE precoders. It is assumed that the UE has the knowledge of interference constellation in MU MIMO mode. It is further assumed that the UE knows its own channel from the eNodeB. So in MU MIMO mode, the UE can find the effective interference channel based on the fact that the eNodeB schedules the second UE on the same RE whose precoder is 180° out of phase of the precoder of the first UE. The UEs employ low complexity MF based detectors for both MU MIMO mode and transmission mode 4 as these detectors have the inherent ability of exploiting the interference structure in the detection of the desired stream. Figs. 5.3 and 5.4 show that the proposed transmission strategy for MU MIMO with LTE precoders (LTE mode 5) significantly outperforms Alamouti transmit diversity scheme (LTE mode 2) and performs better than the SU MIMO schemes for different spectral efficiencies under fast fading. An interesting result is almost the equivalent performance of the unquantized MF EGT

¹The LTE turbo decoder design was performed using the coded modulation library www.iterativesolutions.com

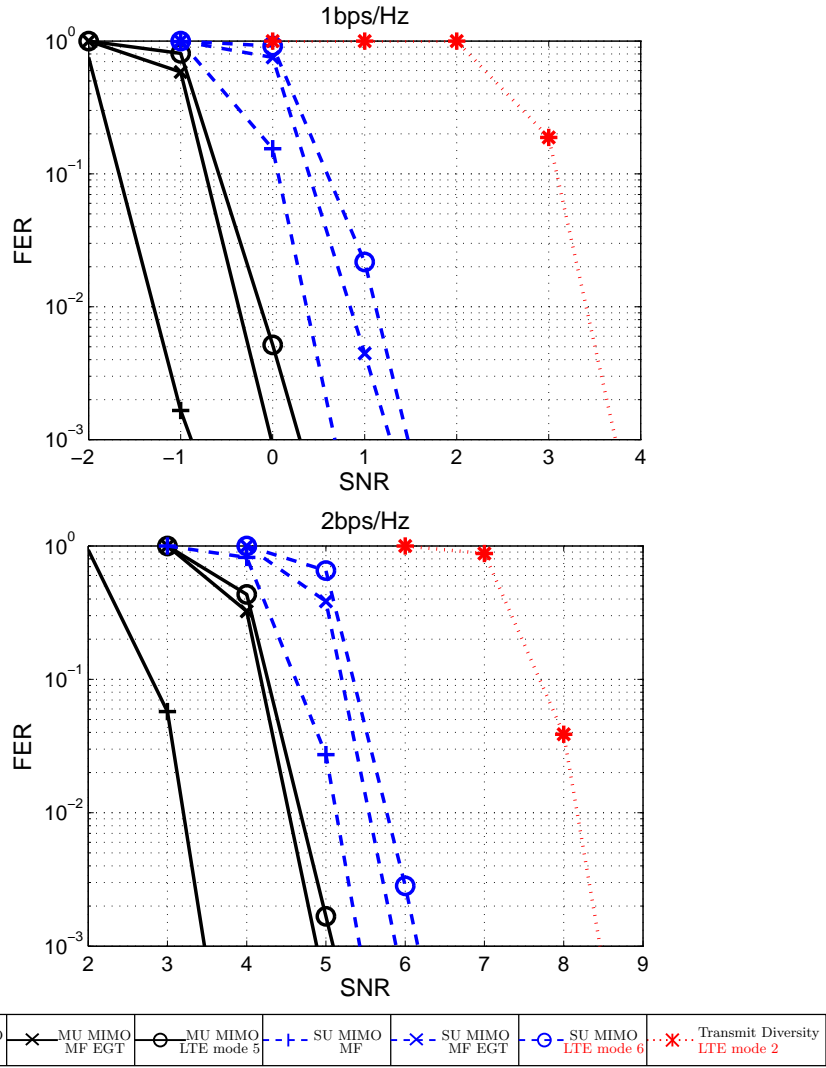


Figure 5.3: MU MIMO mode in LTE. Downlink fast fading channel with $n_t = 2$ and 2 single antenna UEs. 3GPP LTE rate 1/3 turbo code is used with different puncturing patterns.

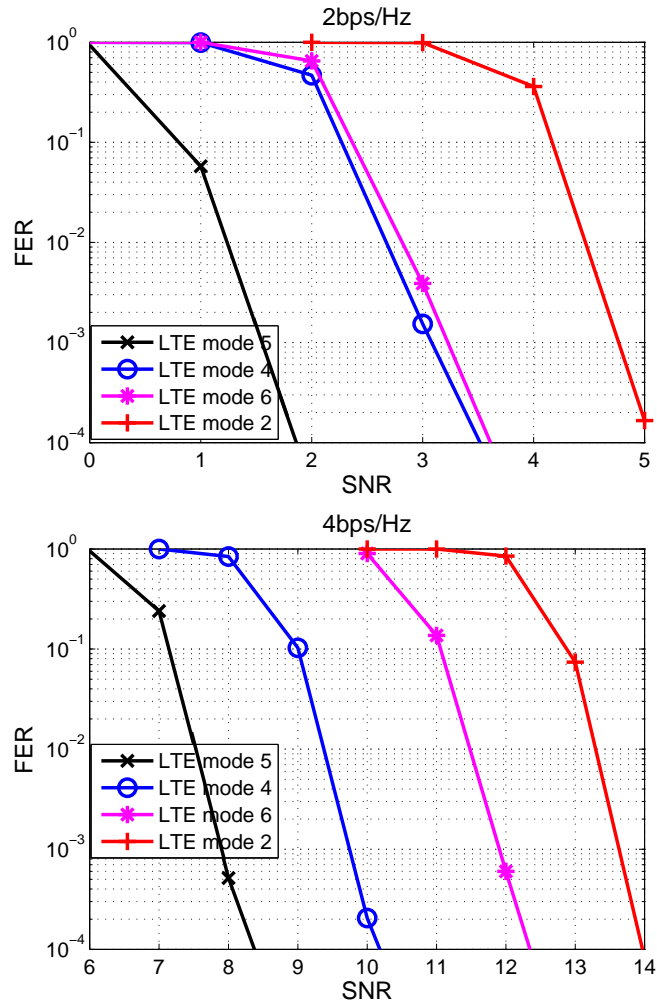


Figure 5.4: MU MIMO mode in LTE. Downlink fast fading channel with eNodeB with 2 antennas and 2 dual antenna UEs. 3GPP LTE rate 1/3 turbo code is used with different puncturing patterns.

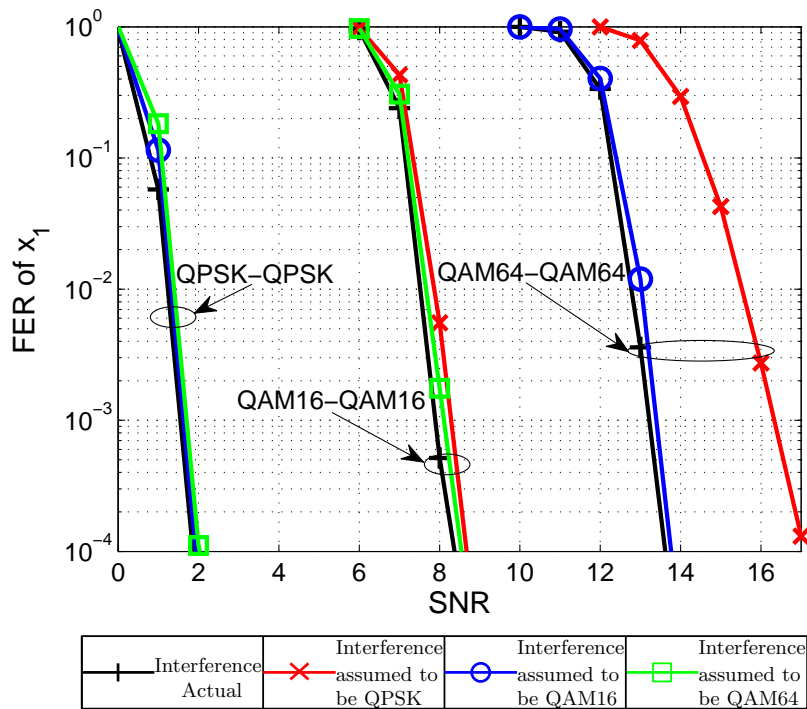


Figure 5.5: Interference sensitivity for MU MIMO mode in LTE. Three sets of simulations are shown. QPSK-QPSK indicates that both x_1 and x_2 both QPSK. 'Interference Actual' implies the case once UE knows the constellation of interference (x_2).

and low resolution LTE precoders which shows that the loss with respect to the unquantized MF precoders is attributed to the EGT rather than the low resolution of LTE precoders. These results substantiate the enhanced performance of MU MIMO mode over the other transmission modes in LTE.

In the second part of simulations, we look at the sensitivity of the proposed algorithm to the knowledge of the interference constellation for MU MIMO mode in LTE. The simulation settings are same as of the first part except that we additionally consider the case when UE has no knowledge of the constellation of interference. Fig. 5.5 compares the FER of UE-1 for the cases when the constellation of UE-2 is known and not known by UE-1. When the interfering constellation is not known by UE-1, it assumes interference to be from QPSK, QAM16 or QAM 64 and the results for these

different assumptions are shown. The results show that there is negligible degradation in the performance of the proposed algorithm if the interfering constellation is assumed to be QAM16 or QAM64. However, there is significant degradation in some cases if the interference is assumed to be QPSK. The results show that assuming interference to be QAM16 leads to the best performance. This postulation not only captures the effect of four quadrants of QPSK constellation points but also encapsulates the spread of QAM64 constellation points in each quadrant thereby leading to a reasonable compromise.

In the third set of simulations, we look at the diversity order of SU MIMO and MU MIMO schemes in LTE. We consider slow fading environment, i.e. the channel remains constant for the duration of one codeword. Fig. 5.6 shows that the MF precoders have full diversity both in MU MIMO and SU MIMO modes. However, once the constraint of EGT is imposed on the MF precoders, MU MIMO mode loses diversity while SU MIMO still exhibits full diversity which is in conformity with the analytical results of Section 5.4. This fundamental result holds even when the low level quantization of LTE is imposed on these EGT precoders. Earlier conclusion that the performance loss is attributed to the EGT rather than the low resolution of LTE precoders is further confirmed. These results give a general guideline for the possible employment of SU MIMO and MU MIMO in LTE under different environments. Once not enough diversity is available in the channel, SU MIMO is the preferred option while MU MIMO is the possible choice once the channel is rich in diversity.

5.6 Conclusion

In this chapter, we have looked at the possible employment of the low resolution LTE precoders for MU MIMO transmission mode. We have proposed a strategy based on the geometric alignment of interference combined with a scheduling algorithm which effectively mitigates the interference seen by each UE. To exploit the structure of the residual interference, we have further proposed the employment of the low complexity MF based detectors, both for single and dual antenna UEs. We have shown both by the information theoretic analysis and the system level simulations that LTE MU MIMO mode outperforms transmit diversity mode while it performs better than SU MIMO mode. We have also shown by PEP analysis that EGT has full diversity in SU MIMO mode while simulation results show that EGT loses diversity in MU MIMO mode. Results have indicated that the per-

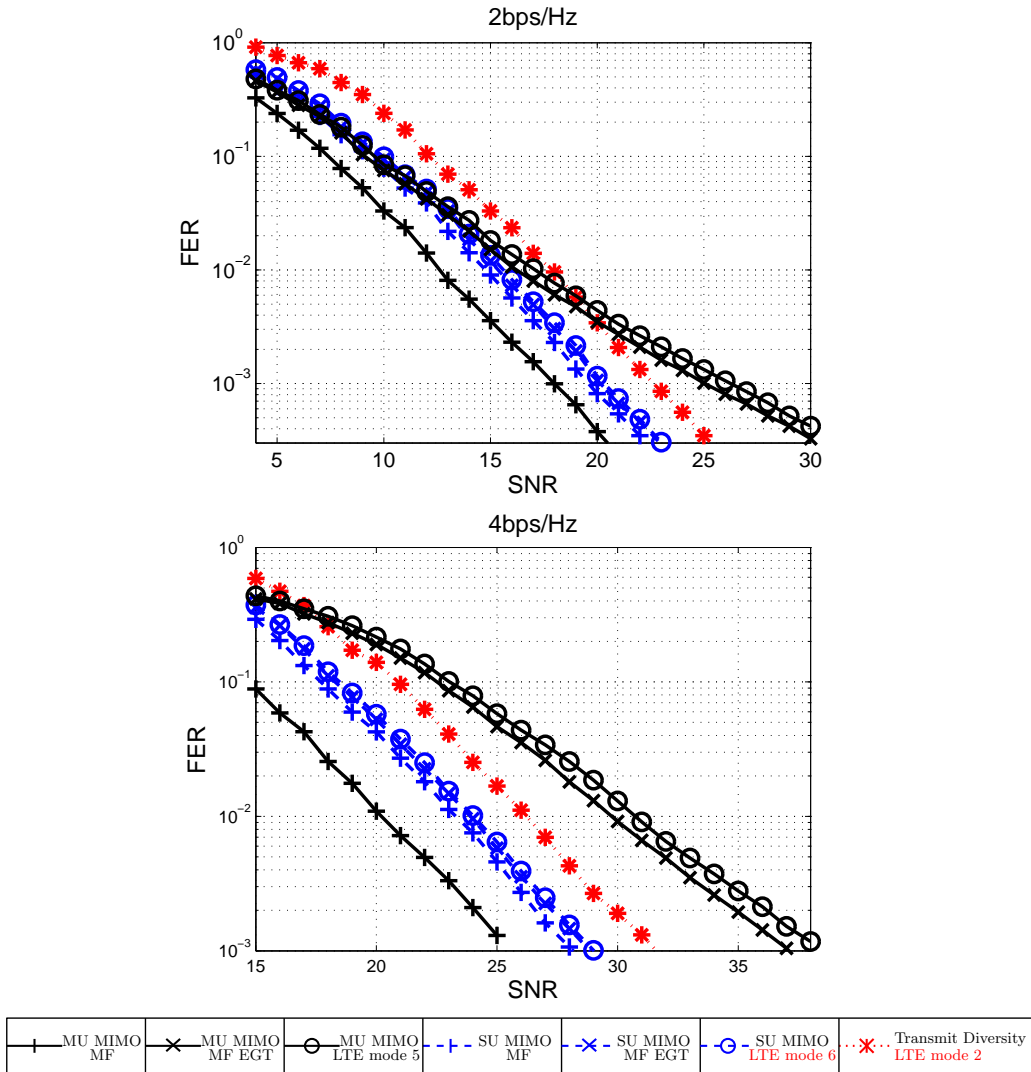


Figure 5.6: Diversity in SU and MU MIMO modes. Downlink slow fading channel (one channel realization per codeword) with $n_t = 2$ and 2 single antenna UEs. 3GPP LTE rate 1/3 turbo code is used with different puncturing patterns.

formance loss of LTE precoders is attributed to their characteristic of EGT rather than their low resolution. We have also looked at the case once the UE in MU MIMO mode is unaware of the interfering constellation and we have proposed a blind detector for this scenario.

5.A Mutual Information for Finite Alphabets

The mutual information for UE-1 for finite size QAM constellation with $|\chi_1| = M_1$ takes the form as

$$\begin{aligned} I(Y_1; X_1 | \mathbf{h}_1^\dagger \mathbf{p}_1, \mathbf{h}_1^\dagger \mathbf{p}_2) &= \mathcal{H}(X_1 | \mathbf{h}_1^\dagger \mathbf{p}_1, \mathbf{h}_1^\dagger \mathbf{p}_2) - \mathcal{H}(X_1 | Y_1, \mathbf{h}_1^\dagger \mathbf{p}_1, \mathbf{h}_1^\dagger \mathbf{p}_2) \\ &= \log M_1 - \mathcal{H}(X_1 | Y_1, \mathbf{h}_1^\dagger \mathbf{p}_1, \mathbf{h}_1^\dagger \mathbf{p}_2) \end{aligned} \quad (5.24)$$

where $\mathcal{H}(\cdot) = -E \log p(\cdot)$ is the entropy function. The second term of (5.24) is given as

$$\begin{aligned} &\mathcal{H}(X_1 | Y_1, \mathbf{h}_1^\dagger \mathbf{p}_1, \mathbf{h}_1^\dagger \mathbf{p}_2) \\ &= \sum_{x_1} \int_{y_1} \int_{\mathbf{h}_1^\dagger \mathbf{p}_1} \int_{\mathbf{h}_1^\dagger \mathbf{p}_2} p(x_1, y_1, \mathbf{h}_1^\dagger \mathbf{p}_1, \mathbf{h}_1^\dagger \mathbf{p}_2) \log \frac{1}{p(x_1 | y_1, \mathbf{h}_1^\dagger \mathbf{p}_1, \mathbf{h}_1^\dagger \mathbf{p}_2)} dy_1 d(\mathbf{h}_1^\dagger \mathbf{p}_1) d(\mathbf{h}_1^\dagger \mathbf{p}_2) \\ &= \sum_{x_1} \sum_{x_2} \int_{y_1} \int_{\mathbf{h}_1^\dagger \mathbf{p}_1} \int_{\mathbf{h}_1^\dagger \mathbf{p}_2} p(x_1, x_2, y_1, \mathbf{h}_1^\dagger \mathbf{p}_1, \mathbf{h}_1^\dagger \mathbf{p}_2) \\ &\quad \times \log \frac{\sum_{x'_1} \sum_{x'_2} p(y_1 | x'_1, x'_2, \mathbf{h}_1^\dagger \mathbf{p}_1, \mathbf{h}_1^\dagger \mathbf{p}_2)}{\sum_{x'_2} p(y_1 | x_1, x'_2, \mathbf{h}_1^\dagger \mathbf{p}_1, \mathbf{h}_1^\dagger \mathbf{p}_2)} dy_1 d(\mathbf{h}_1^\dagger \mathbf{p}_1) d(\mathbf{h}_1^\dagger \mathbf{p}_2) \end{aligned} \quad (5.25)$$

where $x'_1 \in \chi_1$ and $x'_2 \in \chi_2$. Conditioned on the channel and the precoder, there is one source of randomness, i.e. noise. So (5.25) can be extended as

$$\begin{aligned} &\mathcal{H}(X_1 | Y_1, \mathbf{h}_1^\dagger \mathbf{p}_1, \mathbf{h}_1^\dagger \mathbf{p}_2) \\ &= \frac{1}{M_1 M_2} \sum_{\mathbf{x}} E_{z_1} \log \frac{\sum_{\mathbf{x}'} \exp \left[-\frac{1}{N_0} \left| \mathbf{h}_1^\dagger \mathbf{p}_1 x_1 + \mathbf{h}_1^\dagger \mathbf{p}_2 x_2 + z_1 - \mathbf{h}_1^\dagger \mathbf{p}_1 x'_1 - \mathbf{h}_1^\dagger \mathbf{p}_2 x'_2 \right|^2 \right]}{\sum_{x'_2} \exp \left[-\frac{1}{N_0} \left| \mathbf{h}_1^\dagger \mathbf{p}_2 x_2 + z_1 - \mathbf{h}_1^\dagger \mathbf{p}_2 x'_2 \right|^2 \right]} \\ &= \frac{1}{M_1 M_2} \sum_{\mathbf{x}} E_{z_1} \log \frac{\sum_{\mathbf{x}'} \exp \left[-\frac{1}{N_0} \left| \mathbf{h}_1^\dagger \mathbf{P} (\mathbf{x} - \mathbf{x}') + z_1 \right|^2 \right]}{\sum_{x'_2} \exp \left[-\frac{1}{N_0} \left| \mathbf{h}_1^\dagger \mathbf{P} (\mathbf{x} - \mathbf{x}') + z_1 \right|^2 \right]} \end{aligned}$$

where $M_2 = |\chi_2|$, $\mathbf{x} = [x_1 \ x_2]^T$, $\mathbf{x}' = [x'_1 \ x'_2]^T$ and $\mathbf{x}_2' = [x_1 \ x'_2]^T$. The mutual information for UE-1 can be rewritten as

$$I(Y_1; X_1 | \mathbf{h}_1^\dagger, \mathbf{P}) = \log M_1 - \frac{1}{M_1 M_2} \sum_{\mathbf{x}} E_{z_1} \log \frac{\sum_{\mathbf{x}'} p(y_1 | \mathbf{x}', \mathbf{h}_1^\dagger, \mathbf{P})}{\sum_{x_2'} p(y_1 | \mathbf{x}_2', \mathbf{h}_1^\dagger, \mathbf{P})} \quad (5.26)$$

The above quantities can be easily approximated using sampling (Monte-Carlo) methods with N_z realizations of noise and N_{h_1} realizations of the channel \mathbf{h}_1 thereby leading to

$$\begin{aligned} I(Y; X_1 | \mathbf{h}_1^\dagger \mathbf{p}_1, \mathbf{h}_1^\dagger \mathbf{p}_2) \\ &= \log M_1 - \frac{1}{M_1 M_2 N_z N_{h_1}} \sum_{\mathbf{x}} \sum_{\mathbf{h}_1}^{N_{h_1}} \sum_{z_1}^{N_z} \log \frac{\sum_{\mathbf{x}'} \exp \left[-\frac{1}{N_0} |y_1 - \mathbf{h}_1^\dagger \mathbf{p}_1 x'_1 - \mathbf{h}_1^\dagger \mathbf{p}_2 x'_2|^2 \right]}{\sum_{x_2'} \exp \left[-\frac{1}{N_0} |y_1 - \mathbf{h}_1^\dagger \mathbf{p}_1 x_1 - \mathbf{h}_1^\dagger \mathbf{p}_2 x'_2|^2 \right]} \\ &= \log M_1 - \frac{1}{M_1 M_2 N_z N_{h_1}} \sum_{\mathbf{x}} \sum_{\mathbf{h}_1}^{N_{h_1}} \sum_{z_1}^{N_z} \log \frac{\sum_{\mathbf{x}'} \exp \left[-\frac{1}{N_0} |\mathbf{h}_1^\dagger \mathbf{p}_1 (x_1 - x'_1) + \mathbf{h}_1^\dagger \mathbf{p}_2 (x_2 - x'_2) + z_1|^2 \right]}{\sum_{x_2'} \exp \left[-\frac{1}{N_0} |\mathbf{h}_1^\dagger \mathbf{p}_2 x_2 + z_1 - \mathbf{h}_1^\dagger \mathbf{p}_2 x'_2|^2 \right]} \end{aligned} \quad (5.27)$$

Similarly the mutual information for UE-2 is given as

$$I(Y_2; X_2 | \mathbf{h}_2^\dagger, \mathbf{P}) = \log M_2 - \frac{1}{M_1 M_2} \sum_{\mathbf{x}} E_{z_2} \log \frac{\sum_{\mathbf{x}'} p(y_2 | \mathbf{x}', \mathbf{h}_2^\dagger, \mathbf{P})}{\sum_{x_1'} p(y_2 | \mathbf{x}_1', \mathbf{h}_2^\dagger, \mathbf{P})}$$

where $\mathbf{x}'_1 = [x'_1 \ x_2]^T$.

For the case of SU MIMO mode (transmission mode 6), the mutual information is given by

$$I(Y_1; X_1 | \mathbf{h}_1^\dagger \mathbf{p}_1) = \log M_1 - \mathcal{H}(X_1 | Y_1, \mathbf{h}_1^\dagger \mathbf{p}_1)$$

where the second term is given by

$$\begin{aligned}
\mathcal{H}(X_1|Y_1, \mathbf{h}_1^\dagger \mathbf{p}_1) &= \sum_{x_1} \int_{y_1} \int_{\mathbf{h}_1^\dagger \mathbf{p}_1} p(x_1, y_1, \mathbf{h}_1^\dagger \mathbf{p}_1) \log \frac{1}{p(x_1|y_1, \mathbf{h}_1^\dagger \mathbf{p}_1)} dy_1 d(\mathbf{h}_1^\dagger \mathbf{p}_1) \\
&= \sum_{x_1} \int_{y_1} \int_{\mathbf{h}_1^\dagger \mathbf{p}_1} p(x_1, y_1, \mathbf{h}_1^\dagger \mathbf{p}_1) \log \frac{\sum_{x'_1} p(y_1|x'_1, \mathbf{h}_1^\dagger \mathbf{p}_1)}{p(y_1|x_1, \mathbf{h}_1^\dagger \mathbf{p}_1)} dy_1 d(\mathbf{h}_1^\dagger \mathbf{p}_1) \\
&= \frac{1}{M_1 N_z N_{h_1}} \sum_{x_1} \sum_{\mathbf{h}_1^\dagger}^{N_{h_1}} \sum_{z_1}^{N_z} \log \frac{\sum_{x'_1} \exp \left[-\frac{1}{N_0} |y_1 - \mathbf{h}_1^\dagger \mathbf{p}_1 x'_1|^2 \right]}{\exp \left[-\frac{1}{N_0} |y_1 - \mathbf{h}_1^\dagger \mathbf{p}_1 x_1|^2 \right]}
\end{aligned} \tag{5.28}$$

where N_{h_1} are the number of channel realizations of the channel \mathbf{h}_1^\dagger . Note that \mathbf{p}_1 is dependent on the channel \mathbf{h}_1^\dagger .

5.B Near Optimal Linear Precoder

The optimal linear precoder \mathbf{P} can be solved by maximizing the following cost function.

$$\begin{aligned}
J &= I(Y_1; X_1 | \mathbf{h}_1^\dagger, \mathbf{P}) + I(Y_2; X_2 | \mathbf{h}_2^\dagger, \mathbf{P}) + \mathcal{L} \left[\text{Tr}(\mathbf{P}\mathbf{P}^\dagger) - P_t \right] \\
&= \log M_1 M_2 - \frac{1}{M_1 M_2} \left(\sum_{\mathbf{x}} E_{z_1} \log \frac{\sum_{\mathbf{x}'} \exp \left[-\frac{1}{N_0} |\mathbf{h}_1^\dagger \mathbf{P}(\mathbf{x} - \mathbf{x}') + z_1|^2 \right]}{\sum_{\mathbf{x}'_2} \exp \left[-\frac{1}{N_0} |\mathbf{h}_1^\dagger \mathbf{P}(\mathbf{x} - \mathbf{x}'_2) + z_1|^2 \right]} \right. \\
&\quad \left. + \sum_{\mathbf{x}} E_{z_2} \log \frac{\sum_{\mathbf{x}'} \exp \left[-\frac{1}{N_0} |\mathbf{h}_2^\dagger \mathbf{P}(\mathbf{x} - \mathbf{x}') + z_2|^2 \right]}{\sum_{\mathbf{x}'_1} \exp \left[-\frac{1}{N_0} |\mathbf{h}_2^\dagger \mathbf{P}(\mathbf{x} - \mathbf{x}'_1) + z_2|^2 \right]} \right) + \mathcal{L} \left[\text{Tr}(\mathbf{P}\mathbf{P}^\dagger) - P_t \right]
\end{aligned} \tag{5.29}$$

Using the facts that the norm of a vector is convex and the log of the sum of exponentials is also convex, we can write (5.29) as the sum of a convex and a concave function thereby leading to a non-convex cost function which appears to be intractable. However, we now propose a method based on the local optimals to find near optimal linear precoder. The local optimal linear precoders \mathbf{P} which maximize the mutual information are the solutions to

the equations $\nabla_P J = 0$ and $\frac{\partial}{\partial \mathcal{L}} J = 0$, i.e.

$$\begin{aligned} & -\nabla_P \left(\frac{1}{M_1 M_2} \sum_{\mathbf{x}} E_{z_1} \log \frac{\sum_{\mathbf{x}'} p(y_1 | \mathbf{x}', \mathbf{h}_1^\dagger, \mathbf{P})}{\sum_{x_2'} p(y_1 | \mathbf{x}_2', \mathbf{h}_1^\dagger, \mathbf{P})} \right) \\ & -\nabla_P \left(\frac{1}{M_1 M_2} \sum_{\mathbf{x}} E_{z_2} \log \frac{\sum_{\mathbf{x}'} p(y_2 | \mathbf{x}', \mathbf{h}_2^\dagger, \mathbf{P})}{\sum_{x_1'} p(y_2 | \mathbf{x}_1', \mathbf{h}_2^\dagger, \mathbf{P})} \right) + \mathcal{L} \mathbf{P} = 0 \end{aligned} \quad (5.30)$$

where $\nabla_P = \frac{\partial}{\partial \mathbf{P}^*}$. We have used the identities $\nabla_P \text{Tr}(\mathbf{P}^\dagger \mathbf{R}) = \mathbf{R}$ and $\text{Tr}(\mathbf{A}\mathbf{B}) = \text{Tr}(\mathbf{B}\mathbf{A})$. We can interchange the order of the derivative inline with the proof in Appendix A of [76]. Due to similarity, we solve only one derivative in (5.30), i.e.

$$\nabla_P \log \sum_{\mathbf{x}'} \exp\left(-|y_1 - \mathbf{h}_1^\dagger \mathbf{P} \mathbf{x}'|^2\right) = \frac{\sum_{\mathbf{x}'} \exp\left(-|y_1 - \mathbf{h}_1^\dagger \mathbf{P} \mathbf{x}'|^2\right) [\mathbf{h}_1 (y_1 - \mathbf{h}_1^\dagger \mathbf{P} \mathbf{x}') \mathbf{x}'^\dagger]}{\ln 2 \sum_{\mathbf{x}'} \exp\left(-|y_1 - \mathbf{h}_1^\dagger \mathbf{P} \mathbf{x}'|^2\right)}$$

where we have used the relation $\nabla_H (\mathbf{x}^\dagger \mathbf{H}^\dagger \mathbf{y}) = \mathbf{y} \mathbf{x}^\dagger$. Solving (5.30) leads to the following equation

$$\begin{aligned} & \frac{-1}{M_1 M_2} \sum_{\mathbf{x}} E_{z_1} \left\{ \frac{\sum_{\mathbf{x}'} \exp\left(-|y_1 - \mathbf{h}_1^\dagger \mathbf{P} \mathbf{x}'|^2\right) [\mathbf{h}_1 (y_1 - \mathbf{h}_1^\dagger \mathbf{P} \mathbf{x}') \mathbf{x}'^\dagger]}{\ln 2 \sum_{\mathbf{x}'} \exp\left(-|y_1 - \mathbf{h}_1^\dagger \mathbf{P} \mathbf{x}'|^2\right)} \right. \\ & \left. - \frac{\sum_{x_2'} \exp\left(-|y_1 - \mathbf{h}_1^\dagger \mathbf{P} \mathbf{x}_2'|^2\right) [\mathbf{h}_1 (y_1 - \mathbf{h}_1^\dagger \mathbf{P} \mathbf{x}_2') \mathbf{x}_2'^\dagger]}{\ln 2 \sum_{x_2'} \exp\left(-|y_1 - \mathbf{h}_1^\dagger \mathbf{P} \mathbf{x}_2'|^2\right)} \right\} \\ & - \frac{1}{M_1 M_2} \sum_{\mathbf{x}} E_{z_2} \left\{ \frac{\sum_{\mathbf{x}'} \exp\left(-|y_2 - \mathbf{h}_2^\dagger \mathbf{P} \mathbf{x}'|^2\right) [\mathbf{h}_2 (y_2 - \mathbf{h}_2^\dagger \mathbf{P} \mathbf{x}') \mathbf{x}'^\dagger]}{\ln 2 \sum_{\mathbf{x}'} \exp\left(-|y_2 - \mathbf{h}_2^\dagger \mathbf{P} \mathbf{x}'|^2\right)} \right. \\ & \left. - \frac{\sum_{x_1'} \exp\left(-|y_2 - \mathbf{h}_2^\dagger \mathbf{P} \mathbf{x}_1'|^2\right) [\mathbf{h}_2 (y_2 - \mathbf{h}_2^\dagger \mathbf{P} \mathbf{x}_1') \mathbf{x}_1'^\dagger]}{\ln 2 \sum_{x_1'} \exp\left(-|y_2 - \mathbf{h}_2^\dagger \mathbf{P} \mathbf{x}_1'|^2\right)} \right\} + \mathcal{L} \mathbf{P} = 0 \end{aligned} \quad (5.31)$$

Taking partial derivative of (5.29) w.r.t \mathcal{L} we get

$$\text{Tr}(\mathbf{P} \mathbf{P}^\dagger) - P_t = 0 \quad (5.32)$$

So the precoders \mathbf{P} being a function of \mathcal{L} which satisfy (5.31) and (5.32) are the local optimal precoders satisfying the power constraint. It is noted

that it is very difficult to find a closed-form solution (if any) to (5.31) and (5.32) for \mathbf{P} . Nevertheless as we are considering only the two user case, solving the local optimal \mathbf{P} is still feasible. However, when the number of users is large, the computational complexity of solving for local optimal \mathbf{P} is prohibitive. We developed an iterative algorithm employing gradient descent method to solve (5.31) via utilizing the partial derivative $\nabla_{\mathbf{P}} I(\mathbf{P}) = \nabla_{\mathbf{P}} \left[I(Y_1; X_1 | \mathbf{h}_1^\dagger, \mathbf{P}) + I(Y_2; X_2 | \mathbf{h}_2^\dagger, \mathbf{P}) \right]$ which is equal to (5.31) except $\mathcal{L}\mathbf{P}$. The algorithm is as follows:

- \mathbf{P}_0 = initial guess as MF , CI and RCI precoder s.t it satisfies the power constraint
 - $\mathbf{S}_0 = \nabla_{\mathbf{P}_0} I(\mathbf{P}_0)$, $k = 0$
while $I(\mathbf{P}_k)$ is increasing
 - Compute α_k , i.e. step size which is a real number
 - $\mathbf{P}_{k+1} = \mathcal{L}_k(\mathbf{P}_k + \alpha_k \mathbf{S}_k)$, we introduce \mathcal{L}_k once \mathbf{P}_{k+1} does not satisfy the power constraint. It is given as

$$\text{Tr} \left(\mathcal{L}_k(\mathbf{P}_k + \alpha_k \mathbf{S}_k) \mathcal{L}_k(\mathbf{P}_k + \alpha_k \mathbf{S}_k)^\dagger \right) = P_t \implies$$

$$\mathcal{L}_k = \sqrt{\frac{P_t}{\text{Tr} \left((\mathbf{P}_k + \alpha_k \mathbf{S}_k) (\mathbf{P}_k + \alpha_k \mathbf{S}_k)^\dagger \right)}}$$
 - $\mathbf{S}_{k+1} = \frac{\partial}{\partial \mathbf{P}_{k+1}^\dagger} I(\mathbf{P}_{k+1})$
 - $k = k + 1$
- end

So for each channel realization, this algorithm is run for three initializations (MF, CI and RCI). Out of the three local optimals, the near optimal precoder is selected which has the highest sum rate.

5.C Diversity Analysis of EGT in SU MIMO

Consider the system equation (5.4), i.e.

$$y_{1,k} = \frac{1}{\sqrt{2}} (|h_{11,k}| + |h_{21,k}|) x_{1,k} + \frac{h_{11,k}}{|h_{11,k}|} z_{1,k}$$

The max Log MAP bit metric [4] for the bit $c_{k'}$ can be written as

$$\Lambda_1^i(y_k, c_{k'}) \approx \min_{x_1 \in \mathcal{X}_{1,c_{k'}}^i} \left[\frac{1}{N_0} \left| y_{1,k} - \frac{1}{\sqrt{2}} (|h_{11,k}| + |h_{21,k}|) x_1 \right|^2 \right]$$

The conditional PEP i.e $P(\underline{\mathbf{c}}_1 \rightarrow \hat{\underline{\mathbf{c}}}_1 | \mathbf{h}_1)$ is given as

$$\begin{aligned} P(\underline{\mathbf{c}}_1 \rightarrow \hat{\underline{\mathbf{c}}}_1 | \overline{\mathbf{H}}_1) &= P \left(\sum_{k'} \min_{x_1 \in \mathcal{X}_{1,c_{k'}}^i} \frac{1}{N_0} \left| y_{1,k} - \frac{1}{\sqrt{2}} (|h_{11,k}| + |h_{21,k}|) x_1 \right|^2 \right. \\ &\quad \left. \geq \sum_{k'} \min_{x_1 \in \mathcal{X}_{1,\hat{c}_{k'}}^i} \frac{1}{N_0} \left| y_{1,k} - \frac{1}{\sqrt{2}} (|h_{11,k}| + |h_{21,k}|) x_1 \right|^2 \middle| \overline{\mathbf{H}}_1 \right) \end{aligned} \quad (5.33)$$

where $\overline{\mathbf{H}}_1$ indicates the complete channel from the eNodeB to UE-1 for the transmission of the codeword $\underline{\mathbf{c}}_1$. Assume $d(\underline{\mathbf{c}}_1 - \hat{\underline{\mathbf{c}}}_1) = d_{free}$ for $\underline{\mathbf{c}}_1$ and $\hat{\underline{\mathbf{c}}}_1$ under consideration for the PEP analysis, which is the worst case scenario between any two codewords. Therefore, the inequality on the right hand side of (5.33) shares the same terms on all but d_{free} summation points and the summations can be simplified to only d_{free} terms for which $\hat{c}_{k'} = \bar{c}_{k'}$. Let's denote

$$\begin{aligned} \tilde{x}_{1,k} &= \arg \min_{x_1 \in \mathcal{X}_{1,c_{k'}}^i} \frac{1}{N_0} \left| y_{1,k} - \frac{1}{\sqrt{2}} (|h_{11,k}| + |h_{21,k}|) x_1 \right|^2 \\ \hat{x}_{1,k} &= \arg \min_{x_1 \in \mathcal{X}_{1,\hat{c}_{k'}}^i} \frac{1}{N_0} \left| y_{1,k} - \frac{1}{\sqrt{2}} (|h_{11,k}| + |h_{21,k}|) x_1 \right|^2 \end{aligned} \quad (5.34)$$

As $\frac{1}{N_0} \left| y_{1,k} - \frac{1}{\sqrt{2}} (|h_{11,k}| + |h_{21,k}|) x_{1,k} \right|^2 \geq \frac{1}{N_0} \left| y_{1,k} - \frac{1}{\sqrt{2}} (|h_{11,k}| + |h_{21,k}|) \hat{x}_{1,k} \right|^2$, this leads to PEP being given as

$$\begin{aligned}
P(\mathbf{c}_1 \rightarrow \hat{\mathbf{c}}_1 | \overline{\mathbf{H}}_1) &\leq P \left(\sum_{k,d_{free}} \frac{1}{N_0} \left| y_{1,k} - \frac{1}{\sqrt{2}} (|h_{11,k}| + |h_{21,k}|) x_{1,k} \right|^2 \right. \\
&\quad \left. \geq \sum_{k,d_{free}} \frac{1}{N_0} \left| y_{1,k} - \frac{1}{\sqrt{2}} (|h_{11,k}| + |h_{21,k}|) \hat{x}_{1,k} \right|^2 \middle| \overline{\mathbf{H}}_1 \right) \\
&= P \left(\sum_{k,d_{free}} \frac{\sqrt{2} (|h_{11,k}| + |h_{21,k}|)}{N_0} (z_{1,k}^* (\hat{x}_{1,k} - x_{1,k})) \right)_R \\
&\quad \left. \geq \sum_{k,d_{free}} \frac{1}{2N_0} (|h_{11,k}| + |h_{21,k}|)^2 |\hat{x}_{1,k} - x_{1,k}|^2 \right) \\
&= Q \left(\sqrt{\sum_{k,d_{free}} \frac{1}{4N_0} (|h_{11,k}| + |h_{21,k}|)^2 |x_{1,k} - \hat{x}_{1,k}|^2} \right) \\
&\leq \frac{1}{2} \exp \left(- \sum_{k,d_{free}} \frac{1}{8N_0} (|h_{11,k}| + |h_{21,k}|)^2 d_{1,\min}^2 \right) \\
&= \frac{1}{2} \prod_{k,d_{free}} \exp \left(- \frac{1}{8N_0} (|h_{11,k}| + |h_{21,k}|)^2 d_{1,\min}^2 \right)
\end{aligned}$$

where we have used Chernoff bound $Q(x) \leq \frac{1}{2} \exp\left(-\frac{x^2}{2}\right)$. Averaging over channel leads to

$$\begin{aligned}
P(\mathbf{c}_1 \rightarrow \hat{\mathbf{c}}_1) &\leq \frac{1}{2} E_{\overline{\mathbf{H}}_1} \prod_{k,d_{free}} \exp \left(- \frac{1}{8N_0} (|h_{11,k}| + |h_{21,k}|)^2 d_{1,\min}^2 \right) \\
&= \frac{1}{2} \prod_{k,d_{free}} E_{\mathbf{h}_{1,k}} \exp \left(\left(- \frac{\check{d}_{1,\min}^2}{4} \right) \frac{(|h_{11,k}| + |h_{21,k}|)^2 \sigma_1^2}{2N_0} \right)
\end{aligned} \tag{5.35}$$

(5.35) follows from the channel independence at each RE which is the consequence of the interleaving operation. Here we have used the notation $d_{1,\min}^2 = \sigma_1^2 \check{d}_{1,\min}^2$ with $\check{d}_{1,\min}^2$ being the normalized minimum distance of the constellation χ_1 . Using the MGF of the SNR at the output of two branch

EGC as per equations (2) and (23) in [77], PEP at high SNR is upper bounded as

$$\begin{aligned}
P(\underline{\mathbf{c}}_1 \rightarrow \hat{\underline{\mathbf{c}}}_1) \leq & \frac{1}{2} \prod_{d_{free}} \left(\frac{8 \left(\frac{\sigma_1^2}{N_0}\right)^2 + \check{d}_{1,\min}^2 \left(\frac{\sigma_1^2}{N_0}\right)^3}{4 \left(\frac{\sigma_1^2}{N_0}\right)^2 \left(2 + \frac{\sigma_1^2 \check{d}_{1,\min}^2}{4N_0}\right)^2} - \frac{\left(\frac{\check{d}_{1,\min}^2}{2\sqrt{2}}\right) \left(\frac{\sigma_1^2}{N_0}\right)}{\left(2 + \frac{\check{d}_{1,\min}^2}{2} \left(\frac{\sigma_1^2}{N_0}\right)\right)^{3/2}} \right. \\
& \times \left[\pi - 2 \sin^{-1} \left(\sqrt{\frac{\left(\frac{\sigma_1^2}{N_0}\right)^{-1} + \frac{\check{d}_{1,\min}^2}{4}}{2 \left(\frac{\sigma_1^2}{N_0}\right)^{-1} + \frac{\check{d}_{1,\min}^2}{4}}} \right) \right] \\
& \left. + \frac{4 \left(\frac{\sigma_1^2}{N_0}\right)^2 \left(4 + \frac{\check{d}_{1,\min}^2}{2} \left(\frac{\sigma_1^2}{N_0}\right)\right)}{4 \left(\frac{\sigma_1^2}{N_0}\right)^2 \left(2 + \frac{\check{d}_{1,\min}^2}{4} \left(\frac{\sigma_1^2}{N_0}\right)\right)^2 \left(2 + \frac{\check{d}_{1,\min}^2}{2} \left(\frac{\sigma_1^2}{N_0}\right)\right)} \right) \quad (5.36)
\end{aligned}$$

Using the identity $\cos^{-1}(x) = \frac{\pi}{2} - \sin^{-1}(x)$, we have

$$\pi - 2 \sin^{-1} \left(\sqrt{\frac{\left(\frac{\sigma_1^2}{N_0}\right)^{-1} + \frac{\check{d}_{1,\min}^2}{4}}{2 \left(\frac{\sigma_1^2}{N_0}\right)^{-1} + \frac{\check{d}_{1,\min}^2}{4}}} \right) = 2 \cos^{-1} \left(\sqrt{\frac{\left(\frac{\sigma_1^2}{N_0}\right)^{-1} + \frac{\check{d}_{1,\min}^2}{4}}{2 \left(\frac{\sigma_1^2}{N_0}\right)^{-1} + \frac{\check{d}_{1,\min}^2}{4}}} \right) \quad (5.37)$$

Taylor series expansion [78] of $\cos^{-1}(\sqrt{x})$ is given as

$$\cos^{-1}(\sqrt{x}) = \sqrt{2-2\sqrt{x}} \sum_{k=0}^{\infty} \frac{(1-\sqrt{x})^k (1/2)_k}{2^k (k! + 2kk!)} \quad \text{for } |-1 + \sqrt{x}| < 2 \quad (5.38)$$

where $x!$ is the factorial of x while $(x)_n$ is the Pochhammer symbol, i.e. $(x)_n = x(x+1)\cdots(x+n-1)$. For x closer to 1, a case that shall be occurring at high SNR in (5.37), first term will be dominant, i.e.

$$\cos^{-1} \left(\sqrt{\frac{\left(\frac{\sigma_1^2}{N_0}\right)^{-1} + \frac{\check{d}_{1,\min}^2}{4}}{2 \left(\frac{\sigma_1^2}{N_0}\right)^{-1} + \frac{\check{d}_{1,\min}^2}{4}}} \right) \approx \sqrt{2-2 \sqrt{\frac{\left(\frac{\sigma_1^2}{N_0}\right)^{-1} + \frac{\check{d}_{1,\min}^2}{4}}{2 \left(\frac{\sigma_1^2}{N_0}\right)^{-1} + \frac{\check{d}_{1,\min}^2}{4}}}}$$

Taylor series expansion [78] of \sqrt{x} at $x = 1$ is

$$\sqrt{x} = 1 + \frac{x-1}{2} - \frac{(x-1)^2}{8} + \frac{(x-1)^3}{16} - \dots \quad (5.39)$$

In the expansion of $\sqrt{\frac{\left(\frac{\sigma_1^2}{N_0}\right)^{-1} \frac{\check{d}_{1,\min}^2}{4}}{2\left(\frac{\sigma_1^2}{N_0}\right)^{-1} \frac{\check{d}_{1,\min}^2}{4}}}$, first two terms will be dominant at high SNR thereby leading to

$$\begin{aligned} \sqrt{2 - \sqrt{\frac{\left(\frac{\sigma_1^2}{N_0}\right)^{-1} \frac{\check{d}_{1,\min}^2}{4}}{2\left(\frac{\sigma_1^2}{N_0}\right)^{-1} \frac{\check{d}_{1,\min}^2}{4}}}} &\approx \sqrt{2 - 2 \left(1 + \frac{\frac{\left(\frac{\sigma_1^2}{N_0}\right)^{-1} \frac{\check{d}_{1,\min}^2}{4}}{2\left(\frac{\sigma_1^2}{N_0}\right)^{-1} \frac{\check{d}_{1,\min}^2}{4}} - 1 \right)} \\ &= \sqrt{- \left(\frac{\left(\frac{\sigma_1^2}{N_0}\right)^{-1} \frac{\check{d}_{1,\min}^2}{4}}{2\left(\frac{\sigma_1^2}{N_0}\right)^{-1} \frac{\check{d}_{1,\min}^2}{4}} - 1 \right)} \\ &= \frac{1}{\sqrt{2 + \frac{\check{d}_{1,\min}^2}{4} \left(\frac{\sigma_1^2}{N_0}\right)}} \end{aligned}$$

So rewriting (5.36), we get

$$\begin{aligned} P(\mathbf{c}_1 \rightarrow \hat{\mathbf{c}}_1) &\leq \frac{1}{2} \prod_{d_{free}} \left(\frac{2}{\left(2 + \frac{\check{d}_{1,\min}^2}{4} \left(\frac{\sigma_1^2}{N_0}\right)\right)^2} + \frac{\check{d}_{1,\min}^2 \left(\frac{\sigma_1^2}{N_0}\right)}{4 \left(2 + \frac{\check{d}_{1,\min}^2}{4} \left(\frac{\sigma_1^2}{N_0}\right)\right)^2} \right. \\ &\quad \left. - \frac{2 \left(\frac{\check{d}_{1,\min}^2}{2\sqrt{2}}\right) \left(\frac{\sigma_1^2}{N_0}\right)}{\left(2 + \frac{\check{d}_{1,\min}^2}{2} \left(\frac{\sigma_1^2}{N_0}\right)\right)^{3/2} \left(2 + \frac{\check{d}_{1,\min}^2}{4} \left(\frac{\sigma_1^2}{N_0}\right)\right)^{1/2}} \right. \\ &\quad \left. + \frac{\left(4 + \frac{\check{d}_{1,\min}^2}{2} \left(\frac{\sigma_1^2}{N_0}\right)\right)}{\left(2 + \frac{\check{d}_{1,\min}^2}{4} \left(\frac{\sigma_1^2}{N_0}\right)\right)^2 \left(2 + \frac{\check{d}_{1,\min}^2}{2} \left(\frac{\sigma_1^2}{N_0}\right)\right)} \right) \end{aligned}$$

At high SNR, second term converges to $\frac{4}{\check{d}_{1,\min}^2 \left(\frac{\sigma_1^2}{N_0}\right)}$ while the third term

converges to $\frac{-4}{\check{d}_{1,\min}^2\left(\frac{\sigma_1^2}{N_0}\right)}$. So PEP at high SNR is upper bounded as

$$\begin{aligned}
 P(\mathbf{c}_1 \rightarrow \hat{\mathbf{c}}_1) &\leq \frac{1}{2} \prod_{d_{free}} \left(\frac{32}{\left(\check{d}_{1,\min}^2\left(\frac{\sigma_1^2}{N_0}\right)\right)^2} + \frac{16}{\left(\check{d}_{1,\min}^2\left(\frac{\sigma_1^2}{N_0}\right)\right)^2} \right) \\
 &= \frac{1}{2} \prod_{d_{free}} \left(\frac{48}{\left(\check{d}_{1,\min}^2\left(\frac{\sigma_1^2}{N_0}\right)\right)^2} \right) \tag{5.40}
 \end{aligned}$$

Chapter 6

Conclusions and Future Perspectives

6.1 Conclusions

This thesis has mainly dealt with three research directions which become the three parts of the thesis. The first part focuses on SU BICM SISO and MIMO systems. For SISO systems, we have shown that the soft decision bit metrics for the ML decoder can be significantly simplified to a scaled version of the MF output. For MIMO systems, we have proposed a low complexity MF based near ML detector for SIC detection which successfully reduces one complex dimension of the systems. The second part of the thesis principally deals with the dilemma of interference in cellular systems where we have contested the unrealistic assumption of Gaussianity for the interference. Considering interference to be from realistic discrete constellations, we have proposed a low complexity interference suppression strategy which exploits the interference structure in mitigating its effects. The third part is dedicated to the feasibility of MU MIMO for future wireless systems (3GPP LTE) where we have investigated the effectiveness of the low resolution LTE precoders. We have proposed a precoding strategy for MU MIMO mode in LTE which encompasses geometrical interference alignment at the eNodeB and the subsequent exploitation of the residual interference at the UEs. In the following, we briefly discuss the main results and the conclusions of this

thesis on a per chapter basis.

- **Low Complexity Detection in BICM SISO Systems**

In this chapter, low complexity MF based bit metrics for BICM SISO system have been proposed. These proposed metrics are merely scaled versions of the MF outputs thereby evading any distance computations, comparisons or division operations and are therefore suitable for hardware implementations.

- **Low Complexity Detection in BICM MIMO Systems**

This chapter has focused on the dual stream scenario in SU MIMO system. A novel low complexity MF based detector has been proposed which successfully reduces one complex dimension of the system. This detector is characterized by full diversity and higher coding gain as compared to the MMSE detector which has lower diversity and coding gain. Exploiting the UEP of the dual stream scenario, a broadcast strategy has also been proposed to prioritize different data streams to different users.

- **Interference Suppression in Future Cellular Systems**

In this chapter, the inherent problem of interference in wireless communications is addressed. The focus is on the scenario of interference suppression where we have proposed the exploitation of the structure of interference in mitigating its effects. In addition to looking at the diversity of the proposed strategy, we have also looked at the effects of the strength and the rate of interference on the coding gain. It has been shown that the proposed strategy has a coding gain as either the interference gets stronger or its rate trims down whereas the classical MMSE detection suffers from a coding loss as the interference gets stronger. The idea of partial decoding and effective exploitation of interference led to the proposition of a novel FFR scheme in this chapter which is characterized by higher spectral efficiency.

- **Making Multiuser MIMO Work for LTE**

This chapter looks at the possible employment of the low resolution LTE precoders for MU MIMO transmission mode. A novel strategy based on the geometric alignment of the interference combined with a scheduling algorithm has been proposed for MU MIMO mode in LTE. This strategy first mitigates the interference seen by each UE and then the UEs exploit the structure of the residual interference in the detection process. It was shown both by the information theoretic

analysis and the system level simulations that LTE MU MIMO mode outperforms other transmission modes. Another important contribution of this chapter is the diversity analysis of EGT both in SU MIMO and MU MIMO modes. It is shown that EGT is characterized by full diversity of in SU MIMO mode while this transmission scheme loses diversity in MU MIMO mode.

6.2 Future Perspectives

This thesis has been an attempt to solve many relevant problems in wireless communications. As is the usual case with research, the pursuit of the solution for one problem reveals multiple open problems and further research directions and this thesis has certainly been no exception in this regard. In the following, we describe some possible interesting research directions which are either the ideas we came across while working for this thesis or they are the possible future extensions of the work conducted in this thesis.

- We have shown that EGT in SU MIMO has full diversity while simulation results indicate a loss of diversity once EGT is applied to MU MIMO mode. The analytical analysis of EGT in MU MIMO will give more detailed insight into this loss of diversity.
- For MU MIMO, it was shown that exploiting interference by the users is a better strategy than attenuating or canceling the interference at the transmitter. Design of a precoder which manages interference in a way that it can be effectively exploited by the UEs is an interesting problem that we could not address in this thesis.
- The algorithm for MU MIMO mode in LTE has been proposed for the case once the eNodeB is equipped with 2 antennas. It's extension to the case once eNodeB has 4 antennas and consequently the precoder codebook has 16 precoders would be an interesting extension to this work.
- We have derived a near optimal linear precoder for MU MIMO but the problem being non-convex, it was apparently not possible to derive an optimal linear precoder.

Appendices

Appendix A

Summary of the Thesis in French

A.1 Abstract en Français

Atteindre une meilleure efficacité spectrale et une fiabilité accrue sont les objectifs principaux des systèmes sans fil à venir. Dans la poursuite de ces objectifs, il est impératif d'élaborer des stratégies tenant compte des contraintes d'ordre pratique afin que les solutions qui en découlent soient applicables dans le monde réel. Dans cette thèse, l'accent est donc mis sur les systèmes de communication ayant une dimension pratique et réalisable. Dans la première partie de la thèse, nous considérons les systèmes MIMO comprenant peu de dimensions et proposons un récepteur intelligent de faible complexité pour de tels systèmes. Ce récepteur est basé sur les résultats du filtre adapté (matched filter -MF) et réduit avec succès le nombre de dimensions complexes du système par un. Nous comparons le récepteur proposé avec un récepteur MMSE et montrons que le récepteur proposé est caractérisé par l'intégralité de la diversité complet alors que le récepteur MMSE souffre d'une diminution de la diversité. En outre, le récepteur proposé a un gain de codage alors que le récepteur MMSE souffre d'une perte de codage. Dans la deuxième partie de la thèse, nous étudions la suppression d'interférence dans un système cellulaire pour des utilisateurs localisés à la frontière de la cellule. Dans un tel scénario, nous remettons en

question l'hypothèse classique d'interférences Gaussiennes et soulignons que ces interférences ont une structure qui peut être exploitée dans le processus de détection. À cette fin, nous proposons l'extension à ce scénario de la structure précédemment proposée pour le récepteur, et étudions l'influence de l'intensité et du débit de l'interférence. Dans la dernière partie de la thèse, nous considérons le cas du "multi-user" (MU) MIMO mode dans les systèmes "long term evolution" (LTE). Nous proposons une stratégie de précodage pour les précodeurs LTE à base résolution englobant l'alignement géométrique des interférences à la station de base et l'exploitation de la structure des interférences résiduelles par les utilisateurs. Nous examinons également la transmission avec gain égal (EGT), caractéristique des précodeurs LTE, et montrons que si la méthode de transmission EGT atteint la diversité maximale en mode "single-user", il ne l'atteint pas dans le mode MU.

A.2 Introduction

Bien que les normalisations actuelles et en cours sans fil ont convergé vers plusieurs technologies de pointe dans la poursuite des débits plus élevés et une meilleure qualité de service (QoS), ils font toujours face à de nombreux défis de taille. Le défi le plus important, c'est l'interférence qui affecte la réutilisation du spectre et est donc inhérente aux systèmes de communication de données à haut taux. Un autre défi se dégage des contraintes matérielles qui limitent la mise en œuvre des algorithmes sophistiqués et émetteur-récepteur nécessitent des solutions de faible complexité. Un exemple est la difficulté d'atteindre l'antenne requise espacement dans les mobiles qui limite considérablement les gains promis des systèmes MIMO. Il a conduit à une autre application de la dimension spatiale en termes de séparation spatiale des utilisateurs, multi-utilisateur à savoir (multi-user - MU) MIMO. Toutefois, l'emploi efficace de MU MIMO en raison de la contrainte de nombreux commentaires n'est pas encore perçue dans les futurs systèmes sans fil comme le 3GPP LTE citeStefania09. Nous discutons de certains de ces défis dans les paragraphes suivants.

A.2.1 Interférence

En plus de l'incorporation de la dimension spatiale dans la recherche de l'efficacité spectrale supérieure, la réutilisation des ressources spectrales jouera également un rôle important dans les futurs systèmes de communication sans

fil. Lorsque la complexité est le défi de l'intégration de la dimension spatiale, l'interférence limite la réutilisation du spectre. Gérer les interférences peuvent être divisés en cinq catégories comme l'évitement, le confinement, le rejet, la coordination et l'exploitation. Éviter l'interférence se réfère à ce orthogonalisation (temps, fréquence, de l'espace, les codes) qui est basé sur la répartition spatiale de réutilisation. Cette approche conduit à une *a priori* perte de degrés de liberté, quelle que soit la faiblesse de l'interférence potentielle est. Confinement interférence se réfère à des stratégies de fuite des interférences, juste assez pour répondre à une qualité de service (QoS) de contrainte. Rejet des interférences implique la transformation du récepteur de pointe basée dans le domaine spatial. Différentes techniques de rejet ont été fortement contribué à atténuer les interférences nuisibles par l'annulation ou l'atténuation. Un autre domaine de la manipulation d'interférence est la coordination et la coopération [10] qui est une approche plus souple pour réduire les interférences, c'est à dire non-zéro interférence est une fuite de l'émetteur, mais le niveau ou la dimension de l'interférence peut être réduite par l'allocation des ressources de coordination, doux transfert, l'alignement d'interférence, etc. Cette approche s'étend à la notion de réseau MIMO [11] [12] (où BSs adjacents sont reliés pour former un réseau d'antennes) qui exige le partage des CSI et des données utilisateur entre les BSs nécessitant ainsi énorme capacité de backhaul. Une autre catégorie est la suppression des interférences ou de l'exploitation où la structure d'interférence est exploitée au niveau du récepteur à l'atténuation de ses effets. Récemment, l'accent a été mis sur la façon de intelligemment exploiter les connaissances et / ou de la structure de l'interférence d'atteindre une meilleure fiabilité et le débit dans les systèmes de communication sans fil.

A.2.2 De Single-User MIMO à Multiuser MIMO

La dimension spatiale de communication apparaît lorsque plusieurs antennes sont utilisées aux deux extrémités d'une liaison de transmission. Toutefois, les avantages exceptionnels de la SU MIMO sont limités par la condition d'avoir les canaux indépendants entre les antennes émettrices et réceptrices, une exigence qui est difficile à réaliser car les antennes sont rapprochées sur le mobile. Néanmoins, cette dimension spatiale lance aussi quand il ya plusieurs utilisateurs dans le système. Pour la croissance de la capacité d'être linéaire avec le nombre de flux spatiale, la restriction de la disponibilité des " au moins autant (suffisamment espacées) antennes de réception que le flux transmis" dans les systèmes SU MIMO détend de la disponibilité des " au moins autant d'utilisateurs seule antenne que le flux transmis" dans les

systèmes MU MIMO MU [13]. Par conséquent dans le système de communication MU MIMO où un BS équipé n_t antennes est en communication avec n_r utilisateurs (avec une seule antenne), les gains d'efficacité spectrale de l'ordre de (n_t, n_r) sont réalisables par rapport à un système d'exploitation SISO sur le montant même des moyens de communication classiques. En plus de fournir de multiplexage utilisateur de multiplexage et de flux, MU MIMO se caractérise également par la possibilité de sélection sur le nombre excédentaire d'utilisateurs, un gain inventé que la MU diversité [14].

A.3 Contributions et cadre de cette thèse

Nous avons généralement focalisée dans cette thèse sur les systèmes pratiques MIMO comprenant peu de dimensions. Les travaux de recherche menés dans cette thèse peut être divisée en trois parties distinctes. Partie I traite des techniques de transmission et de détection dans les systèmes single-user (SU) MIMO, partie II porte sur la suppression des interférences dans les systèmes cellulaires tandis que la partie III considère précodage dans les systèmes MU MIMO. Partie I, qui comprend les chapitres 2 et 3, se concentre sur la détection de faible complexité en OFDM en fonction SISO BICM et les systèmes MIMO. Partie II, comprenant le chapitre 4 à elle seule l'analyse de suppression des interférences où un nouveau schéma de réutilisation des fréquences fractionnaire est proposé. Partie III, composé du chapitre 5 se concentre sur le précodage pour MU MIMO avec une référence spécifique à la norme 3GPP LTE. Dans les paragraphes suivants, nous donnons un bref aperçu de la thèse et de décrire les contributions sur une base par chapitre.

A.4 Chapitre 2 - Détection de faible complexité dans le système SISO BICM

Dans ce chapitre, nous considérons la détection doux dans BICM SISO OFDM système. Calcul de maximum vraisemblance (maximum likelihood - ML) de ces décisions douces (log likelihood ratio - LLR) impliquent la somme d'un certain nombre de termes exponentielle du nombre de bits par symbole de modulation. Nous montrons que ces mesures ML doux bit de décision peut être considérablement simplifiée pour une version réduite du filtre adapté (MF) de sortie. Cette simplification est facilitée par le découplage des parties réelles et imaginaires de la métrique. La complexité est maintenu à peu près au même niveau pour tous les constellations et les

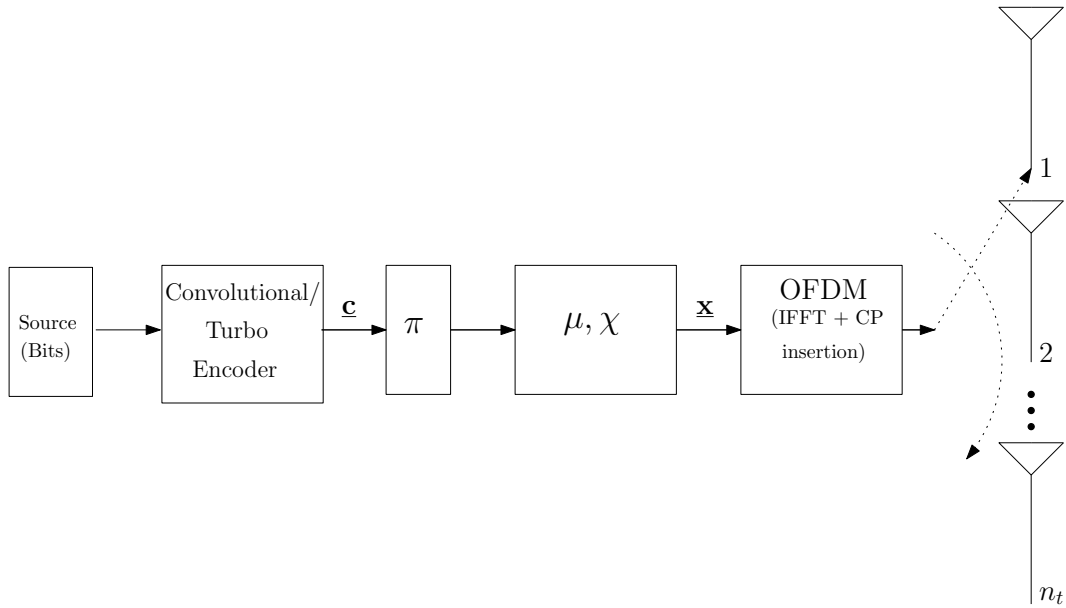


Figure A.1: Schéma de l'émetteur. π indique l'entrelaceur alors que μ et χ indiquent la carte d'étiquetage et de la constellation, respectivement.

mesures en résulte est fondée sur les résultats MF sont appropriés pour la mise en IJuvre dans le matériel. Ce résultat a été publié dans:

- Rizwan Ghaffar and Raymond Knopp, "Low Complexity Metrics for BICM SISO and MIMO systems", *Proceedings of IEEE 71-st Vehicular Technology Conference, VTC-Spring 2010*, Taipei, May, 2010.

A.4.1 Modèle de Système

Le modèle est représenté sur la figure A.1. L'équation du système s'écrit

$$y_k = h_k x_k + z_k, \quad k = 1, 2, \dots, T \quad (\text{A.1})$$

A.4.2 Métriques de Complexité Faible

Ensuite, la métrique peu ML peut être donnée par

$$\begin{aligned}
\Lambda^i(y_k, c_{k'}) &= \log p(c_{k'}|y_k) \\
&\approx \log p(y_k|c_{k'}) \\
&= \log \sum_{x \in \chi_{c_{k'}}^i} p(y_k|x) \\
&= \log \sum_{x \in \chi_{c_{k'}}^i} \frac{1}{\pi N_0} \exp \left[-\frac{1}{N_0} |y_k - h_k x|^2 \right] \\
&\approx \max_{x \in \chi_{c_{k'}}^i} \log \frac{1}{\pi N_0} \exp \left[-\frac{1}{N_0} |y_k - h_k x|^2 \right] \\
&\approx \max_{x \in \chi_{c_{k'}}^i} \left[-\frac{1}{N_0} |y_k - h_k x|^2 \right] \tag{A.2}
\end{aligned}$$

Le LLR bits est donnée à titre

$$\begin{aligned}
\text{LLR}_i(y_k, c_{k'}) &\approx \Lambda^i(y_k, c_{k'} = 1) - \Lambda^i(y_k, c_{k'} = 0) \\
&= \max_{x \in \chi_{c_{k'}=1}^i} \left\{ \frac{-1}{N_0} |y_k - h_k x|^2 \right\} - \max_{x \in \chi_{c_{k'}=0}^i} \left\{ \frac{-1}{N_0} |y_k - h_k x|^2 \right\} \tag{A.3}
\end{aligned}$$

Les parties réelles et imaginaires peuvent être découplés comme indiqué ci-dessous

$$\begin{aligned}
\text{LLR}_i &\approx \max_{x \in \chi_1^i} \left\{ 2\bar{y}_R x_R + 2\bar{y}_I x_I - |h|^2 x_R^2 - |h|^2 x_I^2 \right\} \\
&\quad - \max_{x \in \chi_0^i} \left\{ 2\bar{y}_R x_R + 2\bar{y}_I x_I - |h|^2 x_R^2 - |h|^2 x_I^2 \right\} \\
&= \max_{x_R \in \chi_1^i} \left\{ 2\bar{y}_R x_R - |h|^2 x_R^2 \right\} + \max_{x_I \in \chi_1^i} \left\{ 2\bar{y}_I x_I - |h|^2 x_I^2 \right\} \\
&\quad - \max_{x_R \in \chi_0^i} \left\{ 2\bar{y}_R x_R - |h|^2 x_R^2 \right\} - \max_{x_I \in \chi_0^i} \left\{ 2\bar{y}_I x_I - |h|^2 x_I^2 \right\} \tag{A.4}
\end{aligned}$$

où $\bar{y} = h^* y$ est la sortie MF. x_R est le réel et x_I est la partie imaginaire de x , tandis que \bar{y}_R et \bar{y}_I sont les parties réelle et imaginaire de \bar{y} . Puis, comme par le Gray d'étiquetage, $x_I \in \chi_1^i = x_I \in \chi_0^i$ for $i = 1, 2, \dots, m/2$, LLR est écrit que

$$\text{LLR}_i \approx \max_{x_R \in \chi_1^i} \left\{ 2\bar{y}_R x_R - |h|^2 x_R^2 \right\} - \max_{x_R \in \chi_0^i} \left\{ 2\bar{y}_R x_R - |h|^2 x_R^2 \right\} \tag{A.5}$$

alors que pour $i = m/2 + 1, \dots, m$, $x_R \in \chi_1^i = x_R \in \chi_0^i$, LLR est écrit que

$$\text{LLR}_i \approx \max_{x_I \in \chi_1^i} \left\{ 2\bar{y}_I x_I - |h|^2 x_I^2 \right\} - \max_{x_I \in \chi_0^i} \left\{ 2\bar{y}_I x_I - |h|^2 x_I^2 \right\} \quad (\text{A.6})$$

qui constitue la base de la réduction de la complexité. Les détails peuvent être trouvés dans le papier visés ci-dessus.

A.5 Chapitre 3 - La détection de faible complexité dans les systèmes MIMO BICM

Un double flux BICM MIMO OFDM système est considéré dans ce chapitre. Nous proposons une faible complexité MF basée près de détecteur ML pour la détection de SIC qui réduit avec succès une dimension complexe du système MIMO. C'est à dire la complexité de la détection réduit de $\mathcal{O}(|\chi|^2)$ pour $\mathcal{O}(|\chi|^1)$ dans le scénario à double flux. Le détecteur proposé échappe donc à la complexité exponentielle de MIMO de détection pour le système de double flux considéré. Bien que le décodage du premier flux, ce détecteur prend en compte encore non décodé second flux au lieu d'utiliser un filtre linéaire (MMSE ou ZF) contre elle. Cela conduit à un rendement (taux d'erreur) mieux que les approches standard détecteur linéaire en fonction couplée avec une réduction significative de la complexité. Bien que dans ce chapitre, nous aborderons le détecteur proposé pour le scénario à double flux, il reste valable pour le général multi-flux (multiplexé spatialement) des systèmes MIMO où ce détecteur réduit la complexité de la détection ML à partir de $\mathcal{O}(|\chi|^{n_t})$ pour $\mathcal{O}(|\chi|^{n_t-1})$. Réduction d'une dimension complexe est un résultat fondamental que les contraintes d'espace et de la technologie doit être restreindre les systèmes MIMO avenir de basse dimensionnalité.

Une question naturelle concerne les performances réalisables de ce détecteur. Dans la suite, nous avons poursuivi l'étude codées probabilité d'erreur par paire (PEP) du détecteur proposé d'utiliser *moment generating function* (MGF) approche fondée associée à la forme quadratique d'une variable aléatoire Gaussienne complexe [45]. Nous montrons que le détecteur proposé a pleine diversité. Pour fins de comparaison, nous incluons aussi l'analyse du détecteur MMSE et montrent encore une fois le résultat bien connu que la détection MMSE perd un ordre de diversité dans le scénario à double flux [46]. L'analyse montre également que le détecteur proposé a un meilleur gain de codage de détecteur MMSE. Nous étendons ensuite la détection de faible complexité des systèmes de plus grande dimension en mettant l'accent sur le taux uniforme, la distribution non uniforme de puissance et

de puissance uniforme, la distribution non uniforme entre les taux de flux spatiaux. La performance se dégrade légèrement pour les systèmes de plus élevée dimensions, mais il est en même temps correspond à un coup de pouce dans les économies de la complexité. La distribution de puissance ou de taux entre les flux spatiaux combinés avec codage indépendant sur chaque flux introduit UEP (unequal error protection) qui ajoute de la souplesse au système. Nous proposons également une stratégie de diffusion sur la base des UEP (taux de distribution) qui aide le système à se préparer à un débit plus élevé que les conditions de canal d'améliorer sans aucun ajustement à l'émetteur.

- Rizwan Ghaffar and Raymond Knopp, "Low complexity BICM demodulation for MIMO transmission", *Proceedings of 9th IEEE Workshop on Signal Processing Advances for Wireless Communications, SPAWC 2008*, Recife, July, 2008.
- Rizwan Ghaffar and Raymond Knopp, "Low Complexity Soft Detection for Spatially Multiplexed BICM MIMO OFDM System", *Proceedings of 10th IEEE Workshop on Signal Processing Advances for Wireless Communications, SPAWC 2009*, Perugia, June, 2009.
- Rizwan Ghaffar and Raymond Knopp, "Spatial Interference Cancellation and Pairwise Error Probability Analysis", *Proceedings of IEEE International Conference on Communications, ICC 2009*, Dresden, June, 2009.
- Rizwan Ghaffar and Raymond Knopp, "Performance Analysis of Low Complexity Soft Detection for BICM MIMO System", *Proceedings of IEEE 7th Intl. Symposium on Wireless Communication Systems, ISWCS 2010*, York, Sep, 2010.
- Florian Kaltenberger, Rizwan Ghaffar, Raymond Knopp et. al. "Design and Implementation of a Single-Frequency Mesh Network Using OpenAirInterface", *EURASIP Journal on Wireless Communications and Networking*, 2010.

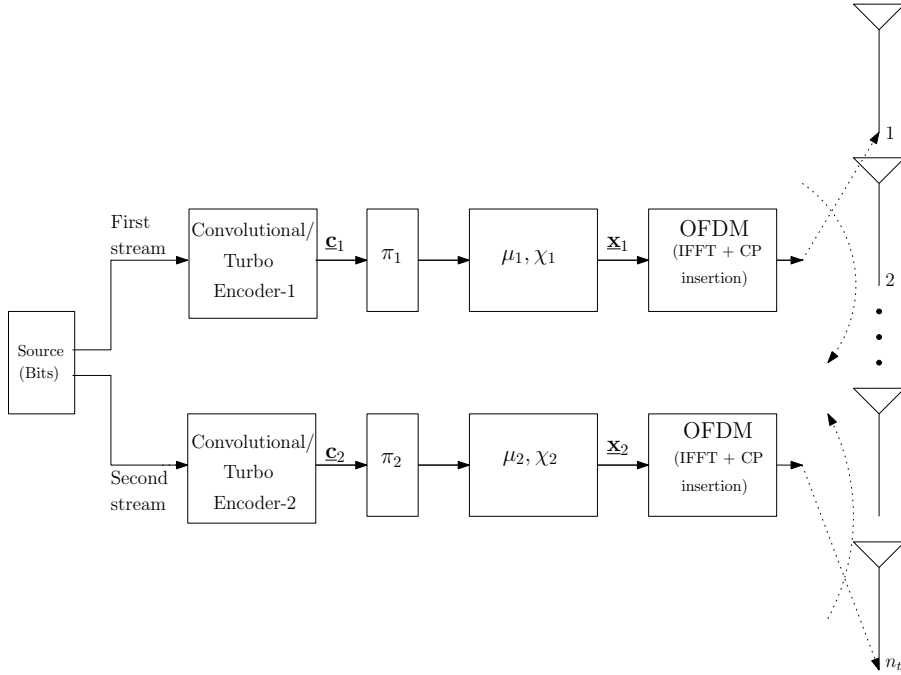


Figure A.2: Schéma de l'émetteur de flux système dual BICM MIMO OFDM. π_1 désigne l'entrelaceur aléatoire pour le premier flux.

A.5.1 Modèle de Système

Le modèle est illustré à la figure A.2. L'équation du système s'écrit

$$\begin{aligned} \mathbf{y}_k &= \mathbf{h}_{1,k}x_{1,k} + \mathbf{h}_{2,k}x_{2,k} + \mathbf{z}_k, & k = 1, 2, \dots, T \\ &= \mathbf{H}_k \mathbf{x}_k + \mathbf{z}_k \end{aligned} \quad (\text{A.7})$$

A.5.2 MF détecteur de faible complexité

Nous considérons maintenant le cas général où n_t flux spatiaux sont transmis dans $n_t \times n_r$ system. Le max log MAP métriques pour le bit $c_{k'}$ sur le premier courant à la sous-porteuse k est donnée à titre

$$\Lambda_1^i(\mathbf{y}_k, c_{k'}) \approx \min_{x_1 \in \mathcal{X}_{1,c_{k'}^i}, x_2 \in \mathcal{X}_2, \dots, x_{n_t} \in \mathcal{X}_{n_t}} \|\mathbf{y}_k - \mathbf{h}_{1,k}x_1 - \dots - \mathbf{h}_{n_t,k}x_{n_t}\|^2 \quad (\text{A.8})$$

(A.8) a la complexité de calcul de $\mathcal{O}(|\chi_1| \cdots |\chi_{n_t}|)$. En développant davantage les bits métriques et de regrouper les termes contenant x_{n_t} , on obtient

$$\begin{aligned}
\Lambda_1^i(\mathbf{y}_k, c_{k'}) &\approx \min_{x_1 \in \chi_{1,c_{k'}}, x_2 \in \chi_2, \dots, x_{n_t} \in \chi_{n_t}} \left\{ \|\mathbf{y}_k\|^2 + \sum_{j=1}^{n_t} \|\mathbf{h}_{j,k} x_j\|^2 - 2 \sum_{j=1}^{n_t} (\mathbf{y}_k^\dagger \mathbf{h}_{j,k} x_j)_R \right. \\
&\quad \left. + 2 \sum_{j=1}^{n_t-1} \sum_{l=j+1}^{n_t} (\mathbf{h}_{j,k}^\dagger \mathbf{h}_{l,k} x_j^* x_l)_R \right\} \\
&= \min_{x_1 \in \chi_{1,c_{k'}}, x_2 \in \chi_2, \dots, x_{n_t} \in \chi_{n_t}} \left\{ \|\mathbf{y}_k\|^2 + \sum_{j=1}^{n_t-1} \|\mathbf{h}_{j,k} x_j\|^2 + 2 \sum_{j=1}^{n_t-1} \sum_{l=j+1}^{n_t-1} (p_{jl,k} x_j^* x_l)_R \right. \\
&\quad \left. - 2 \sum_{j=1}^{n_t-1} (\bar{y}_{j,k}^* x_j)_R + 2 \sum_{j=1}^{n_t-1} (p_{jn_t,k} x_j^* x_{n_t})_R - 2 (\bar{y}_{n_t,k}^* x_{n_t})_R + \|\mathbf{h}_{n_t,k} x_{n_t}\|^2 \right\} \quad (\text{A.9})
\end{aligned}$$

où $\bar{y}_{j,k} = \mathbf{h}_{j,k}^\dagger \mathbf{y}_k$ est la sortie MF pour le j -th flux et $p_{jl,k} = \mathbf{h}_{j,k}^\dagger \mathbf{h}_{l,k}$ est la corrélation croisée entre les chaînes de la j -th and l -th flux à la sous-porteuse k -th. Réécriture certains termes dans leurs parties réelles et imaginaires, nous avons

$$\begin{aligned}
\Lambda_1^i(\mathbf{y}_k, c_{k'}) &\approx \min_{x_1 \in \chi_{1,c_{k'}}, \dots, x_{n_t} \in \chi_{n_t}} \left\{ \sum_{j=1}^{n_t-1} \|\mathbf{h}_{j,k} x_j\|^2 + 2 \sum_{j=1}^{n_t-1} \sum_{l=j+1}^{n_t-1} (p_{jl,k} x_j^* x_l)_R - 2 \sum_{j=1}^{n_t-1} (\bar{y}_{j,k}^* x_j)_R \right. \\
&\quad \left. + 2 \left(\sum_{j=1}^{n_t-1} (p_{jn_t,k,R} x_{j,R} + p_{jn_t,k,I} x_{j,I}) - \bar{y}_{n_t,k,R} \right) x_{n_t,R} + \|\mathbf{h}_{n_t,k}\|^2 x_{n_t,R}^2 \right. \\
&\quad \left. + 2 \left(\sum_{j=1}^{n_t-1} (p_{jn_t,k,R} x_{j,I} - p_{jn_t,k,I} x_{j,R}) - \bar{y}_{n_t,k,I} \right) x_{n_t,I} + \|\mathbf{h}_{n_t,k}\|^2 x_{n_t,I}^2 \right\} \quad (\text{A.10})
\end{aligned}$$

Pour alphabets énergétique égale, la métrique bits est écrit que

$$\begin{aligned}
\Lambda_1^i(\mathbf{y}_k, c_{k'}) &\approx \min_{x_1 \in \chi_{1,c_{k'}}, \dots, x_{n_t-1} \in \chi_{n_t-1}} \left\{ \sum_{j=1}^{n_t-1} \|\mathbf{h}_{j,k} x_j\|^2 + 2 \sum_{j=1}^{n_t-1} \sum_{l=j+1}^{n_t-1} (p_{jl,k} x_j^* x_l)_R - 2 \sum_{j=1}^{n_t-1} (\bar{y}_{j,k}^* x_j)_R \right. \\
&\quad \left. - 2 \left| \sum_{j=1}^{n_t-1} (p_{jn_t,k,R} x_{j,R} + p_{jn_t,k,I} x_{j,I}) - \bar{y}_{n_t,k,R} \right| |x_{n_t,R}| \right. \\
&\quad \left. - 2 \left| \sum_{j=1}^{n_t-1} (p_{jn_t,k,R} x_{j,I} - p_{jn_t,k,I} x_{j,R}) - \bar{y}_{n_t,k,I} \right| |x_{n_t,I}| \right\} \quad (\text{A.11})
\end{aligned}$$

Pour les alphabets non énergétique égale, on a

$$\begin{aligned} |x_{n_t,R}| &\rightarrow \left| \frac{\sum_{j=1}^{n_t-1} (p_{jn_t,k,R}x_{j,R} + p_{jn_t,k,I}x_{j,I}) - \bar{y}_{n_t,k,R}}{\|\mathbf{h}_{n_t,k}\|^2} \right| \\ |x_{n_t,I}| &\rightarrow \left| \frac{\sum_{j=1}^{n_t-1} (p_{jn_t,k,R}x_{j,I} - p_{jn_t,k,I}x_{j,R}) - \bar{y}_{n_t,k,I}}{\|\mathbf{h}_{n_t,k}\|^2} \right| \end{aligned} \quad (\text{A.12})$$

Ce bit métriques implique la réduction d'une dimension complexe, c'est à dire qu'il réduit la complexité de $\mathcal{O}(|\chi_1| \cdots |\chi_{n_t-1}|)$. Cette réduction de complexité sans aucun traitement supplémentaire est un résultat fondamental d'une grande importance pour les systèmes à dimension faible. La complexité de la mise en IJuvre pratique d'un système MIMO dimensions plus élevées en raison de l'espace (l'espacement d'antenne requise) et les contraintes technologiques souligne l'importance des algorithmes de réduction de la complexité des systèmes à dimension faible. En outre ce petit métriques étant basée sur les sorties MF et les corrélations canal signifie que c'est la mise en IJuvre du matériel simple.

A.6 Chapitre 4 - Suppression des interférences dans les futurs systèmes cellulaires

Dans ce chapitre, nous étudions la suppression des interférences dans les futurs systèmes cellulaires. Nous nous concentrons sur les utilisateurs localisés à la frontière de la cellule et de proposer l'emploi de la MF détecteur (précédemment proposé) de faible complexité à base de suppression des interférences. Contrairement aux détecteurs linéaires qui sont fondées sur l'hypothèse irréaliste d'Gaussianité d'interférence, ce détecteur estime d'interférence à partir de constellations discrètes, puis exploite la structure de cette interférence dans l'atténuation de ses effets. Dans la suite, nous avons encore étudier l'effet de la taux et de la puissance d'interférence sur la probabilité d'erreur codé par paires (pairwise error probability - PEP) du détecteur proposé. Pour cette analyse, nous considérons le cas plus réaliste de la chaîne spatialement corrélées. Nous montrons que ce détecteur présente un gain de codage (le déplacement horizontal de la courbe BER) que soit l'interférence devient plus fort ou son taux bas. Nous montrons de plus que la détection MMSE, étant indépendante de la constellation d'interférence, souffre d'une perte de codage que l'interférence devient plus fort qui est évident que ce système de détection n'exploite pas la structure d'interférence dans le processus de détection. Sur la base des caractéristiques de l'exploitation

d'interférence par le détecteur proposé, nous proposerons également une nouvelle réutilisation des fréquences fractionnaire (fractional frequency reuse - FFR), qui est plus spectralement efficace et plus économe en énergie que les stratégies traditionnelles FFR. Les travaux dans ce chapitre ont été publiés dans:

- Rizwan Ghaffar and Raymond Knopp, "Interference Suppression for Next Generation Wireless Systems", *Proceedings of IEEE 69-th Vehicular Technology Conference VTC-Spring 2009*, Barcelona, April, 2009.
- Rizwan Ghaffar and Raymond Knopp, "Spatial Interference Cancellation Algorithm", *Proceedings of IEEE Wireless Communications and Networking Conference WCNC 2009*, Budapest, April, 2009.
- Rizwan Ghaffar and Raymond Knopp, "Analysis of low complexity max log MAP detector and MMSE detector for Interference Suppression in Correlated Fading", *Proceedings of IEEE Global Communications Conference, Globecom 2009*, Hawaii, Dec, 2009.
- Rizwan Ghaffar and Raymond Knopp, "Fractional Frequency Reuse and Interference Suppression for OFDMA Networks", *Proceedings of IEEE 8th Intl. Symposium on Modeling and Optimization in Mobile, Ad Hoc, and Wireless Networks (WiOpt 2010)*, Avignon, June, 2010.

et présenté comme suit:

- Rizwan Ghaffar and Raymond Knopp, "Interference Suppression for future wireless systems", *IEEE transactions on wireless communications*.

Le travail dans le chapitre 3 et chapitre 4 a également été publié sous la forme d'un chapitre de livre en tant que

- Rizwan Ghaffar and Raymond Knopp, "Low dimensional MIMO systems with finite sized constellation inputs" *Radio Communications*, Alessandro Bazzi (Ed.), ISBN: 978-953-307-091-9, IN-TECH, April 2010

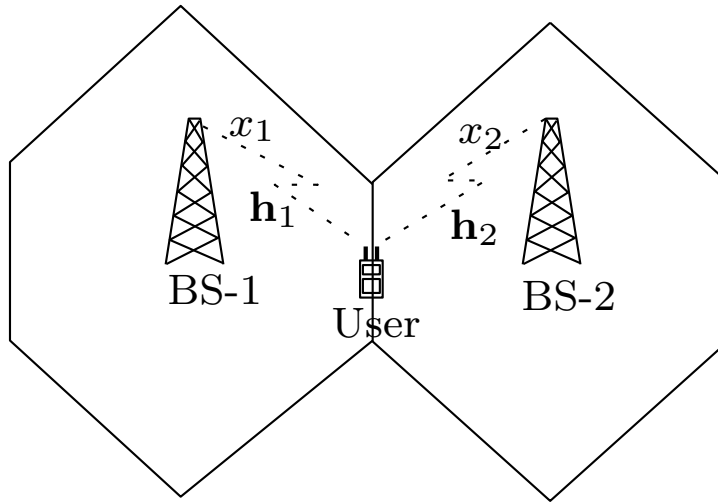


Figure A.3: Intérférence dans un réseau cellulaire. x_1 est le signal désiré alors que x_2 est le signal d'intérférence.

A.6.1 Modèle de Système

Le modèle est représenté sur la figure A.3. L'équation du système s'écrit

$$\begin{aligned} \mathbf{y}_k &= \mathbf{h}_{1,k}x_{1,k} + \mathbf{h}_{2,k}x_{2,k} + \mathbf{z}_k, & k = 1, 2, \dots, T \\ &= \mathbf{H}_k \mathbf{x}_k + \mathbf{z}_k \end{aligned} \quad (\text{A.13})$$

A.6.2 Analyse de l'information mutuelle

Nous examinons l'information mutuelle de flux désiré dans la présence de la interférence. Figure A.4 montre les effets du taux de flux d'interférence sur l'information mutuelle du flux désiré où la puissance d'interference est maintenue constante. Il illustre clairement qu'il ya une croissance significative de l'information mutuelle du flux désiré quand flux interférence sont alphabets discrets par rapport au cas où il appartient à d'autres alphabets Gaussien. Interférences discrets possède la structure qui peuvent être exploitées dans la détection du flux désiré. Toutefois, si l'interférence est Gaussien, il est dépourvu de toute structure et ne peut donc faciliter la détection des flux désiré. Notez que l'écart entre l'information mutuelle des interférences Gaussien et discret rétrécit que le taux de flux d'interférence augmente. Cette diminution de l'écart peut être lié à la proximité du comportement d'interférence taux plus élevé de Gaussianité. Dans un scénario

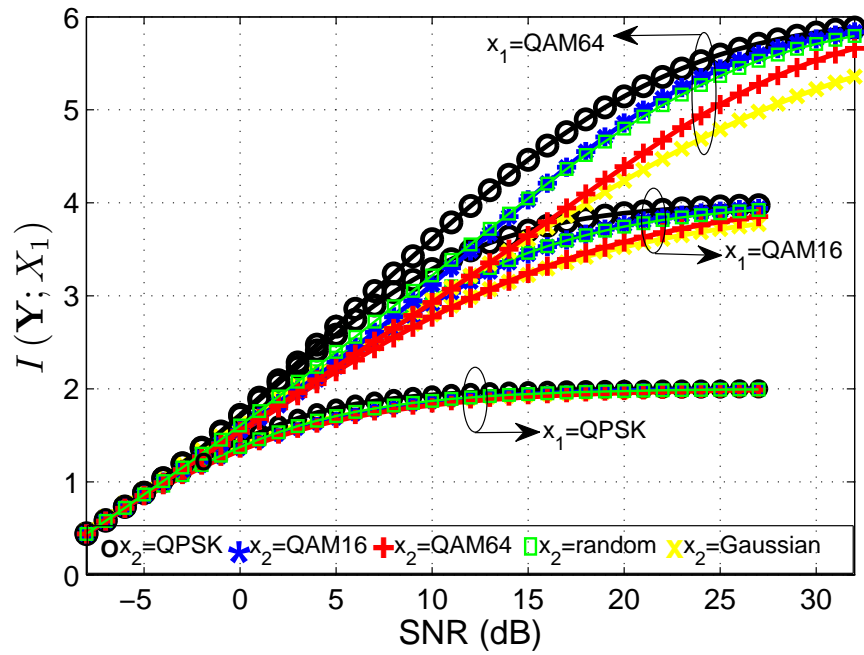


Figure A.4: Effet du taux de flux d'interférence x_2 sur l'information mutuelle du flux désiré x_1 . Les interférences sont la force de la même force que le flux désiré, soit $\sigma_2^2/\sigma_1^2 = 1$. Interférences hasard fait référence à l'affaire une fois l'interférence n'est pas statique, mais change de manière aléatoire entre QPSK, QAM16 et QAM64.

plus réaliste, la répartition des sous-porteuses pour les utilisateurs dans la cellule voisine peut ne pas coïncider avec l'attribution de sous-porteuse pour les utilisateurs dans la cellule à l'étude ce qui a entraîné dans différentes constellations d'interférence sur le sous-porteuses différentes. Pour tenir compte de ce cas, nous avons également examiné le cas d'interférences aléatoires dus à une répartition différente multi-utilisateur dans la cellule d'interférence. Notamment information mutuelle en présence d'interférences aléatoire est aussi bien améliorée par rapport au cas d'interférence Gaussien.

A.6.3 Suppression d'Interférence

Pour l'exploitation de la structure d'interférence, nous avons proposé l'emploi de précédemment proposé MF détecteur de faible complexité. Figure A.5 compare les performances de l'approche de l'exploitation de la structure d'interférence ou de la suppression d'interférences (MF détecteur) et l'atténuation d'interférence (MMSE détecteur). Il montre clairement une meilleure performance de la suppression des interférences en particulier une fois ingérence à un taux plus faible par rapport au flux désiré.

A.6.4 Novel FFR

Sur la base de l'exploitation des interférences, nous avons proposé un schéma FFR pour les systèmes cellulaires. Il existe trois principaux modes de réutilisation des fréquences pour l'atténuation d'interférence inter-cellule: HFR, FFR et SFR [67]. Nous nous concentrons sur FFR qui divise la bande spectrale dans un intérieur et une partie externe comme figure A.6. Il attribue la partie intérieure a des utilisateurs situé à proximité de la BS avec une puissance réduite en appliquant un facteur de réutilisation de fréquence d'un, c'est à dire la partie intérieure est entièrement réutilisés par tous les BSs. Pour les utilisateurs plus près du bord de cellules, une fraction de la partie extérieure de la bande spectrale est dédiée orthogonalement dans les cellules voisines avec le facteur de réutilisation des fréquences de 3. En se concentrant sur les utilisateurs bord de la cellule, nous proposons un schéma FFR qui améliore l'efficacité spectrale en permettant à un out-of-interférence cellule comme montré dans la figure A.7. La FFR a proposé assure le maximum d'une interférence pour les utilisateurs bord de la cellule et le facteur de réutilisation de fréquence réduit par la suite à 1,5. Cela conduit à une amélioration significative de l'efficacité spectrale, mais au prix d'une interférence. Toutefois, l'emploi des détecteurs de MF proposées sur la base par les utilisateurs ne pas augmenter la complexité de la détection.

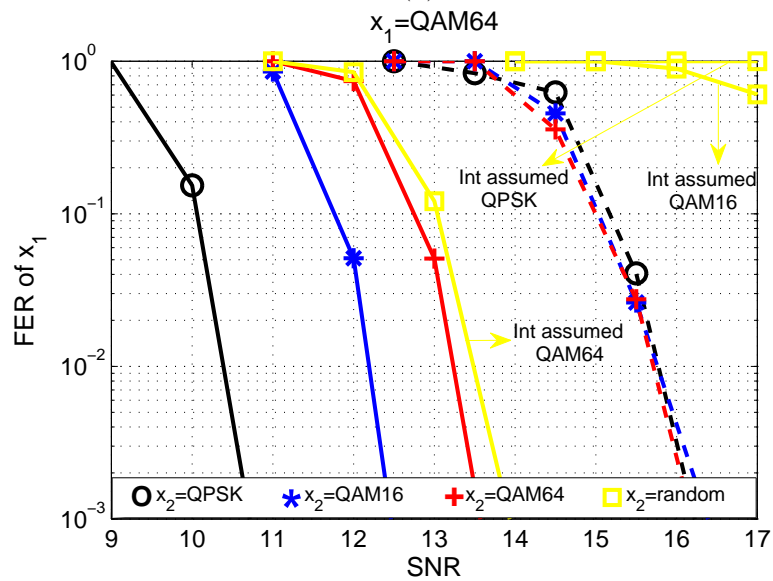
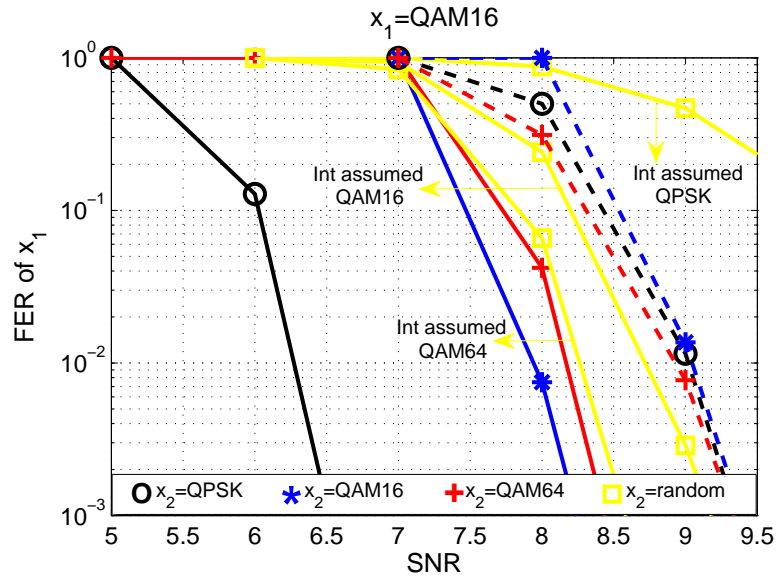


Figure A.5: Comparaison de suppression d'interférence et d'atténuation d'interférence.

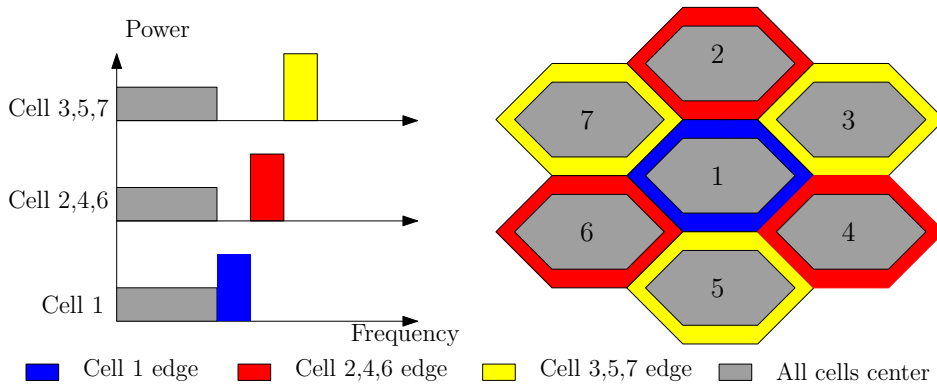


Figure A.6: FFR dans LTE. Facteur de réutilisation de fréquence pour les utilisateurs de bord de la cellule est de 3.

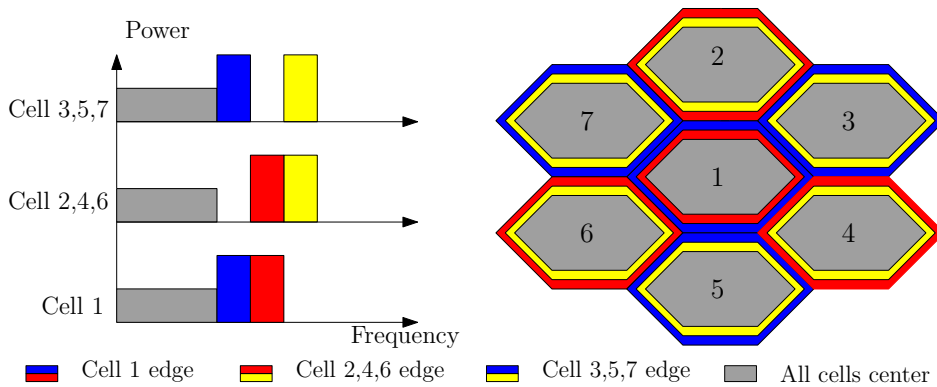


Figure A.7: FFR Proposé en LTE. Une seule interférence est assurée dans le pire des cas. Facteur de réutilisation de fréquence pour les utilisateurs de bord de la cellule est de 1,5.

A.6.5 Chapitre 5 - MIMO multi-utilisateurs (MU MIMO) pour LTE

La faisabilité de MU MIMO pour le LTE est étudié dans ce chapitre. On analyse l'efficacité de la faible résolution de LTE précodeurs. Nous proposons une stratégie de précodage basée sur les précodeurs LTE qui englobe l'alignement géométrique des interférences à la eNodeB (notation de LTE pour la station de base), suivie par l'exploitation de la structure d'interférence résiduelle par l'équipement utilisateur (user equipment - UE). D'une part, cette stratégie relègue l'interférence perçue par chaque UE par un algorithme géométrique tandis que d'autre part, des UEs exploitent la structure de l'interférence résiduelle par des détecteurs de faible complexité. Toutefois, la condition sine qua non de cette stratégie de détection est la connaissance de la constellation d'interférence. Downlink contrôle de l'information (DCI) formats en 3GPP LTE [32] ne permettent pas la transmission de cette information à l'UE. Par conséquent, nous examinons également la sensibilité de ce système de détection à la connaissance de la constellation d'interférence et de proposer un détecteur aveugle qui n'est pas au courant de cette information. Toutefois, l'importance de cette information motive son inclusion dans la normalisation en cours de LTE-Advanced [6]. Nous proposons également dans ce chapitre un algorithme pour l'emploi des précodeurs LTE pour le mode SU MIMO. EGT étant une caractéristique importante de précodeurs LTE, nous examinons les effets de cette stratégie de transmission et montrons que EGT a toute sa diversité en mode SU MIMO alors qu'il souffre d'une perte de diversité dans le mode MU MIMO. Les travaux dans ce chapitre a été publié dans:

- Rizwan Ghaffar and Raymond Knopp, "Channel Capacity for Linearly Precoded Multiuser MIMO for Discrete Constellations", *Proceedings of IEEE 20-th International Symposium on Personal, Indoor and Mobile Radio Communications (PIMRC 2009)*, Tokyo, Sep, 2009.
- Rizwan Ghaffar and Raymond Knopp, "Linear Precoders for Multiuser MIMO for finite constellations and a simplified receiver structure under controlled interference", *Proceedings of Asilomar Conference on Signals, Systems and Computers*, Pacific Grove, Nov, 2009.
- Rizwan Ghaffar and Raymond Knopp, "Near Optimal Linear Precoder for Multiuser MIMO for Discrete Alphabets", *Proceedings of IEEE International Conference on Communications, ICC 2010*, Cape Town,

June, 2010.

- Rizwan Ghaffar and Raymond Knopp, “Making Multiuser MIMO work for LTE”, *Proceedings of IEEE 21-st International Symposium on Personal, Indoor and Mobile Radio Communications (PIMRC 2010)*, Istanbul, Sep, 2010.
- Rizwan Ghaffar and Raymond Knopp, “Diversity Analysis of Equal Gain Transmission for Singleuser and Multiuser MIMO”, *Proceedings of IEEE Global Communications Conference, Globecom 2010*, Miami, Dec, 2010.

et soumis à:

- Rizwan Ghaffar, Raymond Knopp et. al., “MU MIMO in 4G systems : from theory to practice”, *EURASIP Journal on Wireless Communications and Networking, MU-MIMO special issue*.

A.6.6 Modèle de Système

Nous considérons le modèle de système pour le LTE mode de transmission 5, c.-à-MU MIMO mode dans lequel le eNodeB transmet un flux de chacun de deux UE seule antenne en utilisant les mêmes ressources temps-fréquence. En cascade à la IFFT à eNodeB et FFT à l’UE avec l’extension du préfixe cyclique, la transmission à la k -ème RE pour UE-1 en mode 5 peut être exprimée en

$$y_{1,k} = \mathbf{h}_{1,k}^\dagger \mathbf{p}_{1,k} x_{1,k} + \mathbf{h}_{1,k}^\dagger \mathbf{p}_{2,k} x_{2,k} + z_{1,k}$$

A.6.7 Stratégie de précodage at alignement géométrique d’interférence

Notre stratégie de précodage proposé implique le calcul de MF précodeurs à l’UEs. Ayant connaissance du canal, ce calcul implique seulement une opération conjugué tandis que le calcul des autres précodeurs comme CI [21] ou RCI [25] impliquent complexes inversions de matrices. Comme la décision de programmer une UE dans SU MIMO, MU MIMO ou le mode de la diversité de transmettre sera faite par le eNodeB, chaque UE est prévu à la rétroaction du précodeur qui maximise la puissance du signal reçu. Par conséquent, conformément à des LTE précodeurs, les UEs calculent quantifié versions de

leurs précodeurs MF respectifs. L'UE estime que son canal $\mathbf{h}_1^\dagger = [h_{11}^* \ h_{21}^*]$ du eNodeB et calcule par conséquent, le précodeur MF $[h_{11} \ h_{21}]^T$ (la version normalisée implique une division par $\|\mathbf{h}_1\|$). Comme précodeurs LTE sont caractérisés par des coefficients de l'unité, UE normalise le premier coefficient de la précodeur MF sorte que

$$\mathbf{p}_{MF} = \frac{h_{11}^*}{|h_{11}|^2} \begin{bmatrix} h_{11} \\ h_{21} \end{bmatrix} = \begin{bmatrix} 1 \\ h_{11}^* h_{21} / |h_{11}|^2 \end{bmatrix} \quad (\text{A.14})$$

Le deuxième coefficient indique la phase entre les deux coefficients du canal. Maintenant, se basant sur la distance minimale entre \mathbf{p}_{MF} et \mathbf{p} , l'un des quatre précodeurs est sélectionné par l'UE et l'indice de ce précodeur est renvoyé à la eNodeB. Que ce soit précodeur $\mathbf{p}_1 = \frac{1}{\sqrt{2}} \begin{bmatrix} 1 \\ q \end{bmatrix}$, $q \in [\pm 1, \pm j]$.

Du point de vue géométrique, ce précodeur fois employé par le eNodeB tentera d'aligner h_{21}^* avec h_{11}^* dans le plan complexe afin de maximiser la puissance du signal reçu, $|h_{11}^* + qh_{21}^*|^2$ sous la contrainte que le précodeur permet la rotation de h_{21}^* par $0^\circ, \pm 90^\circ$ ou 180° . Par conséquent, cette précodage assure que h_{11}^* et h_{21}^* se trouvent dans le même quadrant que représenté sur la figure A.8 (b). Ces précodeurs requis peut être employé par le eNodeB si elle décide de servir les UEs en mode SU MIMO (mode de transmission 6).

En mode MU MIMO, deux UEs sont servi par le eNodeB sur les meme ressources en temps-fréquence. Nous supposons une cellule densément peuplées, où l'eNodeB a demandé des précodeurs de la plupart des UE dans la cellule. Ici, nous proposons un algorithme d'ordonnancement pour MU MIMO mode où le eNodeB choisit deux UEs sur les mêmes ressources en temps-fréquence qui ont demandé précodeurs inverse, à savoir l'eNodeB choisit comme second UE d'être servi dans chaque groupe de attribuables RBs une des UEs qui a demandé le précodeur \mathbf{p}_2 180° en opposition de phase du précodeur \mathbf{p}_1 de l'UE premiers à être servis sur les même RBs . Le précodeur matrice est donc donné comme $\mathbf{P} = \frac{1}{\sqrt{4}} \begin{bmatrix} 1 & 1 \\ q & -q \end{bmatrix}$. Ainsi, le signal reçu par lw UE-1 est donnée à titre

$$y_1 = \frac{1}{\sqrt{4}} (h_{11}^* + qh_{21}^*) x_1 + \frac{1}{\sqrt{4}} (h_{11}^* - qh_{21}^*) x_2 + z_1 \quad (\text{A.15})$$

où le choix du précodeur pour chaque UE permettrait d'assurer la maximisation de la puissance du signal désiré, soit $|\mathbf{h}_1^\dagger \mathbf{p}_1|^2$ pour UE-1 et $|\mathbf{h}_2^\dagger \mathbf{p}_2|^2$ pour le second UE tandis que la sélection de l'UE avec les paires de précodeurs phase permettrait d'assurer la minimisation de la résistance à l'interférence

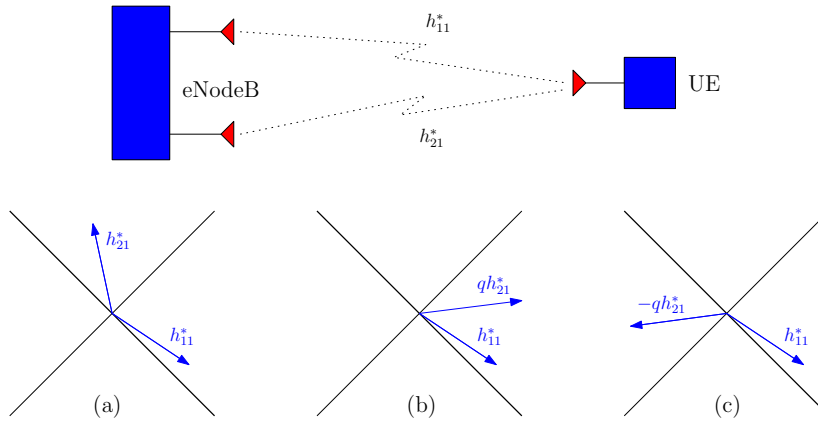


Figure A.8: Aligned géométrique d'interférence. (a) montre la canal originale de la eNodeB à l'UE tandis que (b) montre le canal efficace du signal désiré while (c) montre le canal efficace de l'interférence.

perçue par chaque UE, soit $|\mathbf{h}_1^\dagger \mathbf{p}_2|^2$ pour UE-1 et $|\mathbf{h}_2^\dagger \mathbf{p}_1|^2$ pour le deuxième UE. Notez que ces minimisations et maximisations sont soumis à la contrainte de l'utilisation des précodeurs LTE de faibles résolution. Cette stratégie de planification permettrait de s'assurer que les UE choisies pour être servi en mode MU MIMO sur les ressources en temps-fréquence même ont une bonne séparation des canaux.

Bien que cette stratégie de précodage et d'ordonnancement ferait en sorte de minimisation de l'interférence sous la contrainte de faible résolution LTE précodeurs, l'interférence résiduelle serait toujours significative. Cette interférence appartient à un alphabet fini et sa structure peut être exploitée dans le processus de détection mais cette exploitation se fait au prix d'une complexité accrue. Ici, nous proposons d'utilisation de la précédemment proposé MF détecteur de complexité faible qui réduit une dimension complexe du système et exploite la structure d'interférence dans la détection du flux désiré.

A.6.8 Résultats de la simulation

Figures A.9 montrent que la stratégie proposée pour la transmission MIMO avec MU précodeurs LTE (mode LTE 5) surpasse de manière significative Alamouti schéma de diversité de transmettre (LTE mode 2) et plus performant que les systèmes SU MIMO pour différentes efficacités spectrales.

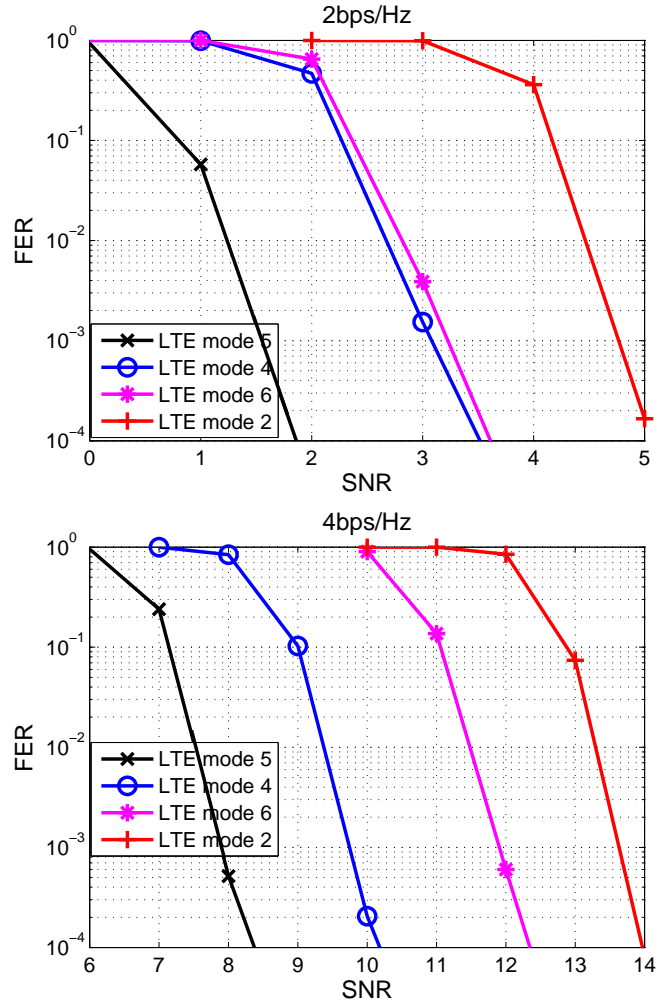


Figure A.9: MU MIMO mode en LTE

Bibliography

- [1] G. J. Foschini and M. J. Gans, "On limits of wireless communication in a fading environment when using multiple antennas," *Wireless Personal Communications*, vol. 6, no. 3, pp. 311–335, March 1998.
- [2] I. E. Telatar, "Capacity of multi-antenna Gaussian channels," *European Transactions on Telecommunications*, vol. 10, no. 6, pp. 585–595, Nov./Dec 1999.
- [3] E. Zehavi, "8-PSK trellis codes on Rayleigh channel," *IEEE Transactions on Communications*, vol. 40, pp. 873–884, May 1992.
- [4] G. Caire, G. Taricco, and E. Biglieri, "Bit-interleaved coded modulation," *IEEE Transactions on Information Theory*, vol. 44, no. 3, pp. 927–946, May 1998.
- [5] LTE, *Evolved Universal Terrestrial Radio Access (E-UTRA); Physical Channels and Modulation, Release 8, V.8.6.0*. 3GPP TS 36.211, 2009.
- [6] LTE-A, *Requirements for Further Advancements for Evolved Universal Terrestrial Radio Access (EUTRA) (LTE-Advanced)*. 3GPP TR 36.913, 2008.
- [7] IEEE 802.11n, *Amendment 5: Enhancements for Higher Throughput*, IEEE-SA, 2009.
- [8] IEEE 802.16m, *System Description Document*. IEEE 802.16m-09/0034r3, 2010.
- [9] S. Sesia, I. Toufik, and M. Baker, *LTE, The UMTS Long Term Evolution: From Theory to Practice*. Wiley, 2009.
- [10] D. Gesbert, S. Hanly, H. Huang, S. Shamai, O. Simeone, and W. Yu, "Multi-cell MIMO cooperative networks: A new look at interference,"

to appear in *IEEE Journal on Selected Areas in Communications*, fall 2010.

- [11] S. Venkatesan, A. Lozano, and R. Valenzuela, "Network MIMO: Overcoming intercell interference in indoor wireless systems," in *41-st Asilomar Conference on Signals Systems and Computers, ACSSC 2007*, vol. 2, Nov. 2007, pp. 83–87.
- [12] O. Somekh, B. Zaidel, and S. Shamai, "Sum rate characterization of joint multiple cell-site processing," *IEEE Transactions on Information Theory*, vol. 53, no. 12, pp. 4473–4497, Dec. 2007.
- [13] D. Gesbert, M. Kountouris, R. Heath, C.-B. Chae, and T. Salzer, "Shifting the MIMO paradigm," *IEEE Signal Processing Magazine*, vol. 24, no. 5, pp. 36–46, Sep. 2007.
- [14] R. Knopp and P. Humblet, "Information capacity and power control in single-cell multiuser communications," in *IEEE International Conference on Communications, ICC 1995, Seattle, USA*, Jun. 1995.
- [15] S. Shamai and A. Steiner, "A broadcast approach for a single-user slowly fading MIMO channel," *IEEE Transactions on Information Theory*, vol. 49, no. 10, pp. 2617–2635, Oct. 2003.
- [16] A. Lozano, A. Tulino, and S. Verdu, "Optimum power allocation for parallel Gaussian channels with arbitrary input distributions," *IEEE Transactions on Information Theory*, vol. 52, no. 7, pp. 3033–3051, July 2006.
- [17] H. Yao and G. Wornell, "Lattice-reduction-aided detectors for MIMO communication systems," in *IEEE Global Telecommunications Conference, GLOBECOM 2002*, vol. 1, Nov. 2002, pp. 424–428.
- [18] C. Windpassinger, L. Lampe, R. Fischer, and T. Hehn, "A performance study of MIMO detectors," *IEEE Transactions on Wireless Communications*, vol. 5, no. 8, pp. 2004–2008, Aug. 2006.
- [19] B. Hassibi and H. Vikalo, "On the expected complexity of sphere decoding," in *35-th Asilomar Conference on Signals Systems and Computers*, vol. 2, Sept. 2001, pp. 1051–1055.
- [20] I. Medvedev, B. Bjerke, R. Walton, J. Ketchum, M. Wallace, and S. Howard, "A comparison of MIMO receiver structures for 802.11N

- WLAN - Performance and complexity,” in *IEEE 17th International Symposium on Personal Indoor and Mobile Radio Communications*, Sept. 2006, pp. 1–5.
- [21] Q. Spencer, A. Swindlehurst, and M. Haardt, “Zero-Forcing methods for downlink spatial multiplexing in multiuser MIMO channels,” *IEEE Transactions on Signal Processing*, vol. 52, no. 2, pp. 461 – 471, Feb. 2004.
- [22] S. H. Muller-Weinfurtner, “Coding approaches for multiple antenna transmission in fast fading and OFDM,” *IEEE Transactions on Signal Processing*, vol. 50, pp. 2442–2450, Oct. 2002.
- [23] A. M. Chan and I. Lee, “A new reduced-complexity sphere decoder for multiple antenna systems,” in *IEEE International Conference on Communications, ICC 2002*, vol. 1, 2002.
- [24] G. Caire and S. Shamai, “On the achievable throughput of a multi-antenna Gaussian broadcast channel,” *IEEE Transactions on Information Theory*, vol. 49, no. 7, pp. 1691–1706, July 2003.
- [25] C. Peel, B. Hochwald, and A. Swindlehurst, “A vector-perturbation technique for near-capacity multiantenna multiuser communication—part I: Channel inversion and regularization,” *IEEE Transactions on Communications*, vol. 53, no. 1, pp. 195–202, Jan. 2005.
- [26] D. Love, R. Heath, V. Lau, D. Gesbert, B. Rao, and M. Andrews, “An overview of limited feedback in wireless communication systems,” *IEEE Journal on Selected Areas in Communications*, vol. 26, no. 8, pp. 1341–1365, Oct. 2008.
- [27] C. Ribeiro, K. Hugl, M. Lampinen, and M. Kuusela, “Performance of linear multi-user MIMO precoding in LTE system,” in *3rd International Symposium on Wireless Pervasive Computing, 2008. ISWPC 2008.*, pp. 410–414.
- [28] A. Carleial, “A case where interference does not reduce capacity (corresp.),” *IEEE Transactions on Information Theory*, vol. 21, no. 5, pp. 569 – 570, Sep 1975.
- [29] T. Han and K. Kobayashi, “A new achievable rate region for the interference channel,” *IEEE Transactions on Information Theory*, vol. 27, no. 1, pp. 49–60, Jan 1981.

-
- [30] E. Dahlman, H. Ekstrom, A. Furuskar, Y. Jading, J. Karlsson, M. Lundvall, and S. Parkvall, "The 3G long-term evolution - Radio interface concepts and performance evaluation," in *IEEE 63rd Vehicular Technology Conference VTC-Spring*, vol. 1, May 2006, pp. 137–141.
- [31] H. Poor and S. Verdú, "Probability of error in MMSE multiuser detection," *IEEE Transactions on Information Theory*, vol. 43, no. 3, pp. 858–871, May 1997.
- [32] LTE, *Evolved Universal Terrestrial Radio Access (E-UTRA); Channel Coding and Multiplexing, Release 8, V.8.6.0*. 3GPP TS 36.212, 2009.
- [33] U. Wachsmann, R. Fischer, and J. Huber, "Multilevel codes: Theoretical concepts and practical design rules," *IEEE Transactions on Information Theory*, vol. 45, no. 5, July 1999.
- [34] X. Li and J. Ritcey, "Trellis-coded modulation with bit interleaving and iterative decoding," *IEEE Journal on Selected Areas in Communications*, vol. 17, no. 4, pp. 715–724, Apr 1999.
- [35] R. Ghaffar and R. Knopp, "Making Multiuser MIMO work for LTE," in *IEEE 21-st International Symposium on Personal, Indoor and Mobile Radio Communications (PIMRC 2010)*, Istanbul, September 2010.
- [36] LTE, *Requirements for Evolved UTRA (E-UTRA) and Evolved UTRAN (E-UTRAN)*. 3GPP TR 25.913 v.7.3.0., 2006.
- [37] F. Tosato and P. Bisaglia, "Simplified soft-output demapper for binary interleaved COFDM with application to HIPERLAN/2," in *IEEE International Conference on Communications, ICC 2002.*, vol. 2, 2002, pp. 664–668.
- [38] E. Akay and E. Ayanoglu, "Low complexity decoding of bit-interleaved coded modulation for M-ary QAM," in *IEEE International Conference on Communications, ICC 2004*, vol. 2, June 2004, pp. 901–905.
- [39] L. Zheng and D. Tse, "Diversity and multiplexing: a fundamental trade-off in multiple-antenna channels," *IEEE Transactions on Information Theory*, vol. 49, no. 5, pp. 1073 – 1096, May 2003.
- [40] S. Alamouti, "A simple transmit diversity technique for wireless communications," *IEEE Journal on Selected Areas in Communications*, vol. 16, no. 8, pp. 1451–1458, Oct 1998.

- [41] M. Gonzalez-Lopez, F. Vazquez-Araujo, L. Castedo, and J. Garcia-Frias, "Optimized serially-concatenated LDGM and Alamouti codes for approaching MIMO Capacity," in *IEEE 17th International Symposium on Personal, Indoor and Mobile Radio Communications, PIMRC 2006*, Sep. 2006, pp. 1–5.
- [42] P. Wolniansky, G. Foschini, G. Golden, and R. Valenzuela, "V-BLAST: An architecture for realizing very high data rates over the rich-scattering wireless channel," in *International Symposium on Signals, Systems, and Electronics, 1998. ISSSE 98*, 29 1998, pp. 295–300.
- [43] S. Verdu, *Multiuser Detection*. Cambridge University Press, U.K, 1998.
- [44] G. Caire, S. Guemghar, A. Roumy, and S. Verdu, "Maximizing the spectral efficiency of coded CDMA under successive decoding," *IEEE Transactions on Information Theory*, vol. 50, no. 1, pp. 152–164, Jan. 2004.
- [45] G. L. Turin, "The characteristic function of Hermitian quadratic forms in complex normal variables," in *Biometrika*, 1960, pp. 199–201.
- [46] D. Tse and P. Viswanath, *Fundamentals of Wireless Communication*. Cambridge University Press, U.K, 2005.
- [47] T. M. Cover and J. A. Thomas, *Elements of Information Theory*. New Jersey, USA: John Wiley & Sons, 2006.
- [48] G. Golden, C. Foschini, R. Valenzuela, and P. Wolniansky, "Detection algorithm and initial laboratory results using V-BLAST space-time communication architecture," *Electronics Letters*, vol. 35, no. 1, pp. 14–16, Jan. 1999.
- [49] R. A. Horn and C. R. Johnson, *Matrix Analysis*. Cambridge University Press, U.K, 1985.
- [50] Y. Liu, K. Lau, O. Takeshita, and M. Fitz, "Optimal rate allocation for superposition coding in quasi-static fading channels," in *IEEE International Symposium on Information Theory, ISIT 2002*, pp. 111–.
- [51] D. Gesbert, S. Kiani, A. Gjendemsj, and G. Oien, "Adaptation, coordination, and distributed resource allocation in interference-limited wireless networks," *Proceedings of the IEEE*, vol. 95, no. 12, pp. 2393–2409, Dec. 2007.

- [52] M. Russell and G. Stuber, "Interchannel interference analysis of OFDM in a mobile environment," in *IEEE 45th Vehicular Technology Conference*, vol. 2, 1995, pp. 820–824.
- [53] G. Caire, S. Ramprasad, and H. Papadopoulos, "Rethinking network MIMO: Cost of CSIT, performance analysis, and architecture comparisons," in *Information Theory and Applications Workshop (ITA)*, Jan. 2010, pp. 1–10.
- [54] D. Bladsjö, A. Furuskär, S. Jäverbring, and E. Larsson, "Interference cancellation using antenna diversity for EDGE - Enhanced data rates in GSM and TDMA/136," in *IEEE Vehicular Technology Conference Proceedings, VTC 1999-Fall*, vol. 4, 1999, pp. 1956–1960.
- [55] M. Debbah, B. Muquet, M. de Courville, M. Muck, S. Simoens, and P. Loubaton, "A MMSE successive interference cancellation scheme for a new adjustable hybrid spread OFDM system," in *IEEE 51st Vehicular Technology Conference Proceedings, VTC 2000-Spring, Tokyo*, vol. 2, pp. 745–749.
- [56] A. Paulraj, R. Nabar, and D. Gore, *Introduction to Space-Time Wireless Communications*. Cambridge University Press, U.K, 2006.
- [57] SFR, *Soft frequency reuse scheme for UTRAN LTE*. 3GPP, Huawei R1-050507, May 2005.
- [58] S. Das, H. Viswanathan, and G. Rittenhouse, "Dynamic load balancing through coordinated scheduling in packet data systems," in *Twenty-Second Annual Joint Conference of the IEEE Computer and Communications Societies, INFOCOM*, vol. 1, Mar. 2003, pp. 786 – 796.
- [59] A. Gjendemsjo, D. Gesbert, G. E. Oien, and S. G. Kiani, "Optimal power allocation and scheduling for two-cell capacity maximization," in *4th International Symposium on Modeling and Optimization in Mobile, Ad Hoc and Wireless Networks, WiOpt*, Apr. 2006, pp. 1–6.
- [60] T. Bonald, S. C. Borst, and A. Proutiere, "Inter-cell scheduling in wireless data networks," in *Proceedings of European Wireless Conference*, 2005.
- [61] G. Foschini, K. Karakayali, and R. Valenzuela, "Coordinating multiple antenna cellular networks to achieve enormous spectral efficiency," *IEEE Proceedings Communications*, vol. 153, no. 4, pp. 548–555, August 2006.

- [62] FFR, *Interference mitigation : considerations and results on frequency reuse*. 3GPP, TSG-RAN R1-050738,, Siemens, Sept. 2005.
- [63] S. Das and H. Viswanathan, "Interference mitigation through intelligent scheduling," in *Asilomar Conference on Signals, Systems and Computers*, Nov. 2006.
- [64] C. Oestges, "Validity of the kronecker model for MIMO correlated channels," in *IEEE 63rd Vehicular Technology Conference, VTC-Spring*, vol. 6, May 2006, pp. 2818 –2822.
- [65] S. Loyka, "Channel capacity of MIMO architecture using the exponential correlation matrix," *IEEE Communications Letters*, vol. 5, no. 9, pp. 369–371, Sep. 2001.
- [66] J. Winters, "Optimum combining in digital mobile radio with cochannel interference," *IEEE Journal on Selected Areas in Communications*, vol. 2, no. 4, pp. 528–539, Jul. 1984.
- [67] R. Ghaffar and R. Knopp, "Fractional frequency reuse and interference suppression for OFDMA networks," in *8th Intl. Symposium on Modeling and Optimization in Mobile, Ad Hoc, and Wireless Networks (WiOpt 2010)*, Avignon, May-June 2010.
- [68] A. Hedayat, H. Shah, and A. Nosratinia, "Analysis of space-time coding in correlated fading channels," *IEEE Transactions on Wireless Communications*, vol. 4, no. 6, pp. 2882–2891, 2005.
- [69] H. Bolcskei and A. J. Paulraj, "Performance of space-time codes in the presence of spatial fading correlation," in *Asilomar Conference on Signals, Systems and Computers, 2000*, pp. 687–693.
- [70] R. Fischer, C. Windpassinger, A. Lampe, and J. Huber, "Tomlinson-Harashima precoding in space-time transmission for low-rate backward channel," in *International Zurich Seminar on Broadband Communications. Access - Transmission - Networking*, 2002.
- [71] R. Zamir, S. Shamai, and U. Erez, "Nested linear/lattice codes for structured multiterminal binning," *IEEE Transactions on Information Theory*, vol. 48, no. 6, pp. 1250 –1276, Jun. 2002.
- [72] LTE, *Evolved Universal Terrestrial Radio Access (E-UTRA); Physical Layer Procedures, Release 8, V.8.6.0*. 3GPP TS 36.213, 2009.

-
- [73] Q. Zhang, "Probability of error for equal-gain combiners over Rayleigh channels: some closed-form solutions," *IEEE Transactions on Communications*, vol. 45, no. 3, pp. 270–273, Mar. 1997.
- [74] D. Love and R. Heath Jr., "Equal gain transmission in multiple-input multiple-output wireless systems," *IEEE Transactions on Communications*, vol. 51, no. 7, pp. 1102–1110, Jul. 2003.
- [75] R. Zakhour, Z. K. M. Ho, and D. Gesbert, "Distributed beamforming coordination in multicellular MIMO systems," in *IEEE 69th Vehicular Technology Conference, VTC-Spring, April, 26-29, 2009, Barcelona, Spain*, Dec 2009.
- [76] D. Palomar and S. Verdu, "Gradient of mutual information in linear vector Gaussian channels," *IEEE Transactions on Information Theory*, vol. 52, no. 1, pp. 141–154, Jan. 2006.
- [77] X. Qi, M.-S. Alouini, and Y.-C. Ko, "Closed-form analysis of dual-diversity equal-gain combining over Rayleigh fading channels," *IEEE Transactions on Wireless Communication*, vol. 2, no. 6, pp. 1120–1125, Nov. 2003.
- [78] I. Gradshteyn and I. Ryzhik, *Table of Integrals, Series, and Products*. Academic Press, San Diego, USA, 2000.